Spring 2014

Elevated temperature mechanical properties of zirconium diboride based ceramics

Eric W. Neuman
Missouri University of Science and Technology, neumane@mst.edu

ELEVATED TEMPERATURE MECHANICAL PROPERTIES OF ZICONIUM DIBORIDE BASED CERAMICS

by

ERIC WILLIAM NEUMAN

A DISSERTATION

Presented to the Faculty of the Graduate School of the

MISSOURI UNIVERSITY OF SCIENCE AND TECHNOLOGY

In Partial Fulfillment of the Requirements for the Degree

DOCTOR OF PHILOSOPHY

in

CERAMIC ENGINEERING

2014

Approved

Gregory E. Hilmas, Advisor

William G. Fahrenholtz

Jeffrey D. Smith

F. Scott Miller

K. Chandrashekhara

PUBLICATION DISSERTATION OPTION

Portions of this dissertation have been prepared in the style for publication in the *Journal of the American Ceramic Society* and the *Journal of the European Ceramic Society.* The literature review contains portions of text that were published as part of a book chapter entitled “Mechanical Properties of Zirconium Diboride Based UHTCs” in *Ultra-High Temperature Ceramics: Materials for Extreme Environment Application*, to be published in September 2014. The manuscript entitled “Strength of Zirconium Diboride to 2300°C” was published in the *Journal of the American Ceramic Society* in volume 96, number 1 in 2013. The manuscript entitled “Mechanical Behavior of Zirconium Diboride – Silicon Carbide Ceramics at Elevated Temperatures in Air” was published in the *Journal of the European Ceramic Society* in volume 33, number 15-16 in 2013. The manuscript entitled “Mechanical Behavior of Zirconium Diboride-Silicon Carbide Ceramics up to 2200°C” will be submitted to the *Journal of the European Ceramic Society* following revisions based on the dissertation committee’s suggestions. The manuscripts entitled “Elevated Temperature Strength Enhancement of ZrB_2-30 vol% SiC Ceramics by Post-sintering Thermal Annealing” and “Ultra-high Temperature Strength, Toughness and Modulus of a Zirconium Diboride-Zirconium Carbide Ceramic” will be submitted to the *Journal of the American Ceramic Society* following revisions based on the dissertation committee’s suggestions. The manuscript entitled “Building an Ultra-high-temperature Mechanical Testing System” was published in the *American Ceramic Society Bulletin* in volume 92, number 1 in 2013.

ABSTRACT

Research presented in this dissertation focused on the mechanical behavior of ZrB_2 based ceramic at elevated temperatures. Flexure strength, fracture toughness, and elastic modulus were measured at temperatures up to 2300°C for three compositions: monolithic ZrB_2 (Z); ZrB_2 – 30 vol% SiC – 2 vol% B_4C (ZS); and ZrB_2 – 10 vol% ZrC (ZC). In argon, Z, ZS, and ZC had strengths of 210 (at 2300°C), 260 (at 2200°C), and 295 MPa (at 2300°C), the highest temperatures tested for each composition. Fractography was used extensively to characterize the strength limiting flaws as a function of temperature. Strength of ZS in argon was controlled by the SiC cluster size up to 1800°C, and the formation of B-O-C-N phases that bridged SiC clusters above 2000°C. For ZC, surface flaws introduced during specimen preparation were the source of critical flaws in the material up to 1400°C, sub-critical crack growth of surface flaws between 1600 and 2000°C, and microvoid coalescence above 2000°C.

It was also shown that thermal annealing at either 1400, 1500, or 1600°C improves the strength and modulus of ZS at temperatures between 800°C and 1600°C. Heat treatment at 1400°C for 10 hours produced the largest improvement in strength, 430 MPa at 1600°C versus 380 MPa for the as processed material. As a whole, the research pointed to several key microstructural features currently limiting the mechanical properties at the highest temperatures. In particular, removal of unfavorable secondary phases, and improved control over microstructure, should be promising methods to improve the elevated temperature properties of ZrB_2 ceramics.

AKNOWLEDGEMENTS

Firstly, I would like to thank my advisor, Dr. Gregory Hilmas for all his assistance and guidance throughout my graduate career. He has allowed me to travel the country as well as abroad to present my work in addition to the research opportunities he has afforded me. He has allowed me a large amount of freedom in my research, and has allowed me to pursue research unrelated to my thesis. I would also like to thank Drs. Fahrenholtz, Watts, and Brown-Shaklee for providing continuous insight and support. I would like to thank my friends and fellow students for all their help and support. The number of people that have helped me with this research is large, and I will not list the names for fear of omitting someone.

I would also like to thank the other members of my committee, Drs. Smith, Miller, and Chandrashekhara. Without them, I could not be in the position that I am. Each of them have provided me with the tools and insights that have allowed me to progress in my research.

I would like to acknowledge that my research was funded through the Air Force Office of Scientific Research through contract number FA9550-09-1-0168 under program manager Ali Sayir.

Finally, thanks go to my wife, Rebecca, my children, Kaelyn, Otto, and Beatrix and my parents, Keith and Richarda. Without their support, I would not have been able to be where I am today.

TABLE OF CONTENTS

LIST OF ILLUSTRATIONS

PAPER I

PAPER II

LIST OF TABLES

PAPER IV

PAPER V

1. INTRODUCTION

Development of structural materials capable of withstanding temperatures in excess of 2000°C for extended periods is critical for the development of hypersonic airframe and propulsion components. Zirconium diboride is of interest to the ultra-high temperature materials community due to its high melting temperature (3245°C), density (6.09 g/cm^3), high thermal conductivity, oxidation resistance, and high strength.[1] The borides generally exhibit higher thermal conductivities and lower electrical resistivities at room temperatures than carbide and nitride ceramics.[2, 3] Borides also show good resistance to chemical attack.[4] These properties have made borides candidates for applications including refractory linings,[5, 6] molten metal crucibles,[7, 8] furnace electrodes,[7] cutting tools,[4, 9] and especially for use on future hypersonic aerospace vehicles.[10, 11] Unfortunately, the mechanical properties of zirconium diboride and other ultra-high temperature ceramics have seen limited study at temperatures up to 1500°C with even fewer studies at higher temperatures. Further, most of these studies have been concerned only with the strength of the material being investigated, with few measurements of the elastic properties, and no measurements of the fracture toughness.

Recent research in ZrB_2 based ceramics has focused on either ZrB_2-SiC or ZrB_2-$MoSi_2$ composites. These materials have exhibited good room temperature properties, with strengths exceeding 1000 MPa and fracture toughness values exceeding 5 MPa·m^{½}.[12, 13] However, these materials would only be expected to have limited lifetimes at temperatures exceeding 2000°C due

to chemical stability issues. This is due to the presence of a eutectic at 2270°C in the ZrB_2-SiC system, and the melting point of $MoSi_2$ at 2030°C. The ZrB_2-ZrC_x system proposed in this dissertation offers promise for use in structural applications above 2000°C, as its eutectic occurs between 2660°C and 2830°C, depending on ZrC stoichiometry.[14, 15]

The purpose of this research has been to develop a better understanding of the mechanical behavior of zirconium diboride based ceramics at the proposed use temperatures for hypersonic flight. Specifically, how microstructure influences strength and toughness at temperature, as well as investigating the sources of failure in the material at temperature. The research addresses several questions:

1. How can the mechanical properties of ultra-high temperature ceramics be measured a temperatures relevant to their intended uses?
2. How have advances in powder purity and processing affected the mechanical behavior of ZrB_2 at elevated temperatures compared to the historical work presented by Manlabs Inc. in the 1960's?
3. What are the mechanical properties (strength, toughness, modulus) of a ZrB_2 – 30 vol% SiC at elevated temperatures, what is controlling the mechanical response, and what is the effect of atmosphere on the mechanical behavior?
4. Can thermal annealing be used to improve the elevated temperature mechanical properties of ZrB_2 based ceramics, such as ZrB_2-SiC?

5. Does a ZrB_2-ZrC composite offer improved mechanical properties at temperatures above 2000°C compared to the more widely studied monolithic ZrB_2, ZrB_2-SiC, and ZrB_2-$MoSi_2$ ceramics? What are its mechanical properties at temperature, and what are failure mechanisms, in flexure, as a function of temperature?

Knowledge of the mechanical properties of ZrB_2 based materials at elevated temperature, and understanding how these materials fail at temperature, is critical for enabling use of these materials in design for advanced aerospace applications. Improving the mechanical properties and refractoriness of ZrB_2 ceramics will allow for ZrB_2 based ceramics to be used for leading and trailing edges in hypersonic flight vehicles.

References

1. W. G. Fahrenholtz, G. E. Hilmas, I. G. Talmy, and J. A. Zaykoski, "Refractory Diborides of Zirconium and Hafnium," *J. Am. Ceram. Soc.,* **95** [5] 1347-64 (2007).

2. M. Rahman, C. C. Wang, W. Chen, S. A. Akbar, and C. Mroz, "Electrical Resistivity of Titanium Diboride and Zirconium Diboride," *J. Am. Ceram. Soc.,* **78** [5] 1380-82 (1995).

3. J. W. Zimmerman, G. E. Hilmas, W. G. Fahrenholtz, R. B. Dinwiddie, W. D. Porter, and H. Wang, "Thermophysical Properties of ZrB_2 and ZrB_2-SiC Ceramics," *J. Am. Ceram. Soc.,* **91** [5] 1405-11 (2008).

4. S. K. Mishra, S. K. Das, and P. Ramachandrarao, "Sintering Studies on Ultrafin ZrB_2 Powder Produced by a Self-propagating High-temperature Synthesis Process," *J. Mater. Res.,* **15** [11] 2499-504 (2000).

5. K. Kuwabara, S. Skamoto, O. Kida, T. Ishino, T. Kodama, T. Nakajima, T. Ito, and Y. Hirakawa, "Corrosion Ressistance and Electrical Resistivity of ZrB_2 Monolithic Refractories," *The Proceedings of UNITECT 2003,* The 8^{th} Biennial Worldwide Conference on Refractories (2003).

6. N. Kaji, H. Shikano, and I. Tanaka, "Developement of ZrB_2-Graphite Protective Sleeve for Submerged Nozzle," *Taikabutsu Overseas,* **14** [2] 39-43 (1992).

7. Z. J. Jin, M. Zhang, D. M. Guo, and R. K. Kang, "Electroforming of Copper/ZrB_2 Composite Coating and Performance as Eltron-Discharge Machining Electrodes," *Key Eng. Mater.,* **291-292** 537-42 (2005).

8. J. Sung, D. M. Goedde, G. S. Girolami, and J. R. Abelson, "Remote-plasma Chemical Vapor Deposition of Conformal ZrB_2 Films at Low Temperature: A Promissing Diffusion Barrier for ltralarge Scale Integrated Electronics," *J. Appl. Phys.,* **91** [6] 3904-11 (2002).

9. Y. Murata, "Cutting Tool Tips and Ceramics Containing Hafnium Nitride and Zirconium Diboride." in., U. S., 1970.

10. A. L. Chamberlain, W. G. Fahrenholtz, and G. E. Hilmas, "Low-Temperature Densification of Zirconium Diboride Ceramics by Reactive Hot Pressing," *J. Am. Ceram. Soc.,* **89** [12] 6368-75 (2006).

11. M. M. Opeka, I. G. Talmy, and J. A. Zaykoski, "Oxidation-based Materials Selection for 2000°C + Hypersonice Aerosurfaces: Theoretical

Considerations and Historical Experience," *J. Mater. Sci.,* **39** [19] 5887-904 (2004).

12. A. L. Chamberlain, W. G. Fahrenholtz, and G. E. Hilmas, "High-Strength Zirconium Diboride-Based Ceramics," *J. Am. Ceram. Soc.,* **87** [6] 1170-72 (2004).

13. A. L. Chamberlain, W. G. Fahrenholtz, G. E. Hilmas, and D. T. Ellerby, "Characterization of Zirconium Diboride-Molybdenum Disilicide Ceramics," pp. 299-308 in *Advances in Ceramic Matrix Composites IX*, Edited by N. P. Bansal, J. P. Singh, W. M. Kriven, and H. Schneider. The American Ceramic Society, Westerville, OH, 2003.

14. E. Rudy and S. Windisch, "Part II: Ternary Systems: Volume XIII: Phase Diagrams of the Systems Ti-B-C, Zr-B-C, and Hf-B-C." AFML-TR-65-2. Air Force Materials Laboratory, Wright-Patterson Air Force Base, OH, 1966.

15. S. S. Ordan'yan and V. I. Unrod, "Reactions in the System ZrC-ZrB_2," *Powder Metall Met Ceram,* **14** [5] 393-95 (1975).

2. LITERATURE REVIEW

Zirconium diboride is of interest to the ultra-high temperature materials community due to its high melting temperature (3245°C), low density (6.09 g/cm^3) compared to refractory metals, high thermal conductivity, oxidation resistance, and high strength.[1] The borides generally exhibit higher thermal conductivities and lower electrical resistivity at room temperatures than carbide and boride ceramics.[2, 3] Borides also show good resistance to chemical attack.[4] These properties have made borides candidates for applications including refractory linings,[5, 6] molten metal crucibles,[7, 8] furnace electrodes,[7] cutting tools,[4, 9] and especially for use on future hypersonic aerospace vehicles.[10, 11]

The purpose of this section is to provide an overview of recent research progress in the study of zirconium diboride based ceramics. First, the crystal structure, physical and chemical properties are discussed. Then, sintering of ZrB, ZrB_2-SiC, and ZrB_2-ZrC is discussed. A brief overview of the oxidation behavior of ZrB_2 and ZrB_2-SiC ceramics is then presented. Finally, the mechanical behavior of ZrB_2 ceramics at both room and elevated temperatures is presented. The influence of composition, processing, and microstructure on the mechanical properties is discussed in detail.

2.1. CRYSTAL STRUCTURE AND PROPERTIES

Zirconium diboride (ZrB_2) is comprised of alternating layers of boron and zirconium atoms, having the AlB_2-type P6/mmm crystal structure (Figure 2.1).[12] Boron atoms form 2D graphene-type sheets alternating with close packed zirconium layers. Zirconium atoms lie in the center of each boron hexagon, in the

middle of two adjacent boron layers. Each zirconium atom has 12 equidistant boron neighbors, and 6 equidistant zirconium neighbors. Each boron atom is surrounded by 3 equidistant boron atoms, and 6 equidistant zirconium atoms. The crystal structure leads to a combination of covalent, metallic, and ionic bonding: B-B bonds are strongly covalent; Zr-Zr bonds exhibit metallic and covalent bonding; Zr-B bonds display covalent and ionic characteristics.

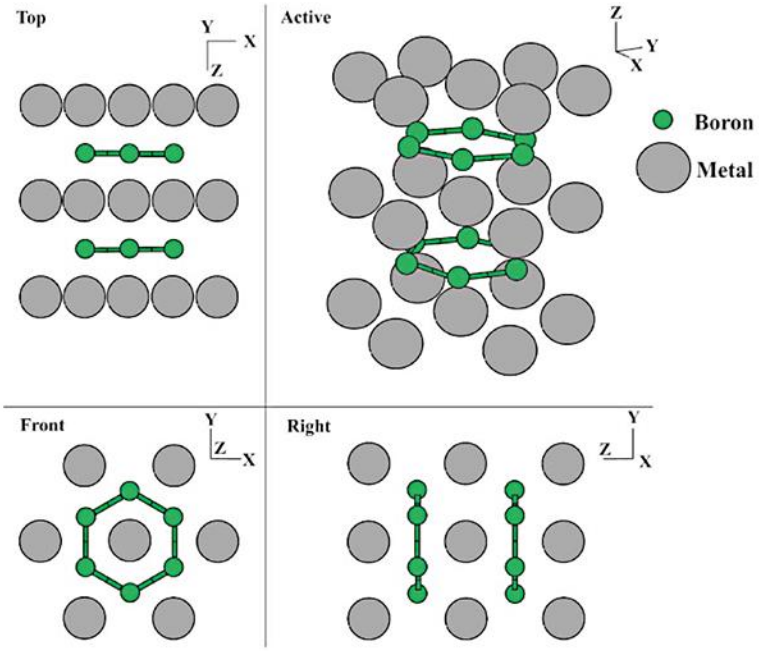

Figure 2.1. Representation of the ZrB_2 crystal structure. Pictures taken from the Crystal Lattice Structures Web page, provided by the Center for Computational Materials Science of the United States Naval Research Laboratory.

The anisotropic nature of the ZrB_2 crystal structure results in many of its physical and mechanical properties being anisotropic. Vickers hardness of ZrB_2 single crystals was measured by Xuan et al. in the temperature range from 25°C to 1000°C.[13] As temperature increased from 25°C to 1000°C, hardness decreased from ~20.9 GPa for all planes to ~7.9 GPa for the (0001) plane and ~4.9 GPa for the $(10\bar{1}0)$ and $(11\bar{2}0)$ planes. The hardness of the $(10\bar{1}0)$ and $(11\bar{2}0)$ planes was ~35% lower than that of the (0001) plane for the temperature range. Okamoto et al. obtained the elastic constants of single crystal ZrB_2 from room temperature to 1400°C (Figure 2.2).[14] While C_{12} is below 100 GPa, C_{33} is above 400 GPa, and C_{11} is greater than 500 GPa. These elastic constants also exhibit different trends with changes in temperature. C_{11}, C_{33}, and C_{44} decrease with increasing temperature, while C_{12} and C_{13} appear to be insensitive to changes in temperature up to 1400°C. The coefficient of thermal expansion (CTE) of ZrB_2 along the a-axis is 6.7 X 10^{-6} /K, and 6.9 X 10^{-6} /K along the c-axis.[14] The similar values along the a and c axes indicate very little anisotropy in CTE along different crystallographic directions. Due to the random orientation of grains in the microstructure, polycrystalline ZrB_2 ceramics do not generally exhibit anisotropic properties on the macroscopic level.

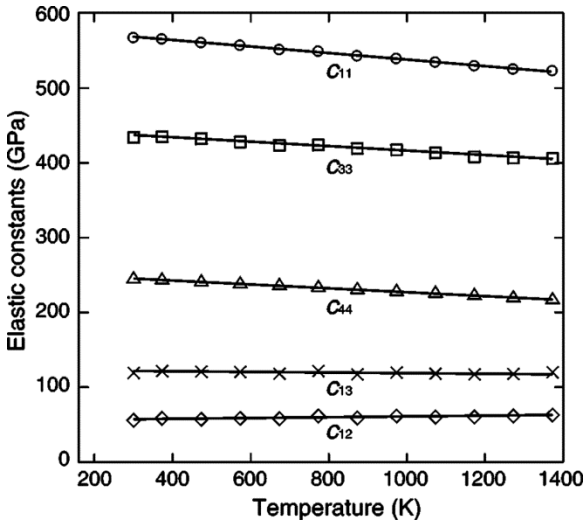

Figure 2.2. Five independent elastic constants of single-crystal ZrB_2 as a function of temperature.[14]

2.2. PROCESSING OF ZIRCONIUM DIBORIDE BASED CERAMICS

2.2.1. Zirconium Diboride. Properties of borides that lend themselves well to high temperature applications also make densification difficult. Historically, temperatures in excess of 2200°C, along with pressure, were required to densify diborides.[1] Recent work at Missouri S&T has focused on lowering the sintering temperature of zirconium diboride. Chamberlain *et al.* was able to achieve 99.8% dense ZrB_2 following hot pressing at 1900°C, a result of reducing the starting particle size by attrition milling.[15] Chamberlain *et al.* later showed that the same milling procedure could be used to produce 98.0% dense ZrB_2 by pressureless sintering at 2150°C.[16] The densification was enhanced by the reduction of the starting ZrB_2 particle size from 2 μm to 0.5 μm, isothermal holds that aided in the removal of surface oxides, and the introduction of tungsten carbide (WC) into the powder via erosion of the grinding media. The

surface of ZrB_2 powder is covered with a layer of ZrO_2 and B_2O_3, which acts as a diffusion barrier during sintering. B_2O_3 can be removed from the surface of the powders by evaporation under mild vacuum at 1340°C.[17, 18] Several vacuum isothermal holds were utilized up to 1650°C, thus B_2O_3 liquid should be completely vaporized. WC aided in the densification of ZrB_2 by reducing the ZrO_2 on the surface of the particles (Equation 1). This reaction was later confirmed by Zhang et at.[18] in addition to an intermediate reaction step that generates W_2C (Equations 2 & 3).

$$ZrO_2 + 3WC \rightarrow ZrC + 2CO(g) + 3W \quad (1)$$

$$2WC \rightarrow W_2C + C \quad (2)$$

$$ZrO_2 + 3W_2C \rightarrow ZrC + 6W + 2CO(g) \quad (3)$$

Further improvements to the densification of ZrB_2 were investigated using reducing agents such as C and B_4C (Figure 2.3).[18-20] Additions of C and B_4C have been shown to react with the surface oxides by the following reactions:

$$2B_2O_3 + 7C \rightarrow B_4C + 6CO(g) \quad (4)$$

$$7ZrO_2 + 5B_4C \rightarrow 7ZrB_2 + 3B_2O_3 + 5CO(g) \quad (5)$$

$$ZrO_2 + 5C + B_2O_3 \rightarrow ZrB_2 + 5CO(g) \quad (6)$$

$$2ZrO_2 + B_4C + 4C \rightarrow 2ZrB_2 + 4CO(g) \quad (7)$$

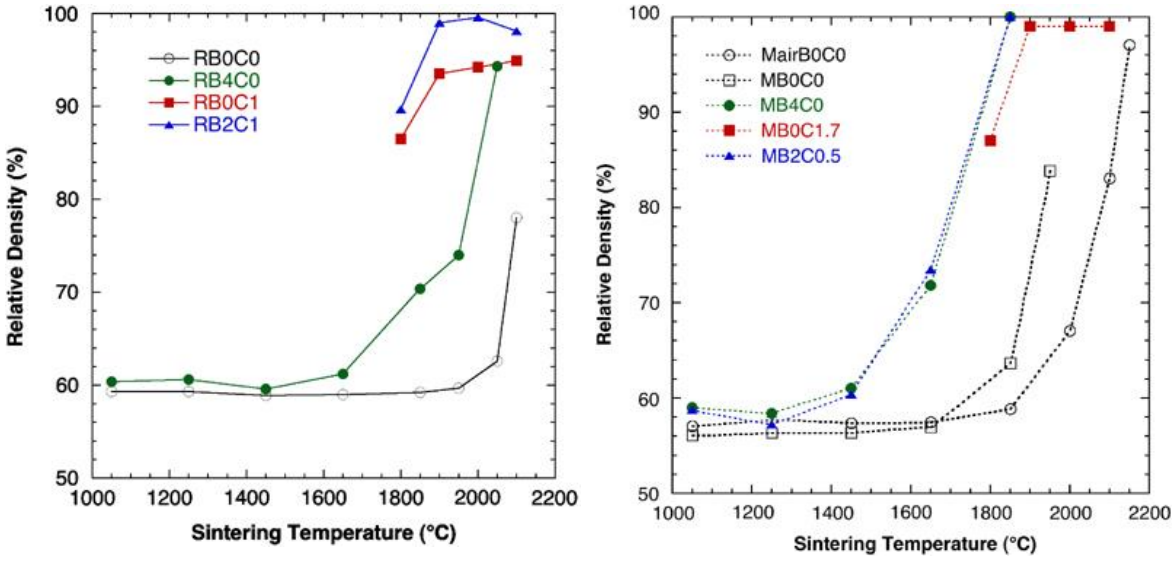

Figure 2.3. Relative density as a function of sintering temperature for as received (R) and attrition milled (M) ZrB_2 with B_4C (B) and carbon (C) additives.[19]

Zhang showed that addition of 4 wt% B_4C to as received powder improved the relative density, following pressureless sintering at 2050°C, from ~62% to ~95%.[18] Attrition milling the powder with 4 wt% B_4C resulted in fully dense microstructures at 1850°C (Figure 2.4). Zhu et al.[21] showed that an addition of 0.5 wt% C to as received ZrB_2 resulted in an increase in density from ~62% to ~90%, and adding 1.0 wt% C to attrition milled powder increased the density from ~68% to ~99%, following pressureless sintering at 1900°C (Figure 2.5).[21] Zhu later showed that a combination of 1 wt% C and 2 wt% B_4C added as sintering aids allows as received ZrB_2 to be sintered to >99% density at 1900°C

(Figure 2.6).[19, 20] Harrington *et al.* showed that additions of ZrH_2 can be used to consume excess B_4C and C by the following reactions:[22]

$$ZrH_2 \rightarrow Zr + H_2(g) \quad (8)$$

$$2Zr + B_4C \rightarrow 2ZrB_2 + C \quad (9)$$

$$3Zr + B_4C \rightarrow 2ZrB_2 + ZrC \quad (10)$$

$$Zr + C \rightarrow ZrC \quad (11)$$

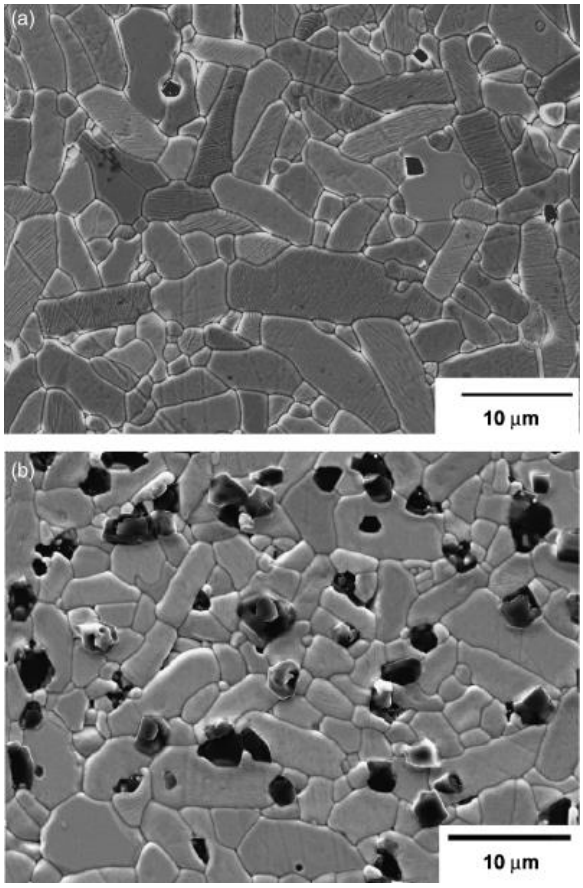

Figure 2.4. SEM images of attrition-milled ZrB_2 with (a) 2 wt% B_4C and (b) 4 wt% B_4C sintered at 1850°C.[1]

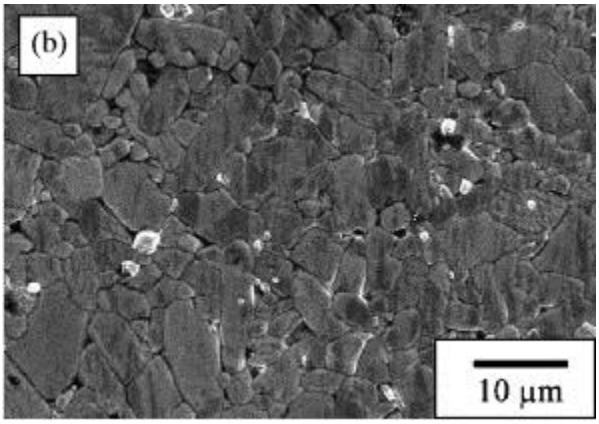

Figure 2.5. SEM micrograph of attrition-milled ZrB_2 with 1.7 wt% carbon addition sintered at 1900°C.[21]

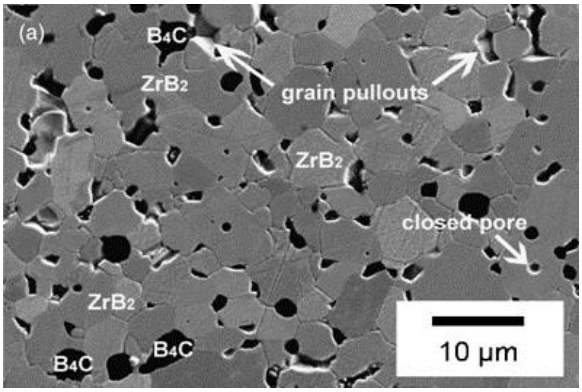

Figure 2.6. SEM image of ZrB_2 with additions of 2 wt% B_4C and 1 wt% C sintered at 1900°C.[20]

2.2.2. Zirconium Diboride – Silicon Carbide. ZrB_2 ceramics with additions of SiC have traditionally been densified by hot pressing.[1, 23, 24] Recent studies have reported improvents in the sinterability of ZrB_2-SiC.[15, 25-28] Chamberlain et al. reported the production of dense ZrB_2 with 10, 20 and 30 vol% SiC by hot-pressing at 1900°C following milling with WC media (Figure 2.7).[15] Rezaie et al. hot-pressed ZrB_2 – 30 vol% SiC to densities of ~97% at

temperatures as low as 1800°C.[25] The improvement in sinterability was attributed to the reduction in starting ZrB_2 and SiC particle size, and the reduction of surface oxides by WC (introduced through media erosion during milling), as discussed above. Zhang et al. showed the ZrB_2 – SiC ceramics could be pressurelessly sintered to full density at 1900°C through a combination of attrition milling with WC media and additions of B_4C and C to remove surface oxides.[26]

Additions of SiC to ZrB_2 have the benefit of reducing the ZrB_2 grain size. Chamberlain reported a reduction in ZrB_2 grain size from 6 μm to 3 μm with the addition of SiC.[15] Rezaie et al. investigated the effect of hot-pressing time and temperature on ZrB_2-SiC ceramics.[25] Hot-pressing temperatures ranged from 1850°C to 2050°C with times ranging from 45 min to 180 min at temperature. The effect of time and temperature on the grain size of both ZrB_2 and SiC were measured. Expectedly, the lowest temperature and shortest time resulted in the finest grain sizes, while the highest temperature and longest time produced the largest grain sizes. The average grain sizes showed some change (2.1 – 4.7 μm for ZrB_2 and 1.2 – 2.7 μm for SiC); however, the maximum grain sizes were substantially larger (6.0 – 20.9 μm for ZrB_2 and 3.5 – 8.0 μm for SiC).

2.2.3. Zirconium Diboride – Zirconium Carbide. Investigations into the effect of zirconium carbide (ZrC) additions on the densification of ZrB_2 have been more limited. Gropyanov *et al.* showed that additions of ZrC to ZrB_2 improve sintering.[29] They showed that additions of 10 vol% ZrC lowered the activation energy for sintering by ~25% and suppress grain growth in the ZrB_2 and ZrC

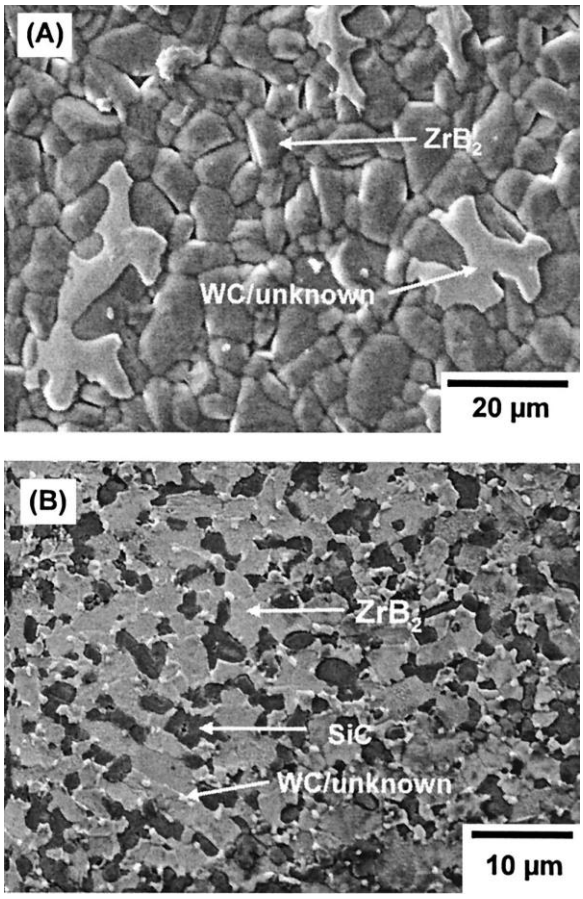

Figure 2.7. SEM images of ZrB_2 (A) and ZrB_2 – 30 vol% SiC (B). [15]

phase. Andrievskii *et al.* hot pressed ZrB_2-5 vol% ZrC with ~5 vol% porosity after hot pressing at 2200°C.[30] They also found that the addition increased the grain size of the ZrB_2 phase from 13 µm to 27 µm for similar hot pressing conditions. Kats *et al.* showed that 20 vol% additions of ZrC into ZrB_2 reduced the porosity to 2.9% from 10.6%, and reduced the grain size of the ZrB_2 from 6-8 µm to 2-4 µm after hot pressing at 2100°C.[31] More recently, Tsuchida *et al.* used spark plasma sintering to produce a 97.5% dense compact of ZrB_2-20 vol% ZrC at 1800°C.[32] The current body of work reports conflicting results for the effect of ZrC on the sintering of ZrB_2 ceramics. This may be a result of unreported variations in

stoichiometry or purity of the ZrB_2 and ZrC powders used. Most other recent work investigating additions of ZrC to ZrB_2 based materials has focused on ZrB_2-SiC-ZrC and ZrB_2-$MoSi_2$-ZrC composites.

2.3. OXIDATION BEHAVIOR

Exposure of ZrB_2 to air above ~700°C results in the formation of ZrO_2 and B_2O_3 by Equation 12.[1] This reaction is favorable at all temperatures.

$$ZrB_2(c) + \frac{5}{2}O_2(g) \rightarrow ZrO_2(g) + B_2O_3(l,g) \quad (12)$$

For nominally pure ZrB_2, oxidation below 1100°C is controlled by diffusion of oxygen through the liquid boria that surrounds the ZrO_2 grains.[33-35] Between 1100°C and 1400°C, the oxidation kinetics display paralinear characteristics due to mass gain from the formation of ZrO_2 and B_2O_3, and mass loss through B_2O_3 evaporation.[35] At temperatures greater than 1400°C, the oxide scale is no longer protective and oxidation proceeds with linear mass gain kinetics.[1, 34] These regimes are shown schematically in Figure 2.8, with an characteristic cross-section of the oxide scale following exposure at 1500°C shown in Figure 2.9.

Additions of SiC to ZrB_2 ceramics have been reported to improve the oxidation resistance compared to nominally pure monolithic ZrB_2.[37] Figure 2.10 shows the evolution of the oxide scale of a ZrB_2 – 30 vol% SiC ceramic between 1000 and 1500°C. During oxidation at elevated temperatures, the silicon from

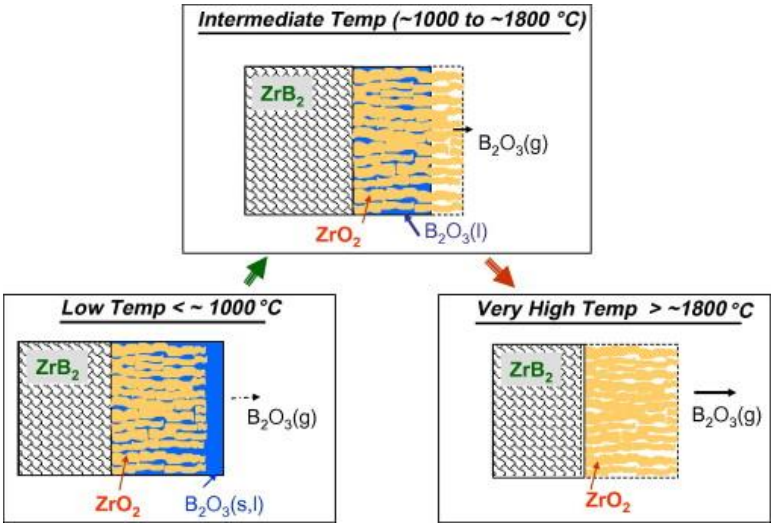

Figure 2.8. Schematic showing the three temperature regimes for the oxidation of ZrB_2.[36]

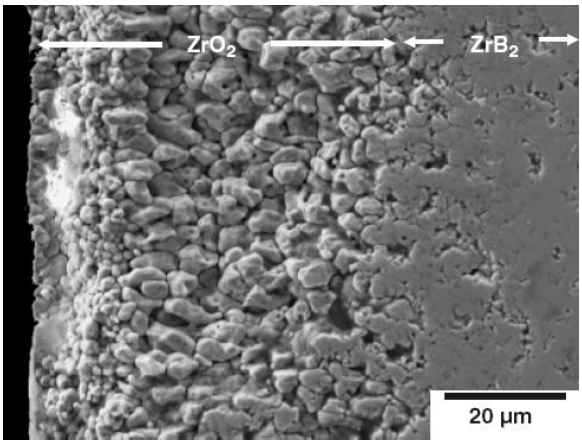

Figure 2.9. A ZrB_2 ceramic oxidized at 1500°C in air for 30 min showing a surface layer composed of porous ZrO_2.[17]

the SiC and the boron from the ZrB_2 are oxidized to form a protective borosilicate glassy layer. The silicon carbide oxidizes according to Equation 13.

$$SiC(c) + \frac{3}{2}O_2(g) \rightarrow SiO_2(l) + CO(g) \quad (13)$$

ZrB_2 containing SiC retains the protective glassy layer for a wider temperature range. However, SiC only improves the oxidation resistance at temperatures above ~1350°C.[1] Below this temperature, SiC does not undergo significant oxidation and SiC inclusions remain in the oxide layer. Above ~1350°C, SiC oxidation increases, as does B2O3 vaporization. The silica-rich liquid provides protection until the passive to active transition of SiC oxidation between 1600-1700°C in air under atmospheric pressure.[38] At these higher temperatures, the silica glassy layer begins to vaporize as a result of the formation of SiO (Equations 14 and 15).

$$SiO_2(l) + CO(g) \rightarrow SiO(g) + CO_2(g) \quad (14)$$

$$2SiO_2(l) + SiC(c) \rightarrow 2SiO(g) + CO(g) \quad (15)$$

Oxidation of SiC results in the formation of a SiC depletion region[39] and pressure within the oxide scale resulting in rupture of the glassy layer.[11] Due to the evaporation of the glassy scale at high temperatures, formation of a porous

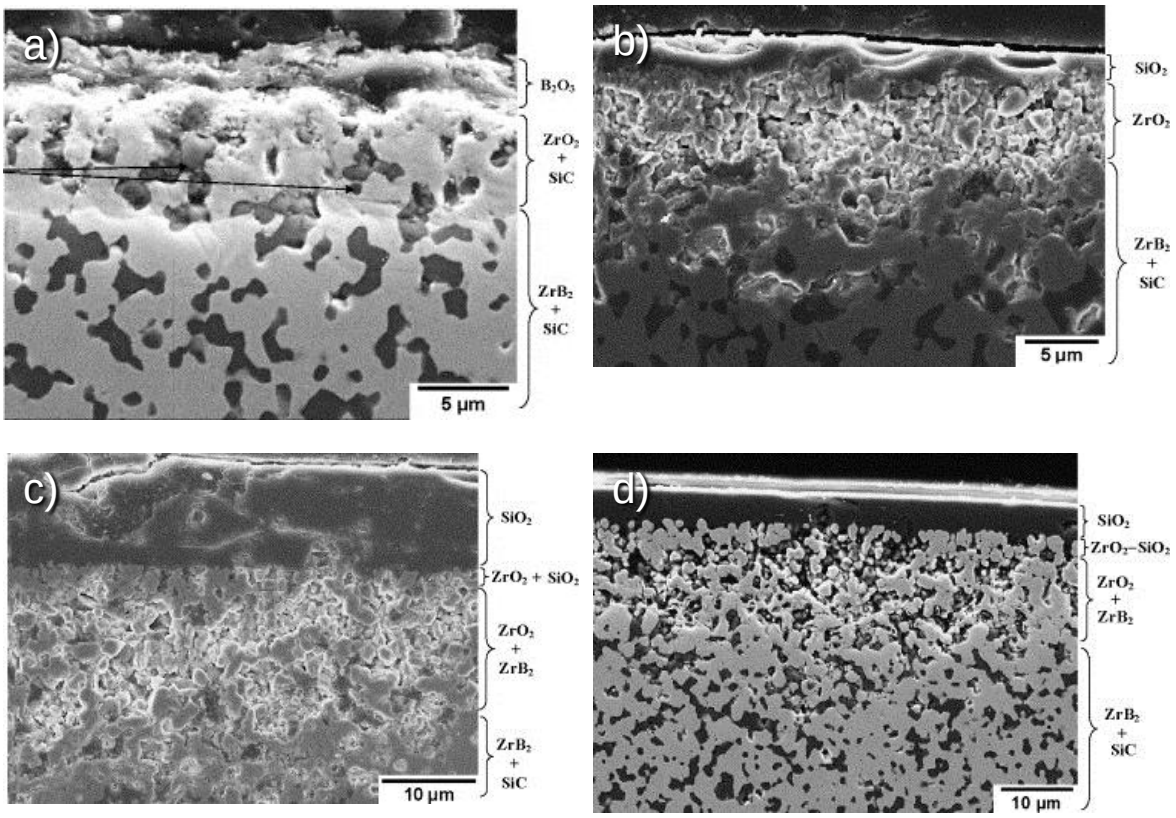

Figure 2.10. SEM image of ZrB_2-SiC ceramic showing the evolution of the oxide scale structure at a) 1000°C, b) 1200°C, c) 1400°C, and d) 1500°C.[37]

SiC depletion region, and rupture of the glassy scale at high temperatures, SiC additions may not be desirable for use at ultra-high temperatures despite their improvements to mechanical properties.

2.4. ROOM TEMPERATURE MECHANICAL PROPERTIES

2.4.1. Zirconium Diboride. Elastic modulus values reported for selected ZrB_2 ceramics, with and without sintering additives, are summarized in Table 2.1. Elastic modulus ranges from ~350 GPa to ~530 GPa depending on porosity and additives (Figure 2.11). Fitting the data to the Einstein (linear),[40] Spriggs,[41] and

Nielson[42, 43] models (Table 2.2) gives a value for fully dense ZrB_2 of 511 GPa compared to measured values of 490 - 500 GPa in previous studies.[44, 45] However, the materials in the historic studies were not fully dense, and fitting the historic data to similar models predicts an elastic modulus of 519 GPa for dense ZrB_2. Zhang et al. calculated the elastic modulus of ZrB_2 from first principles to be 520 GPa, in good agreement with the fitted data.[46] Recent work by Okamoto et al. calculated the polycrystalline elastic modulus of ZrB_2 from single crystal measurements to be 525 GPa.[47] The modulus of 99.8% dense ZrB_2 was measured to be 489 GPa.[15] However, additions of AlN, Si_3N_4, B_4C, and C, as well as impurities picked up during powder milling (i.e., WC, ZrO_2, etc.), affect the elastic modulus of ZrB_2 ceramics. Small additions of B_4C and/or C increase the elastic modulus of ZrB_2.[19, 48] Additions of AlN and Si_3N_4 lower the elastic modulus.[49, 50] Additions affect the elastic modulus primarily through interactions with impurities on the surface of the starting powders. Additives such as C and B_4C remove low modulus surface oxides, which increases modulus, whereas additives such as with AlN (308 GPa)[51] and Si_3N_4 (310 GPa) promote formation of low modulus grain boundary phases, which reduces modulus.[52] The reported modulus values for ZrB_2 are typically impacted by porosity and/or impurities, but the intrinsic elastic modulus seems to be ~525 GPa.

Table 2.1. Elastic modulus, Vickers hardness, fracture toughness by direct crack method, and 4-point flexure strength of ZrB_2 ceramics with and without sintering additives.

Composition (vol%)	Relative density (%)	Grain size (μm)	Elastic modulus (GPa)	Hardness (GPa)	Fracture toughness (MPa·m^{½})	Flexure strength (MPa)	Ref.
ZrB_2	87	10	346 ± 4	8.7 ± 0.4	2.4 ± 0.2^{C}	351 ± 31	24, 28, 49, 53
ZrB_2	90	-	-	16.1 ± 1.1	1.9 ± 0.4	325 ± 35^{3}	54
ZrB_2	90.4	6.1	417	-	4.8 ± 0.4	457 ± 58	55-57
ZrB_2	95.8	10	-	16.5 ± 0.9	3.6 ± 0.3	450 ± 40^{3}	58
ZrB_2	97	8.1	479 ± 8	16.7 ± 0.6	2.8 ± 0.1	452 ± 27	48
ZrB_2	97.2	5.4 ± 2.8	498	-	-	491 ± 22	59
ZrB_2	98	9.1	454	14.5 ± 2.6	-	444 ± 30	16, 19
ZrB_2	> 98	-	-	14.7 ± 0.8	-	300 ± 40	60
ZrB_2	~ 99	20	491 ± 34	-	-	326 ± 46	23
ZrB_2	99.8	~6	489	23 ± 0.9	3.5 ± 0.3^{I}	565 ± 53	15, 61, 62
ZrB_2 + 4 wt% B_4C	100	8	530	18	3.1	473	19
ZrB_2 + 4 wt% Ni	98	5 - 15	496	14.4 ± 0.8	3.4 ± 0.4^{C}	371± 24	24, 63
ZrB_2 + 4.6 AlN	~ 92	-	407 ± 5	9.4 ± 0.5	3.1 ± 0.1^{C}	580± 80	50
ZrB_2 + 5 Si_3N_4	98	3	419 ± 5	13.4 ± 0.6	3.7 ± 0.1^{C}	600 ± 90	49, 64-66
ZrB_2 + 3 YAG	95	7.5	-	-	5.4 ± 0.2^{S}	629 ± 31^{3}	67
ZrB_2 + 2 wt% B_4C + 1 wt% C	100	4.1	507	19.6 ± 0.4	3.5	575± 29	19, 20
ZrB_2 + 2 wt% B_4C + 1 wt% C	100	2.5	509 ± 11	19.7 ± 0.6	3.0 ± 0.1	547 ± 35	48

^{S} Single edge notched beam, ^{C} Chevron notched beam, ^{I} Indentation strength in bending, ^{3} 3-point flexure

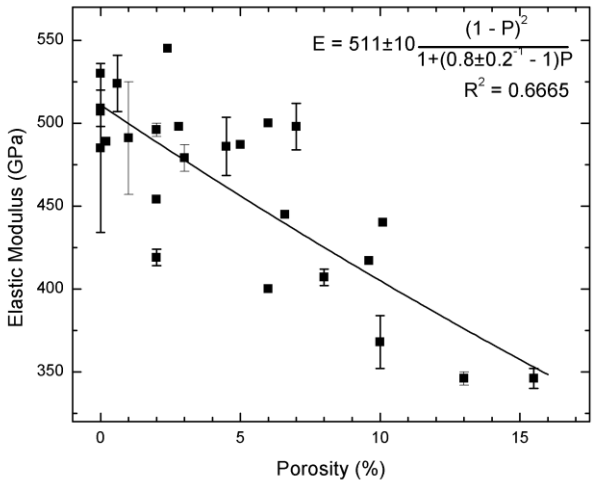

Figure 2.11. Room temperature elastic modulus as a function of porosity for ZrB_2 (left) with and without sintering aids.[15, 16, 19, 20, 23, 24, 28, 44, 48-50, 53, 55, 56, 59, 61-66, 68] Line represents fitted relationship of elastic modulus to porosity according to Nielsen's relationship.[42, 43]

Table 2.2. Summary of various fitted models of elastic modulus as a function of porosity for ZrB_2.

Equation	E_o	b	R^2
$E = E_0(1-bP)$	511 ± 10	2.0 ± 0.3	0.6416
$E = E_0 e^{-bP}$	512 ± 11	2.4 ± 0.4	0.6614
$E = E_0 \frac{(1-P)^2}{1+(b^{-1}-1)P}$	511 ± 11	0.8 ± 0.2	0.6665

Room temperature flexure strengths for ZrB_2 ceramics with and without sintering aids are also given in Table 2.1. The strength ranges from 250 to 630 MPa depending on grain size and additives (Figure 2.12). In general, the strength of ZrB_2 follows an inverse square root relation with grain size ($GS^{-½}$), as expected for ceramics free of other larger flaws. The line in Figure 2.12

highlights the $GS^{-½}$ relationship, but is not intended as a fit of the data. This relation indicates that flaw-free ZrB_2 with a fine grain size has improved strengths.

The fracture toughness of ZrB_2 is generally in the range of 3.0 MPa·$m^{½}$ to 4.5 MPa·$m^{½}$, with most values being reported near ~3.5 MPa·$m^{½}$. Unfortunately, the effects of porosity or grain size on fracture toughness have not been investigated. Also, the possibility of R-curve behavior has not been investigated, even though the CTE mismatch between the a-axis (6.9 x 10^{-6} K^{-1}) and c-axis (6.7 x 10^{-6} K^{-1}) [14]of the hexagonal unit cell leads to residual stresses that could induce R-curve behavior.

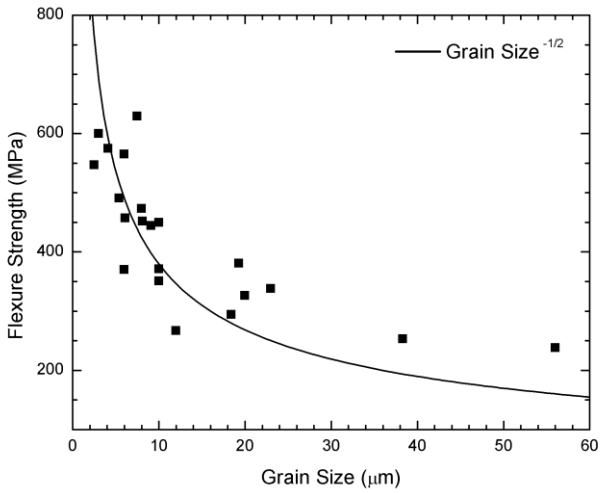

Figure 2.12. Room temperature flexure strength as a function of grain size for ZrB_2 (left) with and without sintering additives.[15, 16, 19, 20, 23, 24, 28, 48, 49, 53, 55-65, 67, 69, 70] Line is not fitted to data, and is meant to guide the eye.

2.4.2. Zirconium Diboride – Silicon Carbide.

2.4.2.1. Size effect of SiC addition. The 4-point flexure strength of ZrB_2-SiC ceramics without additives is shown in Table 2.3. Although ZrB_2 grain size is a factor, the room temperature strength of ZrB_2-SiC is controlled by the size of the dispersed SiC particles or clusters.[25, 74, 75] Rezaie et al.[25] and Watts et al.[75] used linear elastic fracture mechanics to show that critical flaw sizes correlated to the SiC cluster size in ZrB_2-30 vol% SiC ceramics. This conclusion is consistent with the CTE mismatch between ZrB_2 and SiC (for α-SiC: $\alpha_{a\text{-}axis} = 4.3 \times 10^{-6}\ K^{-1}$, $\alpha_{c\text{-}axis} = 4.7 \times 10^{-6}\ K^{-1}$).[76] Watts et al.[77] used neutron diffraction to measure the thermal residual stresses present in ZrB_2-30 vol% SiC. They found that the thermal residual stresses begin to accumulate at ~1400°C, resulting in residual tensile stresses in the ZrB_2 and compressive stresses in the SiC at room temperature. Assuming constant strain across the interface between SiC and ZrB_2, the maximum tensile stress in the ZrB_2 was determined to be ~1000 MPa.[75] Watts predicted a critical grain size range for microcracking between 6.5-13.8 μm. This matches well with the critical SiC particle size of ~11.5 μm observed by Watts experimentally (estimated by fitting the major axis of the clusters to ellipses as discussed below).

Table 2.3. Elastic modulus, Vickers hardness, fracture toughness by direct crack method, and 4-point flexure strength of ZrB_2-SiC ceramics.

Composition (vol%)	Relative density (%)	ZrB_2 Grain size (μm)	SiC Grain size (μm)	Elastic modulus (GPa)	Hardness (GPa)	Fracture toughness ($MPa \cdot m^{½}$)	Flexure strength (MPa)	Ref.
ZrB_2 + 10SiC	-	3	-	507 ± 4	-	4.8 ± 0.3^{C}	835 ± 35	28
ZrB_2 + 10SiC	93.2	~ 3	-	450	24 ± 0.9	4.1 ± 0.3^{I}	713 ± 48	15, 62
ZrB_2 + 10SiC	97.1	2.2	~ 0.2	-	-	5.7 ± 0.2^{S}	720 ± 55^{3}	69
ZrB_2 + 10SiC	97.4	4.5 ± 1.6	0.8 ± 0.4	-	-	-	524 ± 63	55, 57
ZrB_2 + 10SiC	99.8	4.3 ± 1.4	-	500 ± 16	18 ± 0.9	3.8 ± 0.3	393 ± 114^{3}	71
ZrB_2 + 15SiC	96.5	4.4 ± 1.7	0.9 ± 0.5	-	-	-	714 ± 59	55, 57
ZrB_2 + 15SiC	99	2	-	480 ± 4	17.7 ± 0.4	4.1 ± 0.1^{C}	795 ± 105	72
ZrB_2 + 20SiC	-	1.8	~ 0.2	-	-	6.8 ± 0.1^{S}	1009 ± 43^{3}	69
ZrB_2 + 20SiC	97.3	4.2 ± 1.9	0.9 ± 0.5	-	-	-	608 ± 93	55, 57
ZrB_2 + 20SiC	99.7	~ 3	-	466	24 ± 2.8	4.4 ± 0.2^{I}	1003 ± 94	15, 62
ZrB_2 + 20SiC	99.7	4.0 ± 1.1	-	506	22.1 ± 0.1	4.2 ± 0.8	487 ± 68^{3}	71
ZrB_2 + 20SiC	5.62 g/cm^3	4.1 ±0.9	-	505 ± 3	21.3 ± 0.7	3.9 ± 0.3	937 ± 84^{3}	73
ZrB_2 + 30SiC	-	3	~ 0.2	-	-	5.9 ± 0.2^{S}	860 ± 70^{3}	69
ZrB_2 + 30SiC	97.2	2.2 ± 1.2	1.2 ± 0.6	516 ± 3	20 ± 2.0	5.5 ± 0.3^{I}	1063 ± 91	25
ZrB_2 + 30SiC	97.5	3.9 ± 0.9	-	487 ± 12	24.4 ± 0.6	4.4 ± 0.5	425 ± 35^{3}	71
ZrB_2 + 30SiC	99.8	1.5 ± 1.2	-	510	27.0 ± 2.2	2.1 ± 0.1	800 ± 115	10
ZrB_2 + 30SiC	99.4	~ 3	-	-	24.0 ± 0.7	5.3 ± 0.5^{I}	1089 ± 152	15, 62
ZrB_2 + 30SiC	99.8	1.2 ± 0.4	1.0 ± 0.4	520 ± 7	20.7 ± 1.0	4.6 ± 0.1^{I}	909 ± 136	74
ZrB_2 + 30SiC	>99	10.6	1.6	541 ± 22	21.4 ± 0.6	-	1150 ± 115	75

Microstructure-mechanical property relationships for ZrB_2-based ceramics are complex. Because the size of the particulate reinforcing phase controls the strength, a uniform dispersion of SiC is required to maximize strength, even for compositions and starting particle sizes that should be below the percolation threshold for the system. The method of estimating grain size from image analysis data also affects the interpretation of microstructure-property relations. Figure 2.13 shows the flexure strength of ZrB_2-30 vol% SiC as a function of cluster size estimated using equivalent area diameter, one of the most used methods for reporting grain size. This method assumes a spherical particle, and underestimates the critical grain size for microcracking as ~3 μm (Figure 2.13). Figure 2.13 also shows flexure strength as a function of the maximum measured equivalent area diameter (EAD_{max}). Since failure occurs at the largest flaw, a measurement that reports the largest flaw size is more useful, but still may not accurately describe the behavior of the material. From Figure 2.13, below the critical grain size determined by EAD_{max}, the strength shows a linear trend with grain size, instead of the inverse square root relationship predicted by Griffith analysis.

Figure 2.14 shows flexure strength, elastic modulus, and hardness as a function of the SiC cluster size that was estimated using the maximum measured major axis from ellipses (ME_{max}) fitted to the SiC clusters. All three properties experience a sudden, discontinuous decrease at ~11.5 μm. Figure 2.15 shows typical microcracking observed in the ZrB_2-SiC composites with max SiC cluster size larger than ~11.5 μm. Below the critical grain size, the strength follows an

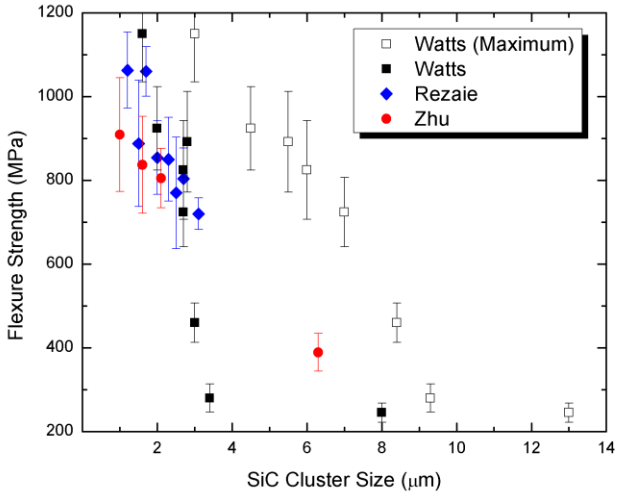

Figure 2.13. Room temperature flexure strength as a function of SiC cluster size (equivalent area diameter) for ZrB_2 – 30 vol% SiC ceramics produced by hot pressing. [25, 74, 75]

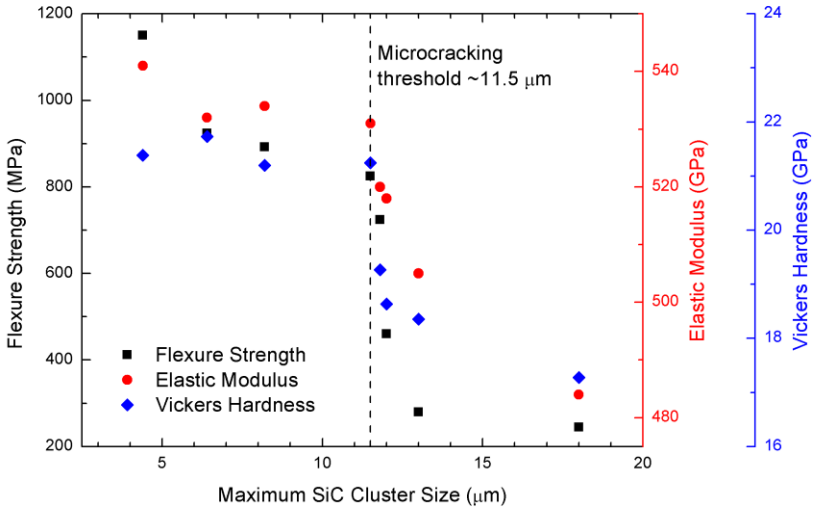

Figure 2.14. Room temperature flexure strength, elastic modulus and Vickers hardness as a function of maximum SiC cluster size (major axis of ellipse) for ZrB_2 – 30 vol% SiC ceramics prepared by hot pressing. The dashed line indicates the microcracking threshold which occurs at a SiC cluster size of ~11.5 μm.[75]

inverse square root relation with cluster size. Fitting ellipses to the clusters is preferred because it more closely resembles the morphology of the clusters. Taking this analysis even further, measuring the maximum Feret's diameter of the cluster, should more accurately correlate to the flaw size by freeing the analysis from assumptions of circularity.

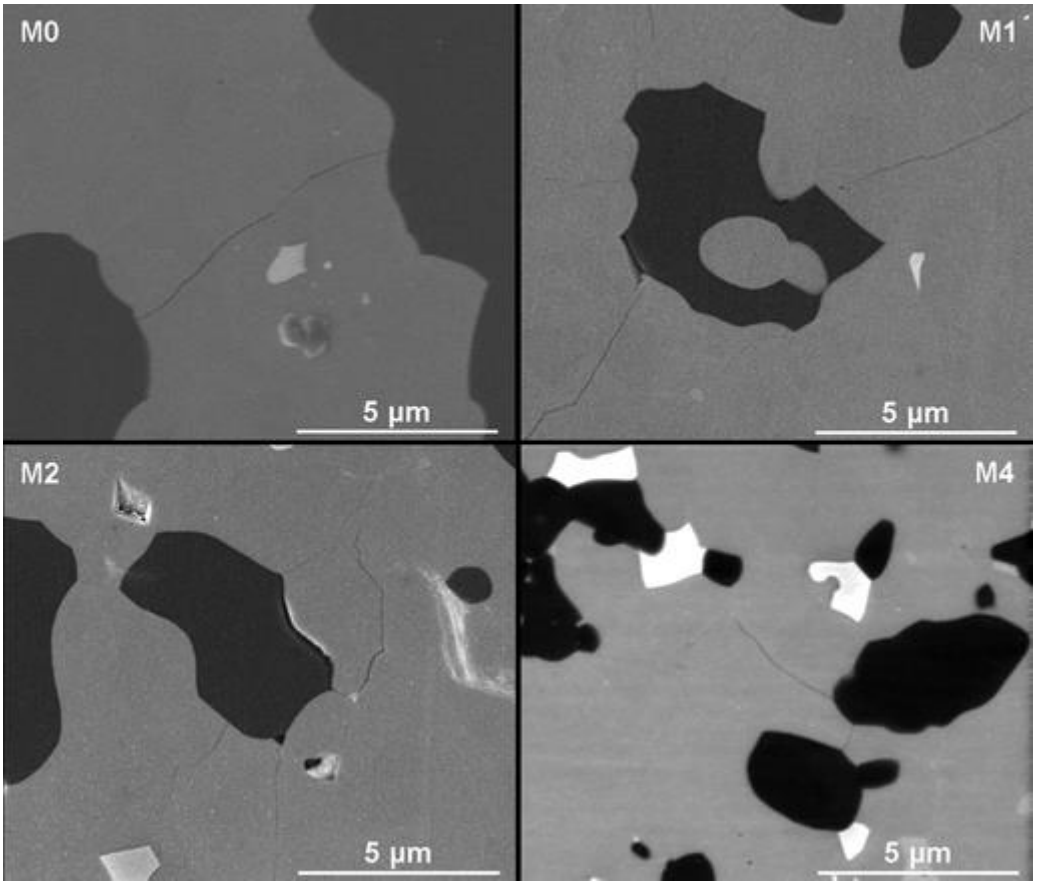

Figure 2.15. SEM micrographs of hot-pressed ZrB_2 – 30 vol% SiC showing microcracking.[75]

2.4.2.2. Effect of SiC concentration. The effect of SiC concentration on the strength of ZrB_2-SiC ceramics is shown in Figure 2.16. In general, the strength (Table 2.3) increases with SiC content. From Chamberlain et al., the strength of ZrB_2 increases from 560 to 1090 MPa with addition of up to 30 vol% SiC.[15] However, the strength is still controlled by the size of the SiC inclusions as discussed previously. Chamberlain was able to achieve high strengths through dispersion of the SiC particulate during processing. When percolation clusters begin to form, or the size of the SiC particles is large, strengths will decrease. Liu et al. produced ZrB_2-SiC ceramics using nanometer sized SiC powder.[69] They produced strengths comparable to Chamberlain, except at the level of 30 vol% additions, where SiC began to form large percolation clusters, resulting in a material with lower strength than expected based solely on the submicron SiC particle size. Zhang *et al.* produced pressurelessly sintered ZrB_2-SiC that resulted in large asymmetric SiC grains from the long isothermal holding times (3 hours) required for densification.[78] Even though Zhang achieved good dispersion of the SiC particles, the resulting SiC grain size (up to 13 μm long) was larger than the critical grain size for microcracking of ~11.5 μm, thus resulting in reduced strengths (490 MPa).

The fracture toughness of ZrB_2-SiC ceramics as a function of SiC additions is also shown in Figure 2.16. In general, fracture toughness (Table 2.3) increases with increasing SiC additions. Chamberlain reported a fracture toughness of 3.5

MPa·m^{½} for pure ZrB_2, increasing to 5.3 MPa·m^{½} for ZrB2-30 vol% SiC. Liu's work showed that toughness followed a similar trend to strength for nanosized SiC, increasing from 3.1 MPa·m^{½} for ZrB_2 to 6.8 MPa·m^{½} for 20 vol% SiC then decreasing to 5.9 MPa·m^{½} for 30 vol% SiC (along with observed formation of percolation clusters).[69] SiC additions increase the fracture toughness of ZrB_2 by increasing the tortuosity of the crack path. Figure 2.17 shows a polished and etched specimen of ZrB_2-SiC exhibiting crack bridging and crack deflection. The ZrB_2 grains typically fail by transgranular fracture, while cracks deflect at or near ZrB_2-SiC interfaces. This behavior is consistent with residual stresses resulting from CTE mismatch between SiC and ZrB_2. Further, R-curve behavior has been observed in ZrB_2-SiC, as expected based on the CTE mismatch between the phases. Kurihara et al.[79] reported falling R-curve behavior for ZrB_2 – 10 vol% SiC and Bird et al.[80] reported rising R-curve behavior for ZrB_2 – 20 vol% SiC. Further increases in fracture toughness will likely require second phase additions with higher aspect ratios, such as whiskers, rods, or platelets (discussed later), or the fabrication of laminate-type architectures.[81]

The elastic modulus of ZrB_2 with SiC (475 GPa)[82] additions follows a simple linear volumetric rule of mixtures trend (Figure 8.18). Small variations in elastic modulus from the expected values may be attributed to the impact of processing impurities on ZrB_2-SiC, such as WC from milling media or the effect of thermal residual stresses.

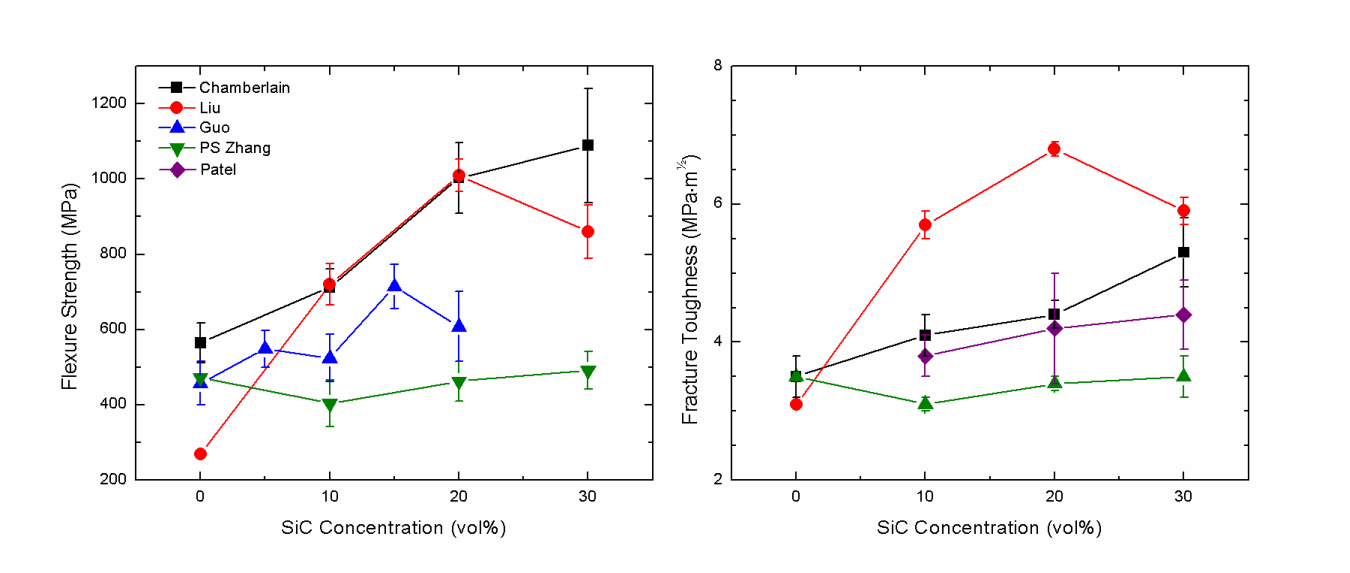

Figure 2.16. Room temperature flexure strength[15, 19, 20, 55, 69, 78] and fracture toughness[15, 19, 20, 55, 69, 71, 78] as a function of SiC concentration for ZrB_2 – SiC ceramics produced by hot pressing and pressureless sintering.

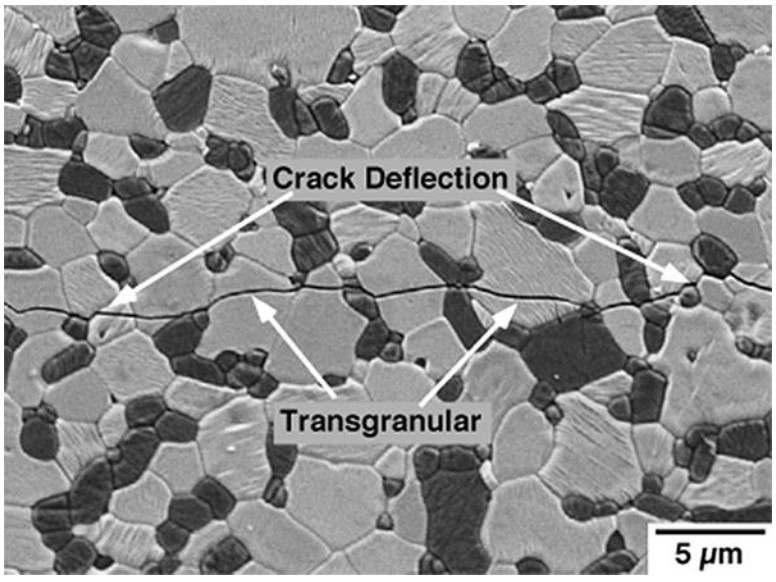

Figure 2.17. Thermally etched cross section of ZrB_2 – 30 vol% SiC. The image shows the crack path from a Vickers indent with arrows indicating predominantly transgranular fracture for the ZrB_2 grains and crack deflection near the ZrB_2-SiC interfaces. Reproduced from Fahrenholtz.[1]

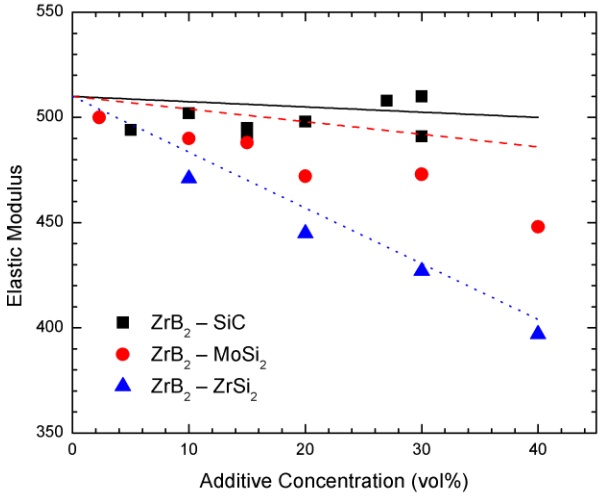

Figure 2.18. Elastic modulus as a function of additive content for selected hot pressed ZrB_2 based composites with SiC,[10, 15, 55, 57, 62, 72, 83] $MoSi_2$,[53, 84-87] and $ZrSi_2$[56] additives. Values have been corrected for porosity using a linear relationship and b = 2.0 (based on Nielsen's relationship – see Table 2.2).

Figure 2.19 shows the hardness of ZrB_2 – SiC ceramics with varying SiC content. The lines represent the expected hardness from a rule of mixtures: ZrB_2, HV = 23 GPa (upper bound) [46] and 14 GPa (lower bound); SiC, HV = 28 GPa [88, 89]. The upper (Equation 16) and lower bounds (Equation 17) were calculated using the following:

$$H_{UB} = f_a H_a + f_b H_b \tag{16}$$

$$H_{LB} = \frac{H_a H_b}{f_a H_b + f_b H_a} \tag{17}$$

where H_{UB} and H_{LB} are the composite hardnesses, H_a and H_b are the hardness of phase a and phase b, and f_a and f_b are the volume fraction of phase a and phase

b. The observed hardness values fall within the upper and lower bounds of the predicted hardness. Evaluation of the effect of SiC on hardness is made difficult by the use of various indentation loads used in the measurement of reported hardness values. However, a general trend can still be observed. Hardness increases with SiC content, from 18 GPa to 24 GPa for ZrB_2 – 10 vol% SiC to 21 GPa to 27 GPa for ZrB_2 – 30 vol% SiC. This is in agreement with the expected effect of SiC's higher hardness on the hardness of ZrB_2-SiC. The ZrB_2 and ZrB_2 – SiC ceramics produced by Chamberlain [15] are in good agreement with the predicted upper bound for ZrB_2 – SiC, and are likely a result of the well dispersed SiC phase and fine ZrB_2 and SiC grain sizes. Hardness is a structure sensitive property, thus variations in grain size and resulting thermal residual stresses can be expected to influence hardness and contribute to the observed scatter in reported hardness values.

2.4.2.3. Effect of additional phases. The effect of various additions to ZrB_2-SiC are summarized in Table 2.4. Additions are typically introduced as sintering aids that may be designed to remove surface oxide impurities, as in the case of C and B_4C, or interacting with surface oxides to form softer grain boundary phases, as in the case of Si_3N_4. ZrB_2-SiC with other additions has similar room temperature mechanical properties to ZrB_2-SiC without additions.

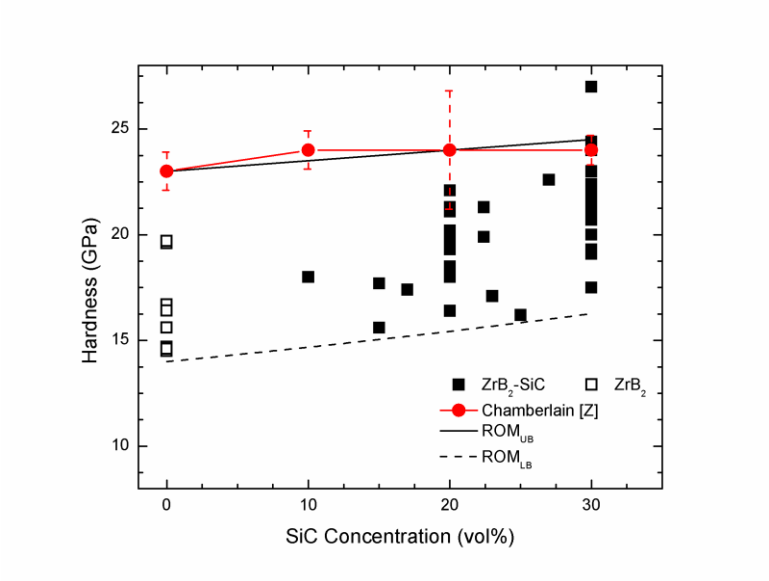

Figure 2.19. Room temperature hardness as a function of SiC concentration for ZrB_2 ceramics. Open squares represent nominally pure ZrB_2. Lines represent expected upper and lower bounds for hardness based on rule of mixtures behavior.

Nitride additions typically increase toughness by formation of a weaker grain boundary phase that increases crack bridging and deflection. Han[90] and Wang[91] observed an increased toughness for ZrB_2 – 20 vol% SiC (from ~4.2 to ~5.5 $MPa \cdot m^{1/2}$) with 5 to 10 vol% additions of aluminum nitride, while retaining a room temperature flexure strength of 830 MPa. This increase was likely due to improved densification, which resulted in a finer grain size, and the presence of weaker grain boundary phases (BN and Al_2O_3) that enhanced crack deflection.

Small additions of oxides (such as YAG[49] and La_2O_3)[58] follow a similar trend to the nitride additions with minimal improvements in toughness. This shows that small additions of nitrides and oxides can be added to ZrB_2-SiC to provide additional means of controlling densification and microstructure without adversely affecting room temperature mechanical properties.

In contrast to oxide and nitride additions, the mechanical properties of ZrB_2-SiC ceramics with ZrC (Table 2.4) typically result in mechanical properties similar to ZrB_2-SiC without ZrC additions (Table 2.3). This is most likely the result of a closer CTE match between ZrC (7.6×10^{-6} K^{-1})[98] and ZrB_2 compared to SiC and ZrB_2, resulting in the SiC phase still dominating the mechanical behavior. With ZrC additions from 5 to 30 vol%, the flexure strength (~500-750 MPa), and fracture toughness (3.5-6.5 $MPa \cdot m^{½}$) are nominally the same as ZrB_2-SiC. Similarly, it is reasonable to assume that the same microstructural controls used in ZrB_2-SiC to improve mechanical properties can be employed in the ZrB_2-SiC-ZrC system. Small additions of other carbides (C, B_4C, VC, and WC) have little effect on the mechanical properties of ZrB_2-SiC. However, these additions improve densification of ZrB_2-SiC in the same manner as when added to ZrB_2, through removal of surface oxides from the starting powders. Thus small additions of carbides can also be used to improve the room temperature mechanical properties by allowing greater control of the microstructure during sintering.

Table 2.4. Elastic modulus, Vickers hardness, fracture toughness by direct crack method, and 4-point flexure strength of ZrB_2-SiC ceramics with various additives.

Composition (vol%)	Relative density (%)	ZrB_2 Grain size (μm)	SiC Grain size (μm)	Elastic modulus (GPa)	Hardness (GPa)	Fracture toughness ($MPa \cdot m^{½}$)	Flexure strength (MPa)	Ref.
ZrB_2 + 20SiC + 1 wt% B	> 99.0	7.3 ± 0.8	3.3 ± 0.5	-	16.0 ± 0.4	-	519 ± 31[3]	92
ZrB_2 + 27SiC + 1B_4C	100	2	1	508 ± 6	22.6 ± 0.9	3.5	720 ± 140	83
ZrB_2 + 20SiC + 3wt%C + 0.5wt%B_4C	99	~ 10	~ 8	374 ± 25	14.7 ± 0.2	5.5 ± 0.5 [S]	361 ± 44[3]	68
ZrB_2 + 30SiC + 4 wt% B_4C[†] + 5 wt% C[‡]	99	2.8 ± 0.2	2 ± 0.8	511 ± 7	-	3.8 ± 0.2[I]	604 ± 69	78
ZrB_2 + 20SiC + 2 wt% La_2O_3	99.6	3.5 ± 0.4	-	-	19.3 ± 0.6	5.2 ± 0.5	600 ± 70[3]	58
ZrB_2 + 20SiC + 4Si_3N_4	98	2.4 ± 0.1	-	-	14.6 ± 0.3	-	730 ± 100[3]	49
ZrB_2 + 20SiC + 5AlN	100	3	-	-	19.4 ± 0.6	5.4 ± 0.3[S]	835 ± 26[3]	90
ZrB_2 + 20SiC + 10AlN	100	2.5	-	-	-	5.6 ± 0.5[S]	831 ± 12[3]	91
ZrB_2 + 15SiC + 4.5ZrN	99	-	-	467 ± 4	15.6 ± 0.3	5.0 ± 0.1[C]	635 ± 60	27
ZrB_2 + 20SiC + 6ZrC	99.1	~ 4	-	-	19.0 ± 0.5	6.5 ± 0.4[S]	622 ± 64[3]	93
ZrB_2 + 21SiC + 5ZrC	97.3	< 2	-	-	17.2 ± 0.8	5.2 ± 0.4	747 ± 101	94
ZrB_2 + 13SiC + 15ZrC	> 99	-	-	-	18.2	4.3	512 ± 50[3]	95
ZrB_2 + 20SiC + 10ZrC	99.8	2.7 ± 0.5	1.6 ± 0.2	-	18.1 ± 0.6	5.3	662 ± 64[3]	96
ZrB_2 + 10SiC + 30ZrC	99	2	-	474	18.8 ± 0.5	3.5 ± 0.2	723 ± 136	87
ZrB_2 + 20SiC + 5VC	> 99	1.9 ± 0.3	1.4 ± 0.3	-	15.8 ± 0.3	5.5 ± 0.5	804 ± 90[3]	97
ZrB_2 + 10HfB_2 + 15SiC	98.2	3	-	508 ±4	18.2 ± 0.5	4.1 ± 0.8	765 ± 75	72
ZrB_2 + 35HfB_2 + 15SiC + 4.5ZrN	99.5	-	-	494 ± 4	16.7 ± 0.7	4.8 ± 0.2[C]	590 ± 25	27
ZrB_2 + 9.6SiC + 28.9ZrC + 3.7Si_3N_4	99.5	2	-	450	21.1 ± 0.8	3.8 ± 0.1	510 ± 160	87
ZrB_2 + 18.5SiC + 3.7Si_3N_4 + 1Al_2O_3+ 0.5Y_2O_3	98	2.5 ± 0.1	-	421 ± 5	14.2 ± 0.6	4.6 ± 0.1	710 ± 110	49

[†]ZrB_2 basis, [‡]SiC basis

2.4.3. Zirconium Diboride With Disilicide Additions

2.4.3.1. Flexure strength. The flexure strength of ZrB_2 with additions of $ZrSi_2$, $MoSi_2$, or $TaSi_2$ is summarized in Table 2.5. Figure 2.20 shows the effect of $MoSi_2$ and $ZrSi_2$ additives on the strength of ZrB_2. Guo[56] reported strengths for ZrB_2-$ZrSi_2$ in the range of 380 to 555 MPa depending on $ZrSi_2$ content. Chamberlain[61] reported the effect of $MoSi_2$ on strength of ZrB_2, increasing from 565 MPa for ZrB_2 to 1150 MPa for 10 vol% $MoSi_2$, decreasing to ~1020 MPa for 20 vol% and 30 vol% additions of $MoSi_2$. Similarly, Guo[84] also reported the strength of ZrB_2 to increase from 460 MPa for ZrB_2[56] to between 750 and 800 MPa for 10 to 40 vol% $MoSi_2$ additions.

The strength of ZrB_2 with $MoSi_2$ additions has been reported by numerous researchers. This has resulted in a wide range of reported strengths: ZrB_2 – 10 vol% $MoSi_2$, 560 to 1150 MPa; ZrB_2 – 20 vol% $MoSi_2$, 460 to 1010 MPa; ZrB_2 – 30 vol% $MoSi_2$, 550 to 1030 MPa. These values highlight the importance of microstructure and processing control similar to the ZrB_2-SiC system. Unfortunately, microstructural effects of disilicide additions on the strength of ZrB_2 have not been thoroughly investigated. This is further complicated by the tendency of the ZrB_2–disilicide systems to form complex grain boundary phases and solid solution phases with the ZrB_2. Silvestroni et al. reported the formation of a ZrB_2 core – $(Zr,Mo)B_2$ rim structures during sintering (Figure 2.21).[104] In addition, ZrC, ZrO_2, MoB, and SiO_2 were detected in the final microstructures.

Table 2.5. Elastic modulus, Vickers hardness, fracture toughness by direct crack method, and 4-point flexure strength of ZrB_2-(Zr, Mo, Ta)Si_2 ceramics.

Composition (vol%)	Relative density (%)	ZrB_2 Grain size (μm)	$MeSi_2$ Grain size (μm)	Elastic modulus (GPa)	Hardness (GPa)	Fracture toughness ($MPa \cdot m^{½}$)	Flexure strength (MPa)	Ref.
ZrB_2 + 10$ZrSi_2$	96.6	2.3 ± 0.9	0.6 ± 0.4	432	-	3.8 ± 0.3	483 ± 22	56
ZrB_2 + 20$ZrSi_2$	99.1	2.5 ± 0.8	0.7 ± 0.6	445	-	4.4 ± 0.5	556 ± 54	56
ZrB_2 + 30$ZrSi_2$	99.8	2.6 ± 1.1	0.7 ± 0.6	427	-	4.4 ± 0.2	555 ± 42	56
ZrB_2 + 40$ZrSi_2$	99.2	2.7 ± 1.0	0.9 ± 0.7	397	-	3.9 ± 0.4	382 ± 78	56
ZrB_2 + 2.3$MoSi_2$	6.04 g/cm^3	5	-	500 ± 2	18.1 ± 0.4	3.4 ± 0.3[C]	750 ± 160	53
ZrB_2 + 5$MoSi_2$	96	2.6	-	516 ± 4	15.2 ± 1.0	2.9 ± 0.1[C]	569 ± 54	99
ZrB_2 + 10$MoSi_2$	99.7	1.9 ± 0.6	1.8 ± 0.5	490 ± 7	15.8 ± 0.7	3.7 ± 0.3	800 ± 108	84
ZrB_2 + 10$MoSi_2$	6.19 g/cm^3	~3	-	516	20.4 ± 2.2	4.1 ± 0.4[I]	1151 ± 52	61, 62
ZrB_2 + 10$MoSi_2$	99.9	-	-	-	17.5 ± 0.4	3.8 ± 0.4	560 ± 115[3]	100
ZrB_2 + 15$MoSi_2$	5.99 g/cm^3	1.9 ± 0.6	-	452 ± 4	14.7 ± 0.6	3.5 ± 0.6[C]	780 ± 87	86
ZrB_2 + 15$MoSi_2$	98.1	1.4	-	479 ± 4	16.2 ± 0.5	2.6 ± 0.3	643 ± 97	85-87
ZrB_2 + 20$MoSi_2$	99.9	-	-	-	14.9 ± 0.1	3.2 ± 0.2	680 ± 40[3]	100
ZrB_2 + 20$MoSi_2$	6.17 g/cm^3	~3	-	523	18.5 ± 2.7	3.0 ± 0.2[I]	1008 ± 137	61, 62
ZrB_2 + 20$MoSi_2$	99.8	1.6 ± 0.6	2.7 ± 0.9	472 ± 6	16.3 ± 0.9	2.8 ± 0.2	750 ± 128	84
ZrB_2 + 20$MoSi_2$	99.1	~2.5	-	489 ± 4	16.0 ± 0.4	2.3 ± 0.2	531 ± 46	85, 99, 101, 102
ZrB_2 + 30$MoSi_2$	99.7	-	-	-	14.3 ± 0.2	3.2 ± 0.3	550 ± 65[3]	100
ZrB_2 + 30$MoSi_2$	99.8	2.1 ± 0.7	2.4 ± 0.6	473 ± 3	15.4 ± 0.7	2.6 ± 0.2	757 ± 76	84
ZrB_2 + 30$MoSi_2$	6.29 g/cm^3	~3	-	494	17.7 ± 1.6	4.0 ± 0.4[I]	1031 ± 150	61, 62
ZrB_2 + 40$MoSi_2$	99.7	1.9 ± 0.7	2.6 ± 0.8	448 ± 4	13.2 ± 0.7	3.1 ± 0.3	790 ± 57	84
ZrB_2 + 15$TaSi_2$	99	2	-	444 ± 24	17.8 ± 0.5	3.8 ± 0.1[C]	840 ± 33	103

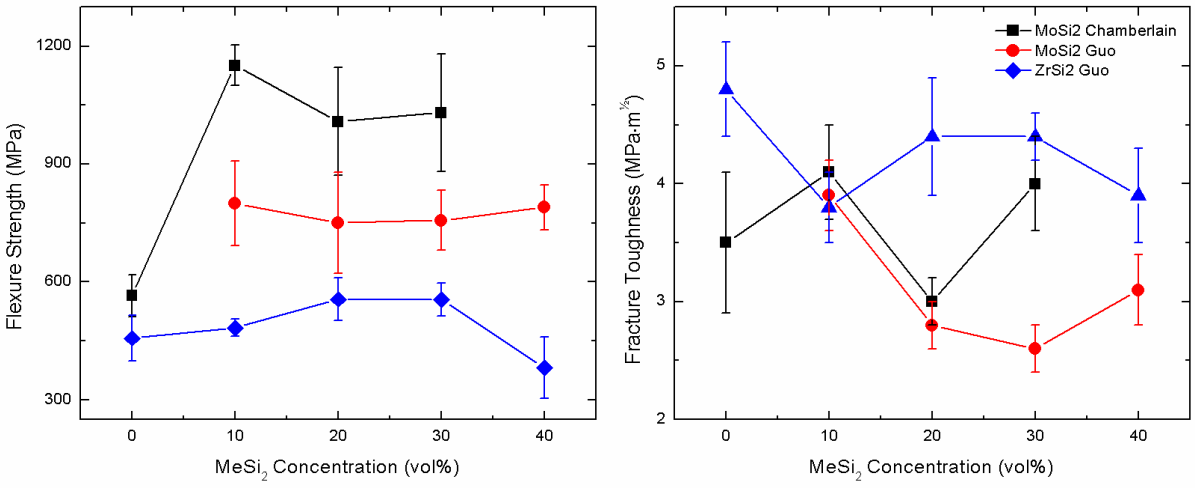

Figure 2.20. Room temperature flexure strength and fracture toughness as a function of disilicide concentration for ZrB_2 – $MeSi_2$ ceramics produced by hot pressing.[56, 61, 84]

Further, they observed various Mo-Zr-B-Si phases that may have also contained C and O, as well as the core-rim structures. These complex chemistries and architectures make analysis of microstructure–mechanical properties effects difficult. Though detailed microstructural analysis has not been performed on the other transition metal disilicide systems, similar processes presumably occur in these systems as well.

2.4.3.2. Fracture toughness. Table 2.5 shows the fracture toughness of ZrB_2 with the addition of $ZrSi_2$, $MoSi_2$, or $TaSi_2$. The effect of $ZrSi_2$ and $MoSi_2$ additions on the fracture toughness of ZrB_2 is also shown in Figure 2.20. In general, $MoSi_2$ additions result in fracture toughness values in the range of 3.2-4.0 $MPa \cdot m^{½}$. Chamberlain [61]reported indentation strength in bending (ISB) fracture toughness values of 3-4 $MPa \cdot m^{½}$ for ZrB_2-$MoSi_2$, but without a trend with

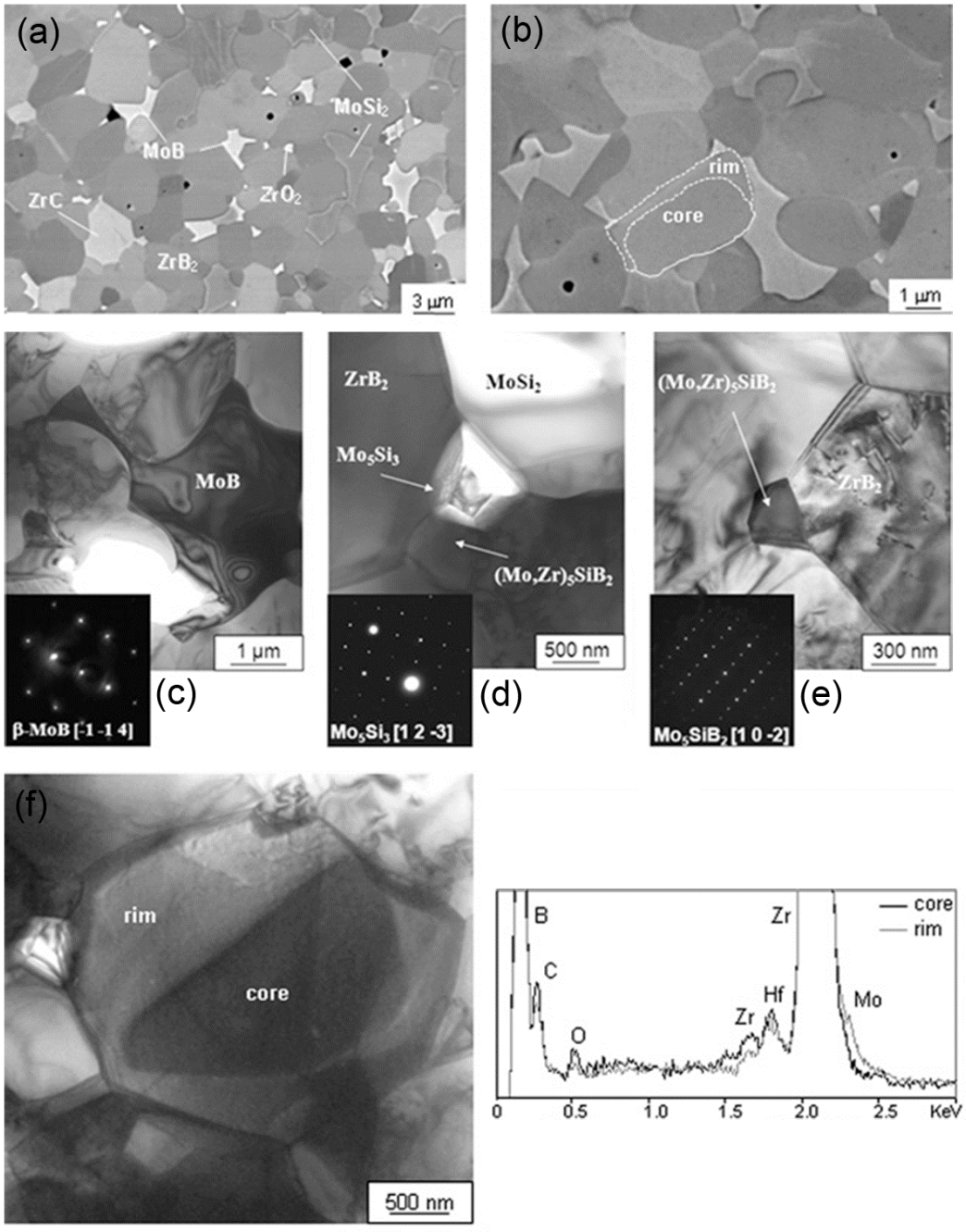

Figure 2.21. SEM images of the polished surface (a,b) and bright-field TEM images of a ZrB_2 – $MoSi_2$ composite. Note the formation of secondary phases in (a) and the core-rim substructure of ZrB_2 grains in (b). The formation of a MoB phase (c) and Mo_5Si_3 and Mo_5SiB_2 phase (d,e) at triple pockets with corresponding diffraction patterns. Morphology and corresponding EDS spectra of the core-rim structure (f). Reproduced from [104]

$MoSi_2$ content. Guo [84] measured fracture toughness of ZrB_2-$MoSi_2$ using the direct crack method (DCM) and reported values that decreased from 4.8 $MPa \cdot m^{½}$ for ZrB_2 [56] to ~2.8 $MPa \cdot m^{½}$ for additions of 20 to 40 vol% $MoSi_2$. Guo also reported DCM toughness for ZrB_2-$ZrSi_2$ as 3.8$MPa \cdot m^{½}$ for 10 vol% additions, increasing to 4.4 $MPa \cdot m^{½}$ for 20 and 30 vol% additions, and then decreasing to 3.9 $MPa \cdot m^{½}$ for 40 vol% $ZrSi_2$ additions.[56] Unlike SiC additions to ZrB_2, no trend was observed for fracture toughness with disilicide additions.

Using the Griffith criteria and a Y-parameter of 1.99 (long, semi-eliptical surface flaw), the ZrB_2-$MoSi_2$ composites produced by Chamberlain and Guo both exhibit critical flaw sizes that correlated to the observed grain sizes. For example, Chamberlain's ZrB_2 – 10 vol% $MoSi_2$ has a calculated flaw size of 3.2 μm and a reported grain size of ~3 μm. However, Guo observed that the calculated critical flaw size was much larger than the observed grain size suggesting that something other than grain size was controlling the strength of the ZrB_2-$ZrSi_2$ composites. From the microstructural analysis of polished cross-sections and fracture surfaces, Guo observed that the $ZrSi_2$ segregated to the grain boundaries during sintering, exhibiting a "string of pearls" type morphology and clustering of $ZrSi_2$ grains. Further, small amounts of porosity were observed in the $ZrSi_2$ clusters between the grains. For ZrB_2-$ZrSi_2$, the size and morphology of the $ZrSi_2$ phase controls the failure behavior of the composite.

2.4.3.3. Elastic modulus. Table 2.5 also summarizes the hardness and elastic modulus of ZrB_2 with the addition of $ZrSi_2$, $MoSi_2$, or $TaSi_2$. The effect of additive concentration on the elastic modulus of ZrB_2-$MoSi_2$ and ZrB_2-$ZrSi_2$ is

shown in Figure 2.18. The dashed lines represent the expected modulus based on linear volumetric rule of mixtures calculations assuming moduli of 510 GPa for ZrB_2, 440 GPa for $MoSi_2$,[105] and 235 GPa for $ZrSi_2$.[106] From Figure 2.18, it can be seen that the ZrB_2-$MoSi_2$ composites follow the rule of mixtures trend, but the values are consistently 10 to 20 GPa lower than expected. This is likely due to the formation of complex phases and solid solutions during densification ZrB_2-$MoSi_2$ composites. Thermal residual stresses resulting from the CTE mismatch between ZrB_2 ($\alpha_{a\text{-}axis} = 6.9 \times 10^{-6}\ K^{-1}$, $\alpha_{c\text{-}axis} = 6.7 \times 10^{-6}\ K^{-1}$)[14] and $MoSi_2$ ($\alpha_{a\text{-}axis} = 8.2 \times 10^{-6}\ K^{-1}$, $\alpha_{c\text{-}axis} = 9.4 \times 10^{-6}\ K^{-1}$)[107] may also play a role in the observed difference between the predicted and observed modulus. In the case of ZrB_2-$ZrSi_2$, the observed modulus is in good agreement with the predicted modulus. Since a tendency to form complex phases has not been observed in the ZrB_2-$ZrSi_2$ system, this likely explains why the elastic modulus of ZrB_2-$ZrSi_2$ follows predictions while ZrB_2-$MoSi_2$ has a more complex behavior.

The strength of ZrB_2 with $MoSi_2$ additions has been reported by numerous researchers. This has resulted in a wide range of strengths being reported for these materials: ZrB_2 – 10 vol% $MoSi_2$, 560 – 1150 MPa; ZrB_2 – 20 vol% $MoSi_2$, 460 – 1010 MPa; ZrB_2 – 30 vol% $MoSi_2$, 550 – 1030 MPa. This wide range of reported strength values highlights the importance of microstructure and processing control with these materials as previously discussed for the ZrB_2 – SiC system. Unfortunately, the microstructural effects of disilicide additions on the strength of ZrB_2 has not been thoroughly investigated. Further complicating this is the tendency of the ZrB_2–disilicide systems to form complex grain

boundary phases, and the tendency of the transition metal to form complex solid solution phases with the ZrB_2, creating a core-rim type structure. Silvestroni *et al*.[104] investigated the microstructural features that form during sintering of ZrB_2 – $MoSi_2$ (Figure 2.21). Their results clearly show the formation of a ZrB_2 core - $(Zr,Mo)B_2$ rim structure. The formation of ZrC, ZrO_2, MoB, and SiO_2 phases are visible in the final microstructure. Further, they show the formation of various Mo-Zr-B-Si phases, with EDS also identifying the presence of C and O in these phases, as well as the core-rim structures. These complex chemistries and architectures make analysis of microstructure–mechanical properties effects difficult. Though similar analysis has not been performed as extensively on the other transition metal disilicide systems, it is reasonable to assume similar processes occurring in these other systems.

2.5. ELEVATED TEMPERATURE MECHANICAL PROPERTIES

While several studies have reported elevated temperature mechanical properties of ZrB_2 ceramics, most have only reported a single property (i.e., strength) for a limited number of temperatures and have not provided a systematic evaluation of the effects of temperature on mechanical behavior. The following discussion highlights studies of the elevated temperature elastic modulus, strength, and fracture toughness of various zirconium diboride based UHTCs.

2.5.1. Elastic modulus. The elevated temperature elastic modulus of hot pressed ZrB_2 with and without additives is shown in Figure 2.22. Only limited data on elastic behavior of ZrB_2 have been published for elevated temperatures. Okamoto et al. reported elastic modulus from single crystal values as being 525 GPa at room temperature, decreasing linearly to 490 GPa at 1100°C.[14] Experimental results of bulk ZrB_2 have resulted in lower values of elastic modulus than those reported by Okamoto. The historical work of Rhodes et al. provided the only reported values for the elastic modulus of bulk ZrB_2 tested in inert atmosphere.[23] A modern study by Zhu et al. and was conducted in air, and thus is affected by the formation of an oxide scale on the test articles.[48] Regardless, the elastic modulus of bulk ZrB_2 decreased more rapidly than expected based on single crystal measurements presumably due to a grain boundary effect. The modulus decreased linearly from room temperature to ~1200°C (450 GPa). Above this temperature, the elastic modulus decreased more rapidly with temperature. The change in slope was thought to be a result of softening of grain boundary phases combined with the activation of grain boundary sliding and diffusional creep mechanisms.[23, 48, 108] Reported modulus values were similar up to 1600°C (250 MPa), despite the differences in testing methods. To date, Rhodes is the only study to report the modulus above 1600°C, where it decreases to 100 GPa at 2000°C.

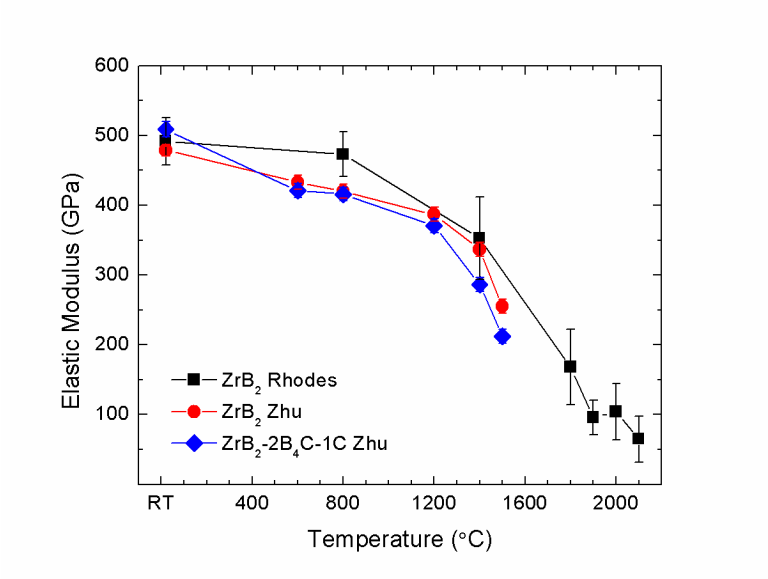

Figure 2.22. Elevated temperature elastic modulus of hot pressed ZrB_2 with and without additives.[23, 48]

The elevated temperature elastic modulus of ZrB_2-SiC ceramics is shown in Figure 2.23. Rhodes observed a steady decrease in modulus from 530 GPa at room temperature to 420 GPa at 1400°C.[23] Above 1400°C, the modulus decreased dramatically to ~100 GPa at 1600°C. As with ZrB_2, the changes in slope of the elastic modulus are likely the result of softening of grain boundary phases, as well as grain boundary sliding and diffusional creep. In ZrB_2-SiC, the softening was expected to occur at a lower temperatures to the presence of SiO_2 (surface oxide impurity from SiC) and its interaction with the B_2O_3 and ZrO_2 present from the ZrB_2. Zou et al. measured the internal damping in ZrB_2-SiC prepared by milling with Si_3N_4 balls, and found that the damping peaks just above 800°C and again around 1400°C.[108] The reduction in modulus with temperature

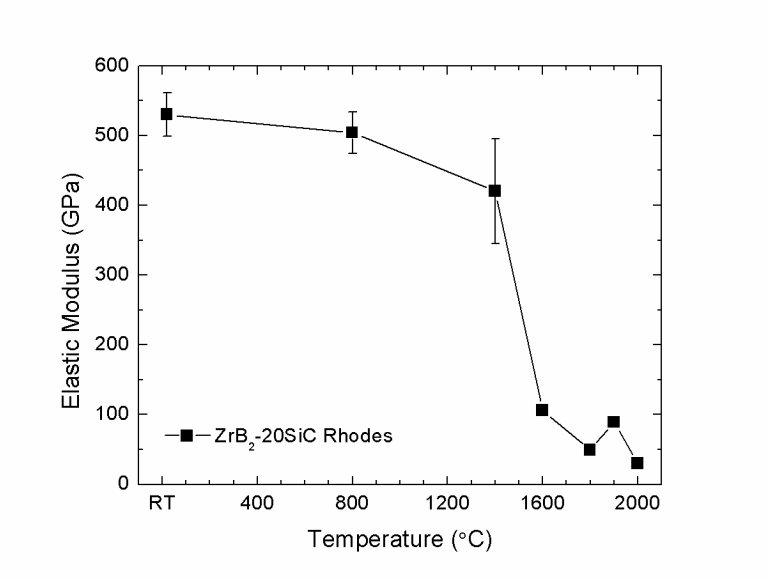

Figure 2.23. Elevated temperature elastic modulus of hot pressed ZrB_2 – SiC with and without additives.[23]

for ZrB_2-SiC ceramics is enhanced by the presence of oxides at the grain boundaries and triple junctions as well as the polycrystalline nature of the material.

2.5.2. Strength Of Zirconium Diboride. The elevated temperature 4-point flexure strength of ZrB2 with and without additives is shown in Figure 2.24. In the historical study of Rhodes, a room temperature strength of 325 MPa was measured for fully dense ZrB2 with a ~20 µm grain size.23 Strength increased between room temperature and 800°C (420 MPa), as a result of relief of thermal residual stresses. Strength decreased to 145 MPa at 1400°C, increased to 200 MPa at 1900°C, and then decreased to 50 MPa at 2200°C. The observed increase in strength from 1400°C to 1900°C was thought to be caused by stress relief during testing through plastic flow, arising from diffusional creep. A general trend was observed that finer grain size, and lower porosity resulted in improved

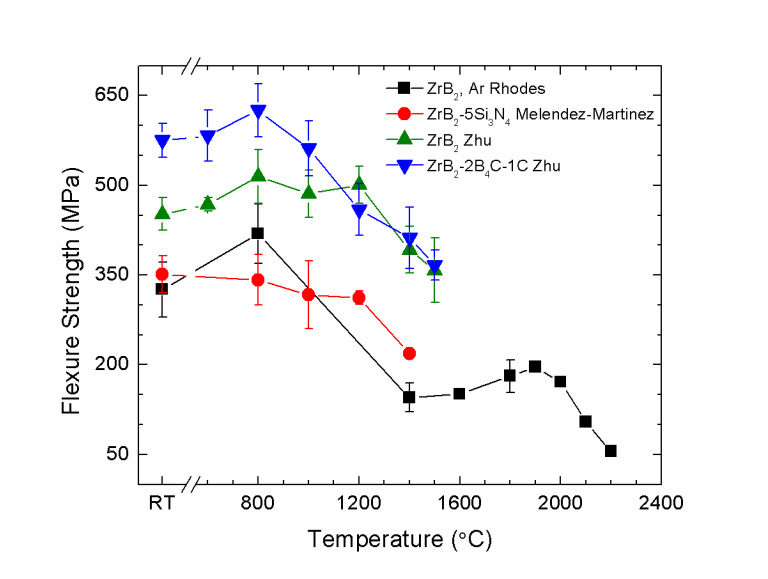

Figure 2.24. Elevated temperature flexure strength of selected hot pressed ZrB_2 ceramics with and without additives in air and argon.[24, 28, 48, 49]

elevated temperature strength, which was offset by enhanced creep in the finer grained material. Similar results have been observed in other structural ceramic systems such as SiC, ZrO2, Al2O3, and Si3N4.

Since the historical work of Rhodes, several modern studies have investigated the strength of ZrB_2 at elevated temperatures. Melendez-Martinez et al. measured the flexure strength of an 87% dense ZrB_2 (350 MPa at room temperature) up to 1400°C in air (220 MPa).[24] Zhu produced dense ZrB_2 and ZrB_2 – 2wt% B_4C – 1wt% C with grain sizes of 8.1 and 2.5 µm, respectively.[48] At room temperature, the ZrB_2 had a strength of 450 MPa compared to 575 MPa for ZrB_2-B_4C-SiC. The ZrB_2 strength increased up to 1200°C (500 MPa) before decreasing to 360 MPa at 1500°C. The strength of ZrB_2-B_4C-C increased to 630 MPa at 800°C, then steadily decreased to 370 MPa at 1500°C. Zhu performed

his testing in air, and even though he used a protective SiO_2 coating, the strength above 1200°C was likely controlled by flaws induced by oxidation damage.

2.5.3. Strength Of Zirconium Diboride – Silicon Carbide. The elevated temperature flexure strength of several hot pressed ZrB_2-SiC ceramics with and without additives is shown in Figure 2.25. The ZrB_2 – 20 vol% SiC studied by Rhodes exhibited an increase in strength from 390 MPa at room temperature to 420 MPa at 800°C.[23] The strength, steadily decreased to 245 MPa at 1800°C and decreased more rapidly to 115 MPa at 2000°C. Modern ZrB_2-SiC exhibited higher strengths at room and elevated temperature compared to Rhodes' material and similarly for all temperatures measured thus far. Zou et al. have reported the three-point bend strengths at elevated temperature for several compositions up to 1600°C in argon.[108, 111] Zou reported a strength of 550 MPa for ZrB_2 – 20 vol% SiC at room temperature, increasing to 680 MPa at 1000°C, then steadily decreasing to 460 MPa at 1600°C. Zou added 5 vol% WC, which resulted in a room temperature strength of 605 MPa that steadily increased to 675 MPa at 1600°C. Interestingly, the composition ZrB_2-20SiC-5ZrC (not shown) exhibited a room temperature strength of 1100 MPa, only slightly decreasing to 1020 MPa at 1000°C. Increasing temperatures resulted in a steep decrease in strength to 320 MPa at 1600°C. Grigoriev measured the strength of a ZrB_2 – 19 vol% SiC composite in air, reporting a room temperature strength of 500 MPa that was maintained up to 1200°C, decreasing to 430 MPa at 1400°C.[54] Not only do the room temperature strengths vary widely for ZrB_2-SiC, but the change in strength with temperature also varies.

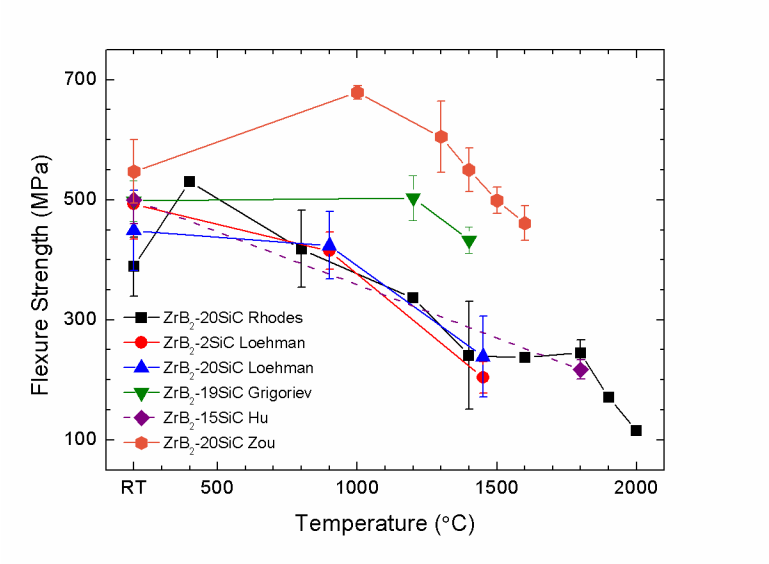

Figure 2.25. Elevated temperature flexure strength of selected hot pressed ZrB_2 – SiC ceramics with and without additives in argon.[23, 54, 108-110]

Zou showed that the addition of WC to ZrB_2-20SiC resulted in a finer ZrB_2 and SiC grain sizes plus enhanced removal of surface oxides from the starting powders. Reducing the amount of low melting point oxides present at the grain boundaries should result in a higher stiffness at elevated temperatures, thus also improving strength and resistance to creep. Similarly, the increase in strength for ZrB_2-20SiC-5ZrC at room temperature was attributed to grain refinement. The steep drop in strength at elevated temperatures was attributed to the softening of residual oxides present at grain boundaries, since no favorable reactions with the surface oxides or ZrC were identified up to the sintering temperature. Further, creep was observed in the material during testing at 1600°C. Hence, the presence of oxide impurities reduces strength and increases creep at elevated temperatures.

Figure 2.26 also shows the elevated temperature flexure strengths of some ZrB_2-SiC ceramics with various additives. Rhodes added graphitic carbon to ZrB_2-SiC to improve the thermal shock resistance. The strength increased from 520 MPa at room temperature to 640 MPa at 600°C in argon and then steadily decreased to 260 MPa at 1800°C. Monteverde added 4 vol% Si_3N_4 as a sintering aid to ZrB_2-20 vol% SiC.[49] The strength decreased from 730 MPa at room temperature to 250 MPa at 1200°C due to formation of various phases containing Zr, Si, and/or B with O and/or N at the grain boundaries and triple junctions. These phases begin to soften at temperatures as low as 800°C, leading to strength degradation with increasing temperatures. Bellosi measured the strength of a ZrB_2-10SiC-30ZrC composite in argon, showing a room temperature strength of 720 MPa which steadily decreased to 420 MPa at 1500°C.[87] The decline in strength between 1200°C and 1500°C was similar to the decline observed by Zou over a similar temperature range. Grigoriev made additions of 4 vol% and 7 vol% $ZrSi_2$ to ZrB_2-18SiC and ZrB_2-17SiC. In the case of the 4% addition, a strength of ~480 MPa was maintained up to 1200°C, before decreasing to 230 MPa. Adding 7 vol% $ZrSi_2$ resulted in a decrease in strength from 400 MPa at room temperature to ~230 MPa at 1200°C and 1400°C. Grigoriev did not speculate as to the effect of $ZrSi_2$ on the response of strength at elevated temperatures, but it is likely due to the relatively low melting point of $ZrSi_2$ of 1620°C and the formation of complex phases at the grain boundaries and triple junctions as seen with in ZrB_2-$MoSi_2$, as discussed below.

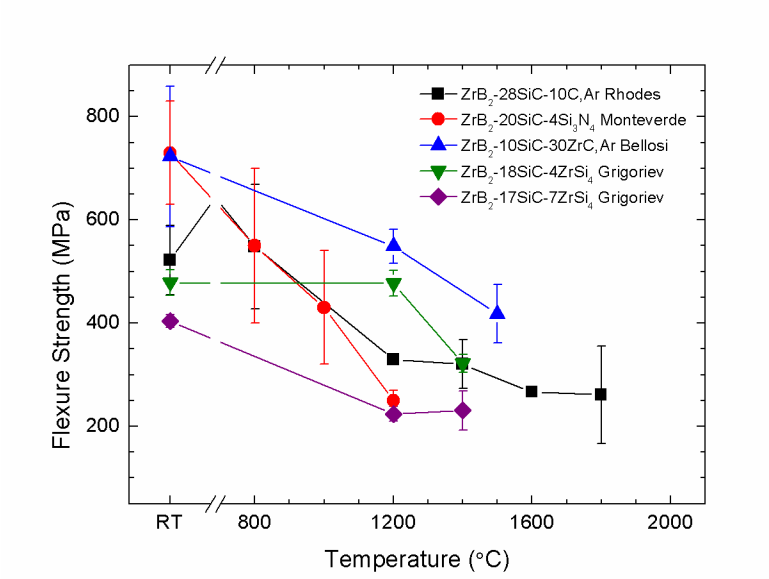

Figure 2.26. Elevated temperature flexure strength of selected hot pressed ZrB_2 – SiC ceramics with various additives in argon.[23, 49, 54, 87]

2.5.4. Strength Of Zirconium Diboride With Molybdenum And Tantalum Disilicide.

Figure 2.27 shows the four-point flexure strengths at elevated temperatures in air for several ZrB_2 ceramics containing $MoSi_2$ or $TaSi_2$. ZrB_2 – 20 vol% SiC prepared by Rhodes is included as a comparison. Silvestroni measured the strength of a pressurelessly sintered ZrB_2 – 5 vol% $MoSi_2$ ceramic, finding that the strength decreased only slightly from 570 MPa at room temperature to 490 MPa at 1500°C.[99] Bellosi reported properties for a spark plasma sintered ZrB_2-15$MoSi_2$ ceramic, finding that the strength remained ~635 MPa from room temperature up to 1200°C, before decreasing to 360 MPa at 1600°C.[87] In a follow up study, Balbo and Sciti reported similar results for a hot pressed material of the same composition, speculating that the decrease in strength at 1500°C was the result of softening of silicate phases present in the material.[86] Sciti et al. also measured the strength of pressurelessly sintered ZrB_2

– 20 vol% $MoSi_2$ ceramics, in this case observing an increase in strength from 530 MPa at room temperature to 655 MPa at 1200°C, declining to 500 MPa at 1500°C.[101] They attributed the increase in strength at 1200°C to healing of surface flaws due to formation of an oxide scale. Sciti et al. also investigate the properties of hot pressed ZrB_2-$TaSi_2$, reporting a strength of 840 MPa at room temperature that decreased to 375 MPa at 1500°C.[103] This strength was slightly higher than they observed for a comparably processed ZrB_2 – 15 vol% $MoSi_2$ (705 MPa at room temperature, 335 MPa at 1500°C), but the strength followed a similar trend. The increased strength of ZrB_2 – $TaSi_2$ was likely a result of the observed increase in fracture toughness between the $MoSi_2$ and $TaSi_2$ containing composites, but no further speculation was offered by the authors.

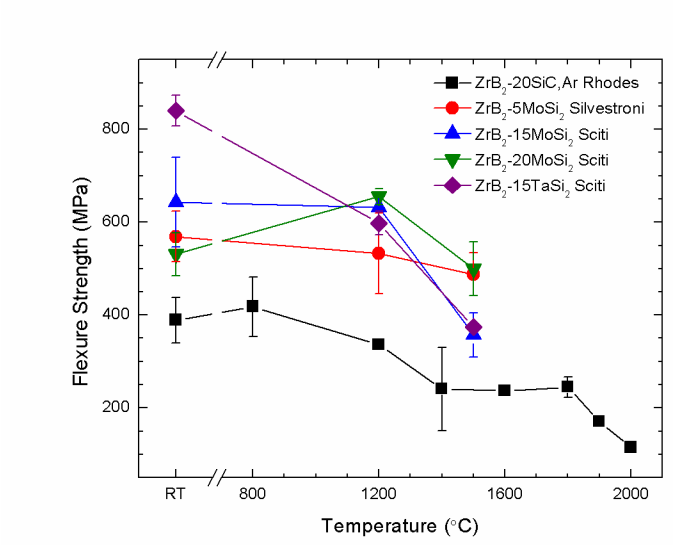

Figure 2.27. Elevated temperature four-point flexure strength of selected ZrB_2 – $MeSi_2$ ceramics in air.[23, 85-87, 99, 102, 103]

The ZrB_2 – transition metal disilicide systems show promise for their retention of strength at elevated temperatures. Unfortunately, few data are available for these systems above 1500°C. In addition, no elastic properties or fracture toughness behavior have been reported at elevated temperatures.

2.5.5. Fracture Toughness. Limited fracture toughness measurements have been reported for ZrB_2 ceramics at elevated temperatures. Kalish et al. reported an increase in the amount of transgranular fracture in ZrB_2 from ~20% at room temperature up to ~60% at 1000°C.[112] The amount of transgranular fracture then decreased to ~10% at 1200°C and 1400°C. Similarly, Bird et al. observed an increase in the amount of intergranular fracture in ZrB_2-20 vol% SiC from ~5% at room temperature to ~95% at 1400°C.[80] The amount of intergranular fracture increased between 800°C and 1000°C. The increase in the amount of intergranular fracture with temperature corresponded to an increase in the observed plateau in toughness (study reported K_R curves from DCB testing), which increased from ~2.8 MPa·$m^{½}$ at room temperature to ~5.8 MPa·$m^{½}$ at 1400°C.

References

1. W. G. Fahrenholtz, G. E. Hilmas, I. G. Talmy, and J. A. Zaykoski, "Refractory Diborides of Zirconium and Hafnium," *J. Am. Ceram. Soc.,* **95** [5] 1347-64 (2007).

2. M. Rahman, C. C. Wamg, W. Chen, S. A. Akbar, and C. Mroz, "Electrical Resistivity of Titanium Diboride and Zirconium Diboride," *J. Am. Ceram. Soc.,* **78** [5] 1380-82 (1995).

3. J. W. Zimmerman, G. E. Hilmas, W. G. Fahrenholtz, R. B. Dinwiddie, W. D. Porter, and H. Wang, "Thermophysical Properties of ZrB_2 and ZrB_2-SiC Ceramics," *J. Am. Ceram. Soc.,* **91** [5] 1405-11 (2008).

4. S. K. Mishra, S. K. Das, and P. Ramachandrarao, "Sintering Studies on Ultrafin ZrB_2 Powder Produced by a Self-propagating High-temperature Synthesis Process," *J. Mater. Res.,* **15** [11] 2499-504 (2000).

5. K. Kuwabara, S. Skamoto, O. Kida, T. Ishino, T. Kodama, T. Nakajima, T. Ito, and Y. Hirakawa, "Corrosion Ressistance and Electrical Resistivity of ZrB_2 Monolithic Refractories," *The Proceedings of UNITECT 2003,* The 8^{th} Biennial Worldwide Conference on Refractories (2003).

6. N. Kaji, H. Shikano, and I. Tanaka, "Developement of ZrB_2-Graphite Protective Sleeve for Submerged Nozzle," *Taikabutsu Overseas,* **14** [2] 39-43 (1992).

7. Z. J. Jin, M. Zhang, D. M. Guo, and R. K. Kang, "Electroforming of Copper/ZrB_2 Composite Coating and Performance as Eltron-Discharge Machining Electrodes," *Key Eng. Mater.,* **291-292** 537-42 (2005).

8. J. Sung, D. M. Goedde, G. S. Girolami, and J. R. Abelson, "Remote-plasma Chemical Vapor Deposition of Conformal ZrB_2 Films at Low Temperature: A Promissing Diffusion Barrier for ltralarge Scale Integrated Electronics," *J. Appl. Phys.,* **91** [6] 3904-11 (2002).

9. Y. Murata, "Cutting Tool Tips and Ceramics Containing Hafnium Nitride and Zirconium Diboride." in., U. S., 1970.

10. A. L. Chamberlain, W. G. Fahrenholtz, and G. E. Hilmas, "Low-Temperature Densification of Zirconium Diboride Ceramics by Reactive Hot Pressing," *J. Am. Ceram. Soc.,* **89** [12] 6368-75 (2006).

11. M. M. Opeka, I. G. Talmy, and J. A. Zaykoski, "Oxidation-based Materials Selection for 2000°C + Hypersonice Aerosurfaces: Theoretical Considerations and Historical Experience," *J. Mater. Sci.,* **39** [19] 5887-904 (2004).

12. P. Vajeeston, P. Ravindran, C. Ravi, and R. Asokamani, "Electronic structure, bonding, and ground-state properties of AlB_2-type transition-metal diborides," *Phys, Rev. B,* **63** [4] 045115 (2001).

13. Y. Xuan, C.-H. Chen, and S. Otani, "High temperature microhardness of ZrB_2 single crystals," *J. Phys. D: Appl. Phys.,* **35** [20] L98 (2002).

14. N. L. Okamoto, M. Kusakari, K. Tanaka, H. Inui, M. Yamaguchi, and S. Otani, "Temperature Dependence of of Thermal Expansion and Elastic Constants of Single Crystals of ZrB_2 and the Suitability of ZrB_2 as a Substrate for GaN Film," *J. Appl. Phys.,* **93** [1] 88-93 (2003).

15. A. L. Chamberlain, W. G. Fahrenholtz, and G. E. Hilmas, "High-Strength Zirconium Diboride-Based Ceramics," *J. Am. Ceram. Soc.,* **87** [6] 1170-72 (2004).

16. A. L. Chamberlain, W. G. Fahrenholtz, and G. E. Hilmas, "Pressureless Sintering of Zirconium Diboride," *J. Eur. Ceram. Soc.,* **89** [2] 450-56 (2006).

17. W. G. Fahrenholtz, "The ZrB_2 Volatility Diagram," *J. Am. Ceram. Soc.,* **88** [12] 3509-12 (2005).

18. S. C. Zhang, G. E. Hilmas, and W. G. Fahrenholtz, "Pressureless Densification of Zirconium Diboride with Boron Carbide Additions," *J. Am. Ceram. Soc.,* **89** [5] 1544-50 (2006).

19. W. G. Fahrenholtz, G. E. Hilmas, S. C. Zhang, and S. Zhu, "Pressureless Sintering of Zirconium Diboride: Particle Size and Additive Effects," *J. Am. Ceram. Soc.,* **91** [5] 1398-404 (2007).

20. S. Zhu, W. G. Fahrenholtz, G. E. Hilmas, and S. C. Zhang, "Pressureless Sintering of Zirconium Diboride Using Boron Carbide and Carbon Additions," *J. Am. Ceram. Soc.,* **90** [11] 3660-63 (2007).

21. S. Zhu, W. G. Fahrenholtz, G. E. Hilmas, and S. C. Zhang, "Pressureless Sintering of Carbon-coated Zirconium Diboride Powders," *Materials Science and Engineering: A,* **459** [1–2] 167-71 (2007).

22. G. J. K. Harrington, G. E. Hilmas, and W. G. Fahrenholtz, "Effect of Carbon and Oxygen on the Densification and Microstructure of Hot Pressed Zirconium Diboride," *J. Am. Ceram. Soc.* (Accepted - In Press).

23. W. H. Rhodes, E. V. Clougherty, and D. Kalish, "Research and Development of Refractory Oxidation-Resistant Diborides Part II, Volume IV: Mechanical Properties." AFML-TR-68-190, Part II, Volume IV. ManLabs Incorporated and Avco Corporation, Wright Patterson Air Forse Base, OH, 1970.

24. J. J. Melendez-Martinez, A. Dominguez-Rodriguez, F. Monteverde, C. Melandri, and G. d. Portu, "Characterization and High Temperature Mechanical Properties of Zirconium Boride-based Materials," *J. Eur. Ceram. Soc.,* **22** 2543-49 (2002).

25. A. Rezaie, W. G. Fahrenholtz, and G. E. Hilmas, "Effect of Hot Pressing Time and Temperature on the Microstructure and Mechanical Properties of ZrB_2-SiC," *J. Mater. Sci.,* **42** [8] 2735-44 (2007).

26. S. C. Zhang, G. E. Hilmas, and W. G. Fahrenholtz, "Pressureless Sintering of ZrB_2–SiC Ceramics," *J. Am. Ceram. Soc.,* **91** [1] 26-32 (2008).

27. F. Monteverde and A. Bellosi, "Development and Characterization of Metal-Diboride-Based Composites Toughened with Ultra-Fine SiC Particulates," *Solid State Sci.,* **7** [5] 622-30 (2005).

28. F. Monteverde, "Beneficial Effects of an Ulta-fine α-SiC Incorporation on the Sinterability and Mechanical Properties of ZrB_2," *Appl. Phys. A,* **82** 329-37 (2006).

29. V. M. Gropyanov and L. M. Bel'tyukova, "Sintering and Recrystallization of ZrC-ZrB_2 Compacts," *Powder Metall Met Ceram,* **7** [7] 527-33 (1968).

30. R. A. Andrievskii, L. A. Korolev, V. V. Klimenko, A. G. Lanin, I. I. Spivak, and I. L. Taubin, "Effect of Zirconium Carbide and Carbon Additions on Some Physicomechanical Properties of Zirconium Diboride," *Powder Metall Met Ceram,* **19** [2] 93-94 (1980).

31. S. M. Kats, S. S. Ordan'yan, and V. I. Unrod, "Compressive Creep of Alloys of the ZrC-ZrB_2 and TiC-TiB_2 Systems," *Powder Metall Met Ceram,* **20** [12] 886-90 (1981).

32. T. Tsuchida and S. Yamamoto, "Spark Plasma Sintering of ZrB_2–ZrC Powder Mixtures Synthesized by MA-SHS in Air," *J. Mater. Sci.,* **42** [3] 772-78 (2007).

33. A. K. Kuriakose and J. L. Margrave, "The Oxidation Kinetics of Zirconium Diboride and Zirconium Carbide at High Temperatures," *J. Electrochem. Soc.,* **111** [7] 827-31 (1964).

34. W. C. Tripp and H. C. Graham, "Thermogravimetric Study of the Oxidation of ZrB_2 in the Temperature Range of 800° to 1500°C," *J. Electrochem. Soc.,* **118** [7] 1195-99 (1971).

35. F. Monteverde and A. Bellosi "Oxidation of ZrB_2-Based Ceramics in Dry Air," *J. Electrochem. Soc.,* **150** [11] B552-B59 (2003).

36. T. A. Parthasarathy, R. A. Rapp, M. Opeka, and R. J. Kerans, "A model for the oxidation of ZrB_2, HfB_2 and TiB_2," *Acta Mater.,* **55** [17] 5999-6010 (2007).

37. A. Rezaie, W. G. Fahrenholtz, and G. E. Hilmas, "Evolution of Structure During the Oxidation of Zirconium Diboride-Silicon Carbide up to 1500°C," *J. Eur. Ceram. Soc.,* **27** 2495-501 (2007).

38. A. H. Heuer and V. L. K. Lou, "Volatility Diagrams for Silica, Silicon Nitride, and Silicon Carbide and Their Application to High-Temperature Decomposition and Oxidation," *J. Am. Ceram. Soc.,* **73** [10] 2789-803 (1990).

39. W. G. Fahrenholtz, "Thermodynamic Analysis of ZrB_2-SiC Oxidation: Formation of a SiC-Depeleted Region," *J. Am. Ceram. Soc.,* **90** [1] 143-8 (2007).

40. E. A. Dean and J. A. Lopez, "Empirical Dependence of Elastic Moduli on Porosity for Ceramic Materials," *J. Am. Ceram. Soc.,* **66** [5] 366-70 (1983).

41. R. M. Spriggs, "Expression for Effect of Porosity on Elastic Modulus of Polycrystalline Refractory Materials, Particularly Aluminum Oxide," *J. Am. Ceram. Soc.,* **44** [12] 628-29 (1961).

42. L. F. Nielsen, "Elastic Properties of Two-phase Materials," *Mater. Sci. Eng.,* **52** [1] 39 (1982).

43. L. F. Nielsen, "Elasticity and Damping of Porous Materials," *J. Am. Ceram. Soc.,* **67** [2] 93-98 (1984).

44. D. E. Wiley, W. R. Manning, and O. Hunter Jr, "Elastic Properties of Polycrystalline TiB_2, ZrB_2 and HfB_2 from room temperature to 1300° K," *J. Less-Common Metals,* **18** [2] 149-57 (1969).

45. R. A. Cutler, "Engineering Properties of Borides," pp. 787-803 in *Ceramics and Glasses: Engineered Materials Handbook,* Vol. 4, Edited by S. J. S. Schneider Jr. ASM International, Materials Park, OH, 1991.

46. X. Zhang, X. Luo, J. Han, J. Li, and W. Han, "Electronic Structure, Elasticity and Hardness of Diborides of Zirconium and Hafnium: First Principles Calculations," *Computational Materials Science,* **44** [2] 411-21 (2008).

47. N. L. Okamoto, M. Kusakari, K. Tanaka, H. Inui, and S. Otani, "Anisotropic Elastic Constants and Thermal Expansivities in Monocrystal CrB_2, TiB_2, and ZrB_2," *Acta Mater.,* **58** [1] 76-84 (2010).

48. S. Zhu, "Densification, Microstructure, and Mechanical Properties of Zirconium Diboride Based Ultra-High Temperature Ceramics," Ph. D. Thesis. Missouri University of Science and Technology, Rolla, MO, 2008.

49. F. Monteverde, S. Guicciardi, and A. Bellosi, "Advances in Microstructure and Mechanical Properties of Zirconium Diboride Based Ceramics," *Mater. Sci. Eng., A,* **346** 310-19 (2003).

50. F. Monteverde and A. Bellosi, "Beneficial Effects of AlN as Sintering Aid on Microstructure and Mechanical Properties of Hot-Pressed ZrB_2," *Adv. Eng. Mater.,* **5** [7] 508-12 (2003).

51. J. B. Wachtman, *Mechanical Properties of Ceramics*. John Wiley & Sons, Inc.: New York, NY, (1996).

52. R. A. Cutler, "Engineering Properties of Borides," pp. 787-803 in *Ceramics and Glasses, Engineered Materials Handbook,* Vol. 4, Edited by S. J. Schneider. ASM International, Materials Park, OH, 1991.

53. F. Monteverde, "The Addition of SiC Particles Into a $MoSi_2$-doped ZrB_2 Matrix: Effects on Densification, Microstructure and Thermo-physical Properties," *Mater. Chem. Phys.,* **113** 626-33 (2009).

54. O. N. Grigoriev, B. A. Galanov, V. A. Kotenko, S. M. Ivanov, A. V. Koroteev, and N. P. Brodnikovsky, "Mechanical Properties of ZrB_2-SiC($ZrSi_2$) Ceramics," *J. Eur. Ceram. Soc.,* **30** 2173-81 (2010).

55. S. Q. Guo, J. M. Yang, H. Tanaka, and Y. Kagawa, "Effect of Thermal Exposure on Strength of ZrB_2-based Composites with Nano-Sized SiC Particles," *Compos. Sci. Technol.,* **68** 3033-40 (2008).

56. S. Q. Guo, Y. Kagawa, and T. Nishimura, "Mechanical Behavior of Two-Step Hot-Pressed ZrB_2-Based Composites with $ZrSi_2$," *J. Eur. Ceram. Soc.,* **29** 787-94 (2009).

57. S. Q. Guo, "Densification of ZrB_2-based Composites and Their Mechanical and Physical Properties: A Review," *J. Eur. Ceram. Soc.,* **29** 995-1011 (2009).

58. E. Zapata-Solvas, D. D. Jayaseelan, P. B. H. T. Lin, and W. E. Lee, "Mechanical Properties of ZrB_2- and HfB_2-Based Ultra-High Temperature Ceramics Fabricated by Spark Plasma Sintering," *J. Eur. Ceram. Soc.,* **33** [7] 1373-86 (2013).

59. S. Guo, T. Nishimura, and Y. Kagawa, "Preparation of Zirconium Diboride Ceramics by Reactive Spark Plasma Sintering of Zirconium Hydride-Boron Powders," *Scripta Mater.,* **65** 1018-21 (2011).

60. I. G. Talmy, J. A. Zaykoski, M. M. Opeka, and A. H. Smith, "Properties of Ceramics in the System ZrB_2-Ta_5Si_3," *J. Mater. Res.,* **21** [10] 2593-99 (2006).

61. A. L. Chamberlain, W. G. Fahrenholtz, G. E. Hilmas, and D. T. Ellerby, "Characterization of Zirconium Diboride-Molybdenum Disilicide Ceramics," pp. 299-308 in *Advances in Ceramic Matrix Composites IX*, Edited by N. P. Bansal, J. P. Singh, W. M. Kriven, and H. Schneider. The American Ceramic Society, Westerville, OH, 2003.

62. A. L. Chamberlain, W. G. Fahrenholtz, G. E. Hilmas, and D. T. Ellerby, "Characterization of Zirconium Diboride for Thermal Protection Systems," *Key Eng. Mater.,* **264-268** 493-96 (2004).

63. F. Monteverde, A. Bellosi, and S. Guicciardi, "Processing and Properties of Zirconium Diboride–Based Composites," *J. Eur. Ceram. Soc.,* **22** 279-88 (2002).

64. S. Guicciardi, L. Silvestroni, M. Nygren, and D. Sciti, "Microstructure and Toughening Mechanisms in Spark Plasma-Sintered ZrB_2 Ceramics Reinforced by SiC Whiskers or SiC-Chopped Fiber," *J. Am. Ceram. Soc.,* **93** [8] 2384-91 (2010).

65. L. Silvestroni, D. Sciti, C. Melandri, and S. Guicciardi, "Toughened ZrB_2-Based Ceramics Through SiC Whisker or SiC Chopped Fiber Additions," *J. Eur. Ceram. Soc.,* **30** [11] 2155-64 (2010).

66. D. Sciti and L. Silvestroni, "Processing, Sintering and Oxidation Behavior of SiC Fibers Reinforced ZrB_2 Composites," *J. Eur. Ceram. Soc.,* **32** 1933-40 (2012).

67. X. Zhang, L. Xu, W. Han, L. Weng, J. Han, and S. Du, "Microstructure and Properties of Silicon Carbide Whisker Reinforced Zirconium Diboride Ultra-High Temperature Ceramics," *Solid State Sci.,* **11** [1] 156-61 (2009).

68. H. Zhang, Y. Yan, Z. Huang, X. Liu, and D. Jiang, "Properties of ZrB2-SiC Ceramics by Pressureless Sintering," *J. Am. Ceram. Soc.,* **92** [7] 1599-602 (2009).

69. Q. Liu, W. Han, and J. Han, "Influence of SiCnp Content on the Microstructure and Mechanical Properties of ZrB_2-SiC Nanocomposite," *Scripta Mater.,* **63** 581-84 (2010).

70. C. W. Li, Y. M. Lin, M. F. Wang, and C. A. Wang, "Preparation and Mechanical Properties of ZrB_2-Based Ceramics Using $MoSi_2$ as Sintering Aids," *Front. Mater. Sci. China,* **4** [3] 271-75 (2010).

71. M. Patel, J. J. Reddy, V. V. B. Prasad, and V. Jayaram, "Strength of Hot Pressed ZrB_2-SiC Composite After Exposure to High Temperatures (1000-1700°C)," *J. Eur. Ceram. Soc.,* **32** [16] 4455-67 (2012).

72. F. Monteverde and L. Scatteia, "Resistance to Thermal Shock and to Oxidation of Metal Diborides-SiC Ceramics for Aerospace Applications," *J. Am. Ceram. Soc.,* **94** [4] 1130-38 (2007).

73. S. Ran, O. V. d. Biest, and J. Vleugels, "ZrB_2-SiC Composites Prepared by Reactive Pulsed Electric Current Sintering," *J. Eur. Ceram. Soc.,* **30** [12] 2633-42 (2010).

74. S. Zhu, W. G. Fahrenholtz, and G. E. Hilmas, "Influence of Silicon Carbide Particle Size on the Microstructure and Mechanical Properties of Zirconium Diboride-Silicon Carbide Ceramics," *J. Eur. Ceram. Soc.,* **27** [4] 2077-83 (2007).

75. J. Watts, G. E. Hilmas, and W. G. Fahrenholtz, "Mechanical Characterization of ZrB_2-SiC Composites with Varying SiC Particle Sizes," *J. Am. Ceram. Soc.,* **94** [12] 4410-18 (2011).

76. E. L. Kern, D. W. Hamil, H. W. Deam, and H. D. Sheets, "Thermal Properties of Silicon Carbide from 20 to 2000 C," *Mater. Res. Bull.,* **4** S25-32 (1969).

77. J. L. Watts, G. E. Hilmas, W. G. Fahrenholtz, D. Brown, and B. Clausen, "Measurement of Thermal Residual Stresses in ZrB_2–SiC Composites," *J. Eur. Ceram. Soc.,* **31** [9] 1811-20 (2011).

78. S. C. Zhang, G. E. Hilmas, and W. G. Fahrenholtz, "Mechanical Properties of Sintered ZrB_2-SiC Ceramics," *J. Eur. Ceram. Soc.,* **31** [5] 893-901 (2011).

79. J. K. Kurihara, T. Tomimatsu, Y. F. Liu, S. Q. Guo, and Y. Kagawa, "Mode I Fracture Toughness of SiC particel-dispersed ZrB_2 Matrix Composied Measured Using DCDC Specimen," *Ceram. Int.,* **36** 381-84 (2010).

80. M. W. Bird, R. P. Aune, A. F. Thomas, P. F. Becher, and K. W. White, "Temperature-Dependent Mechanical and Long Crack Behavior of Zirconium Diboride–Silicon Carbide Composite," *J. Eur. Ceram. Soc.,* **32** [12] 3453-62 (2012).

81. D. Kovar, B. H. King, R. W. Trice, and J. W. Halloran, "Fibrous Monolithic Ceramics," *J. Am. Ceram. Soc.,* **80** [10] 2471-87 (1997).

82. P. T. B. Shaffer and C. K. Jun, "The Elastic Modulus of Dense Polycystalline Silicon Carbide," *Mater. Res. Bull.,* **7** [1] 63-70 (1972).

83. J. W. Zimmerman, G. E. Hilmas, W. G. Fahrenholtz, F. Monteverde, and A. Bellosi, "Fabrication and Properties of Reactively Hot Pressed ZrB_2-SiC Ceramics," *J. Eur. Ceram. Soc.,* **27** [7] 2729-36 (2007).

84. S. Q. Guo, T. Nishimura, T. Mizuguchi, and Y. Kagawa, "Mechanical Properties of Hot-Pressed ZrB_2-$MoSi_2$-SiC Composites," *J. Eur. Ceram. Soc.,* **28** 1891-98 (2008).

85. D. Sciti, F. Monteverde, S. Guicciardi, G. Pezzotti, and A. Bellosi, "Microstructure and Mechanical Properties of ZrB_2-$MoSi_2$ Ceramic Composites Produced by Different Sintering Techniques," *Mater. Sci. Eng., A,* **434** 303-09 (2006).

86. A. Balbo and D. Sciti, "Spark Plasma Sintering and Hot Pressing of ZrB_2-$MoSi_2$ Ultra-High-Temperature Ceramics," *Mater. Sci. Eng., A,* **475** 108-12 (2008).

87. A. Bellosi, F. Monteverde, and D. Sciti, "Fast Densification of Ultra-High-Temperature Ceramics by Spark Plasma Sintering," *Int. J. Appl. Ceram. Technol.,* **3** [1] 32-40 (2006).

88. H. Kodama and T. Miyoshi, "Study of Fracture Behavior of Very Fine-Grained Silicon Carbide Ceramics," *J. Am. Ceram. Soc.,* **73** [10] 3081-86 (1990).

89. A. K. Bhattacharya and J. J. Petrovic, "Hardness and Fracture Toughness of SiC-Particle-Reinforced $MoSi_2$ Composites," *J. Am. Ceram. Soc.,* **74** [10] 2700-03 (1991).

90. W. Han, G. Li, X. Zhang, and J. Han, "Effect of AlN as Sintering Aid on Hot-Pressed ZrB_2-SiC Ceramic Composite," *J. Alloys Compd.,* **471** [1] 488-91 (2009).

91. Y. Wang, J. Liang, W. Han, and X. Zhang, "Mechanical Properties and Thermal Shock Behavior of Hot-Pressed ZrB_2-SiC-AlN Composites," *J. Alloys Compd.,* **475** [1] 762-65 (2009).

92. X. G. Wang, W. M. Guo, and G. J. Zhang, "Pressureless Sintering Mechanism and Microstructure of ZrB_2-SiC Ceramics Doped with Boron," *Scripta Mater.,* **61** [2] 177-80 (2009).

93. Q. Qiang, Z. Xinghong, M. Songhe, H. Wenbo, H. Changqing, and H. Jiecai, "Reactive Hot Pressing and Sintering Characterization of ZrB_2–SiC–ZrC composites," *Mater. Sci. Eng., A,* **491** [1] 117-23 (2008).

94. W. W. Wu, G. J. Zhang, Y. M. Kan, and P. L. Wang, "Reactive Hot Pressing of ZrB_2–SiC–ZrC Composites at 1600°C," *J. Am. Ceram. Soc.,* **91** [8] 2501-08 (2008).

95. W. W. Wu, G. J. Zhang, Y. M. Kan, and P. L. Wang, "Reactive Synthesis and Mechanical Properties of ZrB_2-SiC-ZrC Composites," *Key Eng. Mater.,* **368** 1758-60 (2008).

96. W. M. Guo and G. J. Zhang, "Microstructures and Mechanical Properties of Hot-Pressed ZrB_2-Based Ceramics from Synthesized ZrB_2 and ZrB_2-ZrC Powders," *Adv. Eng. Mater.,* **11** [3] 206-10 (2009).

97. J. Zou, G. J. Zhang, Y. M. Kan, and P. L. Wang, "Hot-Pressed ZrB_2–SiC Ceramics with VC Addition: Chemical Reactions, Microstructures, and Mechanical Properties," *J. Am. Ceram. Soc.,* **92** [12] 2838-46 (2009).

98. J. H. Richardson, "Thermal Expansion of Three Group IVA Carbides to 2700°C," *J. Am. Ceram. Soc.,* **48** [10] 497-99 (1965).

99. L. Silvestroni and D. Sciti, "Effects of $MoSi_2$ Additions on the Properties of Hf–and Zr–B_2 Composites Produced by Pressureless Sintering," *Scripta Mater.,* **57** [2] 165-68 (2007).

100. H. T. Liu, W. W. Wu, J. Zou, D. W. Ni, Y. M. Kan, and G. J. Zhang, "In Situ Synthesis of ZrB_2–$MoSi_2$ Platelet Composites: Reactive Hot Pressing Process, Microstructure and Mechanical Properties," *Ceram. Int.,* **38** [6] 4751-60 (2012).

101. D. Sciti, S. Guicciardi, A. Bellosi, and G. Pezzotti, "Properties of a Pressureless-Sintered ZrB_2–$MoSi_2$ Ceramic Composite," *J. Am. Ceram. Soc.,* **89** [7] 2320-22 (2006).

102. L. Silvestroni, D. Sciti, and A. Bellosi, "Microstructure and Properties of Pressureless Sintered HfB_2-Based Composites with Additions of ZrB_2 or HfC," *Adv. Eng. Mater.,* **9** [10] 915-20 (2007).

103. D. Sciti, L. Silvestroni, G. Celotti, C. Melandri, and S. Guicciardi, "Sintering and Mechanical Properties of ZrB_2–$TaSi_2$ and HfB_2–$TaSi_2$ Ceramic Composites," *J. Am. Ceram. Soc.,* **91** [10] 3285-91 (2008).

104. L. Silvestroni, H. J. Kleebe, S. Lauterbach, M. Müller, and D. Sciti, "Transmission Electron Microscopy on Zr- and Hf-borides with $MoSi_2$ Addition: Densification Mechanisms," *J. Mater. Res.,* **25** [5] 828-34 (2010).

105. M. Nakamura, S. Matsumoto, and T. Hirano, "Elastic Constants of $MoSi_2$ and WSi_2 Single Crystals," *J. Mater. Sci.,* **25** 3309-13 (1990).

106. R. Rosenkranz and G. Frommeyer, "Microstructures and Properties of the Refractory Compounds $TiSi_2$ and $ZrSi_2$," *ZMetl,* **83** [9] 685-89 (1992).

107. O. Thomas, J. P. Senateur, R. Madar, O. Laborde, and E. Rosencher, "Molybdenum Disilicide: Crystal Growth, Thermal Expansion and Resistivity," *Solid State Commun.,* **55** [7] 629-32 (1985).

108. J. Zou, G. J. Zhang, C. F. Hu, T. Nishimura, Y. Sakka, H. Tanaka, J. Vleugels, and O. Van der Biest, "High-Temperature Bending Strength, Internal Friction and Stiffness of ZrB_2–20vol% SiC ceramics," *J. Eur. Ceram. Soc.,* **32** [10] 2519-27 (2012).

109. R. Loehman, E. Corral, H. P. Dumm, P. Kotula, and R. Tandon, "Ultra High Temperature Ceramics for Hypersonic Vehicle Applications." SAND 2006-2925. Sandia National Laboratories, Albuquerque, NM, 2006.

110. P. Hu and Z. Wang, "Flexural Strength and Fracture Behavior of ZrB_2–SiC Ultra-high Temperature Ceramic Composites at 1800°C," *J. Eur. Ceram. Soc.,* **30** [4] 1021-26 (2010).

111. J. Zou, G. J. Zhang, C. F. Hu, T. Nishimura, Y. Sakka, J. Vleugels, and O. Van der Biest, "Strong ZrB_2–SiC–WC Ceramics at 1600°C," *J. Am. Ceram. Soc.,* **95** [3] 874-78 (2012).

112. D. Kalish, E. V. Clougherty, and K. Kreder, "Strength, Fracture Mode, and Thermal Stress Resistance of HfB_2 and ZrB_2," *J. Am. Ceram. Soc.,* **52** [1] 30-36 (1969).

PAPER

I. STRENGTH OF ZIRCONIUM DIBORIDE TO 2300°C

Eric W. Neuman, Gregory E. Hilmas, William G. Fahrenholtz

Department of Materials Science and Engineering, Missouri University of Science and Technology, Rolla, Missouri 65409

Abstract

The strength of zirconium diboride (ZrB_2) ceramics was measured up to 2300°C, which are the first reported measurements above 1500°C since 1970. ZrB_2 ceramics were prepared from commercially available powder by hot pressing. A mechanical testing apparatus capable of testing material in the ultrahigh temperature regime with atmosphere control was built, evaluated, and used. Four point bend strength was measured as a function of temperature up to 1600°C in air and between 1500°C and 2300°C in argon. Strength between room temperature and 1200°C was ~390 MPa, decreasing to a minimum of ~170 MPa between 1400°C and 1500°C, with strength increasing to ~220 MPa between 1600°C and 2300°C.

I. Introduction

Zirconium diboride (ZrB_2) is a transition metal boride that is part of a class of materials known as ultra-high temperature ceramics (UHTCs). This family of compounds has melting points of 3000°C or higher.[1,2] The borides generally exhibit higher thermal conductivities [60-125 $W \cdot (m \cdot K)^{-1}$] and lower electrical resistivities (7.8 – 22 μΩ·cm) at room temperature than carbides or nitrides.[3] Borides are also resistant to chemical attack.[1,2] As a result, borides are candidates for applications including molten metal crucibles, electrodes, microelectronics, cutting tools and hypersonic aerospace vehicles.[2]

The strength of ZrB_2 composites has been reported to decrease at 1200°C and above,[4-7] but the elevated temperature mechanical properties of ZrB_2 ceramics have not been studied systematically. In one of the few studies, Rhodes *et al.* reported strengths of hot pressed ZrB_2 up to 2200°C in argon in 1970.[4] Hot pressing at 2000°C or 2100°C produced a relative density of 99.3% and a grain size between 18 and 23 μm, but the resulting ZrB_2 contained 6.3 vol% ZrO_2 and 0.2 vol% ZrC.[4,8] More recent studies have reported strengths of ZrB_2 ceramics up to 1500°C in air.[5,9]. Melendez-Martinez et al. studied the strength of ZrB_2 in air up to 1400°C, but the specimens contained 13.5% porosity.[9] Zhu *et al.* showed additions of B_4C and carbon to ZrB_2 could improve the density and reduce grain size, which increased strength from 450 MPa to 580 MPa at room temperature and from 490 MPa to 560 MPa at 1000°C in air; strengths were similar to nominally pure ZrB_2 above 1200°C, with strengths reaching ~360MPa at 1500°C in air.[5] Limited data have been published for the

strength of ZrB_2 based ceramics over 1500°C. In addition to Rhodes *et al.,* Hu and Wang reported the strength of ZrB_2 with 15 and 30 vol% SiC to be 112 MPa and 48 MPa at 1800°C in argon[10], while Zou *et al.* reported a strength of 460 MPa for ZrB_2 with 30 vol% at 1600°C in argon.[11]

The purpose of this communication is to report the strength of fully dense ZrB_2 ceramics at elevated temperatures using a custom built mechanical testing apparatus with an environmentally controlled furnace capable of reaching temperatures of 2600°C.

II. Experimental Procedure

(1) Processing

This study used commercially available ZrB_2 powder (Grade B, H.C. Starck, Newton, MA) with a purity of 98.2% and an average particle size of 2 μm. Carbon was added as a densification aid in the amount of 0.5wt% using phenolic resin (Type GP 2074, Georgia Pacific, Atlanta, GA) as a precursor. The carbon yield of the phenolic resin was 41 wt% after charring at 800°C in an argon-10% hydrogen ($Ar/10H_2$) atmosphere. The ZrB_2 powder was ball milled with WC-6Co media in hexanes. After ball milling for 24 hours, the slurry was dried by rotary evaporation at a temperature of 70°C, under low vacuum (~27 kPa), and at a rotation speed of 60 rpm. Grinding media were weighed before and after milling to estimate WC contamination. The phenolic resin was dissolved in acetone, and pre-milled ZrB_2 powder was added. The powder was dispersed in the phenolic resin solution in an ultrasonic bath. The resulting slurry was dried by rotary

evaporation. The dried powders were lightly ground and passed through a 50 mesh screen prior to hot pressing.

Milled powders were hot-pressed (Model HP50-7010G, Thermal Technology, Santa Rosa, CA) in 63.5 mm square graphite dies lined with BN coated graphite foil. Powders were cold compacted at ~2 MPa and then heated under flowing Ar/10H_2 to 800°C with an average heating rate of 5°C/min. After holding for one hour at 800°C, the chamber was evacuated and heated at 20°C under vacuum (~13 Pa) to 1250°C. The powders were held for two hours at 1250°C and then heated at 20°C to 1450°C. After holding for two hours at 1450°C, the temperature was increased to 1600°C at 20°C/min. The furnace was held for one hour at 1600°C and then backfilled with helium and a uniaxial load of 32 MPa was applied. The isothermal holds were used to remove surface oxides from the powder particles.[12,13] The furnace was then heated at ~20°C/min to 2150°C. After one hour, the furnace was cooled at ~20°C/min. The load was removed when the die temperature dropped below 1600°C.

(2) Characterization

Bulk density of hot pressed specimens was measured by Archimedes' method using distilled water as the immersing medium according to ASTM C373-88. Relative density was calculated by dividing the Archimedes' density by the density predicted from the nominal ZrB_2, C, and WC contents. Microstructures were examined using scanning electron microscopy (SEM; S570, Hitachi, Tokyo, Japan) with simultaneous chemical analysis by energy dispersive spectroscopy (EDS; Oxford EDS, FEI, Hillsboro, OR). Specimens were prepared for

microscopy by cutting cross sections perpendicular to the hot-pressing direction and polishing to a 0.25 μm finish using successively finer diamond abrasives. The ZrB_2 was etched using molten $(Na_{0.5}K_{0.5})OH$ at ~300°C for 1 s. Grain sizes were determined from SEM images using image analysis software (ImageJ, National Institutes of Health, Bethesda, MD) by measuring the equivalent area diameter of at least 4000 grains.

(3) Mechanical Testing

Room and elevated temperature flexure strengths were measured following ASTM C1161 and ASTM C1211, respectively, in four-point bending using a fully-articulated test fixture and type-B bars (45 mm x 4 mm x 3 mm). Five specimens were tested at room temperature and three at each elevated temperature (Table I). Bars were machined from the hot-pressed billets by diamond grinding on a fully automated surface grinder (FSG-3A818, Chevalier, Santa Fe Springs, CA). Tensile surfaces were polished to 1 μm using diamond abrasives. Specimens tested in air were coated with silica by dipping in a sol prepared from tetraethylorthosilicate,[14] then heat treating to 800°C in air. Tests in air were performed using a screw-driven instrumented load frame (5881, Instron, Norwood, MA) and a molybdenum disilicide element furnace (MDS66C, Instron SFL, Thornbury, Bristol). A deflectometer was used to record bar displacement. The heating rate for all elevated temperature tests was 10°C/min followed by an isothermal hold for 10 min at the desired temperature. Room temperature elastic constants were determined by impulse excitation (MK4-I Grindosonic, J.W. Lemmens, St. Louis, MO) according to ASTM C1259. The

static bend test method was used to determine the elevated temperature elastic modulus of specimens tested in air according to ASTM standard E111. A minimum of three measurements were averaged to calculate the reported values.

A mechanical testing apparatus consisting of a screw-driven instrumented load frame (33R4204, Instron, Norwood, MA), induction heated (SI-30KWLF, Superior Induction Technology, Pasadena, CA) graphite hot zone inside an environmental chamber was built to perform testing up to 2600°C. Temperature was controlled using a two-color optical pyrometer (SR-35C15, Ircon Inc., Santa Cruz, CA) and a programmable PID controller (2404, Eurotherm, Ashburn, VA). Water cooled graphite pushrods and a fully articulated graphite 4-point bend fixture based on Grathwohl's design were used.[15] Specimens were loaded onto the fixture and secured using a cyanoacrylate adhesive. The environmental chamber was evacuated to ~35kPa and backfilled with argon five times and then argon purged for an additional 30 minutes prior to heating. Specimens were heated at ~100°C/min to 200°C below the test temperature, then heated at 50°C/min to the test temperature followed by a 5 min isothermal hold. Tests were conducted at a crosshead rate of 10mm/min to 10N, followed by the minimum crosshead rate that resulted in linear elastic behavior (Table I) until failure.

III. Results and discussion

Bulk densities were 6.04 g/cm^3 for the hot-pressed specimens. The theoretical density was calculated from the nominal composition plus contamination from milling (0.34 wt% WC-6Co) to be 6.09 g/cm^3. The theoretical

density assumed a density of 6.15 g/cm^3 for ZrB_2 based on the reported Hf content of the powder (1.9 wt%). The resulting relative density of the test specimens was 99.4%. Figure 1 shows a typical cross section of polished and chemically etched ZrB_2. The grain size was 19.4 ± 13.0 μm. Approximately 0.4% porosity was observed within grains, on the grain boundaries, and at triple grain junctions. The size of the closed pores was in the range of 0.5 to 2.5 μm. No residual C was observed. The amount of carbon added as a sintering aid (~0.5 wt%) was less than the reported solubility limit (~1.2 wt%) at the processing temperature (2150°C).[16] Likewise, no WC was observed as its content was below its reported solubility limit of ~8 mol%.[17] Thus, both C and WC dissolved into the ZrB_2 matrix.

Elastic modulus was measured for specimens tested in air. The room temperature modulus was 524 GPa, which was higher than values of 490 GPa to 500 GPa that are typically reported for nominally pure ZrB_2.[1,6,18] However, the values are similar to those reported for ZrB_2 with B_4C and C additives, which lie in the range of 510 GPa to 530 GPa[12,19]. As temperature increased, the modulus decreased in an apparent linear trend from ~524 GPa at room temperature to~370 GPa at 1300°C (Figure 2). The modulus decreased more rapidly above 1300°C to ~260 GPa at 1600°C. These elastic moduli values were similar to values reported by Rhodes[4] and Zhu[5]. As also reported by Zhu, the values exhibited a transition around 1300°C. This change in behavior was previously attributed to softening of grain boundaries or second phases isolated at triple grain junctions by Rhodes.[4]

Figure 3 shows the flexure strength as a function of temperature and testing atmosphere. Strengths were tested in air up to 1600°C and in argon from 1500°C to 2300°C (Table). Strengths did not change significantly up to 1200°C (~390 MPa), but dropped from ~390 MPa at 1200°C to ~110 MPa at 1600°C. However, testing in argon revealed that strength increased from ~170 MPa at 1500°C to ~210 MPa at 1600°C. Previous analysis by Watts et al. determined that residual thermal stresses in ZrB_2 ceramics relaxed at 1400°C,[20] which could account for the drop in strength between 1200°C and 1400°C. The strength increased to ~220 MPa at 1800°C and 2000°C. A similar increase in strength was observed by Rhodes *et al.*, and was attributed to stress relief through plastic flow. Whereas Rhodes observed a strength maximum at 1800°C, the present study observed near constant strength between 1600°C and 2000°C. The drop in strength above 1800°C reported by Rhodes is likely due to creep above 1600°C that resulted from the use of a constant strain rate for all temperatures. In the present study, strain rate was increased with temperature to achieve linear elastic failure and avoid creep as called for in ASTM C1211. The strength increased to nearly 300 MPa at 2200°C, which was above the processing temperature of 2150°C. The increase in strength at 2200°C could be due to further sintering of the material or solutionization reactions, but requires further analysis. Testing was limited to 2300°C due to the ZrB_2-C eutectic at ~2390°C, which would result in melting due to interaction of the specimen with the test fixture at higher temperatures. Use of a ZrC test fixture could enable testing up to ~2600°C.

Strength at room temperature was ~380 MPa, which was higher than that reported by Rhodes (326 MPa)[4] for ZrB_2 with similar grain size and density. Strengths in the range of 380 MPa to 570 MPa have been reported for ZrB_2 with smaller average grain sizes and/or second phases.[5,17,18] The ceramic examined in the present work had an average grain size of nearly 20 μm, which reduced its room temperature strength compared to finer grained ZrB_2, but should reduce creep and improve strength at elevated temperatures compared to the finer grained ceramics. In addition, the strength of the ceramic used in the present study increased above 2000°C, maintaining a value of ~220 MPa, whereas Rhodes reported degradation of strength above 1900°C. The improved strength above 1900°C could due to the higher purity of the modern powders compared those used by Rhodes. The improved purity would reduce the presence of second phases (e.g., ZrO_2 in Rhodes material), which could reduce grain boundary softening and result in a stiffer material at elevated temperatures. Further, unlike the work reported by Rhodes, which noted significant creep, higher strain rates were used at elevated temperatures to achieve brittle failure without creep during testing. The ZrB_2 in this study exhibited a room strength similar to that found previously in ZrB_2 with a finer microstructure, while elevated temperature strength benefited from a lower impurity content.

IV. Summary

Flexure strengths of ZrB_2 were measured up to 2300°C using an apparatus with atmosphere control. These are the first results reported for ZrB_2 at temperatures over 1500°C since 1970. Dense billets of ZrB_2 with a grain size

of ~19 μm were produced by hot pressing. Four point bend strength was measured as a function of temperature up to 1600°C in air and between 1500°C and 2300°C in argon. Strength between room temperature and 1200°C was ~390 MPa, decreasing to a minimum of ~170 MPa between 1400°C and 1500°C. The strength increased to ~220 MPa between 1600°C and 2300°C. The ultrahigh temperature mechanical testing apparatus described in this communication allows for testing at temperatures up to 2600°C with atmosphere control, which is crucial to understanding the behavior of UHTCs and other materials at proposed use temperatures.

Acknowledgements

The authors would like to thank Dr. Jeremy Watts and Dr. Harlan Brown-Shaklee (now at Sandia National Laboratories) for their assistance in the fabrication of the environmental test chamber.

References

1. R.A. Cutler, "Engineering Properties of Borides"; pp. 787-803 in *Ceramics and Glasses, Engineered Materials Handbook,* Vol. 4, Edited by S.J. Schneider, ASM International, Materials Park, OH, 1991.
2. W.G. Fahrenholtz, G.E. Hilmas, I.G. Talmy, and J.A. Zaykoski, "Refractory Diborides of Zirconium and Hafnium," *J. Am. Ceram. Soc.,* **90** [5] 1347-64 (2007).
3. J.W. Zimmerman, G.E. Hilmas, W.G. Fahrenholtz, R.B. Dinwiddie, W.D. Porter, and H. Wang, "Thermophysical Properties of ZrB_2 and ZrB_2-SiC Ceramics," *J. Am. Ceram. Soc.,* **91** [5] 1405-11 (2008).
4. W.H. Rhodes, E.V. Clougherty, and D. Kalish, "Research and Development of Refractory Oxidation-Resistant Diborides Part II, Volume IV: Mechanical Properties," Technical Report AFML-TR-68-190, Part II, Volume IV, ManLabs Incorporated and Avco Corporation, Wright Patterson Air Forse Base, OH, 1970.
5. S. Zhu, "Densification, Microstructure, and Mechanical Properties of Zirconium Diboride Based Ultra-High Temperature Ceramics"; Ph.D. Thesis. Missouri University of Science and Technology, Rolla, 2008.
6. F. Monteverde, S. Guicciardi, and A. Bellosi, "Advances in Microstructure and Mechanical Properties of Zirconium Diboride Based Ceramics," *Mater. Sci. Eng., A,* **346** 310-9 (2003).

7. R. Loehman, E. Corral, H.P. Dumm, P. Kotula, and R. Tandon, "Ultra High Temperature Ceramics for Hypersonic Vehicle Applications," SAND 2006-2925, Sandia National Laboratories, Albuquerque, NM, 2006.

8. E.V. Clougherty, D. Kalish, and E.T. Peters, "Research and Developement of Refractory Oxidation-Resistant Diborides," Technical Report AFML-TR-68-190, ManLabs Incorporated and Avco Corporation, Wright Patterson Air Forse Base, OH, 1968.

9. J.J. Melendez-Martinez, A. Dominquez-Rodriguez, F. Monteverde, C. Melandri, and G.D. Portu, "Characterization and High Temperature Mechanical Properties of Zirconium Diboride-Based Materials," *J. Eur. Ceram. Soc.,* **22** 2543-9 (2002).

10. P. Hu and Z. Wang, "Flexure Strength and Fracture Behavior of ZrB_2-SiC Ultra-High Temperature Ceramic Composites at 1800°C," *J. Eur. Ceram. Soc.,* **30** [4] 1021-6 (2010).

11. J. Zou, G.J. Zhang, C.F. Hu, T. Nishimura, Y. Sakka, H. Tanaka, J. Vleugels, and O. Van der Beist, "High-Temperature Bending Strength, Internal Friction and Stiffness of ZrB_2-20vol% SiC Ceramics," *J. Eur. Ceram. Soc.,* **32** 2519-27 (2012).

12. S. Zhu, W.G. Fahrenholtz, G.E. Hilmas, and S.C. Zhang, "Pressureless Sintering of Zirconium Diboride Using Boron Carbide and Carbon Additions," *J. Am. Ceram. Soc.,* **90** [11] 3660-3 (2007).

13. S.C. Zhang, G.E. Hilmas, and W.G. Fahrenholtz, "Pressureless Densification of Zirconium Diboride with Boron Carbide Additions," *J. Am. Ceram. Soc.,* **89** [5] 1544-50 (2006).

14. M. Nogami and Y. Moriya, "Glass formation Through Hydrolysis of $Si(OC_2H_5)_4$ with NH_4OH and HCl Solution," *J. Non-Cryst. Solids,* **37** 191-201 (1980).

15. G. Grathwohl, "Current Testing Methods: A Critical Assessment," *Int. J. High Techn. Ceram.,* **4** [4] 211-25 (1988).

16. Figure 8874-C in Phase Diagrams for Ceramists Volume X: Borides, Carbides, and Nitrides, Edited by A.E. McHale, The American Ceramics Society, Westerville, OH, (1994).

17. A.L. Chamberlain, W.G. Fahrenholtz, and G.E. Hilmas, "Pressureless Sintering of Zirconium Diboride," *J. Am. Ceram. Soc.,* **89** [2] 450-6 (2006).

18. A.L. Chamberlain, W.G. Fahrenholtz, and G.E. Hilmas, "High Strength ZrB_2-Based Ceramics," *J. Am. Ceram. Soc.,* **87** [6] 1170-2 (2004).

19. W.G. Fahrenholtz, G.E. Hilmas, S.C. Zhang, and S. Zhu, "Pressureless Sintering of Zirconium Diboride: Particle Size and Additive Effects," *J. Am. Ceram. Soc.,* **91** [5] 1398-404 (2007).

20. J. Watts, G.E. Hilmas, W.G. Fahrenholtz, D. Brown, and B. Clausen, "Measurement of Thermal Residual Stresses in ZrB_2-SiC Composites," *J. Eur. Ceram. Soc.,* **31** [9] 1811-20 (2011).

Table I. Elevated temperature mechanical properties measured for ZrB_2 ceramics.

Temperature (°C)	Atmosphere	Crosshead rate (mm/min)	Elastic modulus (GPa)	Strength (MPa)
RT	Air	0.5	524 ± 17	381 ± 41
1000	Air	0.5	414 ± 34	399 ± 37
1200	Air	0.5	392 ± 36	392 ± 37
1300	Air	0.5	368 ± 16	236 ± 3
1400	Air	1.0	297 ± 6	176 ± 18
1500	Argon	1.5	--	173 ± 6
1600	Air	2.0	263 ± 23	110 ± 11
1600	Argon	2.0	--	212 ±26
1800	Argon	2.5	--	220 ±18
2000	Argon	3.0	--	223 ± 18
2200	Argon	3.5	--	299 ± 5
2300	Argon	5.0	--	216 ± 40

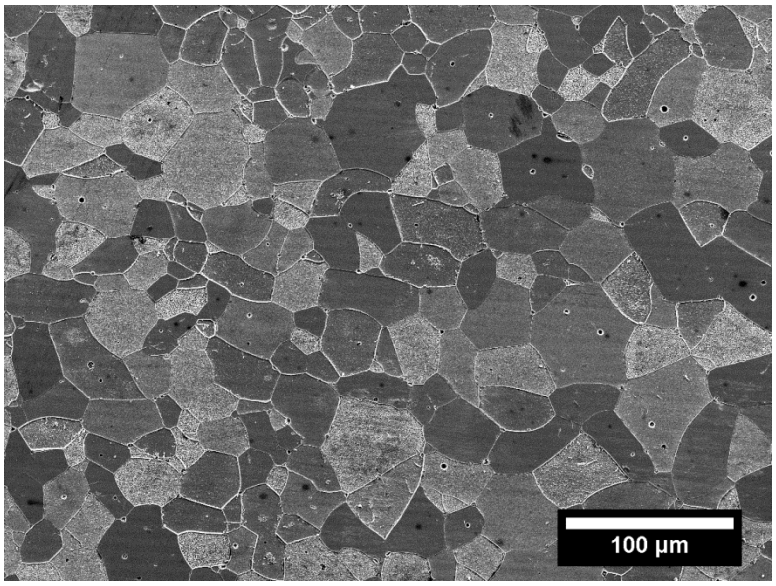

Figure 1. SEM image of a polished and chemically etched cross-section of ZrB_2 ceramic.

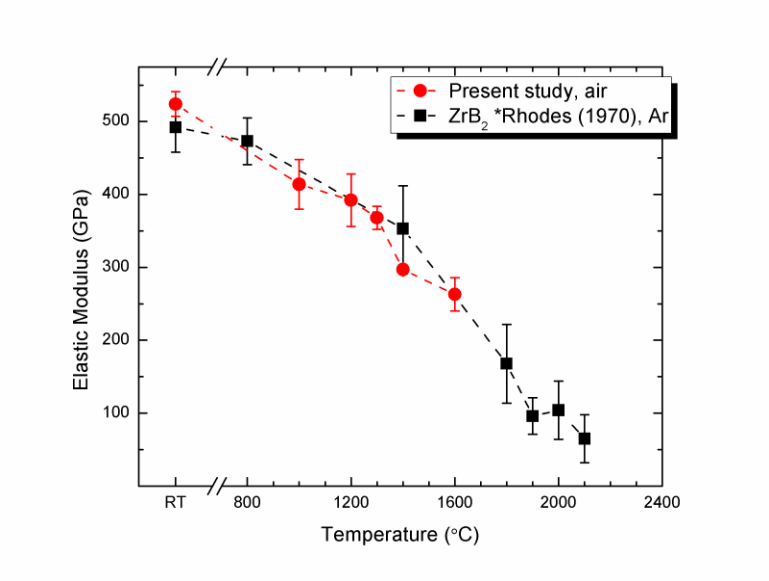

Figure 2. Elastic modulus of ZrB_2 tested in air atmosphere as a function of temperature.

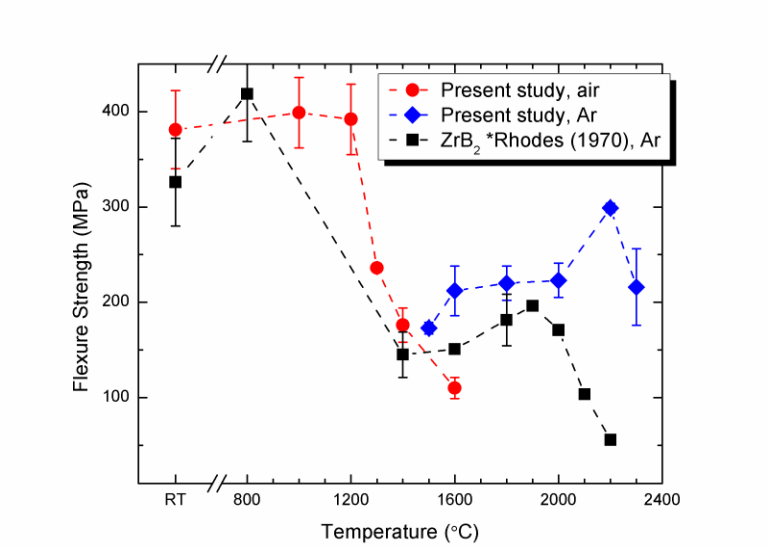

Figure 3. Four-point flexure strength of ZrB_2 ceramics tested in air (circles) and argon (diamonds) atmospheres as a function of temperature. For comparison, the data of Rhodes et al. (squares) are also shown.[4]

II. MECHANICAL BEHAVIOR OF ZIRCONIUM DIBORIDE-SILICON CARBIDE CERAMICS AT ELEVATED TEMPERATURE IN AIR

Eric W. Neuman*, Gregory E. Hilmas, William G. Fahrenholtz

Department of Materials Science and Engineering, Missouri University of Science and Technology, Rolla, Missouri 65409

Abstract

The mechanical properties of zirconium diboride-silicon carbide (ZrB_2-SiC) ceramics were characterized from room temperature up to 1600°C in air. ZrB_2 containing nominally 30 vol% SiC was hot pressed to full density at 1950°C using B_4C as a sintering aid. After hot pressing, the composition was determined to be 68.5 vol% ZrB_2, 29.5 vol% SiC, and 2.0 vol% B_4C using image analysis. The average ZrB_2 grain size was 1.9 μm. The average SiC particles size was 1.2 μm, but the SiC particles formed larger clusters. The room temperature flexural strength was 680 MPa and strength increased to 750 MPa at 800°C. Strength decreased to ~360 MPa at 1500°C and 1600°C. The elastic modulus at room temperature was 510 GPa. Modulus decreased nearly linearly with temperature to 210 GPa at 1500°C, with a more rapid decrease to 110 GPa at 1600°C. The fracture toughness was 3.6 $MPa \cdot m^{½}$ at room temperature, increased to 4.8 $MPa \cdot m^{½}$ at 800°C, and then decreased linearly to 3.3 $MPa \cdot m^{½}$ at 1600°C. The

strength was controlled by the SiC cluster size up to 1000°C, and oxidation damage above 1200°C.

Keywords: zirconium diboride, silicon carbide, hot pressing, mechanical properties, failure analysis

1. Introduction

Zirconium diboride (ZrB_2), a transition metal boride compound, is part of a class of materials known as ultra-high temperature ceramics (UHTCs). This family of compounds is characterized by melting points in excess of 3000°C.[1] The borides generally exhibit higher thermal conductivities (60-125 $W \cdot (m \cdot K)^{-1}$) and lower electrical resistivities (7.8 – 22 $\mu\Omega \cdot cm$) at room temperature than carbide or nitride ceramics.[2, 3] Borides are also resistant to chemical attack.[4] These properties have made borides candidates for applications including molten metal crucibles,[5, 6] furnace electrodes,[5] cutting tools,[4, 7] and wing leading edges on future hypersonic aerospace vehicles.[8, 9] Additionally, ZrB_2 based particulate composites, especially those with silicon carbide (SiC) additives, have displayed enhanced properties. ZrB_2-SiC composites exhibit room temperature strengths in excess of 1000 MPa,[10-12] fracture toughness values as high as 5.5 $MPa \cdot m^{½}$,[10, 11, 13] and hardness values exceeding 22 GPa.[8, 10, 12] Chamberlain et al. showed that the room temperature strength increased from 565 MPa for nominally pure ZrB_2 to over 1000 MPa with the addition of 20 or 30 vol% SiC.[10] Similarly, the fracture toughness increased from 3.5 $MPa \cdot m^{½}$ for nominally pure ZrB_2 to 4.4 $MPa \cdot m^{½}$ for the addition of 20 vol% SiC and 5.3 $MPa \cdot m^{½}$ for 30 vol% SiC.

Zhang et al. showed that the hardness of pressureless sintered ZrB_2-SiC ceramics increased with increasing SiC content, from 15.3 GPa for 10 vol% SiC to 22.4 GPa for 30 vol% SiC,[14] while Chamberlain et al. found the hardness to be ~23-24 GPa for ZrB_2 with up to 30 vol% additions of SiC. Chamberlain also found the modulus of hot pressed, nominally pure ZrB_2 was 489 GPa, which decreased to 466 GPa for 20 vol% and 484 GPa for 30 vol% SiC.[10] For pressureless sintered ZrB_2-SiC, Zhang et al. found that the modulus increased from 404 GPa for 10 vol% SiC to 492 GPa for 30 vol%. These studies showed that the addition of SiC not only increased strength, fracture toughness, and hardness, but also influenced the oxidation rate of ZrB_2 by forming a silica rich oxide layer on the surface, slowing the rate of oxidation of the underlying material.[15-17] This combination of properties has resulted in ZrB_2-SiC composites being studied for aerospace applications related to hypersonic flight. For the present study, ZrB_2 containing nominally 30 vol% SiC was selected based on its combination of room temperature mechanical properties and oxidation resistance.

While several studies have reported the elevated temperature mechanical properties of ZrB_2 ceramics, most of the studies have reported a single property (i.e., strength) for a limited number of temperatures and have not provided a systematic evaluation of the effects of temperature on mechanical behavior. Previous studies have shown that the strength of ZrB_2 composites generally decreases above about ~800°C.[18-23]

Figure 1 summarizes previous studies of the strength of ZrB_2-SiC ceramics at elevated temperatures. Rhodes et al. reported the strengths in argon for hot pressed ZrB_2 up to 2200°C and ZrB_2-20 vol% SiC up to 2000°C in argon in 1970.[18] They reported the strength of ZrB_2-20 vol% SiC to be 390 MPa at room temperature, which decreased to ~240 MPa at 1400°C to 1800°C, and then decreased again to 115 MPa at 2000°C. Rhodes et al. also produced ZrB_2-SiC-C composites with strengths between 220 and 350 MPa at 1400°C and 1800°C in an argon atmosphere.[18] More recent studies have reported the elevated temperature strengths of ZrB_2[19, 24] and ZrB_2-SiC[22, 23, 25] ceramics up to 1500°C in air. While these studies used ceramics with higher room temperature strengths that are more representative of current UHTCs, the ceramics included nitride or disilicide additives as sintering aids. For example, Monteverde et al. reported that a 4 wt% addition of Si_3N_4 to ZrB_2-20vol%SiC could produce a ceramic with a room temperature strength of 730 MPa, but the strength dropped to 250 MPa at 1200°C.[22] For ZrB_2-15 vol% SiC, Monteverde et al. reported a room temperature strength of 887 MPa that dropped to 255 MPa at 1500°C. Loehman et al. examined ZrB_2-20vol% SiC with a room temperature strength of 450 MPa that decreased to 240 MPa at 1450°C.[23] Disilicide additions can improve the elevated temperature strength of ZrB_2 ceramics.[20, 21, 26] Sciti et al. measured strengths of 330 and 370 MPa at 1500°C for ZrB_2 with 15 vol% additions $MoSi_2$ or $TaSi_2$.[20, 21] Silvestroni et al. reported strengths for ZrB_2 with 5 vol% $MoSi_2$ to be 570 MPa at room temperature and 490 MPa at 1500°C.[26]

Since the Rhodes studies, most studies have only reported strength at one or two elevated temperatures.

Studies of other elevated temperature mechanical properties of ZrB_2 ceramics such as elastic modulus and fracture toughness have been limited. Rhodes et al. measured the elastic modulus in argon up to 2100°C for ZrB_2 and up to 2000°C for ZrB_2-20vol% SiC.[18] Zhu measured the modulus of ZrB_2 and ZrB_2 with B_4C and C additions up to 1500°C in air.[19] Rhodes reported a modulus of ~520 GPa for ZrB_2-20 vol% SiC at room temperature, which decreased to 445 GPa at 1400°C, and to 106 GPa at 1600°C. Based on these recent studies, strength data for ZrB_2 based ceramics have not been measured systematically at regular temperature intervals. In addition, no recent studies report the elevated temperature fracture toughness of these materials. Most studies report strength at room temperature and 1200°C with either 1400°C or 1500°C as the highest reported test temperature.

As with other brittle materials, the strength of ZrB_2-SiC ceramics is controlled by the largest flaws present in the microstructure. Previous research has identified the size of the SiC inclusions as the critical flaw in dense, fine grained ZrB_2-SiC.[11-13] At some critical level of thermal expansion mismatch and cluster size, spontaneous microcracking of the matrix can occur, which has been studied by a number of authors.[12, 27, 28] The CTE mismatch between ZrB_2 (~5.2 ppm/K at 298 K),[1, 29] SiC (~3.3 ppm/K at 298 K)[29] and B_4C (~5.7 ppm/K from 300-1970K)[30] results in residual compressive stress in the SiC and tensile stresses in the ZrB_2 matrix and B_4C reinforcing phase. Watts et al. showed that a

decrease in hardness (21 to 18 GPa) occurred at a maximum SiC particle size of 11.5 μm due to stress induced microcracking.[12] Watts et al. directly measured the residual stresses that accumulate in ZrB_2-30vol% SiC upon cooling, finding a compressive stress of 880 MPa in the SiC phase and a tensile stress of 450 MPa in the ZrB_2 phase prior to the onset of microcracking.[31, 32] Additionally, they found that the residual stresses begin to accumulate at ~1400°C upon cooling and that the maximum stress was at the ZrB_2-SiC interface with stress decreasing when moving away from the interface. Previous studies have not examined the critical flaw size in ZrB_2-SiC at elevated temperatures.

The purpose of this paper is to report the mechanical properties of a ZrB_2-30 vol% SiC ceramic for temperatures up to 1600°C. The roles of microstructure and oxidation behavior on the mechanical properties were examined.

2. Experimental Procedure

2.1. Processing

Commercially available powders were used in this study. The ZrB_2 powder (Grade B, H.C. Starck, Newton, MA) had a reported purity of 98.2% and a particle size of 2 μm. The SiC powder (Grade UF-10, H.C. Starck) was predominantly α-SiC, having a reported purity of 98.5% and a particle size of 0.7 μm. The B_4C powder (Grade HD-20, H.C. Starck) had a B:C ratio of 3.8, a reported purity of 97.6%, and a particle size of 0.5 μm. The powders were batched in the ratio of 70 vol% ZrB_2 to 30 vol% SiC with a super addition of 2 wt% B_4C (ZrB_2 basis). The powders were mixed by ball milling with WC-6Co media in acetone with dispersant (DISPERBYK®-110, BYK-Gardner USA,

Columbia, MD). After ball milling for 24 hours, the slurry was dried by rotary evaporation (Model Rotavapor R-124, Buchi, Flawil, Germany) at a temperature of 70°C, low vacuum (~27 kPa), and a rotation speed of 60 rpm. The dried powders were lightly ground to pass through a 50 mesh screen prior to densification.

Milled powders were hot-pressed (Model HP50-7010G, Thermal Technology, Santa Rosa, CA) in 63.5 mm square graphite dies lined with BN coated (SP-108, Cerac, Milwaukee, WI) graphite foil. Prior to hot pressing, the powders were cold compacted in a uniaxial press at ~2 MPa. Powder compacts were heated under vacuum to (~13 Pa) to 1450°C with an average heating rate of 20°C/min. After holding for 1 hour, the temperature was increased to 1650°C at an average heating rate of 20°C/min. After holding for 1 hour, the furnace was back filled with argon and a uniaxial load of 32 MPa was applied. Following previous studies, the isothermal holds were used to promote reactions between surface oxides on the starting powders and boron carbide to remove the oxides as gaseous species.[33, 34] The furnace was then heated at ~90°C/min to 1950°C. After 10 min, the power was shut off and the furnace allowed to cool at a natural rate of ~60°C/min. The load was removed when the die temperature dropped below 1650°C.

2.2. Characterization

The bulk density of the hot pressed specimens was measured by Archimedes' method using distilled water as the immersing medium as described in ASTM C373-88. Microstructures were examined using scanning electron

microscopy (SEM; S570, Hitachi, Tokyo, Japan). Specimens were prepared for microscopy by cutting cross sections perpendicular to the hot-pressing direction and polishing to a 0.25 μm finish using diamond abrasives. The ZrB_2 was etched using molten KOH at 450°C for 1 s. The SiC was etched using boiling Hall's Reagent for 20 min. ZrB_2 and SiC grain sizes were measured from SEM images using computerized image analysis (ImageJ, National Institutes of Health, Bethesda, MD). The grain size distribution was determined by measuring the equivalent area diameter of at least 1000 grains of both ZrB_2 and SiC. The SiC and B_4C cluster size distribution was determined from the polished cross sections by measuring the Feret's diameter approximately 45,000 and 15,000 clusters.

2.3. Mechanical testing

Hardness was measured by Vickers' indentation (Duramin 5, Struers, Cleveland, OH) according to ASTM C1327-08. Indentation loads ranged from 0.49 N (0.05 kg) to 19.8 N (2 kg) with a dwell time of 15 s. A minimum of 10 indents was measured for each load to determine the average values. Room temperature flexure strengths were measured in four-point bending using a fully-articulated test fixture using type-B bars (45 mm x 4 mm x 3 mm) according to ASTM C1161-02c. Flexure strength was measured at elevated temperatures (800, 1000, 1200, 1400, 1500, and 1600°C) using the same type-B bars and following the testing procedures outlined in ASTM C1211-08. Nine specimens were tested at room temperature and a minimum of five specimens were tested at each elevated temperature. Bars were machined from the hot-pressed billets by diamond grinding on a fully automated surface grinder (FSG-3A818,

Chevalier, Santa Fe Springs, CA). The flexure surface was polished to 1 μm using diamond abrasives. Tests were performed using a screw-driven instrumented load frame (5881, Instron, Norwood, MA). Elevated temperature testing was performed in a molybdenum disilicide element furnace (MDS66C, Instron SFL, Thornbury, Bristol). A deflectometer was used to record the displacement of the test bars during loading. A crosshead rate of 0.5 mm/min was used up to 1200°C, 1.5 mm/min at 1400°C, 2.0 mm/min at 1500°C, and 2.5 mm/min at 1600°C. The heating rate for all of the high temperature tests was 10°C/min followed by an isothermal hold for 10 min at the desired temperature before testing.

Room temperature elastic constants were determined by impulse excitation (MK4-I Grindosonic, J.W. Lemmens, St. Louis, MO) according to ASTM C1259-08. The static bend test method was used to determine the elevated temperature elastic modulus according to ASTM standard E111-04. The elastic modulus was calculated from the slope of the load displacement curves. At least 10 measurements were averaged to calculate the reported values. Fracture toughness was measured by the chevron notch beam (CNB) method in four-point bending using a fully articulated test fixture using chevron notch type-A bars (45 mm x 3 mm x 4 mm) according to ASTM Standard C1421-01b. The chevron notch was machined using a dicing saw (Accu-cut 5200, Aremco Products, Ossining, NY) with a 0.006 in thick diamond wafering blade. Prior to testing, the chevron notch tip was loaded in cyclic compression between 20 N and 100 N of the maximum failure load. A crosshead rate of 0.03 mm/min,

0.015 mm/min, and 0.02 mm/min was used for specimens tested at room temperature, 800°C, and between 1000°C and 1600°C respectively. For elevated temperature testing, a heating rate of 10°C/min was used along with an isothermal hold of 10 min at the desired temperature. The notch dimensions were measured after testing using a digital microscope (KH-3000, Hirox-USA, Hackensack, NJ). Six specimens were tested at room temperature, and a minimum of three specimens were tested at the same elevated temperatures used for flexure testing.

3. Results and discussion

The measured bulk densities of the hot-pressed specimens were 5.22 g/cm^3. The theoretical density calculated from the nominal composition (67.75 vol% ZrB_2, 29.00 vol% SiC, and 3.27 vol% B_4C) plus milling contamination (0.24 – 0.32 wt% WC-6Co) was determined to be 5.15g/cm^3. The composition after hot pressing was determined by image analysis to be 68.5 vol% ZrB_2, 29.5 vol% SiC, and 2.0 vol% B_4C, giving a theoretical density of 5.18 g/cm^3. Porosity was not observed in the hot pressed specimens. Further, if the density of ZrB_2 is adjusted for the reported hafnium content in the starting powder (~1.9 wt%), the predicted theoretical density increases to 5.22 g/cm^3. Therefore, the measured bulk density is consistent with SEM observations that the specimens were fully dense.

Figure 2 shows a typical cross section of a polished and a chemically etched specimen. The ZrB_2 and SiC grain sizes were 1.9 ± 0.9 μm and 1.2 ± 0.5 μm respectively. Approximately 2.0 vol% B_4C, which was added as a sintering

aid, was observed in the microstructure following hot pressing. The B_4C grain size was not measured, as a suitable etch could not be found to reveal the B_4C grain boundaries. The B_4C cluster size was 1.2 ± 1.0 μm with a maximum cluster size of 14.4 μm. The SiC particles were found to form large clusters with an average size of 6.1 ± 4.4 μm and a maximum cluster size of 58.9 μm.

The Vickers' hardness, measured with a load of 9.8 N (1 kg), was 20.2 ± 0.5 GPa. This value was lower than those previously measured for similar ZrB_2-30SiC, which had a hardness of 24 GPa.[10] The lower hardness could be due to microcracking. As shown in Figure. 3, SEM analysis revealed the presence of microcracks in the ZrB_2 matrix. The maximum observed SiC cluster size was 58.9 μm, which is well above the microcracking threshold for ZrB_2-SiC of 11.5 μm reported by Watts.[12] The microcracks observed in the present study were typically several microns in lengths, originating from SiC grains or clusters. The microcracks appear to either link with other microcracks, or terminate in the ZrB_2 matrix, shown by the arrows in Figure. 3. Thus, the matrix microcracking is a result of the large SiC clusters present in the microstructure.

Measured values for the elastic modulus, flexure strength, and fracture toughness from room temperature to 1600°C are included in Table I with typical stress versus strain curves shown in Figure 4. All of the specimens exhibited linear-elastic behavior to failure, and no creep was observed in the bars following fracture at the elevated temperatures (Figure 5). Figure 6 summarizes the flexural strength as a function of test temperature. Based on the observed

trends, the discussion below is divided into temperature regimes of similar behavior.

In the lowest temperature regime, the average strength increased from ~680 MPa at room temperature to ~750 MPa at 800°C. An increase in strength from room temperature to 1000°C or 1200 °C has been previously observed in ZrB_2 and HfB_2 based composites, and has been attributed to healing of surface flaws by the formation of oxide scale and the relief of thermal residual stresses.[19, 20, 26, 35] Figure 7a shows that the tensile surface of the bar tested at 800°C was covered by a dense oxide layer ~3.2 μm thick consisting of ZrO_2+ZrB_2+SiC. The formation of this dense oxide layer may heal flaws present on the surface (i.e. machining damage, microcracking), thus decreasing the flaw size. Kalish et al. observed that an increase in the amount of transgranular fracture corresponded to an increase in the strength of ZrB_2.[35] Because the present tests were conducted in an oxidizing environment (i.e., air), any information regarding the type of fracture was lost due to the formation of the oxide scale (Figures 8 and 9) on the fracture surface, so the amount of transgranular and intragranular fracture could not be determined after fracture in air. The increase in strength observed between room temperature and 1000°C is attributed to a decrease in surface flaw size and the transition to transgranular fracture.

The second behavior regime is from 1000°C to 1500°C in which the strength decreased nearly linearly from ~725 MPa at 1000°C to ~360 MPa at 1500°C. At 1000°C the oxide scale (Figure 7b) was ~7 μm thick and appeared to be partially dense. Rhodes et al. attributed the decrease in strength to relaxation

of thermal stresses that arose during cooling from the processing temperature due to the difference in CTE values between ZrB_2 and SiC.[23] More recently, Watts et al. measured residual stresses as a function of temperature and concluded that the stresses were completely relaxed by ~1400°C.[44,45] Thus, the decrease in strength between 1000°C and 1500°C is consistent with relaxation of thermal stresses.

In the third regime, strength increased from ~360 MPa at 1500°C to ~380 MPa at 1600°C. Since the residual stresses were expected to relax by about 1400°C on heating to the testing temperature, some other mechanism is needed to explain the increase in strength observed between 1500°C and 1600°C. For example, a change in the fracture behavior or the morphology of the oxidation scale could account for the change in strength. A minimum in strength for ZrB_2 was also observed by Rhodes et al.[18] to occur around 1400°C, followed by an increase in strength up to 1800 °C. The increase in strength was attributed to plastic flow of the material. Rhodes did not observe the same phenomenon in ZrB_2-20vol% SiC, but did observe a consistent strength between 1400°C and 1800°C. Creep was observed by Rhodes[18] in ZrB_2-20vol% SiC beginning at 1600°C. The strength testing by Rhodes was performed using a constant strain rate. This may have allowed the macroscopic creep effects to counter the benefit of stress relief by plastic flow. The strain rates used in the present study were selected to attain linear elastic fracture at all temperatures as suggested in ASTM C1211-08. This minimizes creep effects that would be detrimental to strength,

and should allow the stress relief associated with plastic flow to increase the strength in this temperature regime.

Following testing, the bars were cross-sectioned to determine the thickness and morphology of the oxidation scale on the tensile surfaces (Figure 7). The measured oxide scale thicknesses are plotted as a function of test temperature for the samples tested between 1200°C and 1600°C (Figure 8). At 800°C and 1000°C (Figure 7b and b) a B_2O_3 glassy layer was observed on the surfaces of the samples with a ZrO_2+ZrB_2+SiC layer beneath the outer B_2O_3 layer. The total thickness of the oxide scale was ~3.2 μm at 800°C and ~7.3 μm at 1000°C. The oxide scale was dense at 800°C, but porosity developed at 1000°C.

At 1200°C (Figure 7c), an outer glassy layer that was about 1.3 μm thick was observed. The outer layer presumably contained SiO_2 and B_2O_3. Beneath the outer glassy layer was a partially oxidized layer ~5.0 μm thick. The partially oxidized layer consisted of ZrO_2 along with partially oxidized ZrB_2 and SiC grains and some porosity. The outer glassy layer grew to ~2.2 μm thick at 1400°C and ~4.8 μm thick at 1500°C (Figure 7d and e). In addition, the glassy phase penetrated into the partially oxidized layer. It can also be seen that partially oxidized SiC grains were present in the ZrO_2 layer at these temperatures, likely due to their large size and the relatively short time at temperature (10 minutes). At some test conditions, a relatively thin (~5.0 μm to 8.8 μm) but pronounced ZrO_2 layer was observed between the outer glassy layer and the partially oxidized layer. The thickness of the partially oxidized layer increased to ~7.2 μm

after testing at 1400°C and ~8.8 μm after oxidation at 1500°C. At these temperatures, the formation of a SiC depleted zone was observed due to the active oxidation of SiC grains. SiC depletion by active oxidation resulted in the formation of porosity in the partially oxidized layer.

The oxidation scale microstructure at 1600°C (Figure 7f) was similar to that observed at 1400°C and 1500°C. The major difference at 1600°C was near full penetration of the glassy phase into the ZrO_2 layer. Additionally, the ZrO_2 layer at 1600°C appears to have a higher density, suggesting that the ZrO_2 grains formed during oxidation had begun to sinter at 1600°C. A number of ZrO_2 islands began to form across the surface (Figure 5e) at 1500°C. At 1600°C, the ZrO_2 islands on the oxidized surface became larger and the glassy phase transitioned from a smooth to a reticulated coating (Figure 5f). The average thickness of the outer glassy layer was ~5.6 μm after testing at 1600°C, with the ZrO_2 and partially oxidized layers having a thickness of ~9.7 μm. The structure of the oxidation scales resembled those presented by Rezaie et al.,[16, 17] albeit for lower temperatures due to the shorter time at temperature (~10 minutes) compared to those presented by Rezaie for longer times (30 minutes).

The elastic modulus of ZrB_2-SiC decreased as temperature increased (Figure 11). The elastic modulus was 513 GPa at room temperature, which is similar to the values reported by Rezaie et al. (503-516 GPa),[11] Zhu et al. (509-520 GPa),[13] and Zhang et al. (511 GPa).[14] The modulus decreased to 432 GPa at 800°C. Between 1000°C and 1500°C, the elastic modulus decreased from 408 GPa to 209 GPa in a trend that appeared to be linear with temperature. The

modulus decreased more rapidly above 1500°C, decreasing to 110 GPa at 1600°C. The change in slope of the trend lines for temperatures from RT to 1000°C and 1000°C to 1500°C may be the result of oxidation. Similar temperature dependencies for modulus and strength have been observed for other oxide and non-oxide ceramics.[19, 36-39] Wachtman et al. found that the elastic modulus of polycrystalline ceramics displayed a gradual linear decrease with increasing temperature in a low temperature range followed by a more rapid, non-linear decrease at higher temperatures.[38] Zhu et al. found a similar trend in ZrB_2, with a slow, linear decrease up to ~1200°C followed by a more rapid decrease above this temperature.[19] Rhodes et al. observed a similar trend in the ZrB_2-20 vol% SiC system, where the modulus decreased slowly from 530 GPa at room temperature to 446 GPa at 1400°C, then experienced a rapid decrease to 1600°C to 110 GPa.[18] This rapid decrease in modulus at elevated temperatures has been attributed primarily to grain boundary sliding and diffusional creep.[38] Talmy et al. found that grain boundary sliding of SiC was the controlling creep mechanism in ZrB_2-SiC ceramics in air.[40] Talmy concluded that increasing the size of the SiC particles in ZrB_2-50vol% SiC from 2 μm to 10 μm increased the creep activation energy from 209 kJ/mol to 511 kJ/mol, which also decreased the amount of creep observed. Further, increasing the amount of SiC (2 μm particle size) present in the ZrB_2 from 0 vol% to 50 vol% increased the creep activation energy from 130 kJ/mol to 511 kJ/mol, increasing the amount of creep observed as SiC content increased. The material produced by Rhodes had ZrB_2 and SiC grain sizes of ~8 μm and ~4 μm. The larger grain size and reduced SiC content

of the Rhodes material, compared to the present material, may explain why Rhodes observed more retention of the elastic modulus to higher temperature. These results suggest that increasing the ZrB_2 and SiC grain sizes should increase the stiffness of the material at elevated temperatures.

The fracture toughness as a function of temperature is shown in Figure 10. At room temperature, the fracture toughness was 4.9 ± 0.4 MPa·m^{½}, which is comparable to values previously measured for ZrB_2 containing 30 vol% SiC ranging from 4.6 MPa·m$^{1/2}$ to 5.5 MPa·m^{½}.[10, 11, 13] The fracture toughness was 4.8 ± 0.2 MPa·m^{½} at 800°C, steadily decreasing to 3.3 ± 0.2 MPa·m^{½} at 1600°C. The fracture toughness at room temperature in the present study may be affected by the presence of stress-induced microcracks (Figure. 3), which have been shown to decrease toughness in previous studies.[41-47] In contrast to the spontaneous microcracking observed in the present ZrB_2-SiC, stress induced microcracking can improve the fracture toughness of ceramics by shielding the crack tip and dissipating the fracture energy during crack propagation.[41, 42, 46] However, pre-existing microcracks, such as the spontaneous formed by thermal expansion mismatch in the present ZrB_2-SiC, do not contribute to crack tip shielding.[47] Rose et al. proposed that spontaneous microcracks reduce the fracture toughness by two mechanisms: 1) reducing the initial modulus; and 2) linking with the main crack during fracture. Therefore, the room temperature fracture toughness of the ceramics examined in the present study may be lower than otherwise expected based on the presence of spontaneous microcracks.

The fracture toughness measured by CNB at 1500°C was 4.6 ± 0.6 MPa•$m^{1/2}$ (filled square at 1500°C in Figure 10). This value did not follow the trend observed for the other elevated temperature tests. The reason for the variation from the observed trend is not known, but may be a result of a change in stress state or the influence of oxidation at the CNB tip. To further evaluate the behavior at 1500°C, the fracture toughness was calculated from the critical flaw size observed from three specimens. Using the observed critical flaw sizes and the measured strengths, the fracture toughness was calculated to be 3.4 ± 0.4 MPa·$m^{½}$ at 1500°C (open square in Figure 10), which is in agreement with the observed trend of fracture toughness with temperature.

The room temperature values for strength and toughness were 682 ± 98 MPa and 4.9 ± 0.4 MPa•$m^{1/2}$. Both were lower than expected from previous studies of ZrB_2-SiC due spontaneous microcracking. The critical flaw size was predicted for the ZrB_2-30 vol% SiC produced in this study using the Griffith criteria and a Y parameter of 1.28 for a semi-elliptical surface flaw.[48] For room temperature, the predicted critical flaw size was 63 ± 10 μm. Repeating the calculation for the elevated temperatures resulted in critical flaw size predictions ranging from ~63 μm at room temperature to ~90 μm at 1400°C and 1600°C. The predicted flaw sizes were significantly larger than the average SiC grain size (1.9 μm), B_4C grain size (1.1. μm) and B_4C cluster size (14.4 μm max) at all temperatures. In addition, the oxide scale thicknesses were less than the predicted critical flaw size for all temperatures. The sizes of the largest SiC clusters (~32 to 59 μm for the largest 0.1% of SiC clusters) fell within the range of

critical flaw sizes up to 1000°C. The flaw size predicted from strength and fracture toughness at room temperature was ~63 μm, which was larger than the largest observed SiC clusters (up to ~59 μm) due to microcracking. Microcracking effectively increases the size of the flaw by either linking clusters, or extending the flaw formed by the SiC cluster further into the ZrB_2 matrix. Further, the predicted critical flaw sizes decreased from ~63 μm at room temperature to ~49 μm and ~47 μm at 800°C and 1000°C, which is consistent with flaw healing, as discussed above.

Above 1000°C, the predicted critical flaw size became larger than the largest SiC clusters. This could mean that the type of critical flaw has changed, which could also mean that the stress intensity factor of 1.28 is no longer valid. For example, a stress intensity factor of $Y = \pi^{½}$ (small central, double ended through crack)[49] brings the predicted critical flaw size into the range the largest SiC clusters. Another possibility is that a larger flaw forms at higher temperatures. For example, oxidation damage could produce larger flaws. Another possibility is that thermal strain on heating above 1000°C provides enough energy to drive the growth of cracks already present in the microstructure. However, thermal stresses have been shown to relax by ~1400°C in ZrB_2-SiC,[31] so thermal strain should be decreasing in this temperature regime and may no longer be able drive crack growth.

Fractography could not be performed on the specimens after testing at elevated temperatures due to oxidation damage on the fracture surfaces (Figure 11). Oxidation damage resulted in the growth of B_2O_3 and ZrO_2 phase

interspersed SiC at 800°C. Above 1000°C, a glassy surface layer with interspersed submicron ZrO_2 islands formed. At 1400°C and above, the glassy phase became discontinuous, forming macroscopic ZrO_2 islands that increased in size with temperature. As these surface oxides grew, details on the fracture surfaces were consumed and covered by the resulting scale.

To search for strength-limiting flaws for materials tested at elevated temperatures, fragments of the specimens oxidized in the testing furnace and fixture at elevated temperatures were subsequently fractured in 3-point bending at room temperature, using a support span of 20 mm, and a crosshead rate of 0.5 mm/min. Figure 12 shows examples of flaws found in specimens fractured at room temperature after exposure to temperatures of 800°C, 1000°C, 1400°C, and 1600°C. Analysis of the fracture surfaces (ASTM C1322-05b) revealed the critical flaw to be SiC agglomerates from room temperature up to 1000°C. These flaws were typically surface, or near surface, flaws exhibiting circular or semicircular morphologies. At 1200°C and above, oxidation damage was determined to be the critical flaw. The failure origins were characterized by regions of increased penetration of the oxide scale into the bulk material. These regions of increased oxidation damage showed semicircular or long semicircular surface flaw morphologies. The critical flaw sizes calculated from the measured fracture toughness and strength values using a Y parameter of 1.99 (long semicircular surface flaws) were consistent with the depth of oxidation damage that was observed. For example, at 1400°C calculated critical flaw size is 18.9 ±

2.0 μm, similar to the measured total oxide scale thickness of 16.7 ± 2.1 μm observed in Figure 7d.

Eliminating the critical flaws could result in ZrB_2-SiC ceramics with improved strength. Below 1200°C, SiC clusters were the strength-limiting flaws. The formation of SiC clusters could be caused by two mechanisms: (1) insufficient dispersion of the powders during processing; and (2) a volume fraction of reinforcing phase that is at or above the percolation threshold. Improved processing methods are needed to ensure more uniform dispersion of the SiC reinforcing phase. He et al. conducted computer modeling of particle packing in two phase systems to determine the effect of particle size ratio and volume fraction of additives on percolation threshold.[50] Using the model of He et al., the percolation threshold for the present system is ~25 vol% SiC, which is consistent with the observation of large clusters of SiC in the microstructures of the specimens. The model suggests that the tendency to form SiC clusters could be reduced by using a SiC powder that has a larger particle size than the ZrB_2 powder or by reducing the volume fraction of SiC. Increasing the starting particle sizes should also reduce creep, which could also improve the elevated temperature strength and stiffness of ZrB_2-SiC. Talmy et al. showed that decreasing the amount of SiC, or increasing the grain size of SiC, improved the creep resistance.[40] Watts et al. showed that a SiC cluster size above 11.5 μm caused spontaneous microcracking in ZrB_2-30vol% SiC, and that increasing the SiC particle size up to this point gradually reduced strength.[12] Therefore, a ZrB_2 based ceramic containing between 15 and 20 vol% SiC and minimal residual

sintering additives that had a maximum SiC particle size just below 11.5 μm could produce a ceramic that was stronger and more creep resistant at elevated temperatures.

Summary

The flexure strength, fracture toughness, and elastic modulus were measured for a ZrB_2-SiC ceramic as a function of temperature. ZrB_2 containing nominally 30 vol% SiC was hot pressed to full density at 1950°C using B_4C as a sintering aid. The ZrB_2 had an average grain size of ~1.9 μm while SiC had a particle size of ~1.2 μm, but a maximum cluster size of ~59 μm. The SiC cluster size led to spontaneous microcracking in the ceramic, which reduced the room temperature strength and modulus compared to similar materials that were not microcracked. The elastic modulus was ~510 GPa at room temperature, but decreased with increasing temperature to ~210 GPa at 1500°C and ~110 GPa at 1600°C. The room temperature strength was ~680 MPa. The strength increased to ~750 MPa at 800°C and decreased ~380 MPa at 1600°C. The fracture toughness was 3.6 $MPa \cdot m^{½}$ at room temperature and increased to 4.8 $MPa \cdot m^{½}$ at 800°C, but decreased to 3.3 $MPa \cdot m^{½}$ at 1600°C. Analysis of the critical flaw sizes indicated that SiC clusters were the critical flaws between room temperature and 1000°C, with oxidation damage being the critical flaw at temperatures above 1200°C. Improved dispersion of SiC, reducing the amount of SiC, reducing the amount of residual B_4C sintering aid, and increasing the SiC and ZrB_2 grain sizes would be expected to improve the strength and creep resistance of ZrB_2-SiC ceramics. Improvements to the oxidation resistance or

coatings to reduce oxide scale penetration in these materials could offer the most benefit for improved strength at elevated temperatures in air.

Acknowledgements

Research at Missouri S&T was supported by the High Temperature Aerospace Materials Program (Dr. Ali Sayir, program manager) in the Air Force Office of Scientific Research through grant FA9550-09-1-0168.

References

[1] Fahrenholtz WG, Hilmas GE, Talmy IG, Zaykoski JA. Refractory diborides of zirconium and hafnium. *J. Am. Ceram. Soc.* 2007;**90**(5):1347-64.

[2] Rahman M, Wang CC, Chen W, Akbar SA, Mroz C. Electrical resistivity of titanium diboride and zirconium diboride. *J. Am. Ceram. Soc.* 1995;**78**(5):1380-2.

[3] Zimmerman JW, Hilmas GE, Fahrenholtz WG, Dinwiddie RB, Porter WD, Wang H. Thermophysical properties of ZrB_2 and ZrB_2-SiC ceramics. *J. Am. Ceram. Soc.* 2008;**91**(5):1405-11.

[4] Mishra SK, Das S, Das SK, Ramachandrarao P. Sintering studies on ultrafine ZrB_2 powder produced by a self-propagating high-temperature synthesis process. *J. Mater. Res.* 2000;**15**(11):2499-504.

[5] Jin ZJ, Zhang M, Guo DM, Kang RK. Electroforming of copper/ZrB_2 composite coating and its performance as electro-discharge machining electrodes. *Key Eng. Mater.* 2005;**291-292**:537-42.

[6] Sung J, Goedde DM, Girolami GS, Abelson JR. Remote-plasma chemical vapor deposition of conformal ZrB_2 films at low temperature: A promising diffusion barrier for ultralarge scale integrated electronics. *J. Appl. Phys.* 2002;**91**(6):3904-11.

[7] Murata Y, "Cutting tool tips and ceramics containing hafnium nitride and zirconium diboride." in., U. S., 1970.

[8] Chamberlain AL, Fahrenholtz WG, Hilmas GE. Low-temperature densification of zirconium diboride ceramics by reactive hot pressing. *J. Am. Ceram. Soc.* 2006;**89**(12):3638-45.

[9] Opeka MM, Talmy IG, Zaykoski JA. Oxidation-based materials selection for 2000°C + hypersonic aerosurfaces: Theoretical considerations and historical experience. *J. Mater. Sci.* 2004;**39**(19):5887-904.

[10] Chamberlain AL, Fahrenholtz WG, Hilmas GE. High strength ZrB_2-based ceramics. *J. Am. Ceram. Soc.* 2004;**87**(6):1170-2.

[11] Rezaie A, Fahrenholtz WG, Hilmas GE. Effect of hot pressing time and temperature on the microstructure and mechanical properties of ZrB_2-SiC. *J. Mater. Sci.* 2007;**42**(8):2735-44.

[12] Watts J, Hilmas GE, Fahrenholtz WG. Mechanical characterization of ZrB_2-SiC composites with varying sic particle sizes. *J. Am. Ceram. Soc.* 2011;**94**(12):4410-8.

[13] Zhu S, Fahrenholtz WG, Hilmas GE. Influence of silicon carbide particle size on the microstructure and mechanical properties of zirconium diboride-silicon carbide ceramics. *J. Eur. Ceram. Soc.* 2007;**27**:2077-83.

[14] Zhang SC, Hilmas GE, Fahrenholtz WG. Mechanical properties of sintered ZrB_2-SiC ceramics. *J. Eur. Ceram. Soc.* 2011;**31**:893-901.

[15] Fahrenholtz WG. Thermodynamic analysis of ZrB_2-SiC oxidation: Formation of a SiC-depeleted region. *J. Am. Ceram. Soc.* 2007;**90**(1):143-8.

[16] Rezaie A, Fahrenholtz WG, Hilmas GE. Evolution of structure during the oxidation of zirconium diboride-silicon carbide up to 1500°C. *J. Eur. Ceram. Soc.* 2007;**27**:2495-501.

[17] Rezaie A, Fahrenholtz WG, Hilmas GE. Oxidation of zirconium diboride-silicon carbide at 1500°C at a low partial pressure of oxygen. *J. Am. Ceram. Soc.* 2006;**89**(10):3240-5.

[18] Rhodes WH, Clougherty EV, Kalish D. Research and development of refractory oxidation-resistant diborides Part II, Volume IV: Mechanical properties. Technical Report AFML-TR-68-190, Part II, Volume IV. Air Force Materials Laboratory, Air Force Systems Command: Wright Patterson Air Forse Base, OH; 1970.

[19] Zhu S. Densification, microstructure, and mechanical properties of zirconium diboride based ultra-high temperature ceramics [Ph.D. Thesis]. Rolla, MO. Missouri University of Science and Technology; 2008.

[20] Sciti D, Monteverde F, Guicciardi S, Pezzotti G, Bellosi A. Microstructure and mechanical properties of ZrB_2-$MoSi_2$ ceramic composites produced by different sintering techniques. *Mater. Sci. Eng., A* 2006;**434**:303-9.

[21] Sciti D, Silvestroni L, Celotti G, Melandri C, Guicciardi S. Sintering and mechanical properties of ZrB_2-$TaSi_2$ and HfB_2-$TaSi_2$ ceramic composites. *J. Am. Ceram. Soc.* 2008;**91**(10):3285-91.

[22] Monteverde F, Guicciardi S, Bellosi A. Advances in microstructure and mechanical properties of zirconium diboride based ceramics. *Mater. Sci. Eng., A* 2003;**346**:310-9.

[23] Loehman R, Corral E, Dumm HP, Kotula P, Tandon R. Ultra high temperature ceramics for hypersonic vehicle applications. SAND 2006-2925. Sandia National Laboratories: Albuquerque, NM; 2006.

[24] Melendez-Martinez JJ, Dominquez-Rodriguez A, Monteverde F, Melandri C, Portu GD. Characterization and high temperature mechanical properties of zirconium diboride-based materials. *J. Eur. Ceram. Soc.* 2002;**22**:2543-9.

[25] Grigoriev ON, Galanov BA, Kotenko VA, Ivanov SM, Koroteev AV, Brodnikovsky NP. Mechanical properties of ZrB_2–SiC($ZrSi_2$) ceramics. *J. Eur. Ceram. Soc.* 2010;**30**(11):2173-81.

[26] Silvestroni L, Sciti D. Effects of $mosi_2$ additions on the properties of Hf- and Zr-B_2 composites produced by pressureless sintering. *Scripta Mater.* 2007;**57**:165-8.

[27] Magley DJ, Winholtz RA, Faber KT. Residual stresses in a two-phase microcracking ceramic. *J. Am. Ceram. Soc.* 1990;**72**(6):1641-44.

[28] Tvergaard V, Hutchinson JW. Microcracking in ceramics induced by thermal expansion or elastic anisotropy. *J. Am. Ceram. Soc.* 1988;**71**(3):157-66.

[29] Touloukian YS, Ho C, Dewitt D. In: Touloukian, editor. Vol. 13, *Thermal expansion: Nonmetallic solids*: New York: IFI/Plenu; 1977.

[30] Tsagareishvili GV, Nakashidze TG, Jobava JS, Lomidze GP, Khulelidze DE, Tsagareishvili DS, et al. Thermal expansion of boron and boron carbide. *Journal of the Less Common Metals.* 1986;**117**(1–2):159-61.

[31] Watts J, Hilmas G, Fahrenholtz WG, Brown D, Clausen B. Stress measurements in ZrB_2–SiC composites using raman spectroscopy and neutron diffraction. *J. Eur. Ceram. Soc.* 2010;**30**(11):2165-71.

[32] Watts J, Hilmas GE, Fahrenholtz WG, Brown D, Clausen B. Measurement of thermal residual stresses in ZrB_2-SiC composites. *J. Eur. Ceram. Soc.* 2011;**31**(9):1811-20.

[33] Zhu S, Fahrenholtz WG, Hilmas GE, Zhang SC. Pressureless sintering of zirconium diboride using boron carbide and carbon additions. *J. Am. Ceram. Soc.* 2007;**90**(11):3660-3.

[34] Zhang SC, Hilmas GE, Fahrenholtz WG. Pressureless densification of zirconium diboride with boron carbide additions. *J. Am. Ceram. Soc.* 2006;**89**(5):1544-50.

[35] Kalish D, Clougherty EV, Kreder K. Strength, fracture mode, and thermal stress resistance of HfB_2 and ZrB_2. *J. Am. Ceram. Soc.* 1969;**52**(1):30-6.

[36] Chen I-W, Liu S-Y, Jacobs D. Effects of temperature, rate, and cyclic loading on the strength and toughness of monolithic ceramics. *Acta. Metall. Mater.* 1995;**43**(4):1439-46.

[37] Chakraborty D, Mukhopadhyay AK. High temperature young's modulus of reaction-bonded Si_3N_4, liquid phase sintered si_3n_4 and sialon. *Ceram. Int.* 1988;**14**:127-32.

[38] Wachtman JB, Lam DG. Young's modulus of refractory materials as a function of temperature. *J. Am. Ceram. Soc.* 1959;**42**(5):254-60.

[39] Stavrolakis JA, Norton FH. Measurement of the torsion properties of alumina and zirconia at elevated temperatures. *J. Am. Ceram. Soc.* 1950;**33**(9):263-8.

[40] Talmy IG, Zaykoski JA, Martin CA. Flexural creep deformation of ZrB_2/SiC ceramics in oxidizing atmosphere. *J. Am. Ceram. Soc.* 2008;**91**(5):1441-7.

[41] Evans AG, Faber KT. Crack-growth resistance of microcracking brittle materials. *J. Am. Ceram. Soc.* 1984;**67**(4):255-60.

[42] Evans AG, Fu Y. Some effects of microcracks on the mechanical properties of brittle solids–II. Microcrack toughening. *Acta Metall.* 1985;**33**(8):1525-31.

[43] Rice RW, Freiman SW, Becher PF. Grain-size dependence of fracture energy in ceramics: I. Experiment. *J. Am. Ceram. Soc.* 1981;**64**(6):345-50.

[44] Rice RW, Freiman SW. Grain-size dependence on fracture energy in ceramics: II. A model for noncubic materials. *J. Am. Ceram. Soc.* 1981;**64**(6):350-4.

[45] Mussler B, Swain MV, Claussen N. Dependence of fracture toughness of alumina on grain size and test technique. *J. Am. Ceram. Soc.* 1982;**65**(11):566-72.

[46] Evans AG, Faber KT. Toughening of ceramics by circumferential microcracking. *J. Am. Ceram. Soc.* 1981;**64**(7):394-8.

[47] Rose LRF. Effective fracture toughness of microcracked materials. *J. Am. Ceram. Soc.* 1986;**69**(3):212-4.

[48] Kaur S, Shetty DK, Cutler RA. R curves and crack-stability map: Application to Ce-TZP/Al_2O_3. *J. Am. Ceram. Soc.* 2007;**90**(11):3554-8.

[49] Wachtman JB. Mechanical properties of ceramics. New York, NY: John Wiley & Sons, Inc.; 1996.

[50] He D, Ekere NN. Effect of particle size ratio on the conducting percolation threshold of granular conductive–insulating composites. *J. Phys. D: Appl. Phys.* 2004;**37**(13):1848.

[51] Hu P, Wang Z. Flexure strength and fracture behavior of ZrB_2-SiC ultra-high temperature ceramic composites at 1800°C. *J. Eur. Ceram. Soc.* 2010;**30**(4):1021-6.

Table I. Elevated temperature mechanical properties of ZrB_2 - 30 vol% SiC. Number of samples tested given in parenthesis.

Temperature (°C)	**Strength (MPa)**	**Modulus (GPa)**	**Toughness (MPa·m^{½})**
RT	682 ± 98 (9)	513 ± 24	4.9 ± 0.4 (6)
800	754 ± 99 (9)	432 ± 17	4.8 ± 0.2 (3)
1000	726 ± 68 (10)	408 ± 26	4.5 ± 0.2 (4)
1200	521 ± 107 (10)	326 ± 66	3.9 ± 0.2 (4)
1400	439 ± 41 (8)	247 ± 17	3.8 ± 0.2 (4)
1500	359 ± 23 (5)	209 ± 21	4.6 ± 0.6 (5) 3.5 ± 0.4 (3)†
1600	384 ± 42 (5)	110 ± 14	3.3 ± 0.2 (5)

† Measured by failure analysis

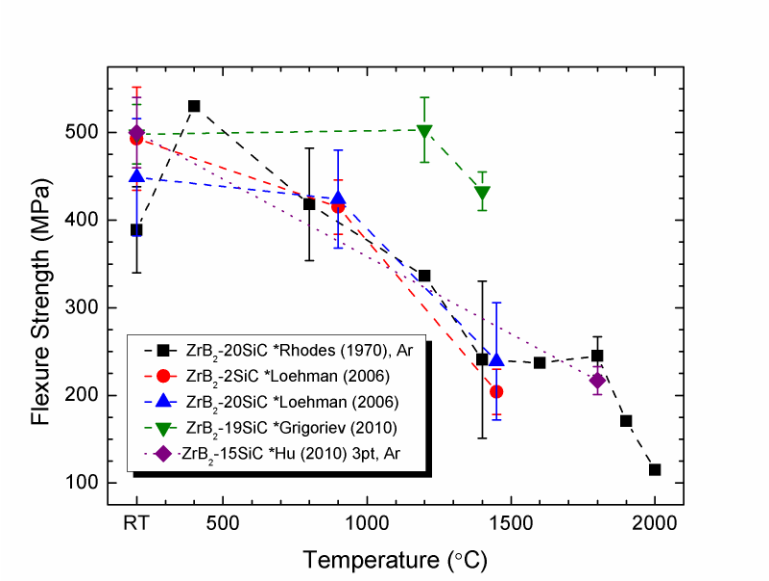

Figure 1. Summary of the strength of ZrB_2-SiC ceramics at elevated temperature from selected studies.[18, 23, 25, 51] Tests were performed using 4-pt flexure in air unless noted.

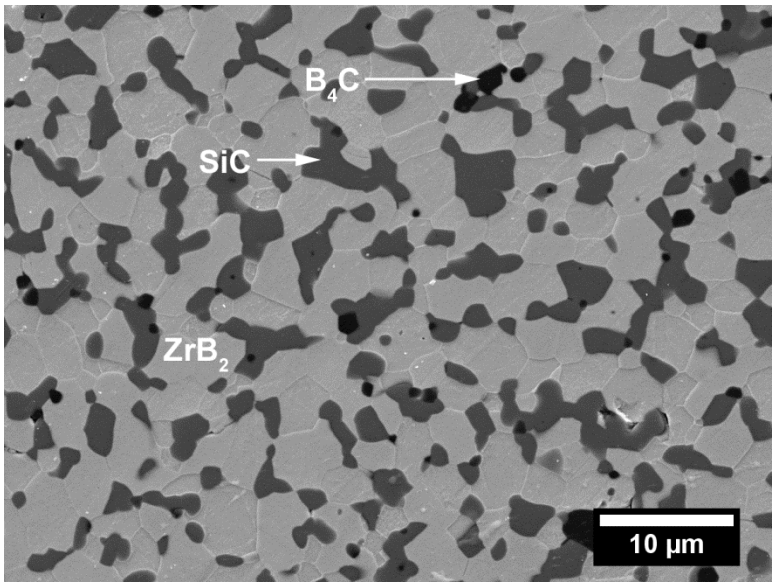

Figure 2. SEM image of a polished and chemically etched cross-section of ZrB_2-30SiC.

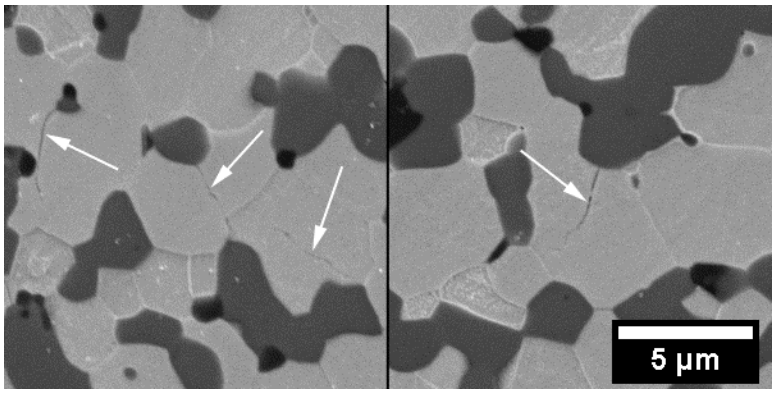

Figure. 3. SEM images of chemically etched cross sections of ZrB_2-30SiC with arrows showing microcracking.

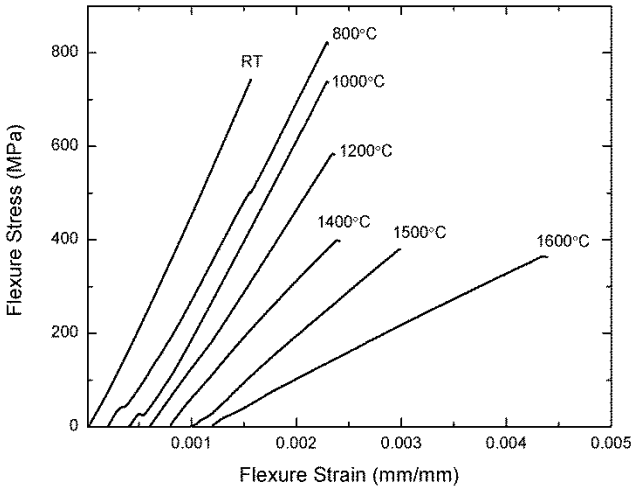

Figure 4. Stress versus strain curves for ZrB_2-30SiC tested in air atmosphere for various temperatures.

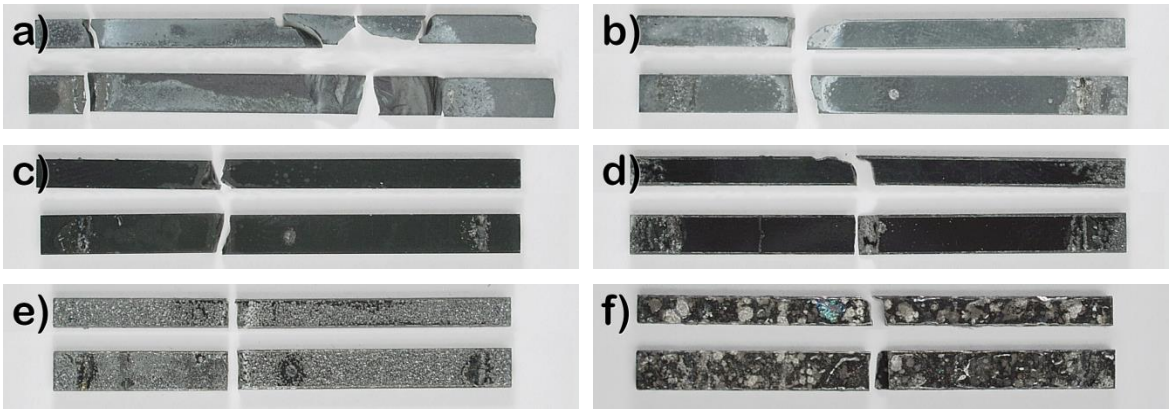

Figure 5. Optical macrographs of ZrB_2-30SiC flexure bars fractured at a) 800°C, b) 1000°C, c) 1200°C, d) 1400°C, e) 1500°C, and f) 1600°C in air. Each image shows the side (top) and tensile surface (bottom) of each bar. The bars are approximately 50 mm in length.

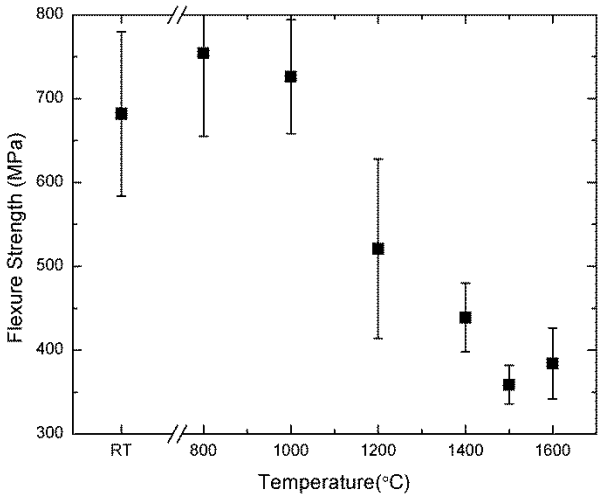

Figure 6. Four-point flexure strength of ZrB_2-30SiC tested in air atmosphere as a function of temperature.

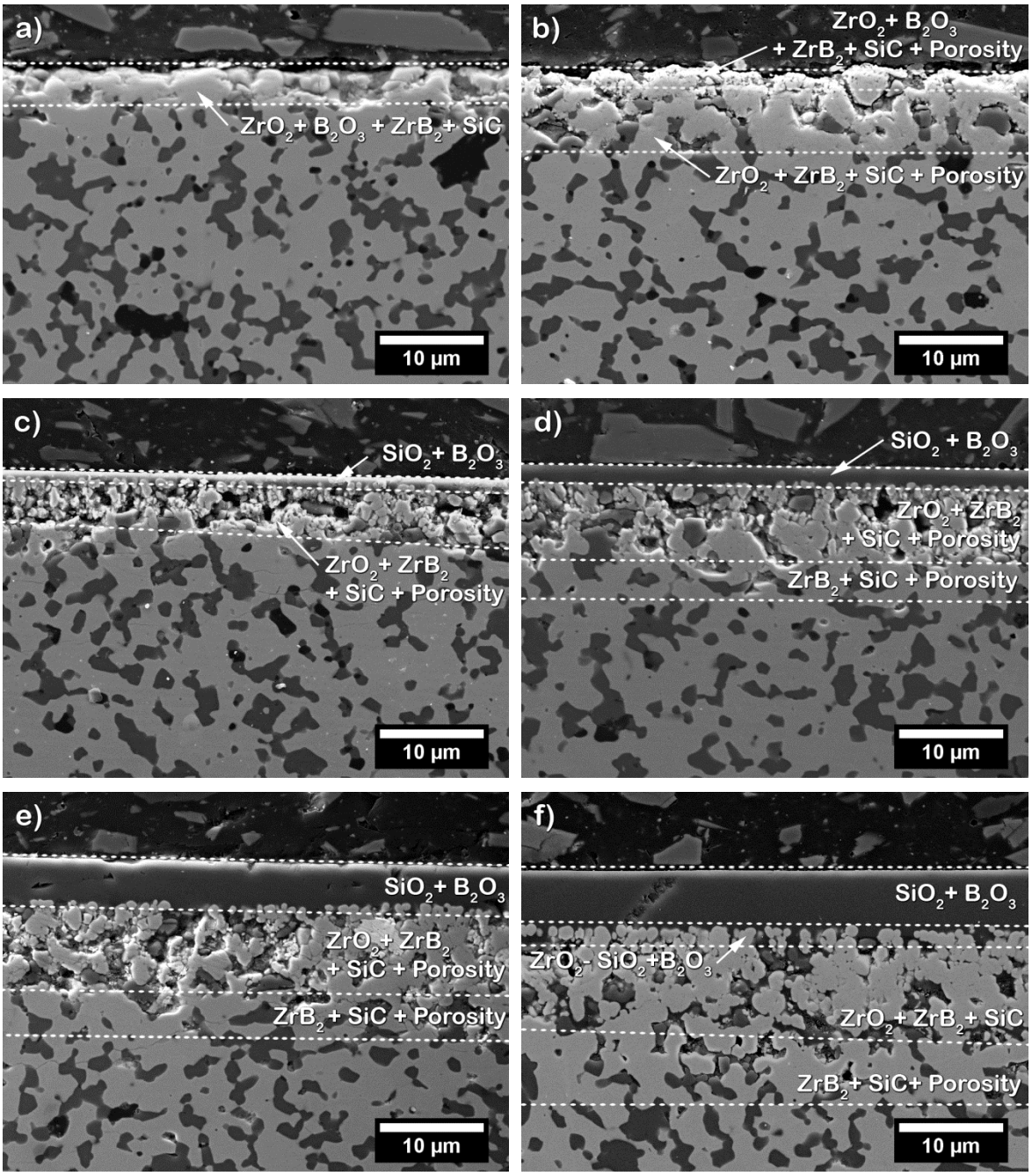

Figure 7. Cross sectional SEM images of the tensile surface of test bars of ZrB_2-30SiC after four-point flexure testing at various temperatures in air atmosphere: (a) 800°C; (b) 1000°C; (c) 1200°C; (d) 1400°C; (e) 1500°C; (f) 1600°C

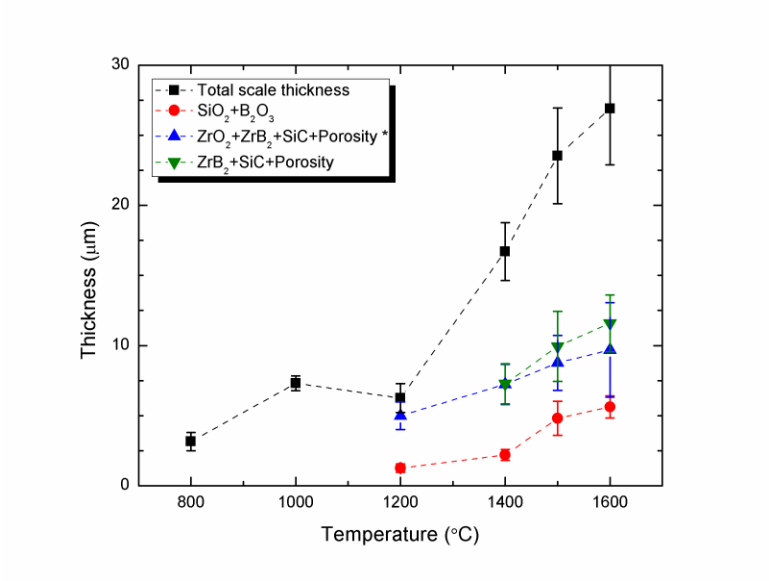

Figure 8. Measured layer thicknesses of ZrB_2-30vol% SiC oxidation scale following mechanical testing between 800°C and 1600°C. *Combines thickness of ZrO_2-SiO_2+B_2O_3 and ZrO_2+ZrB_2+SiC layers at 1600°C. Only the total thickness is reported for 800°C and 1000°C.

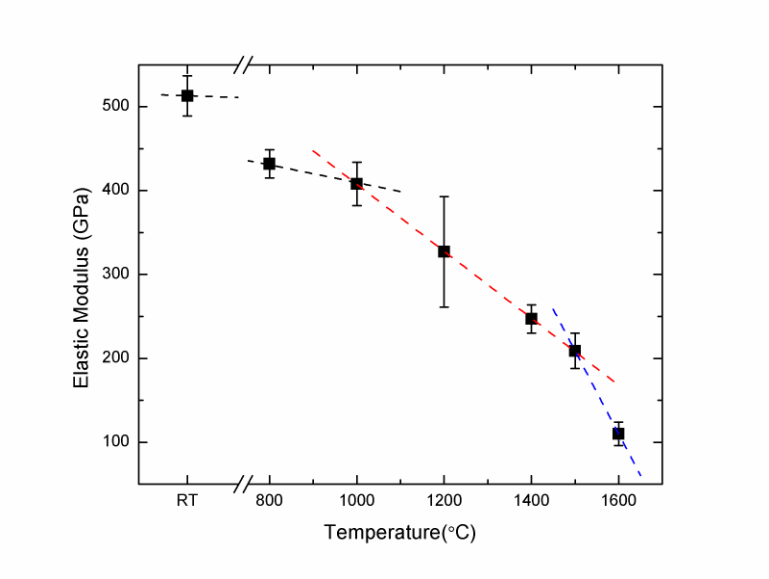

Figure 9. Elastic modulus of ZrB_2-30SiC tested in air atmosphere as a function of temperature. Dashed lines show the linear trend for the three modulus regimes.

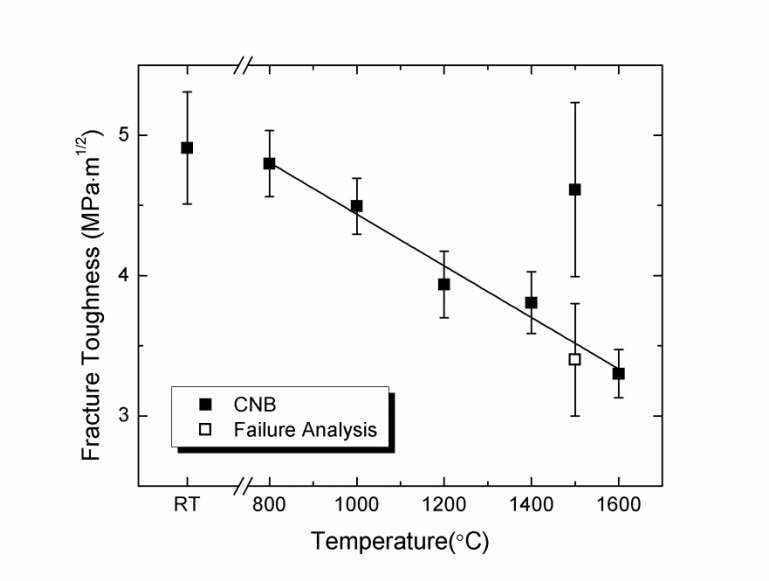

Figure 10. Chevron notch beam, in four point flexure, fracture toughness of ZrB_2-30SiC tested in air atmosphere as a function of temperature.

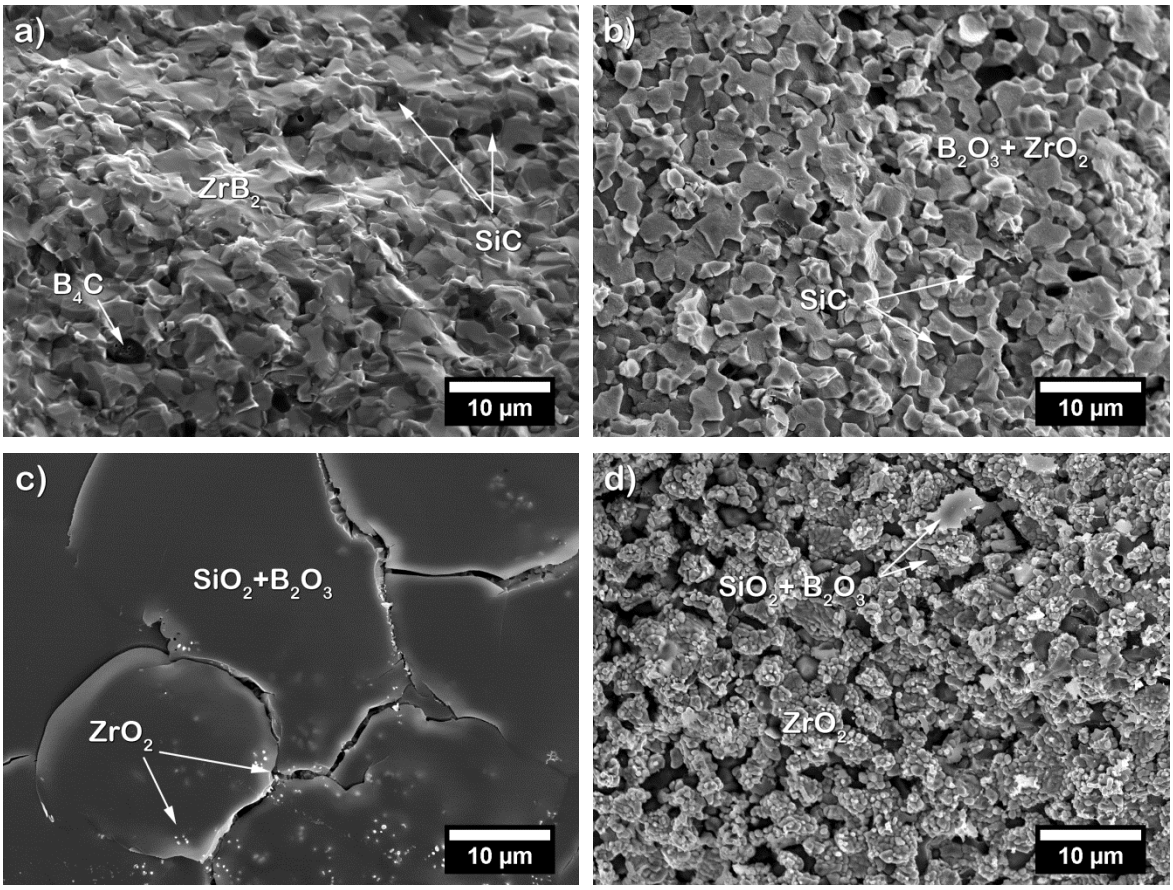

Figure 11. SEM images showing the fracture surface of ZrB_2-30SiC in air at a) room temperature and b) 800°C. A fractured glassy surface layer with interspersed submicron ZrO_2 islands forms beginning at c) 1000°C. Above d) 1400°C, the glassy layer becomes discontinuous, forming macroscopic ZrO_2 islands that grow in size with temperature.

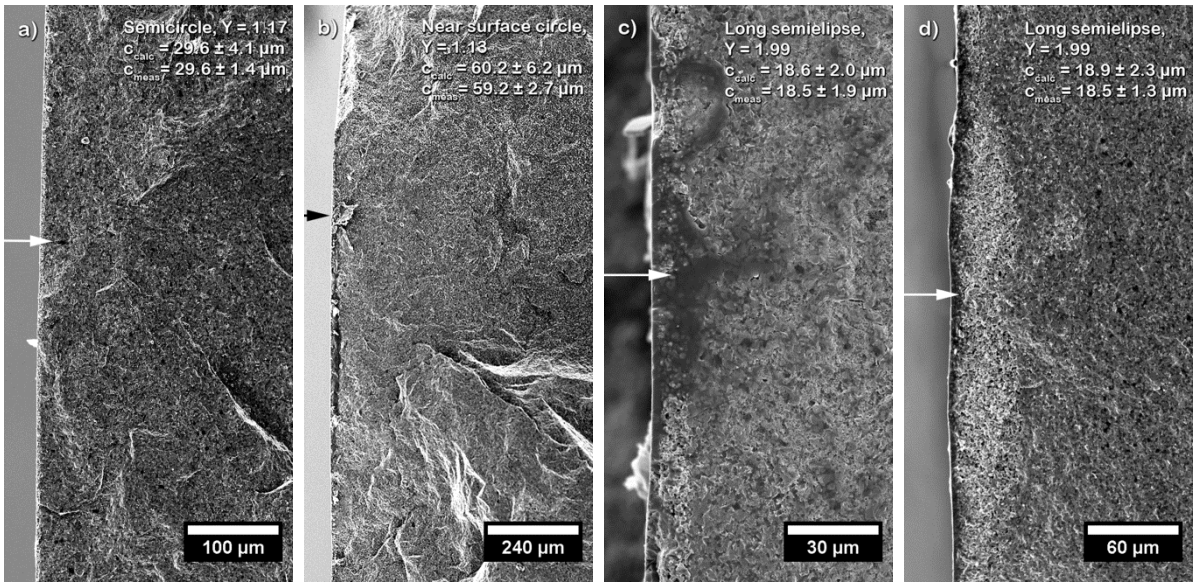

Figure 12. SEM images of the fracture surfaces of a) 800°C, b) 1000°C, c) 1400°C, and d)1600 test bar fragments broken at room temperature in 3-point flexure. The failure origin is marked by the arrow, and the calculated and measured flaw size for each specimen is given.

III. MECHANICAL BEHAVIOR OF ZIRCONIUM DIBORIDE-SILICON CARBIDE CERAMICS UP TO 2200°C

Eric W. Neuman, Gregory E. Hilmas, William G. Fahrenholtz

Department of Materials Science and Engineering, Missouri University of Science and Technology Rolla, MO 65409 USA

Abstract

The mechanical properties of zirconium diboride-silicon carbide (ZrB_2-SiC) ceramics were characterized from room temperature up to 2200°C in an argon atmosphere. ZrB_2 containing 30 vol% SiC was hot pressed to full density at 1950°C using B_4C as a sintering aid. After hot pressing, the composition was determined to be 68.5 vol% ZrB_2, 29.5 vol% SiC, and 2.0 vol% B_4C using image analysis. The average ZrB_2 grain size was 1.9 μm. The SiC particles segregated into larger clusters that were 4.4 ± 4.2 μm, with the largest clusters in excess of 30 μm in diameter. The room temperature flexural strength was 700 MPa and strength decreased to 540 MPa at 1800°C, further decreasing to 260 MPa at 2200°C. The elastic modulus at room temperature was 510 GPa, steadily decreasing with temperature to 340 GPa at 1800°C, with a more rapid decrease to 160 GPa at 2200°C. The fracture toughness was 4.9 MPa·$m^{½}$ at room temperature, decreasing to 4.0 and 3.5 MPa·$m^{½}$ at 2000°C and 2200°C. The strength was controlled by the SiC cluster size up to 1800°C. At higher

temperatures, strength was controlled by formation of liquid phases, and precipitation of large BN and B-O-C-N inclusions within the microstructure.

Keywords: zirconium diboride, silicon carbide, hot pressing, mechanical properties, failure analysis

1. Introduction

Zirconium diboride (ZrB_2) is member of a class of materials known as ultra-high temperature ceramics (UHTCs), characterized by melting points in excess of 3000°C.[1] Borides generally exhibit higher thermal conductivities (60-125 $W\cdot(m\cdot K)^{-1}$) and lower electrical resistivity (7.8 – 22 μΩ·cm) at room temperature compared to carbide or nitride ceramics.[2, 3] Borides also exhibit resistance to chemical attack.[4] These properties have made borides candidates for a range of applications including molten metal crucibles,[5, 6] furnace electrodes,[5] cutting tools,[7, 8] and wing leading edges on future hypersonic aerospace vehicles.[9, 10] Additionally, ZrB_2 based particulate composites, especially those with silicon carbide (SiC) additives, display enhanced mechanical properties. ZrB_2-SiC composites have demonstrated room temperature strengths in excess of 1000 MPa,[11-13] fracture toughness as high as 5.5 $MPa\cdot m^{½}$,[11, 12, 14] and hardness exceeding 22 GPa.[9, 11, 13] Chamberlain et al. showed that the room temperature strength increased from 565 MPa for nominally pure ZrB_2 to over 1000 MPa with the addition of 20 or 30 vol% SiC.[11] Similarly, the fracture toughness increased from 3.5 $MPa\cdot m^{½}$ for ZrB_2 to 5.3 $MPa\cdot m^{½}$ with 30 vol% SiC. Chamberlain measured the modulus of hot pressed

ZrB_2 as 489 GPa, which decreased to 484 GPa with the 30 vol% SiC addition.[11] These studies showed that the addition of SiC not only increased strength, fracture toughness, and hardness, but also influenced the oxidation rate of ZrB_2 by forming a silica rich oxide layer on the surface, slowing the rate of oxidation of the underlying material.[15-17] These properties have resulted in ZrB_2-SiC composites being investigated for aerospace applications related to hypersonic flight.

Previous studies have shown that the strength of ZrB_2-SiC composites generally decreases above about ~800°C.[18-23] Figure 1 summarizes previous studies of the strength of ZrB_2-SiC ceramics at elevated temperatures. Rhodes et al. reported the strengths in argon for hot pressed ZrB_2-20 vol% SiC up to 2000°C in argon in 1970.[18] They reported the strength of ZrB_2-20 vol% SiC to be 390 MPa at room temperature, decreasing to ~240 MPa at 1400°C to 1800°C, and 115 MPa at 2000°C. More recent studies have reported the elevated temperature strengths of ZrB_2-SiC ceramics up to 1600°C.[20-24] While these studies used ceramics with higher room temperature strengths, which are more representative of current UHTCs, the ceramics included nitride or disilicide additives as sintering aids. For example, Monteverde et al. reported that a 4 wt% addition of Si_3N_4 to ZrB_2-20 vol% SiC could produce a ceramic with a room temperature strength of 730 MPa, but the strength dropped to 250 MPa at 1200°C.[20] Loehman et al. examined ZrB_2-20vol% SiC with a room temperature strength of 450 MPa that decreased to 240 MPa at 1450°C.[21] Grigoriev et al. reported the strength of ZrB_2-19 vol% SiC in air to be ~500 MPa up to 1200°C

and 430 MPa at 1400°C.[24] Zou et al. reported the strengths of ZrB_2-20 vol% SiC, tested in an argon atmosphere, with[23] and without[22] additions of 5 vol% WC. For ZrB_2-20SiC, the strength was reported to increase from 550 MPa at ambient to 680 MPa at 1000°C, decreasing to 460 MPa at 1600°C. ZrB_2-20SiC-5WC showed the greatest retained strength at elevated temperature, increasing from 605 MPa at room temperature to 675 MPa at 1600°C. This enhancement in strength was attributed to the removal of surface oxides from the starting powders (ZrB_2 and SiC) by reaction with WC during sintering.

Studies of other elevated temperature mechanical properties of ZrB_2 based ceramics, such as elastic modulus and fracture toughness, have been limited. Rhodes evaluated the elastic modulus in argon up to 2100°C for ZrB_2 and up to 2000°C for ZrB_2-20vol% SiC.[18] Zhu reported the modulus of ZrB_2 and ZrB_2 with B_4C and C additions up to 1500°C in air.[19] Rhodes reported a modulus of ~520 GPa for ZrB_2-20 vol% SiC at room temperature, decreasing to 445 GPa at 1400°C and 106 GPa at 1600°C. Zou measured the modulus of ZrB_2-20 vol% SiC up to 1300°C.[22] The modulus was ~505 GPa at ambient, linearly decreasing to ~480 at ~780°C, and decreasing more rapidly to ~445 GPa at 1300°C. The change in trend occurring at 780°C was attributed to the softening of oxide phases present in the microstructure. Based on these recent studies, strength data for ZrB_2 based ceramics have not been measured systematically at regular temperature intervals, nor have they been tested at the temperatures proposed for applications such as hypersonic flight (i.e., >2000°C). Most studies have

report strength at room temperature and 1200°C with 1400, 1500, or 1600°C as the highest reported test temperature.

Typical of brittle materials, the strength of ZrB_2-SiC ceramics is controlled by the largest flaws present in the microstructure. SiC inclusions have been identified as the critical flaw in dense, fine grained ZrB_2-SiC.[12-14] At some critical level of thermal expansion mismatch and cluster size, spontaneous microcracking of the matrix can occur.[13, 25, 26] The CTE mismatch between ZrB_2 (~5.2 ppm/K at 298 K),[1, 27] SiC (~3.3 ppm/K at 298 K)[27] and B_4C (~5.7 ppm/K from 300-1970K)[28] results in residual compressive stress in the SiC and tensile stresses in the ZrB_2 matrix and B_4C reinforcing phase. Watts reported a decrease in hardness (21 to 18 GPa) with a maximum SiC cluster size of 11.5 μm, a result of stress induced microcracking.[13] Watts directly measured the residual stresses that accumulate in ZrB_2-30vol% SiC upon cooling, compressive stresses of 880 MPa in the SiC phase and tensile stresses of 450 MPa in the ZrB_2 matrix phase, prior to the onset of microcracking.[29, 30] The residual stresses began to accumulate at ~1400°C upon cooling and that the maximum stress occurs at the ZrB_2-SiC interface with stress decreasing with distance from the interface.

Previous work on the material of this study investigated the mechanical behavior up to 1600°C in air.[31] The strength was reported to increase from 680 MPa to 750 MPa between room temperature and 800°C, decreasing to 385 MPa at 1600°C. The elastic modulus at room temperature was 510 GPa, decreasing to 325 GPa at 1000°C, decreasing to 110 GPa at 1600°C. The fracture

toughness was 4.9 MPa·$m^{½}$ at room temperature, 4.8 MPa·$m^{½}$ at 800°C, decreasing linearly to 3.3 MPa·$m^{½}$ at 1600°C. Strength was controlled by the largest SiC clusters up to 1000°C, and oxidation damage above 1200°C. The purpose of this paper is to investigate the mechanical properties of a ZrB_2-30 vol% SiC ceramic for temperatures up to 2200°C. Testing was performed in an argon atmosphere to minimize extrinsic effects on strength (i.e., oxidation damage). The role of microstructure on the mechanical properties was examined.

2. Experimental Procedure

2.1. Processing

The material used for this study was processed as described previously.[31] The ZrB_2 powder (Grade B, H.C. Starck, Newton, MA) had a reported purity of 98.2% and a particle size of 2 μm. The SiC powder (Grade UF-10, H.C. Starck) was predominantly α-SiC, having a reported purity of 98.5% and a particle size of 0.7 μm. The B_4C powder (Grade HD-20, H.C. Starck) had a reported purity of 97.6%, and a particle size of 0.5 μm. The powders were batched in the ratio of 70 vol% ZrB_2 to 30 vol% SiC with a super addition of 2 wt% B_4C (ZrB_2 basis). The powders were ball milled in methyl ethyl ketone with WC-6Co media for 48 hours. Contamination from media erosion was 0.28 ± 0.04wt%. Following milling, the slurry was dried by rotary evaporation. The mixed powder was hot pressed at 1950°C for 10 min under an applied pressure of 32 MPa with isothermal holds at 1450°C and 1650°C used during heating to aid in the removal of surface oxides, discussed in more detail elsewhere.[32, 33]

2.2. Characterization

Microstructures of specimens were examined following elevated testing using scanning electron microscopy (SEM; Helios Nanolab 600, FEI, Hillsboro, OR) equipped for energy dispersive spectroscopy (EDS; X-Max, Oxford Instruments, Abingdon, UK). The tensile surfaces of the specimens following testing were examined both as-tested and polished, and the fracture surfaces examined as-tested. The as-tested specimens were ultrasonically cleaned to remove furnace deposits. The polished specimens were initially plane ground using a diamond grinding wheel on a fully automated surface grinder (FSG-3A818, Chevalier, Santa Fe Springs, CA) to remove ~100 μm from the tensile surface. The specimens were then polished to a 0.05 μm finish using diamond abrasives and etched using molten KOH at 200°C for ~2 s to reveal the grain boundaries. ZrB_2 and SiC grain sizes were measured from SEM images using computerized image analysis (ImageJ, National Institutes of Health, Bethesda, MD). The grain size distribution of the ZrB_2 phase was estimated by fitting ellipses to at least 1000 grains of both ZrB_2. The SiC and B_4C cluster size distributions were determined from the polished cross sections by measuring the Feret's diameter of at least 2,000 clusters and fitting ellipses to at least 1,000 clusters, respectively.

2.3. Mechanical testing

Room temperature flexure strengths were measured in four-point bending using a fully-articulated test fixture using type-B bars (45 mm x 4 mm x 3 mm) according to ASTM C1161-02c. Flexure strength was measured at elevated

temperatures (1000, 1200, 1400, 1600, 1800, 2000, and 2200°C) using the same type-B bars and following the testing procedures outlined in ASTM C1211-08. Twenty specimens were tested at room temperature and a minimum of five specimens were tested at each elevated temperature. Bars were machined from the hot-pressed billets by diamond grinding. The flexure surface was polished to a 1 μm finish using diamond abrasives. Tests were performed using a screw-driven instrumented load frame (33R4204, Instron, Norwood, MA). Elevated temperature testing was performed in an environmental chamber using an induction heated graphite hot zone and load train, under a flowing argon atmosphere.[34] The heating profile was 100°C/min to 100°C below the test temperature, then 50°C/min to the test temperature, followed by a 5 min isothermal hold. The crosshead rate was varied with temperature (Table I) such that the load-displacement curve was linear to failure.

Room temperature elastic constants were determined by impulse excitation (MK4-I Grindosonic, J.W. Lemmens, St. Louis, MO) according to ASTM C1259-08. The static bend test method was used to determine the elevated temperature elastic modulus according to ASTM standard E111-04. The elastic modulus was calculated from the slope of the load displacement curves, with the beam displacement estimated from the crosshead displacement. A minimum of five measurements were averaged at each temperature to calculate the reported values.

Fracture toughness was measured by the chevron notch beam method in four-point bending using a fully articulated test fixture using chevron notch type-A

bars (45 mm x 3 mm x 4 mm) according to ASTM Standard C1421-01b. The chevron notch was machined using a dicing saw (Accu-cut 5200, Aremco Products, Ossining, NY) with a 0.006 in thick diamond wafering blade. The crosshead rate was varied with temperature (Table I). For elevated temperature testing, a heating rate of 50°C/min was used, followed by an isothermal hold of 5 min at the desired temperature. The notch dimensions were measured after testing using a digital microscope (KH-3000, Hirox-USA, Hackensack, NJ). Eight specimens were tested at room temperature, and a minimum of three specimens were tested at the same elevated temperatures used for flexure testing.

3. Results and discussion

The measured bulk densities of the hot-pressed specimens were 5.22 g/cm^3 and no porosity was observed in the microstructure using SEM. The composition following hot-pressing was determined to be 68.5 vol% ZrB_2, 29.5 vol% SiC, and 2.0 vol% B_4C by SEM image analysis. Figure 2a shows a typical cross section of a polished and etched specimen prior to testing. The ZrB_2 grain size was 2.99 ± 1.54 μm with a maximum observed grain size of 10.6 μm. The average SiC cluster size was 3.61 ± 3.40 μm with a maximum observed cluster size of 32.8 μm. The B_4C had an average cluster size of 0.97 ± 0.84 μm and a maximum observed size of 11.0 μm. The B_4C clusters were found to contain internal ZrB_2 and SiC grains, as well as entrapped porosity (Figure 3). The SiC formed large clusters because the amount of SiC present is greater than the percolation threshold, ~25 vol%, for the observed ZrB_2/SiC grain size ratio, 1.9/1.2 μm.[31]

Since the SiC cluster size is above the ~11.5 μm microcracking threshold for ZrB_2-SiC, microcracking was observed in the microstructure.[31]

3.1. Mechanical Properties

Measured values for the elastic modulus, flexure strength, and fracture toughness from room temperature to 2200°C are included in Table I, with typical load versus displacement curves shown in Figure 4. All specimens exhibited linear-elastic behavior to failure, and no creep was observed in the bars following fracture at elevated temperature (Figure 5). Figure 6 summarizes the flexural strength as a function of temperature. Changes to the grain and cluster sizes, following exposure to high temperature testing, are summarized in Table II. Based on the observed trends, the discussion below is divided into two temperature regimes: room temperature to 1800°C, and 1800°C to 2200°C.

In the first regime, strength decreased near linearly from ~700 MPa at room temperature to ~540 MPa at 1800°C. Unlike previous studies regarding ZrB_2-SiC, an increase in strength was not observed between room temperature and 1000°C. This increase in strength has been attributed to flaw healing by formation of a continuous oxide scale on the specimen surface, which is not observed in this material due to testing in an inert atmosphere.[19] However, an oxide layer was identified by EDS on the surface of ZrB_2 grains during up to temperatures of 1800°C (Figure 7). The formation of this oxide scale is a result of the low pO_2, estimated to be between 10^{-14} and 10^{-12} atm from the Zr-B-O phase stability diagram (Figure 7a).[35] A similar oxide scale has been reported during high temperature testing of ZrB_2-SiC in a flowing argon atmosphere by

Bird et al..[36, 37] Additionally, the microstructure, shown in Figure 2, remains relatively unchanged throughout this regime with an average and maximum ZrB_2 grain size of 3.0 and 11 μm, respectively. Similarly, the average and maximum SiC and B_4C cluster sizes were approximately 3.8 and 32, and 1 and 11 μm, respectively. Finally, the fracture surfaces in the tensile region of the flexure specimens are shown in Figure 8, with the measured fraction of intergranular fracture (IGF) in the ZrB_2 phase shown in Figure 9. The amount of IGF was observed to steadily increase from ~20% at ambient to ~95% at 2200°C. This is contrary to the behavior observed by Kalish et al.[38] who observed a decrease in IGF up to 700°C followed by a sudden increase at 1000°C for $ZrB_{1.89}$, and Bird et al.[36] who observed an increasing amount of IGF between ambient and 1400°C with a similar transition between 750°C and 1000°C.

In the second regime, strength decreased from ~540 to ~260 MPa between 1800°C and 2200°C. Again, an oxide scale is observed on the surface of ZrB_2 grains at 1800°C, but is no longer present at 2000°C and 2200°C, allowing the pO_2 of the test furnace to be estimated at between 10^{-14} and 10^{-12} atm. At these temperatures, a coating is still observed on the surface of the ZrB_2 grains; however, EDS identifies the constituents of the surface coating to be Zr, C, and B. Further, active oxidation can be observed in the SiC and B_4C phases. The SiC is expected to experience active oxidation under these conditions based on the work of Heuer and Lou.[39] The active oxidation of the B_4C phase is also expected since Lavrenko and Gogotsi showed that B_4C actively oxidizes above 1250°C in air through the evaporation of B_2O_3.[40] Active oxidation results in the

recession of SiC and B_4C grains at the surface of the specimen, effectively creating a porous surface layer, which is expected to reduce the measured strength. Further, while the average and maximum ZrB_2 grain size and B_4C cluster size remain unchanged, the average SiC cluster size increased slightly to ~4.1 μm and the maximum cluster size increased from ~32 μm at 1800°C, to ~38 and 47 μm at 2000°C and 2200°C. Since the largest SiC clusters are acting as flaws, increases in the size of the clusters will reduce the strength. Further, the formation of several additional solid and liquid phases is observed above 1800°C, which may affect the measured properties and will be discussed in more detail below. At these highest temperatures, additional phases, especially liquid phases, would be expected to enhance creep effects. As an example, liquid phases are known to enhance creep cavitation, leading to micro void coalescence, and a reduction in strength.[41] Finally, it is important to keep in mind that the reported eutectic for the ZrB_2-SiC system is ~2270°C;[42] further, the specimens also contain residual B_4C sintering aid, and that the ternary ZrB_2-SiC-B_4C eutectic would be expected to occur at an even lower temperature. This suggests that more liquid than otherwise expected at these temperatures could be present, resulting in a reduction of strength.

The elastic modulus decreased as temperature increased (Figure 10). At room temperature, the elastic modulus was 513 GPa, which is similar to the values reported by Zhu et al. (509-520 GPa)[18], Rezaie et al. (503-516 GPa)[16], and Watts et al. (505-520 GPa)[58] for ZrB_2-30 vol% SiC with a similar maximum SiC cluster size (13-11.8 μm).[13] The elastic modulus decreased nearly linearly to

~350 GPa at 1800°C, decreasing more rapidly to ~165 GPa at 2200°C. Similar temperature dependencies for modulus and strength have been observed for other oxide and non-oxide ceramics.[19, 43-46] Wachtman et al. showed that the elastic modulus of polycrystalline ceramics display a gradual linear decrease with increasing temperature in a low temperature range followed by a more rapid, non-linear decrease at higher temperatures.[45] Zhu et al. found a similar trend in ZrB_2, with a linear decrease up to ~1200°C followed by a more rapid decrease above this temperature.[19] Rhodes et al. observed a similar trend in the ZrB_2-20 vol% SiC system, where the modulus decreased slowly from ~530 GPa at room temperature to ~445 GPa at 1400°C, then experienced a rapid decrease to 1600°C to ~110 GPa.[18] This rapid decrease in modulus at elevated temperatures has been attributed primarily to grain boundary sliding and diffusional creep.[45] Zou et al. observed a similar decrease in modulus to ~480 GPa at 800°C from ~505 GPa at ambient, followed by a more rapid decrease to ~445 GPa at 1300°C.[22] In Zou's work, the change in the slope of the modulus at 800°C was attributed to the glass transition temperature of the $CaO{\cdot}SiO_2{\cdot}ZrO_2$ glassy phase that was observed in the microstructure. Similarly, the formation of new phases was observed in the present material following testing above 1800°C. These phases are discussed in more detail below, but are expected to have a lower modulus than ZrB_2-SiC, and thus result in a decrease in the calculated modulus of the bulk material.

Fracture toughness as a function of temperature is shown in Figure 11. At room temperature, the fracture toughness was 4.9 ± 0.7 $MPa{\cdot}m^{½}$, which is

similar to previously reported values ranging from 4.6 MPa·$m^{1/2}$ to 5.5 MPa·$m^{½}$ for ZrB_2-30 vol% SiC ceramics.[14, 16, 47] Toughness decreased steadily to 4.0 MPa·$m^{1/2}$ at 2000°C, and decreased further to 3.5 MPa·$m^{1/2}$ at 2200°C. The measured toughness at 1200°C, 4.2 MPa·$m^{1/2}$, is below the trend, and correlates with a decrease in modulus at the same temperature. From the Griffith formulation of fracture mechanics, K_{IC} can be written in terms of elastic modulus and surface energy.[48] Thus, the trend in toughness from room temperature to 2000°C may not be linear, and the decrease in toughness at 1200°C may simply be a result of a decrease in elastic modulus. Additionally, the decrease in toughness correlates well with the decrease in modulus up to 2200°C.

This decrease in toughness and modulus must be a result of changes in the microstructure and/or the stress state of the material. If a change in the internal stress state of the material was occurring, it might be expected to observe a discontinuous change in toughness around 1400°C, the stress relaxation temperature in ZrB_2-SiC as reported by Watts.[29] Improvements in the toughness of two-phase particulate ceramics have been shown to be a result of thermal residual stresses generated from the CTE mismatch between the phases upon cooling from processing temperatures.[48-50] Upon heating, these stresses are reduced and the toughness decreases.[50] In the present material, some amount of the residual stress has already been relieved by spontaneous matrix microcracking.[31] Thus, it is most likely that changes in the microstructure, and not changes in stress state, are resulting in the decrease in modulus and toughness with increasing temperature.

The room temperature values for strength and toughness were 695 ± 69 MPa and 4.9 ± 0.4 MPa·$m^{½}$. Compared to previous studies of ZrB_2-SiC, both are lower because of matrix microcracking. The critical flaw size was predicted for the material in this study using the Griffith criteria and a Y-parameter of $\pi^{½}$ (Table II). At room temperature, the predicted critical flaw size is 32 ± 6 μm. This is in agreement with the maximum measured SiC cluster size of 33 μm. Repeating the calculation results in critical flaw sizes of 30-40 μm between room temperature and 1600°C, 60 μm at 2200°C, and 120 μm at 2200°C. The measured maximum SiC cluster size is in reasonable agreement with the predicted flaw size up to 1800°C. However, the maximum SiC cluster size and predicted flaw size differ by a factor of two and four at 2000°C and 2200°C. This suggests that something other than the largest SiC clusters are acting as critical flaws at these temperatures.

3.2. Changes in Microstructure

Following testing at elevated temperatures, the specimens were polished to remove the any scale that formed on the surface of the bars during testing, and then examined to discover if any changes to the microstructure had occurred. The change in the ZrB_2 grain size, and SiC and B_4C cluster sizes, were discussed above. Of primary interest in this section is the presence of additional phases in the as-processed material, and the phases that form following further exposure to the testing temperatures.

First, the as-processed material contains several additional phases in addition to ZrB_2, SiC, and B_4C. There are two main additional phases. The first is

BN (not shown), and has been previously seen by numerous researchers in ZrB_2 based ceramics.[20, 22, 51, 52] Whereas the BN present in the material produced by Zou et al.[22] and Monteverde et al.[20, 52] is a primarily a result of Si_3N_4 contamination or additions, the BN in the present material, and that of Eakins,[51] is likely formed due to reaction with the nitrogen in the raw ZrB_2 powder (~0.25 wt% reported by the manufacturer). The second is a predominantly Fe-Co phase (Figure 12a) that also contains some O, W, and U. It may also contain some Zr, Si, and B, but is confounded by the interaction volume of the electron beam. This phase appears to have been liquid at the processing temperatures used. The Fe is present in the starting powders as a minor impurity (~0.1 wt% in ZrB_2, and ~ 0.05 wt% in SiC), along with the U as a trace impurity. The W and Co are introduced from wear of the WC-6Co grinding media, and whereas the W will enter into solid solution with the ZrB_2, the Co will not, instead forming an alloy with the Fe. From the Fe impurity in the raw powder, and the Co introduced by media wear, the Fe-Co phase comprises between 0.1-0.2 vol% of the microstructure. Finally there are small inclusions, less than several hundreds of nm, of varying combinations of Zr-Y-Al-O that are primarily at grain boundaries and triple junctions of ZrB_2, but also appear occasionally intragranular to ZrB_2. Finally, a boron rich silicon phase is present at the junctions of some SiC and B_4C grains, which appears to have been liquid at the processing temperature. These features remain unchanged through 1600°C.

At 1800°C, several new phases begin to appear. The first is another liquid phase (Figure 12b). It is composed primarily of varying combinations of primarily

Zr, Si, B, Y, Ca, Th, and various rare earths (RE; typically Ce, Nd, Gd) and sometimes containing O or C. The previously mentioned Fe-Co-U phase is still present as a separate phase. The previously mentioned Zr-Y-Al-O phases appear to be more numerous, and have also formed Zr-O and Y-Al-O features within the ZrB_2 grains (Figure 14). At 2200°C. the previously discussed liquid phases can be seen to corrode the ZrB_2, SiC, and B_4C grains that contact them (Figure 12c). Finally, various B-O-C-N phases (white arrows) begin to form starting at 1800°C (Figure 15a), along with additional BN inclusions (black arrows). By 2200°C these inclusions are ubiquitous in the microstructure, and exhibit themselves as large, over 10 μm in size, high aspect ratio BN grains in a chain like morphology (Figure 15b and c). These typically span the ZrB_2 matrix, linking previously separated SiC and B_4C clusters. If the B-O-C-N type phases link several SiC clusters, it is reasonable to assume the size of these cluster networks could reach the 60-120 μm range that is calculated as the critical flaw size based on the flexure strengths at 2000°C and 2200°C.

Fracture in ceramics at elevated temperature typically involves the nucleation, growth, and coalescence of microvoids.[41] Figure 16 shows typical cavity formation at 1200°C, 1600°C, 2000°C, and 2200°C. Etching was used to enhance the visibility of the cavities, and it is important to remember that as a result, the cavities shown are larger than they would otherwise be. The microstructure of the present study exhibits an equiaxed grain structure with no grain boundary phase, but with dispersed BN grains and an Fe-Co rich phase. Cavities are observed to form primarily at three and four grain junctions where

SiC, B_4C, BN, or Fe-Co phases are present up to 1800°C. There are few cavities observed at 1000°C, increasing in presence as the testing temperature increases. At 1800°C, cavities are also observed between grain boundaries, in addition to grain junctions. At 2000°C, the cavities span nearly the full length of grain boundaries between SiC, B_4C, and/or BN/B-O-C-N and ZrB_2. At 2200°C, cavitation is widespread and prevalent at every type of grain boundary and junction. Further, the size of cavities are 0.2 to 0.4 μm in size at 2000°C and 2200°C compared to temperatures below 1800°C, where they are typically only ~0.1 μm in size.

In these cases, cavities are presumed to nucleate predominantly near triple points as a result of grain boundary sliding, extending along grain boundaries until sufficient continuous boundaries have cavitated such that a microcrack develops, capable of self-extension to failure.[41, 53] The presence of amorphous/liquid phases assists in the cavity extension by providing enhanced atomic mobility and modifying the equilibrium condition at the cavity tip.[41] Below 1800°C, cavitation at the ZrB_2-SiC boundaries is a likely candidate for the formation of critical flaws that correlate with the largest SiC cluster sizes, as the crack formed is more likely to extend along the ZrB_2-SiC cluster boundary. In concert with the growth of large B-O-C-N phases with lower stiffness than the ZrB_2-SiC bulk, cavitation may lead to enhancing the critical flaw size in the material above 1800°C. It is the formation of these liquid phases, B-O-C-N type inclusions, and cavitation that are most likely contributing to the observed degradation in strength, modulus, and toughness at 2000°C and 2200°C.

4. Summary

The flexure strength, elastic modulus, and fracture toughness were measured for a ZrB_2-30 vol% SiC ceramics from room temperature to 2200°C. The material was hot pressed to full density at 1950°C using B_4C as a sintering aid. The average ZrB_2 grain size was 1.9 μm. The SiC particles segregated into larger clusters that were 4.4 ± 4.2 μm, with the largest clusters between 30 and 33 μm in diameter, resulting in matrix microcracking. The average ZrB_2 grain size and SiC cluster size remained relatively constant with testing temperature. The largest SiC clusters increased in size to 38 and 47 μm after testing at 2000°C and 2200°C. The room temperature flexural strength was 700 MPa, which steadily decreased to 540 MPa at 1800°C, further decreasing to 260 MPa at 2200°C. The elastic modulus at room temperature was 510 GPa, decreasing with temperature to 340 GPa at 1800°C, with a more rapid decrease to 160 GPa at 2200°C. The fracture toughness was 4.9 $MPa \cdot m^{½}$ at room temperature, decreasing to 4.0 and 3.5 $MPa \cdot m^{½}$ at 2000°C and 2200°C. Up to 1800°C, the critical flaw size in the material correlated with the maximum SiC cluster size. Analysis of the microstructure revealed the formation liquid phases and large B-O-C-N phase regions at the grain interfaces at temperature of 1800°C and above. The B-O-C-N phases were large enough at 2000°C and 2200°C to span the ZrB_2 matrix, linking SiC clusters. The proposed strength controlling features are the largest SiC clusters up to 1800°C, and the formation of various liquid phases and large B-O-C-N type inclusions above 1800°C. Reducing the amount of SiC present, and/or decreasing the ZrB_2/SiC grain size ratio, to below the

percolation threshold, should eliminate the microcracking caused by SiC percolation cluster and improve mechanical properties. Further, improvements in starting powder purity and processing methods are needed to enhance the properties at ultra-high temperatures. Reducing the amount of oxygen, nitrogen, and iron in the starting powders, and reducing contamination from milling media, could offer benefits in improving the mechanical properties at ultra-high temperatures.

Acknowledgements

The authors would like to thank Dr. Jeremy Watts for his assistance in the design and fabrication of the ultra-high temperature mechanical testing furnace. We would also like to thank Dr. Clarissa Wisner and Dr. Jessica Terbush of the Advanced Materials Characterization Laboratory at Missouri S&T for their assistance with SEM and TEM characterization. Research at Missouri S&T was supported by the High Temperature Aerospace Materials Program (Dr. Ali Sayir, program manager) in the Air Force Office of Scientific Research through grant FA9550-09-1-0168.

References

1. W. G. Fahrenholtz, G. E. Hilmas, I. G. Talmy, and J. A. Zaykoski, "Refractory Diborides of Zirconium and Hafnium," *J. Am. Ceram. Soc.,* **95** [5] 1347-64 (2007).
2. M. Rahman, C. C. Wang, W. Chen, S. A. Akbar, and C. Mroz, "Electrical Resistivity of Titanium Diboride and Zirconium Diboride," *J. Am. Ceram. Soc.,* **78** [5] 1380-82 (1995).
3. J. W. Zimmerman, G. E. Hilmas, W. G. Fahrenholtz, R. B. Dinwiddie, W. D. Porter, and H. Wang, "Thermophysical Properties of ZrB_2 and ZrB_2-SiC Ceramics," *J. Am. Ceram. Soc.,* **91** [5] 1405-11 (2008).
4. S. K. Mishra, S. K. Das, and P. Ramachandrarao, "Sintering Studies on Ultrafine ZrB_2 Powder Produced by a Self-propagating High-temperature Synthesis Process," *J. Mater. Res.,* **15** [11] 2499-504 (2000).
5. Z. J. Jin, M. Zhang, D. M. Guo, and R. K. Kang, "Electroforming of Copper/ZrB_2 Composite Coating and Performance as Eltron-Discharge Machining Electrodes," *Key Eng. Mater.,* **291-292** 537-42 (2005).
6. J. Sung, D. M. Goedde, G. S. Girolami, and J. R. Abelson, "Remote-plasma Chemical Vapor Deposition of Conformal ZrB_2 Films at Low Temperature: A Promising Diffusion Barrier for Ultra Large Scale Integrated Electronics," *J. Appl. Phys.,* **91** [6] 3904-11 (2002).

7. S. K. Mishra, S. Das, S. K. Das, and P. Ramachandrarao, "Sintering Studies on Ultrafine ZrB_2 Powder Produced by a Self-Propagating High-Temperature Synthesis Process," *J. Mater. Res.,* **15** [11] 2499-504 (2000).

8. Y. Murata, "Cutting Tool Tips and Ceramics Containing Hafnium Nitride and Zirconium Diboride." in., U. S., 1970.

9. A. L. Chamberlain, W. G. Fahrenholtz, and G. E. Hilmas, "Low-Temperature Densification of Zirconium Diboride Ceramics by Reactive Hot Pressing," *J. Am. Ceram. Soc.,* **89** [12] 6368-75 (2006).

10. M. M. Opeka, I. G. Talmy, and J. A. Zaykoski, "Oxidation-based Materials Selection for 2000°C + Hypersonice Aerosurfaces: Theoretical Considerations and Historical Experience," *J. Mater. Sci.,* **39** [19] 5887-904 (2004).

11. A. L. Chamberlain, W. G. Fahrenholtz, and G. E. Hilmas, "High-Strength Zirconium Diboride-Based Ceramics," *J. Am. Ceram. Soc.,* **87** [6] 1170-72 (2004).

12. A. Rezaie, W. G. Fahrenholtz, and G. E. Hilmas, "Effect of Hot Pressing Time and Temperature on the Microstructure and Mechanical Properties of ZrB_2-SiC," *J. Mater. Sci.,* **42** [8] 2735-44 (2007).

13. J. Watts, G. E. Hilmas, and W. G. Fahrenholtz, "Mechanical Characterization of ZrB_2-SiC Composites with Varying SiC Particle Sizes," *J. Am. Ceram. Soc.,* **94** [12] 4410-18 (2011).

14. S. Zhu, W. G. Fahrenholtz, and G. E. Hilmas, "Influence of Silicon Carbide Particle Size on the Microstructure and Mechanical Properties of

Zirconium Diboride-Silicon Carbide Ceramics," *J. Eur. Ceram. Soc.,* **27** [4] 2077-83 (2007).

15. W. G. Fahrenholtz, "Thermodynamic Analysis of ZrB_2-SiC Oxidation: Formation of a SiC-Depeleted Region," *J. Am. Ceram. Soc.,* **90** [1] 143-8 (2007).
16. A. Rezaie, W. G. Fahrenholtz, and G. E. Hilmas, "Evolution of Structure During the Oxidation of Zirconium Diboride-Silicon Carbide up to 1500°C," *J. Eur. Ceram. Soc.,* **27** 2495-501 (2007).
17. A. Rezaie, W. G. Fahrenholtz, and G. E. Hilmas, "Oxidation of Zirconium Diboride-SIlicon Carbide at 1500°C at a Low Partial Pressure of Oxygen," *J. Am. Ceram. Soc.,* **89** [10] 3240-45 (2006).
18. W. H. Rhodes, E. V. Clougherty, and D. Kalish, "Research and Development of Refractory Oxidation-Resistant Diborides Part II, Volume IV: Mechanical Properties." Technical Report AFML-TR-68-190, Part II, Volume IV, Wright Patterson Air Forse Base, OH, 1970.
19. S. Zhu, "Densification, Microstructure, and Mechanical Properties of Zirconium Diboride Based Ultra-High Temperature Ceramics," Ph. D. Thesis. Missouri University of Science and Technology, Rolla, MO, 2008.
20. F. Monteverde, S. Guicciardi, and A. Bellosi, "Advances in Microstructure and Mechanical Properties of Zirconium Diboride Based Ceramics," *Mater. Sci. Eng., A,* **346** 310-19 (2003).

21. R. Loehman, E. Corral, H. P. Dumm, P. Kotula, and R. Tandon, "Ultra High Temperature Ceramics for Hypersonic Vehicle Applications." SAND 2006-2925. Sandia National Laboratories, Albuquerque, NM, 2006.

22. J. Zou, G. J. Zhang, C. F. Hu, T. Nishimura, Y. Sakka, H. Tanaka, J. Vleugels, and O. Van der Biest, "High-Temperature Bending Strength, Internal Friction and Stiffness of ZrB_2–20vol% SiC ceramics," *J. Eur. Ceram. Soc.,* **32** [10] 2519-27 (2012).

23. J. Zou, G. J. Zhang, C. F. Hu, T. Nishimura, Y. Sakka, J. Vleugels, and O. Van der Biest, "Strong ZrB_2–SiC–WC Ceramics at 1600°C," *J. Am. Ceram. Soc.,* **95** [3] 874-78 (2012).

24. O. N. Grigoriev, B. A. Galanov, V. A. Kotenko, S. M. Ivanov, A. V. Koroteev, and N. P. Brodnikovsky, "Mechanical Properties of ZrB_2-SiC($ZrSi_2$) Ceramics," *J. Eur. Ceram. Soc.,* **30** 2173-81 (2010).

25. D. J. Magley, R. A. Winholtz, and K. T. Faber, "Residual Stresses in a Two-Phase Microcracking Ceramic," *J. Am. Ceram. Soc.,* **72** [6] 1641-44 (1990).

26. V. Tvergaard and J. W. Hutchinson, "Microcracking in Ceramics Induced by Thermal Expansion or Elastic Anisotropy," *J. Am. Ceram. Soc.,* **71** [3] 157-66 (1988).

27. Y. S. Touloukian, C. Ho, and D. Dewitt, in *Thermal Expansion: Nonmetallic Solids,* Vol. 13, Edited by Touloukian. New York: IFI/Plenu, 1977.

28. G. V. Tsagareishvili, T. G. Nakashidze, J. S. Jobava, G. P. Lomidze, D. E. Khulelidze, D. S. Tsagareishvili, and O. A. Tsagareishvili, "Thermal expansion of boron and boron carbide," *J. Less-Common Metals,* **117** [1–2] 159-61 (1986).

29. J. Watts, G. Hilmas, W. G. Fahrenholtz, D. Brown, and B. Clausen, "Stress measurements in ZrB_2–SiC composites using Raman spectroscopy and neutron diffraction," *J. Eur. Ceram. Soc.,* **30** [11] 2165-71 (2010).

30. J. Watts, G. E. Hilmas, W. G. Fahrenholtz, D. Brown, and B. Clausen, "Measurement of Thermal Residual Stresses in ZrB_2-SiC Composites," *J. Eur. Ceram. Soc.,* **31** [9] 1811-20 (2011).

31. E. W. Neuman, G. E. Hilmas, and W. G. Fahrenholtz, "Mechanical Behavior of Zirconium Diboride-Silicon Carbide Ceramics at Elevated Temperature In Air " *J. Eur. Ceram. Soc.,* **35** 2889-99 (2013).

32. S. C. Zhang, G. E. Hilmas, and W. G. Fahrenholtz, "Pressureless Sintering of ZrB2–SiC Ceramics," *J. Am. Ceram. Soc.,* **91** [1] 26-32 (2008).

33. W. G. Fahrenholtz, G. E. Hilmas, S. C. Zhang, and S. Zhu, "Pressureless Sintering of Zirconium Diboride: Particle Size and Additive Effects," *J. Am. Ceram. Soc.,* **91** [5] 1398-404 (2007).

34. I. Tanaka, G. Pezzotti, T. Okamoto, Y. Miyamoto, and M. Koizumi, "Hot Isostatic Press Sintering and Properties of Silicon Nitride without Additives," *J. Am. Ceram. Soc.,* **72** [9] 1656-60 (1989).

35. W. G. Fahrenholtz, "The ZrB_2 Volatility Diagram," *J. Am. Ceram. Soc.,* **88** [12] 3509-12 (2005).

36. M. W. Bird, R. P. Aune, A. F. Thomas, P. F. Becher, and K. W. White, "Temperature-Dependent Mechanical and Long Crack Behavior of Zirconium Diboride–Silicon Carbide Composite," *J. Eur. Ceram. Soc.,* **32** [12] 3453-62 (2012).

37. M. W. Bird, R. P. Aune, F. Yu, P. F. Becher, and K. W. White, "Creep Behavior of a Zirconium Diboride-Silicon Carbide Composite," *J. Eur. Ceram. Soc.,* **33** 2407-20 (2013).

38. D. Kalish, E. V. Clougherty, and K. Kreder, "Strength, Fracture Mode, and Thermal Stress Resistance of HfB_2 and ZrB_2," *J. Am. Ceram. Soc.,* **52** [1] 30-36 (1969).

39. A. H. Heuer and V. L. K. Lou, "Volatility Diagrams for Silica, Silicon Nitride, and Silicon Carbide and Their Application to High-Temperature Decomposition and Oxidation," *J. Am. Ceram. Soc.,* **73** [10] 2789-803 (1990).

40. V. A. Lavrenko and Y. G. Gogotsi, "Influence of oxidation on the composition and structure of the surface layer of hot-pressed boron carbide," *Oxid. Met.,* **29** [3-4] 193-202 (1988).

41. A. G. Evans and A. Rana, "High temperature failure mechanicsms in ceramics," *Acta Metall.,* **28** 129-41 (1980).

42. S. S. Ordan'yan, A. I. Dmitriev, and E. S. Moroshkina, "Reaction of Silicon Carbide with Zirconium Diboride," *Inorg. Mater.,* **25** [10] 1487-89 (1989).

43. I. W. Chen, S.-Y. Liu, and D. Jacobs, "Effects of Temperature, Rate, and Cyclic Loading on the Strength and Toughness of Monolithic Ceramics," *AcM&M,* **43** [4] 1439-46 (1995).

44. D. Chakraborty and A. K. Mukhopadhyay, "High Temperature Young's Modulus of Reaction-bonded Si_3N_4, Liquid Phase Sintered Si_3N_4 and Sialon," *Ceram. Int.,* **14** 127-32 (1988).

45. J. B. Wachtman and D. G. Lam, "Young's Modulus of Refractory Materials as a Function of Temperature," *J. Am. Ceram. Soc.,* **42** [5] 254-60 (1959).

46. J. A. Stavrolakis and F. H. Norton, "Measurement of the Torsion Properties of Alumina and Zirconia at Elevated Temperatures," *J. Am. Ceram. Soc.,* **33** [9] 263-68 (1950).

47. A. L. Chamberlain, W. G. Fahrenholtz, and G. E. Hilmas, "High Strength ZrB_2-Based Ceramics," *J. Am. Ceram. Soc.,* **87** [6] 1170-72 (2004).

48. J. Wachtman, *Mechanical Properties of Ceramics*. John Wiley & Sons, Inc.: New York, (1996).

49. M. Taya, S. Hayashi, A. S. Kobayashi, and H. S. Yoon, "Toughening of a particulate-reinforced ceramics-matrix composite by thermal residual stress.," *J. Am. Ceram. Soc.,* **73** [5] 1382-91 (1990).

50. R. L. Brett and P. Bowen, "Fracture toughness assessment of silicon carbide-based ceramics and particulate-reinforced composites," *Compo,* **24** [2] 177-83 (1993).

51. E. Eakins, "Nanoscale Characterisation of Effect of SiC on Microstructure and Oxidation Behavior of ZrB_2-Based Ceramics," Department of Materials, Ph.D. Thesis. Imperial College London, London, England, 2011.

52. F. Monteverde and A. Bellosi, "Development and Characterization of Metal-Diboride-Based Composites Toughened with Ultra-Fine SiC Particulates," *Solid State Sci.,* **7** [5] 622-30 (2005).

53. J. S. Haggerty and D. W. Lee, "Plastic deformation of ZrB_2 single crystals," *J. Am. Ceram. Soc.,* **54** [11] 572-76 (1971).

54. O. N. Grigoriev, B. A. Galanov, V. A. Kotenko, S. M. Ivanov, A. V. Koroteev, and N. P. Brodnikovsky, "Mechanical properties of ZrB_2–SiC($ZrSi_2$) ceramics," *J. Eur. Ceram. Soc.,* **30** [11] 2173-81 (2010).

Table I. Elevated temperature mechanical properties of ZrB_2-30 vol% SiC in argon.

Temperature (°C)	Crosshead Rate (Strength, Toughness) (mm/min)	Strength (MPa)	Modulus (GPa)	Toughness ($MPa \cdot m^{½}$)
RT	0.5, 0.03	695 ± 69	513 ± 24	4.9 ± 0.4
1000	0.5, 0.03	674 ± 81	501 ± 77	4.5 ± 0.5
1200	0.5, 0.03	633 ± 42	431 ± 55	4.2 ± 0.2
1400	1.0, 0.05	608 ± 55	427 ± 56	4.4 ± 0.4
1600	2.5, 0.05	569 ± 56	399 ± 92	4.3 ± 0.1
1800	5.0, 0.07	538 ± 16	345 ± 93	4.2 ± 0.1
2000	7.5, 0.10	419 ± 46	283 ± 78	4.0 ± 0.6
2200	15, 1.0	262 ± 28	164 ± 55	3.5 ± 0.4

Table II. Summary of average and maximum grain size of ZrB_2, average and maximum cluster size of SiC and B_4C following exposure to elevated temperature during testing, and calculated critical flaw size ($Y = \pi^{½}$). AP refers to the as processed material. All values are in microns.

Temperature (°C)	ZrB_2		SiC		B_4C		Calculated Critical Flaw Size, $Y = \pi^{½}$
	Average Grain Size	Maximum Grain Size	Average Cluster Size	Maximum Cluster Size	Average Cluster Size	Maximum Cluster Size	
AP	2.99 ± 1.54	10.6	3.61 ± 3.40	32.8	0.97 ± 0.84	11.0	31.6 ± 5.6
1000	2.94 ± 1.50	9.12	3.78 ± 3.91	28.4	0.95 ± 0.89	8.11	30.8 ± 7.6
1200	2.60 ± 1.48	8.69	3.29 ± 3.46	32.6	0.82 ± 0.74	11.4	34.7 ± 6.2
1400	3.06 ± 1.63	11.6	3.92 ± 3.95	31.0	0.95 ± 0.88	10.6	33.9 ± 5.9
1600	3.06 ± 1.52	8.58	3.86 ±3.95	33.2	1.09 ± 1.08	12.2	47.7 ± 7.6
1800	3.08 ± 1.68	14.8	3.81 ± 3.75	32.5	0.95 ± 0.76	7.20	39.0 ± 1.2
2000	3.13 ± 1.58	8.91	4.07 ± 3.95	38.4	1.01 ± 0.89	11.3	58.1 ± 19.1
2200	3.24 ± 1.67	10.9	4.12 ± 4.02	46.5	1.01 ± 0.78	6.00	116 ± 29

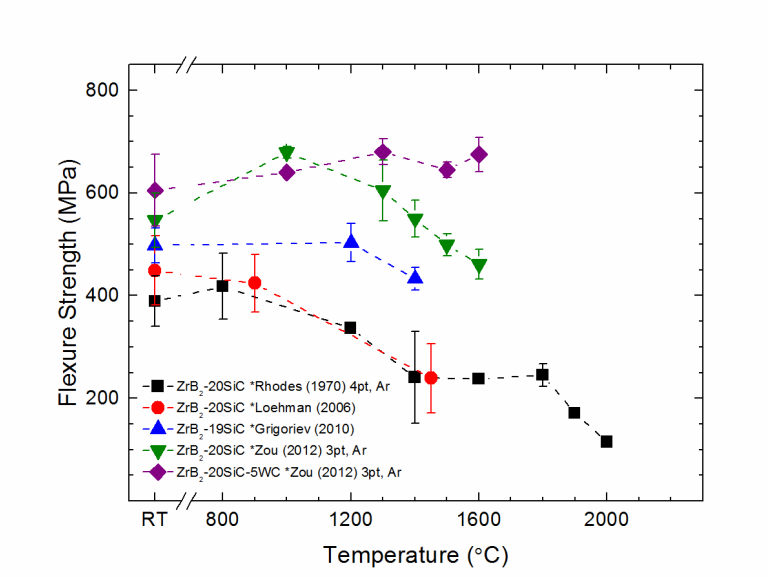

Figure 1. Summary of the strength of ZrB_2-SiC ceramics at elevated temperature from selected studies.[18, 21-23, 54] Tests were performed using 4-pt flexure in air unless noted.

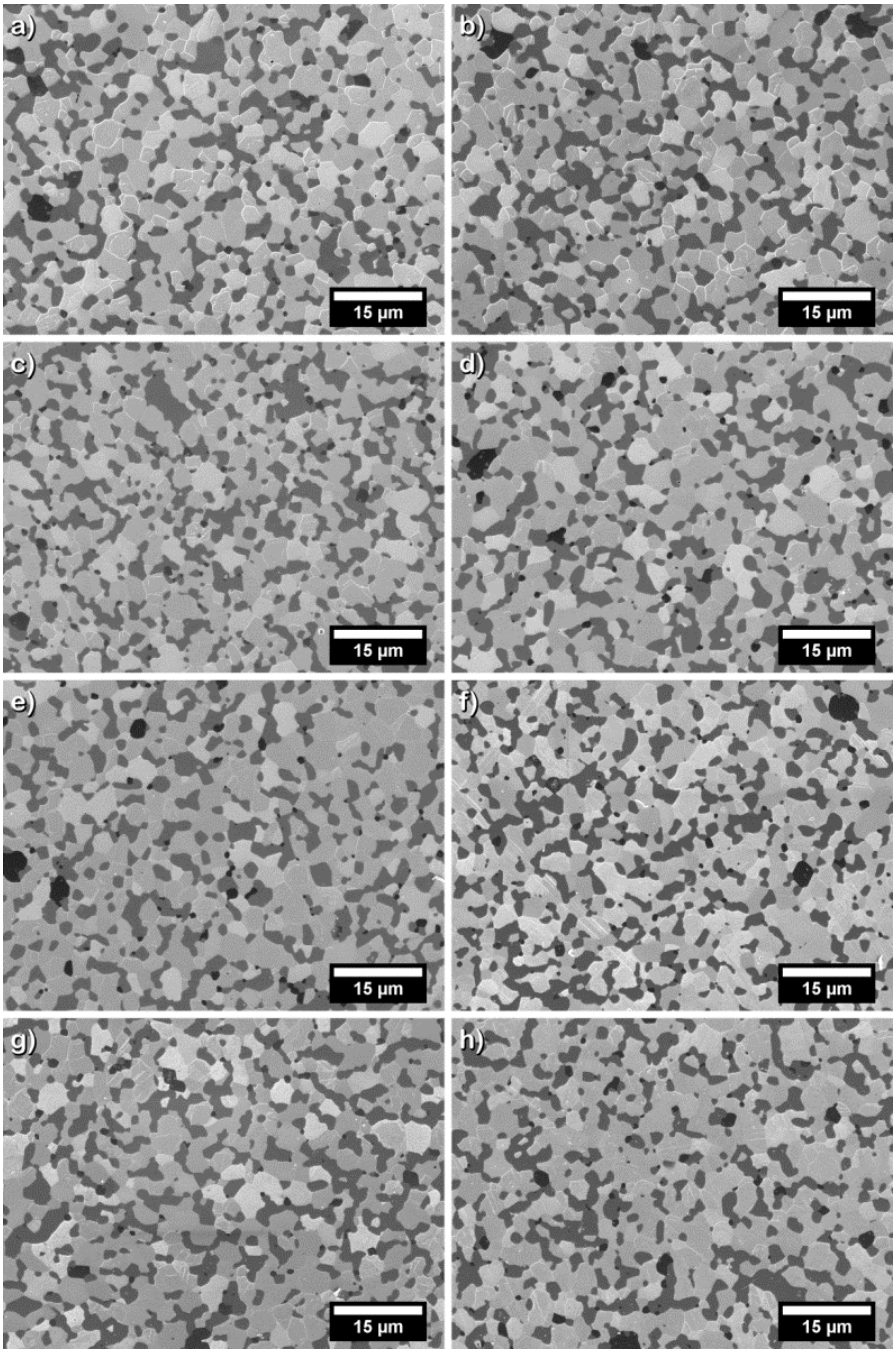

Figure 2. SEM images of polished and etched tensile surface of ZrB_2-30SiC following elevated temperature testing at a) RT, b) 1000°C, c) 1200°C, d) 1400°C, e) 1600°C, f) 1800°C, g) 2000°C, h) 2200°C.

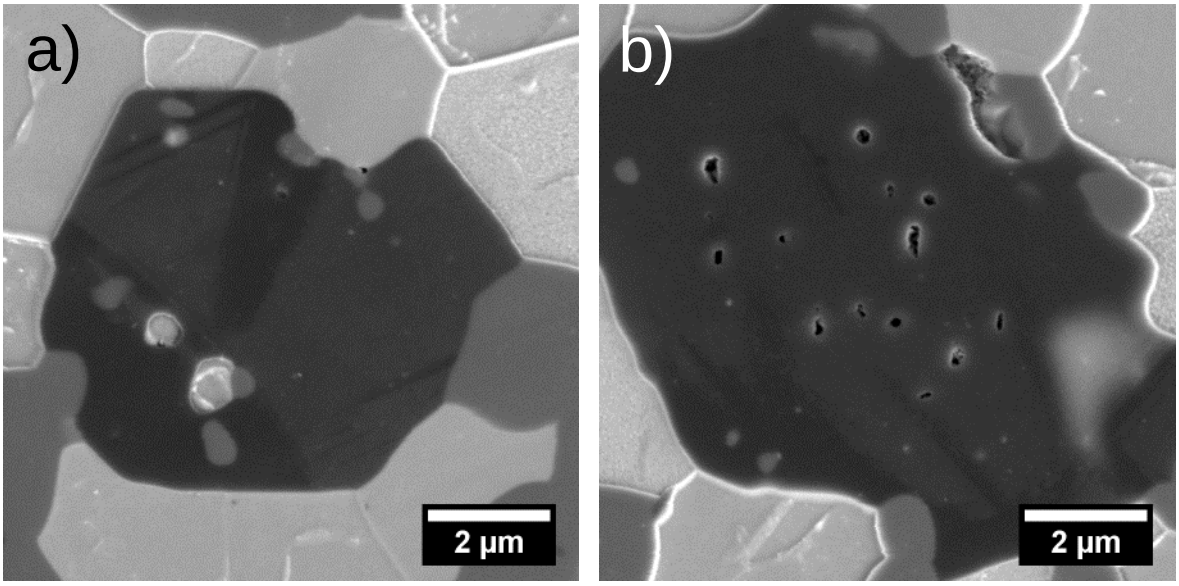

Figure 3. SEM images of polished and etched cross-section of ZrB_2-30SiC showing B_4C clusters with entrapped a) ZrB_2 and SiC and b) entrapped porosity.

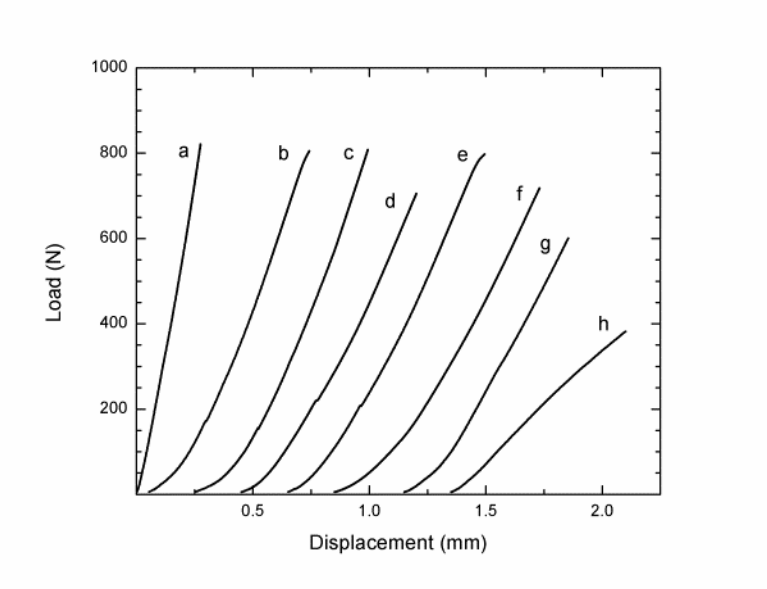

Figure 4. Load versus displacement curves for ZrB_2-30SiC tested at: a, RT; b, 1000°C; c, 1200°C; d, 1400°C; e, 1600°C; f, 1800°C; g, 2000°C; and h, 2200°C. Displacement measured by LVDT for a, and crosshead displacement for b through h.

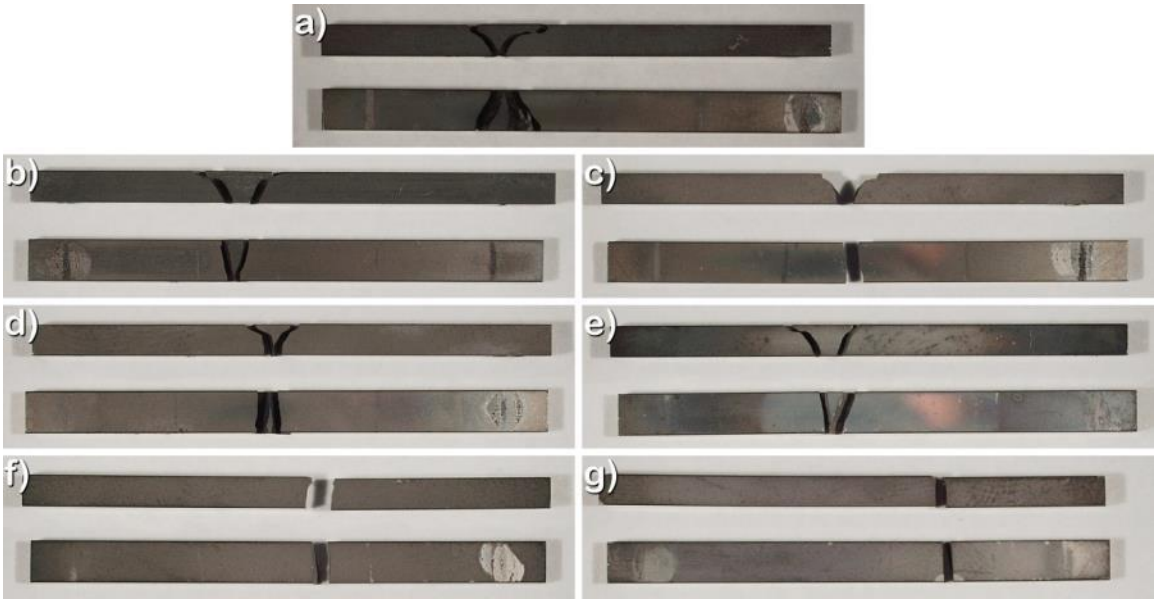

Figure 5. Optical macrographs ZrB_2-30SiC flexure bars fractured at a) 1000°C, b) 1200°C, c) 1400°C, d) 1600°C, e) 1800°C, f) 2000°C, g) 2200°C. Each image shows the side (top) and tensile surface (bottom) of each bar. The bars are approximately 50 mm in length.

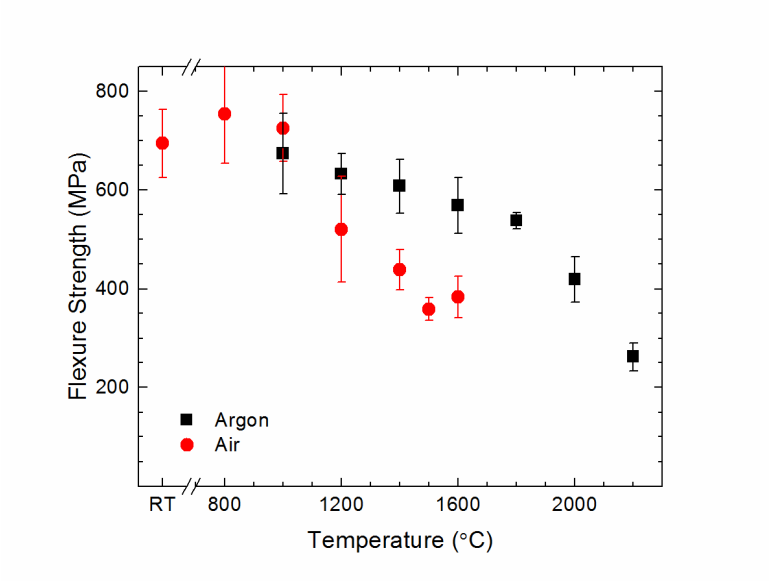

Figure 6. Four-point flexure strength of ZrB_2-30SiC tested in air and argon atmospheres as function of temperature

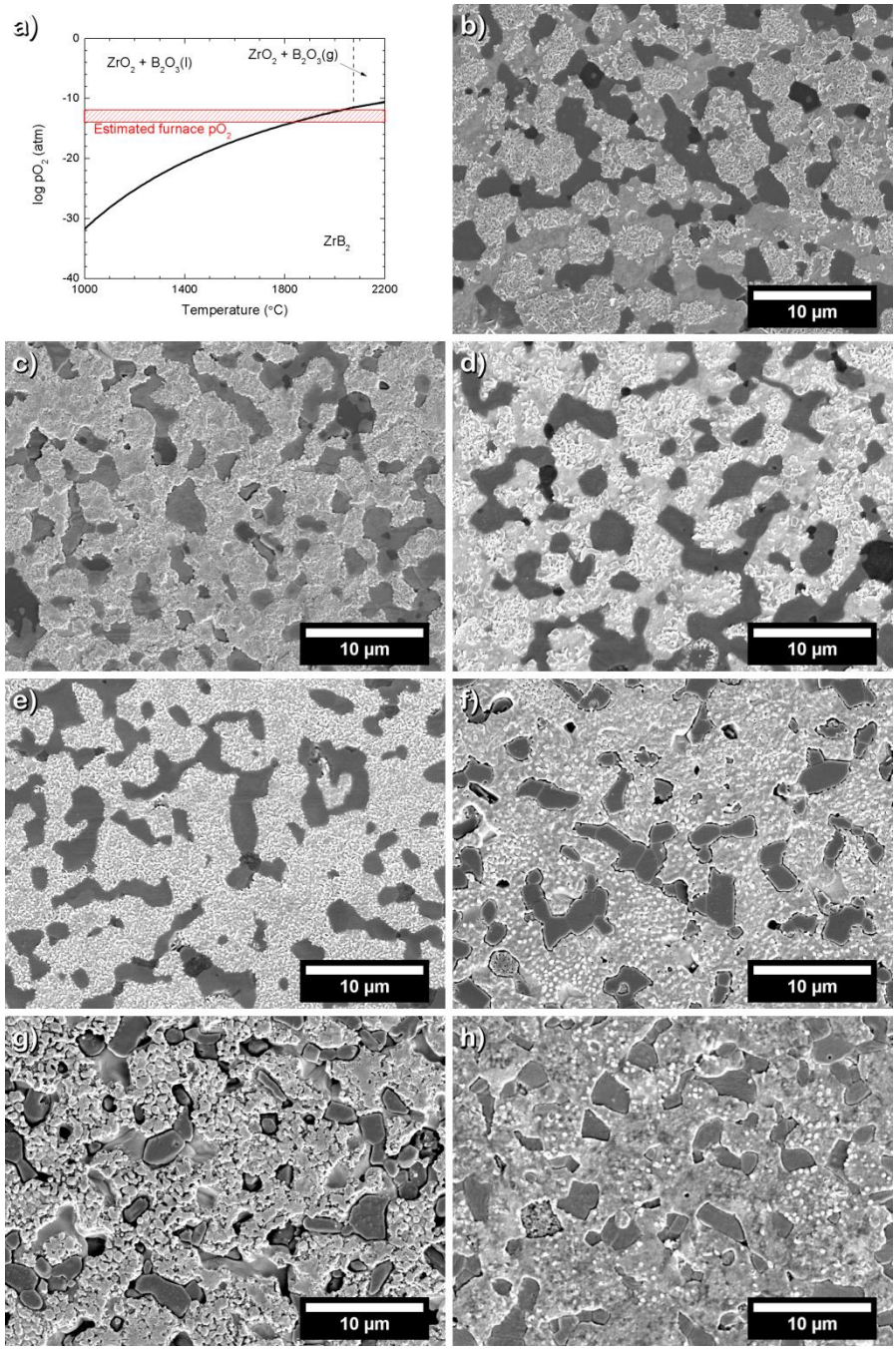

Figure 7. ZrB_2 phase stability diagram, a), and SEM images of as-is tensile surface of ZrB_2-30SiC tested at b) 1000°C, c) 1200°C, d) 1400°C, e) 1600°C, f) 1800°C, g) 2000°C, h) 2200°C. Surfaces of b-e) consist of Zr-B-O phase (bright), SiC,(medium grey) and B_4C (dark grey). Surfaces of f-h) consist of Zr-B-C phase, and etched and/or receding SiC and B_4C grains.

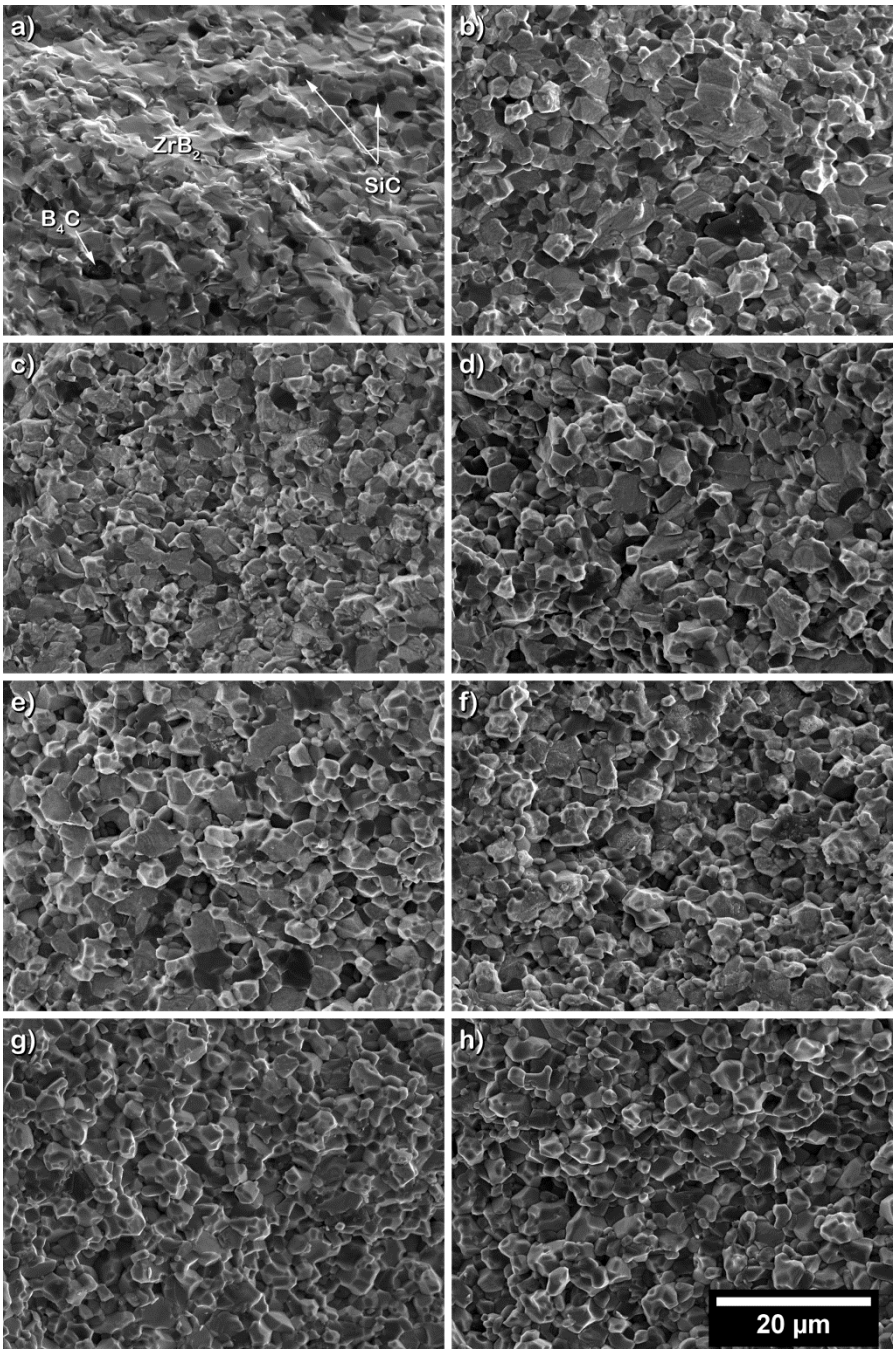

Figure 8. SEM images of tensile region of fracture surface of ZrB_2-30SiC tested at a) RT, b) 1000°C, c) 1200°C, d) 1400°C, e) 1600°C, f) 1800°C, g) 2000°C, h) 2200°C.

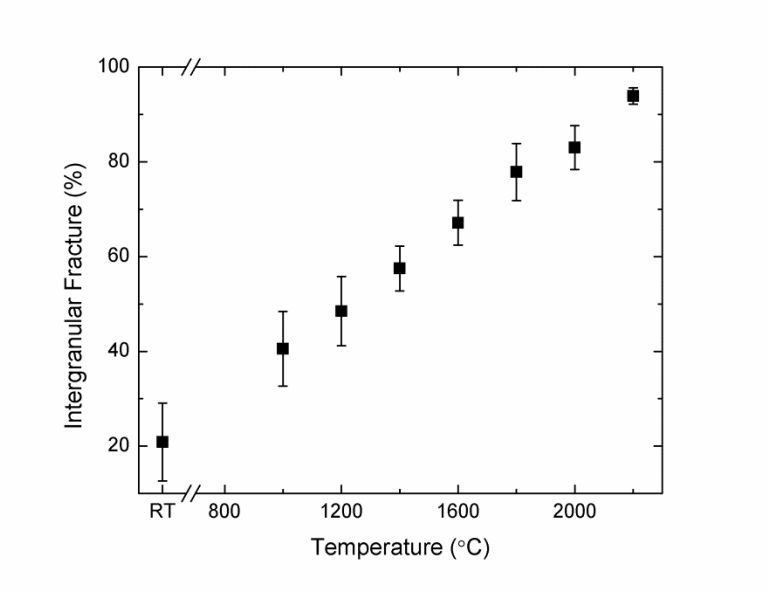

Figure 9. Fraction of ZrB_2 grains observed to fail by intergranular fracture as a function of temperature.

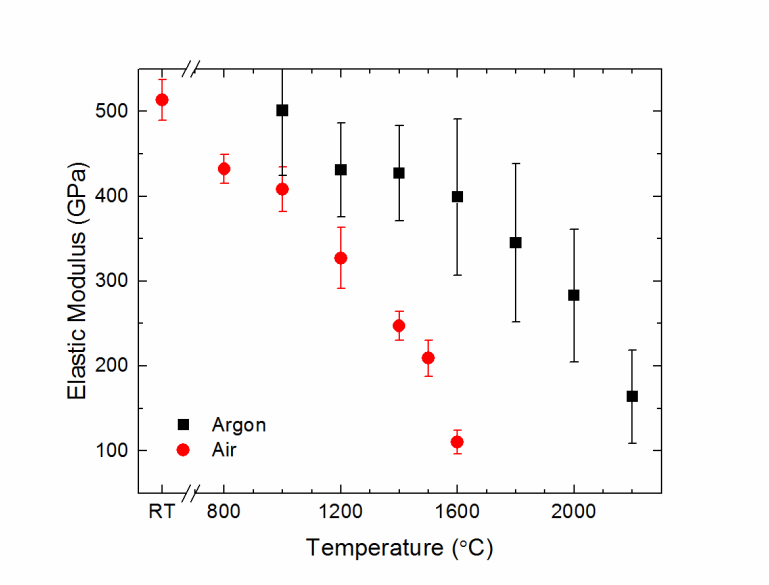

Figure 10. Elastic modulus of ZrB_2-30SiC tested in air and argon atmospheres as a function of temperature. Note modulus of specimens tested in argon estimated using crosshead displacement.

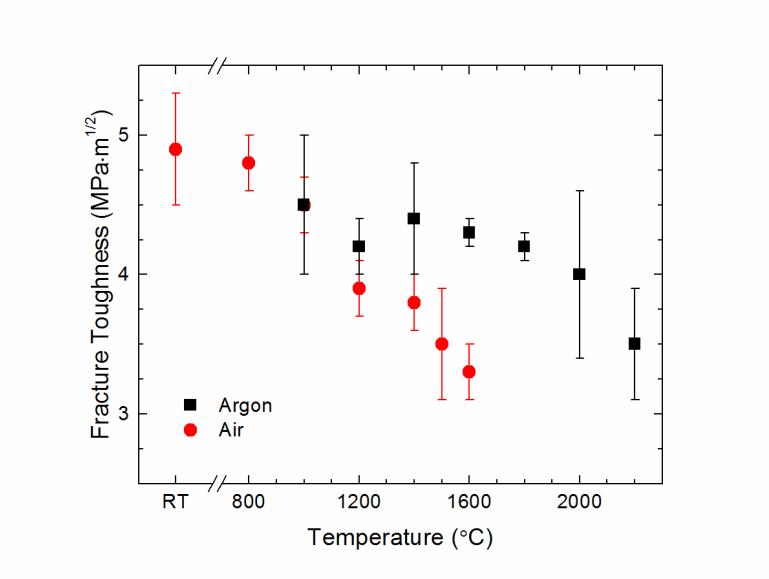

Figure 11. Chevron notch beam, in four-point flexure, fracture toughness of ZrB_2-30SiC tested in air and argon atmospheres as a function of temperature.

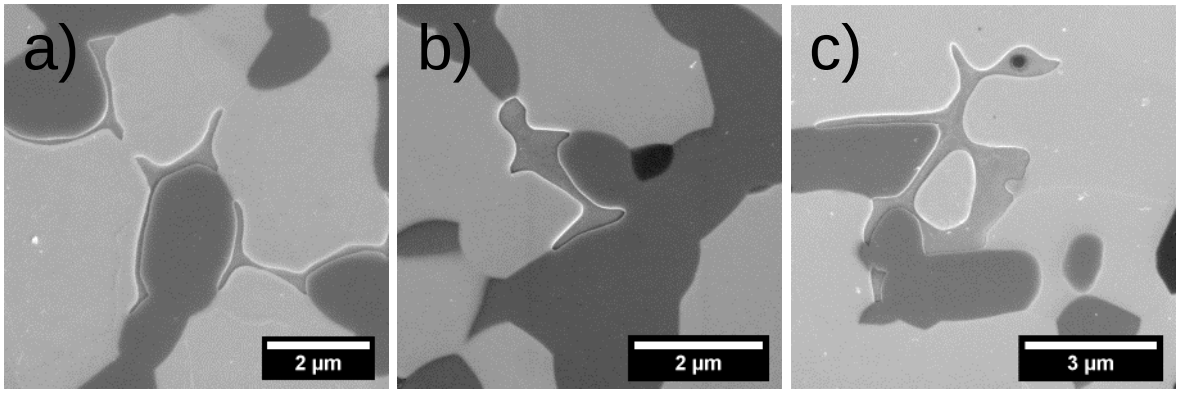

Figure 12. SEM images of polished cross-section of ZrB_2-30SiC showing metallic liquid phases present in microstructure: a)Fe-Co-U phase present in the as processed material, and Zr-Si-Th-B-O-RE containing phases present following testing at b) 1800°C and c)2200°C.

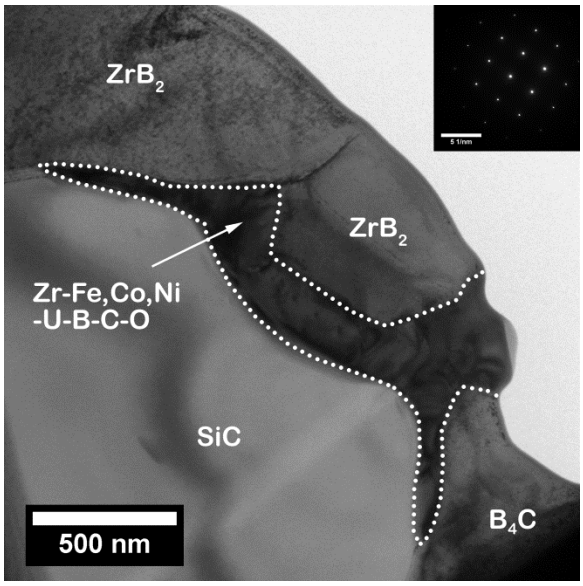

Figure 13. TEM micrograph highlighting the Fe-Co-U type phase present in the as processed material. Arrow also indicates region where SADP was taken.

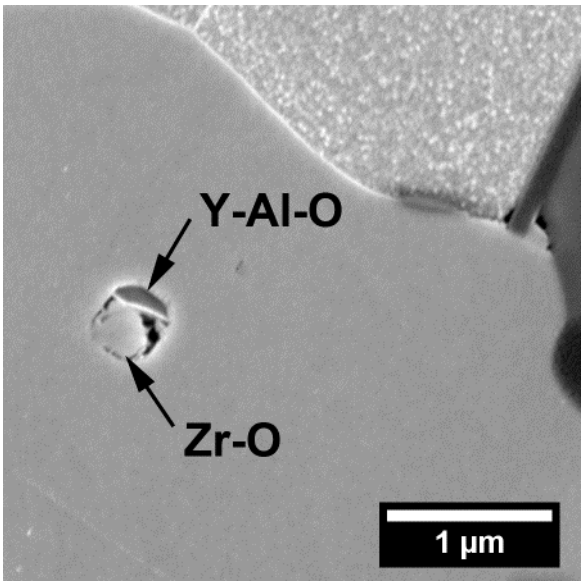

Figure 14. SEM image of polished and etched cross-section of ZrB_2-30SiC following testing at 1800°C showing the presence of a typical zirconium oxide and yttrium aluminum oxide precipitate feature within a ZrB_2 grain.

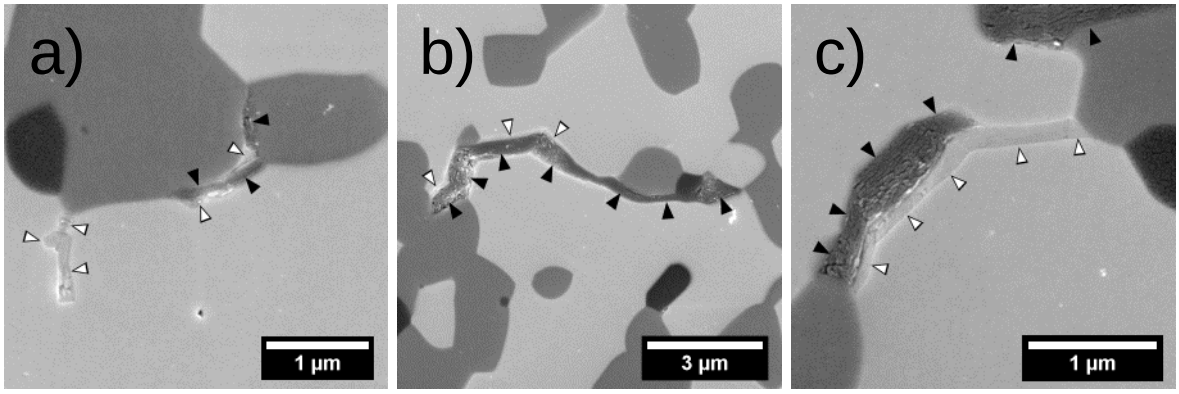

Figure 15. SEM images of polished cross-section of ZrB_2-30SiC showing the examples of BN (solid) and B-O-C-N phases (hollow) following testing at 1800°C (left), and 2200°C (middle and right).

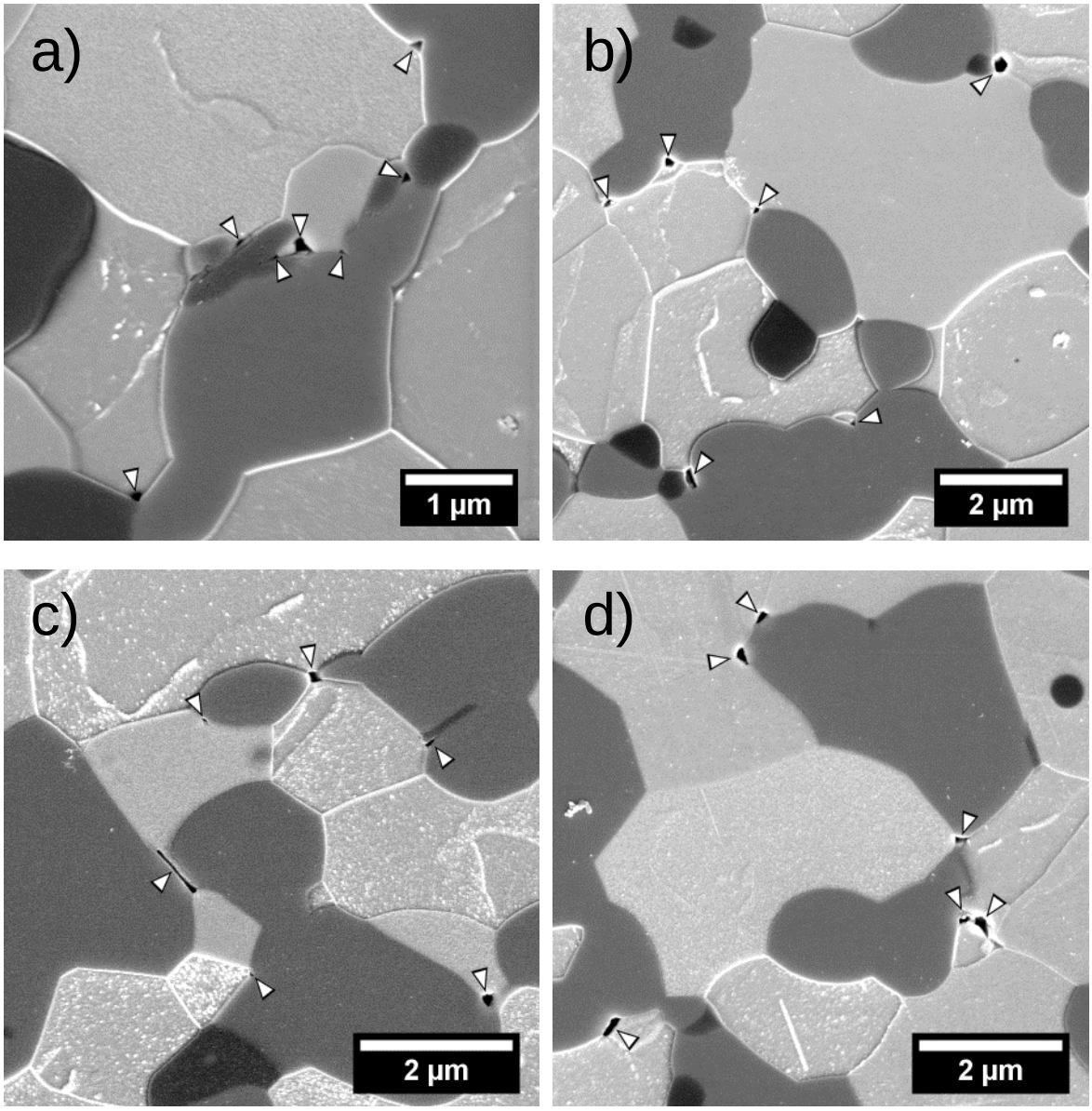

Figure 16. SEM images of polished and etched tensile surface of ZrB_2-30SiC showing examples of cavitation following testing at a) 1200°C, b) 1600°C, c) 2000°C, and d) 2200°C.

IV. ELEVATED TEMPERATURE STRENGTH ENHANCEMENT OF ZrB_2-30 VOL% SiC CERAMICS BY POST-SINTERING THERMAL ANNEALING

Eric W. Neuman, Gregory E. Hilmas, William G. Fahrenholtz

Department of Materials Science and Engineering, Missouri University of Science and Technology Rolla, MO 65409 USA

Abstract

The mechanical properties of dense, hot-pressed ZrB_2-3 0 vol% SiC ceramics were characterized from room temperature up to 1600°C in air. Specimens were tested as hot pressed or after being hot pressed followed by annealing heat-treatments at 1400°C, 1500°C, 1600°C, or 1800°C for 10 hours. Annealing at 1400°C resulted in the largest increases in flexure strengths at the highest test temperatures, with strengths of 470, 385, and 425 MPa at 1400, 1500, and 1600°C, corresponding to increases of 7, 8, and 12% compared to as hot pressed ZrB_2-SiC. Thermal treatment at 1500°C resulted in the largest increase in elastic modulus, with values of 270, 240, and 120 GPa at 1400, 1500, and 1600°C, corresponding to increases of 6, 12, and 18%. Changes in ZrB_2 grain size and SiC cluster size were not observed for these heat-treatment temperatures. Instead, additional phases may be forming during heat-treatment or in dislocation density may be changing. This study shows that thermal

annealing may be a useful method for improving the elevated temperature mechanical properties of ZrB_2 based ceramics.

Keywords: zirconium diboride, silicon carbide, hot pressing, strength, modulus, heat-treatment

1. Introduction

Zirconium diboride (ZrB_2) has generated much interest in its potential for use as a structural material in extreme environments. It belongs to a class of materials known as ultra-high temperature ceramics (UHTCs), characterized by melting points exceeding 3000°C.[1, 2] ZrB_2 based particulate composites, especially those with silicon carbide (SiC) additives, display enhanced properties. ZrB_2-SiC composites have demonstrated room temperature strengths exceeding 1000 MPa,[3-5] fracture toughness values as high as 5.5 MPa·$m^{½}$,[3, 4, 6] and hardness values over 22 GPa.[3, 5, 7] These properties make zirconium diboride ceramics a candidate for a range of applications including molten metal crucibles, furnace electrodes, cutting tools, and wing leading edges on future hypersonic aerospace vehicles.[2]

Recent studies have reported the elevated temperature strengths and elastic moduli of ZrB_2-SiC ceramics up to 1600°C.[8-12] Monteverde et al. reported that a 4 wt% addition of Si_3N_4 to ZrB_2-20 vol% SiC could produce a ceramic with a room temperature strength of 730 MPa, but the strength dropped to 250 MPa at 1200°C.[8] Loehman et al. examined ZrB_2-20vol% SiC with a room temperature strength of 450 MPa that decreased to 240 MPa at 1450°C.[9] Zou et al. reported

the strengths of ZrB_2-20 vol% SiC with[12] and without[11] additions of 5 vol% WC in an argon atmosphere. For ZrB_2-20SiC, the strength was reported to increase to 680 MPa at 1000°C from 550 MPa at ambient, then decrease to 460 MPa at 1600°C. ZrB_2-20SiC-5WC showed the greatest retained strength at elevated temperature, increasing to 675 MPa at 1600°C from 605 MPa at room temperature. This enhancement in strength was attributed to the removal of surface oxides from the starting powders by reaction with WC during sintering. Studies of the elastic properties of ZrB_2 ceramics have also been limited. Rhodes evaluated the elastic modulus in argon up to 2100°C for ZrB_2 and up to 2000°C for ZrB_2-20vol% SiC.[13] Zhu reported the modulus of ZrB_2 and ZrB_2 with B_4C and C additions up to 1500°C in air.[14] Rhodes reported a modulus of ~520 GPa for ZrB_2-20 vol% SiC at room temperature, decreasing 445 GPa at 1400°C and 106 GPa at 1600°C. Zou measured the modulus of ZrB_2-20 vol% SiC up to 1300°C.[11] The modulus was ~505 GPa at ambient, linearly decreasing to ~480 at ~780°C, decreasing more rapidly to ~445 GPa at 1300°C. The change in trend occurring at 780°C was attributed to the softening of oxide phases present in the microstructure.

SiC inclusions have been identified as the critical flaw in dense, fine grained ZrB_2-SiC.[4-6] At some critical level of thermal expansion mismatch and cluster size, spontaneous microcracking of the matrix can occur.[5, 15, 16] The CTE mismatch between ZrB_2 (~5.2 ppm/K at 298 K),[2, 17] SiC (~3.3 ppm/K at 298 K)[17] and B_4C (~5.7 ppm/K from 300-1970K)[18] results in residual compressive stress in the SiC and tensile stresses in the ZrB_2 matrix and B_4C reinforcing phase. Watts

reported a decrease in hardness (21 to 18 GPa) occurred with a maximum SiC cluster size of 11.5 μm, a result of stress induced microcracking.[5] Watts directly measured the residual stresses that accumulate in ZrB_2-30vol% SiC upon cooling, compressive stresses of 880 MPa in the SiC phase and tensile stresses of 450 MPa in the ZrB_2 phase, prior to the onset of microcracking.[19, 20] Residual stresses began to accumulate at ~1400°C upon cooling, with the maximum stress occurring at the ZrB_2-SiC interface.

In-situ toughening of SiC and Si_3N_4 ceramics has been investigated by many authors through various routes, some based on selection of starting powders, sintering schedules, and post-sintering thermal processing.[21-29] Toughening is typically obtained through either the growth of elongated grains or the modification of grain boundary phases. In the case of elongated grains, the increase in toughness is obtained via crack bridging or crack deflection mechanisms due to weak interface boundaries. However, the coarsening that occurs during thermal treatments at high temperatures can lead to an increase in the critical flaw size, diminishing strength. Modification of the grain boundary phase can occur through several means. Enhancement in toughness can occur through redistribution and/or partial elimination due to movement of liquid to the sample surface and evaporation into the atmosphere. It can also occur through recrystallization of the liquid phase and/or phase transitions in crystalline phases, resulting in new phases that are more refractory and can even have improved oxidation resistance. These toughening mechanisms can improve the elevated temperature mechanical properties as well as the room temperature properties.

One example is the work of Cinibulk et al. where they showed an improvement in flexure strength at 1300°C from ~200 to ~400 MPa for Si_3N_4 following recrystallization of the YSiALON grain boundary phase to β-$Y_2Si_2O_7$.[27]

Thermal annealing is being investigated for the ZrB_2-SiC system as a means of improving strength. Improvements are predicted to occur through the relief of thermal residual stresses and the modification of residual grain boundary phases which occur from the incomplete removal of surface oxides during processing. In this work, the microstructure and mechanical properties of hot pressed ZrB_2-30 vol% SiC were compared for as-hot pressed materials and materials that were hot pressed and subsequently heat-treated (annealed). Of particular interest was the effect of annealing on the high temperature mechanical properties, thus flexure strength and elastic modulus were measured up to a temperature of 1600°C in air.

2. Experimental Procedure

2.1. Processing

Commercially available powders were used in this study. The ZrB_2 powder (Grade B, H.C. Starck, Newton, MA) had a reported purity of 98.2% and a particle size of 2 μm. The SiC powder (Grade UF-10, H.C. Starck) was predominantly α-SiC, having a reported purity of 98.5% and a particle size of 0.7 μm. The B_4C powder (Grade HD-20, H.C. Starck) had a B:C ratio of 3.8, a reported purity of 97.6%, and a particle size of 0.5 μm. The powders were batched in the ratio of 70 vol% ZrB_2 to 30 vol% SiC with a super addition of 2 wt% B_4C (ZrB_2 basis). The powders were mixed by ball milling with WC-6Co

media in acetone with a dispersant (DISPERBYK®-110, BYK-Gardner USA, Columbia, MD). After ball milling for 24 hours, the slurry was dried by rotary evaporation (Model Rotavapor R-124, Buchi, Flawil, Germany) at a temperature of 70°C, low vacuum (~27 kPa), and a rotation speed of 60 rpm. The dried powders were lightly ground to pass through a 50 mesh screen prior to densification.

Milled powders were hot-pressed (Model HP50-7010G, Thermal Technology, Santa Rosa, CA) in 63.5 mm square graphite dies lined with BN coated (SP-108, Cerac, Milwaukee, WI) graphite foil. Prior to hot pressing, the powders were cold compacted in a uniaxial press at ~2 MPa. Powder compacts were heated under vacuum to (~13 Pa) to 1450°C with an average heating rate of 20°C/min. After holding for 1 hour, the temperature was increased to 1650°C at an average heating rate of 20°C/min. After holding for 1 hour, the furnace was back filled with argon and a uniaxial load of 32 MPa was applied. Following previous studies, the isothermal holds were used to promote reactions between surface oxides on the starting powders and boron carbide to remove the oxides as gaseous species.[33, 34] The furnace was then heated at ~90°C/min to 1950°C. After 10 min, the power was shut off and the furnace allowed to cool naturally at a rate of ~60°C/min. The load was removed when the die temperature dropped below 1650°C.

Heat-treatment of the specimens was performed following the sectioning of the raw billets into blanks (45 mm x ~5 mm x ~4 mm) prior to grinding to final dimensions. A resistively heated graphite vacuum furnace (Model 3060-FP20,

Thermal Technology, Santa Rosa, CA) was used to heat treat the specimens. The specimens were stacked in a cross-hatch pattern on sacrificial ZrB_2-SiC setters in a graphite-foil lined graphite crucible. The specimens were heated at 20°C/min to 1400°C, 1500°C, 1600°C, or 1800°C for 10 hours (HT14, HT15, HT16, and HT18), then cooled at 20°C/min to room temperature. Heat-treatment was conducted in an argon atmosphere at a pressure of 124 kPa to suppress the oxidation of the SiC and B_4C phases through evaporation of volatile species.[30-32]

2.2. Characterization

Bulk density was measured by Archimedes' method using distilled water as the immersing medium as described in ASTM C373-88. Microstructures were examined using scanning electron microscopy (SEM; S570, Hitachi, Tokyo, Japan) and transmission electron microscopy (TEM, Tecnai F-20, FEI, Hillsboro, OR). Specimens were prepared for microscopy by cutting cross-sections perpendicular to the hot-pressing direction and polishing to a 0.25 μm finish using diamond abrasives. TEM specimens were prepared from the polished cross-sections using a focused ion beam (FIB, Helios NanoLab 600, FEI, Hillsboro, OR). In order to reveal the grain boundaries for image analysis, the ZrB_2 phase was etched using 3:1:1 HNO_3:HF:H_2O, while the SiC phase was etched using boiling Hall's Reagent for 20 min. ZrB_2 and SiC grain sizes were measured from SEM images using computerized image analysis (ImageJ, National Institutes of Health, Bethesda, MD). Grain size was determined by measuring the equivalent area diameter of at least 1000 grains of both ZrB_2 and SiC. Cluster size was determined from the polished cross sections by measuring the Feret's diameter

(SiC) and the major axis of fitted ellipses (B_4C) for at least 10,000 and 2,000 clusters, respectively.

2.3. Mechanical testing

Room temperature flexure strengths were measured in four-point bending using a fully-articulated test fixture using type-B bars (45 mm x 4 mm x 3 mm) according to ASTM C1161-02c. Flexure strength was measured at elevated temperatures (800, 1000, 1200, 1400, 1500, and 1600°C) using the same type-B bars and following the testing procedures outlined in ASTM C1211-08. Bars were machined from the hot-pressed billets by diamond grinding on a fully automated surface grinder (FSG-3A818, Chevalier, Santa Fe Springs, CA). The flexure surface was polished to a 1 μm finish using diamond abrasives. Tests were performed using a screw-driven instrumented load frame (5881, Instron, Norwood, MA). Elevated temperature testing was performed in a molybdenum disilicide element furnace (MDS66C, Instron SFL, Thornbury, Bristol). A deflectometer was used to record the displacement of the test bars during loading. A crosshead rate of 0.5 mm/min was used up to 1200°C, 1.5 mm/min at 1400°C, 2.0 mm/min at 1500°C, and 2.5 mm/min at 1600°C. The heating rate for all of the high temperature tests was 10°C/min followed by an isothermal hold for 10 min at the desired temperature before testing.

Room temperature elastic constants were determined by impulse excitation (MK4-I Grindosonic, J.W. Lemmens, St. Louis, MO) according to ASTM C1259-08. The static bend test method was used to determine the elevated temperature elastic modulus according to ASTM standard E111-04.

The elastic modulus was calculated from the slope of the load displacement curves. At least 10 measurements were averaged to calculate the reported values.

3. Results and Discussion

The measured bulk densities of the hot pressed, as-processed (AP) specimens were 5.22 g/cm^3. The theoretical density based off of the nominal composition (67.75 vol% ZrB_2, 29.00 vol% SiC, and 3.27 vol% B_4C), milling contamination (0.24-0.32 wt% WC-6Co), and the measured crystallographic density of the ZrB_2 (6.14 g/cm^3, primarily due Hf impurity)[33] is 5.22 g/cm^3. Following heat-treatment, the bulk densities of the specimens were 5.21-5.22 g/cm^3. The compositions of the as-processed and heat-treated specimens from image analysis are summarized in Table I, having theoretical densities of 5.21 to 5.27 g/cm^3. Porosity was not observed in the as-processed or heat-treated specimens. Therefore, measured bulk densities are consistent with SEM observations that the specimens are fully dense. Figure 1 shows typical cross-sections of polished as-processed and heat-treated specimens. The ZrB_2 and SiC grain sizes, and SiC and B_4C cluster sizes are summarized in Table II. ZrB_2 and SiC grain sizes were measured to be ~1.9 and ~1.2 µm. Average SiC and B_4C cluster sizes were ~3.6 and ~1.6 µm, with maximum cluster sizes of ~32 and ~12 µm, respectively. ZrB_2 and SiC grain sizes were consistent across the heat-treatment conditions, for the temperatures measured. Average SiC cluster increased for HT18 to ~4.6 µm, and the maximum SiC cluster size increased to ~38 µm. Average B_4C cluster size did not change with heat-treatment

temperature, instead showing a positive correlation with the amount of B_4C observed, and the maximum B_4C cluster size did not change. Matrix microcracking was observed in both the as-processed and heat-treated specimens. This is consistent with previous studies of ZrB_2-30 vol% SiC.[5, 33] The amount of SiC in the microstructure is above the percolation threshold for the observed grain sizes (~25 vol%), thus forming percolation clusters.[34] These clusters are larger than the microcracking threshold for ZrB_2-SiC (~11.5 μm), giving rise to spontaneous matrix microcracking.[5]

Measured values for flexure strength and elastic modulus from room temperature to 1600°C of as-processed and heat-treated samples are given in Table III and Table IV, respectively. All specimens exhibited linear-elastic behavior to failure, and no macroscopic creep was observed in the bars following fracture at elevated temperatures. Figure 2 summarizes the flexure strength and elastic modulus as a function of test temperature. The trends observed in the as-processed material have been discussed in more detail elsewhere.[33] Since the heat-treated specimens follow similar trends, the focus of this discussion will be the differences between the as-processed and heat-treated specimens.

The change in flexure strength from the as-processed material is shown in Figure 3. For the sake of simplicity, a change of ±5% (shaded area) will be considered to be no change. In general, it can be seen that the strength improves for all nearly all test temperatures, regardless of heat-treatment temperature. However, it is also seen that the heat-treatment has negligible impact on the observed room temperature strength, which is consistent with the

observations of Watts et al., who reported no change in strength for ZrB_2-30SiC ceramics thermally annealed above 1400°C.[35] The largest improvements in strength are seen between 800 and 1200°C, with improvements of 10 to 20% over the baseline. Above 1200°C, Figure 3b shows a general negative trend with heat-treatment temperature for change in strength. HT14 exhibited an ~8 to 12% increase in strength between 1400 and 1600°C. HT15 and HT16 only showed improvement at 1600°C, and HT18 showed reduced strength at 1400°C.

Modulus followed previously observed trends, with a decrease in modulus with increasing test temperature.[33] Three regimes are observed for the as-processed and heat-treated materials (RT to 1200°C, 1200 to 1500°C, and 1500 to 1600°C). The change in elastic modulus from the as-processed material is shown in Figure 4. The modulus is generally unchanging with heat-treatment temperature up to 1200°C, aside from the HT15 outlier at 800°C. HT14 shows a small, 5 to 8%, improvement in modulus between 1000 and 1400°C, with HT18 showing a at 1000 and 1200°C. Above 1200°C, Figure 4b shows an increase in modulus between from HT14 to HT15, followed by a decreasing trend to HT18. HT14 and HT18 showed no improvement, while HT15 and HT16 showed a 12 to 18% and 10% increase in modulus, respectively, at 1500 and 1600°C.

Since previous studies have identified inhomogeneous oxide scale growth as the critical flaw and cause of strength degradation in ZrB_2-SiC above 1200°C,[33] it is curious that these temperatures are where improvements in strength following heat-treatment were observed. Assuming heat-treatment did not alter the oxidation behavior of the materials, it would be expected that the

strengths would be quite similar under oxidizing conditions above 1200°C. However, assuming that the oxidation behavior of the materials didn't change, but measuring that the strength did change, it is reasonable to suspect that the toughness of the materials changed as a result of heat-treatment. From Griffith and Irwin type analysis, it is known that toughness, and by extension strength, is a function of elastic modulus and surface free energy.[36] Increases in elastic moduli were observed following heat-treatment, thus some of the improvement in strength can be attributed to the increase in modulus. However, since not all increases in strength were accompanied by increases in modulus, changes in surface energy might be responsible.

Heat-treatment may be affecting strength and modulus in several ways. Raw boride and carbide based ceramic powders typically contain surface oxides. Though various methods are used to remove these oxides during sintering, some amount of oxide is expected to remain and form grain boundary phases/films in the sintered microstructure.[2, 37] Further, commercial ZrB_2 powder contains other impurities such as iron, aluminum, and yttrium, as well as oxygen, nitrogen, and carbon which can also form grain boundary films and precipitates. Tungsten and cobalt were also likely added through grinding media erosion during powder processing. Following densification, several additional phases were observed in the microstructure in addition to ZrB_2, SiC, and B_4C. The two most common additional phases were hexagonal boron nitride (h-BN) and a Zr-Fe-Co-Si rich phase (Figure 5). The h-BN has been observed previously in ZrB_2 based ceramics, and typically occurs at grain interfaces, either as individual grains or

clusters.[37, 38] The Zr-Fe-Co-Si rich phases appear at grain boundaries and junctions, and have a morphology that suggests liquid at the processing temperatures. This phase has not been observed previously, and is thought to be a result of the iron impurity in the raw powders and the cobalt added through media erosion. Both iron and cobalt have been previously shown to form silicides and free carbon when heated in contact with SiC.[39, 40] Further, iron and cobalt both form borides, however, their reactions with ZrB_2 have not been studied. Finally, ZrB_2 and α-SiC belonging to hexagonal crystal systems, and have active slip systems along the basal and prismatic planes, allowing for the formation of dislocations; α-SiC also forms stacking faults as a result of its many polymorphs. Thus it is possible that heat-treatment could alter oxide phases already present at grain interfaces, allow for the precipitation of new phases from dissolved species, allow further reaction of Fe-Co, and change the dislocation density in the ZrB_2 and SiC phases.

Figure 5 shows TEM micrographs of several typical features in AP. Figure 5a and b highlight typical dislocation and stacking fault densities. It can be seen that a majority of the dislocations appear to originate from grain interfaces. Figure 5c shows a typical h-BN grain along a ZrB_2-SiC interface, in addition to a SiC grain exhibiting stacking faults. Figure 5d demonstrates the Zr-Fe-Co-Si containing phase. The rounded morphology of the phase suggests that it was liquid at the processing temperatures used. In this instance, there is a ZrB_2-ZrB_2- ZrB_2 triple junction (bottom) and ZrB_2- ZrB_2- ZrB_2-SiC quadruple junction (top) that contain a discrete amount of the phase, with a grain boundary film of

the same phase connecting the two pockets. Figure 6 shows TEM micrographs of several typical features in HT14 that are not present in AP. Although it had not been quantitatively measured, the dislocation densities in HT14 appear to be increased from AP. There does not appear to be a change in the amount of h-BN present, but the Zr-Fe-Co-Si containing phase appears to be reduced. The most notable change between AP and HT14 is the increased appearance of Zr-Al-Y-O containing phases both at the grain boundaries and triple junctions and intergranular to the ZrB_2. Finally, Figure 6d shows the appearance of nano-scale intragranular oxide precipitates in ZrB_2 grains (lighter grey/white spots). These results are not conclusive, but suggest more detailed micrographic studies would be beneficial in determining the mechanisms by which heat-treatment is affecting the properties of this material.

4. Summary

The flexure strength and elastic modulus of dense, hot-pressed ZrB_2- 30 vol% SiC ceramics were characterized as a function of temperature up to 1600°C in air. Hot pressed specimens were tested as-processed or following an annealing heat-treatment at 1400°C, 1500°C, 1600°C, or 1800°C for 10 hours in an argon atmosphere. Annealing had minimal impact on the room temperature strength, increasing the strength from 690 to 710 MPa. All heat-treatment conditions improved the strength at test temperatures between 800 and 1200°C, with increases of 10 to 20% over the as-processed material. Annealing at 1400°C resulted in the largest improvement in flexure strength, with increases of 7, 8, and 12% at 1400, 1500, and 1600°C, respectively. Elastic modulus was

nominally unchanged following heat-treatment at test temperatures up to 1200°C. Above this temperature, the heat-treatments at 1500 and 1600°C resulted in an increase in modulus, while heat-treatments at 1400 and 1800°C resulted in a decrease in modulus. Heat-treatment at 1500°C resulted in a 6, 12, and 18% improvement in modulus at temperatures of 1400, 1500, and 1600°C compared to the as-processed material. Changes in ZrB_2 and SiC grain size were not observed for these heat-treatment conditions. SiC and B_4C cluster size was largely unchanged, with a slight increase observed following the 1800°C annealing condition. TEM analysis suggests that additional phases may be forming during heat-treatment and/or changes in dislocation and stacking fault density may be occurring. This study shows that thermal annealing may be a useful method for improving the elevated temperature mechanical properties of ZrB_2 based ceramics. Further testing in inert atmosphere to remove the complicating effects of oxidation, as well as additional micrographic studies to better determine the microstructural changes occurring during thermal annealing are recommended.

Acknowledgements

The authors would like to thank Dr. Jessica Terbush of the Advanced Materials Characterization Laboratory at Missouri S&T for her assistance with TEM characterization, and Dr. Jeffrey Smith for technical discussions. Research at Missouri S&T was supported by the High Temperature Aerospace Materials Program (Dr. Ali Sayir, program manager) in the Air Force Office of Scientific Research through grant FA9550-09-1-0168.

References

1. R. A. Cutler, "Engineering Properties of Borides," pp. 787-803. in Ceramics and Glasses: Engineered Materials Handbook, Vol. 4**.** Edited by S. J. S. Schneider Jr. ASM International, Materials Park, OH, 1991.
2. W. G. Fahrenholtz, G. E. Hilmas, I. G. Talmy, and J. A. Zaykoski, "Refractory Diborides of Zirconium and Hafnium," *J. Am. Ceram. Soc.,* **95**[5] 1347-64 (2007).
3. A. L. Chamberlain, W. G. Fahrenholtz, and G. E. Hilmas, "High-Strength Zirconium Diboride-Based Ceramics," *J. Am. Ceram. Soc.,* **87**[6] 1170-72 (2004).
4. A. Rezaie, W. G. Fahrenholtz, and G. E. Hilmas, "Effect of Hot Pressing Time and Temperature on the Microstructure and Mechanical Properties of ZrB_2-SiC," *J. Mater. Sci.,* **42**[8] 2735-44 (2007).
5. J. Watts, G. E. Hilmas, and W. G. Fahrenholtz, "Mechanical Characterization of ZrB_2-SiC Composites with Varying SiC Particle Sizes," *J. Am. Ceram. Soc.,* **94**[12] 4410-18 (2011).
6. S. Zhu, W. G. Fahrenholtz, and G. E. Hilmas, "Influence of Silicon Carbide Particle Size on the Microstructure and Mechanical Properties of Zirconium Diboride-Silicon Carbide Ceramics," *J. Eur. Ceram. Soc.,* **27**[4] 2077-83 (2007).

7. A. L. Chamberlain, W. G. Fahrenholtz, and G. E. Hilmas, "Low-Temperature Densification of Zirconium Diboride Ceramics by Reactive Hot Pressing," *J. Am. Ceram. Soc.,* **89**[12] 6368-75 (2006).

8. F. Monteverde, S. Guicciardi, and A. Bellosi, "Advances in Microstructure and Mechanical Properties of Zirconium Diboride Based Ceramics," *Mater. Sci. Eng., A,* **346** 310-19 (2003).

9. R. Loehman, E. Corral, H. P. Dumm, P. Kotula, and R. Tandon, "Ultra High Temperature Ceramics for Hypersonic Vehicle Applications", Report No. SAND 2006-2925, Sandia National Laboratories, Albuquerque, NM, (2006).

10. O. N. Grigoriev, B. A. Galanov, V. A. Kotenko, S. M. Ivanov, A. V. Koroteev, and N. P. Brodnikovsky, "Mechanical Properties of ZrB_2-SiC($ZrSi_2$) Ceramics," *J. Eur. Ceram. Soc.,* **30** 2173-81 (2010).

11. J. Zou, G. J. Zhang, C. F. Hu, T. Nishimura, Y. Sakka, H. Tanaka, J. Vleugels, and O. Van der Biest, "High-Temperature Bending Strength, Internal Friction and Stiffness of ZrB_2–20vol% SiC ceramics," *J. Eur. Ceram. Soc.,* **32**[10] 2519-27 (2012).

12. J. Zou, G. J. Zhang, C. F. Hu, T. Nishimura, Y. Sakka, J. Vleugels, and O. Van der Biest, "Strong ZrB_2–SiC–WC Ceramics at 1600°C," *J. Am. Ceram. Soc.,* **95**[3] 874-78 (2012).

13. W. H. Rhodes, E. V. Clougherty, and D. Kalish, "Research and Development of Refractory Oxidation-Resistant Diborides Part II, Volume

IV: Mechanical Properties", Report No. Technical Report AFML-TR-68-190, Part II, Volume IV, Wright Patterson Air Forse Base, OH, (1970).

14. S. Zhu, *Densification, Microstructure, and Mechanical Properties of Zirconium Diboride Based Ultra-High Temperature Ceramics*, Ph. D. thesis., Missouri University of Science and Technology, Rolla, MO, (2008).

15. D. J. Magley, R. A. Winholtz, and K. T. Faber, "Residual Stresses in a Two-Phase Microcracking Ceramic," *J. Am. Ceram. Soc.,* **72**[6] 1641-44 (1990).

16. V. Tvergaard and J. W. Hutchinson, "Microcracking in Ceramics Induced by Thermal Expansion or Elastic Anisotropy," *J. Am. Ceram. Soc.,* **71**[3] 157-66 (1988).

17. Y. S. Touloukian, C. Ho, and D. Dewitt. in Thermal Expansion: Nonmetallic Solids, Vol. 13**.** Edited by Touloukian. New York: IFI/Plenu, 1977.

18. G. V. Tsagareishvili, T. G. Nakashidze, J. S. Jobava, G. P. Lomidze, D. E. Khulelidze, D. S. Tsagareishvili, and O. A. Tsagareishvili, "Thermal expansion of boron and boron carbide," *J. Less-Common Metals,* **117**[1–2] 159-61 (1986).

19. J. Watts, G. Hilmas, W. G. Fahrenholtz, D. Brown, and B. Clausen, "Stress measurements in ZrB_2–SiC composites using Raman spectroscopy and neutron diffraction," *J. Eur. Ceram. Soc.,* **30**[11] 2165-71 (2010).

20. J. Watts, G. E. Hilmas, W. G. Fahrenholtz, D. Brown, and B. Clausen, "Measurement of Thermal Residual Stresses in ZrB_2-SiC Composites," *J. Eur. Ceram. Soc.,* **31**[9] 1811-20 (2011).

21. C.-W. Li, S.-C. Lui, and J. Goldacker, "Relation between Strength, Microstructure, and Grain-Bridging Characteristics in In Situ Reinforced Silicon Nitride," *J. Am. Ceram. Soc.,* **78**[2] 449-59 (1995).

22. J. J. Cao, W. J. Moberly-Chan, L. C. De Jonghe, C. J. Gilbert, and R. O. Ritchie, "In Situ Toughened Silicon Carbide with Al-B-C Additions," *J. Am. Ceram. Soc.,* **79**[2] 461-69 (1996).

23. N. P. Padture, "In Situ-Toughened Silicon Carbide," *J. Am. Ceram. Soc.,* **77**[2] 519-23 (1994).

24. S. K. Lee, Y. C. Kim, and C. H. Kim, "Microstructural developement and mechanical properties of pressureless-sintered SiC with plate-like grains using Al_2O_3-Y_2O_3 additives," *J. Mater. Sci.,* **29**[5324-5326] (1994).

25. D. Sciti, S. Guicciardi, and A. Bellosi, "Effect of annealing treatments on microstructure and mechanical properties of liquid-phase-sintered silicon carbide," *J. Eur. Ceram. Soc.,* **21**[5] 621-32 (2001).

26. H. J. Kleebe, "SiC and Si_3N_4 materials with improved fracture resistance," *J. Eur. Ceram. Soc.,* **10**[3] 151-59 (1992).

27. M. K. Cinibulk, G. Thomas, and S. M. Johnson, "Grain-Boundary-Phase Crystallization and Strength of Silicon Nitride Sintered with a YSlAlON Glass," *J. Am. Ceram. Soc.,* **73**[6] 1606-12 (1990).

28. M. K. Cinibulk, G. Thomas, and S. M. Johnson, "Fabrication and Secondary-Phase Crystallization of Rare-Earth Disilicate–Silicon Nitride Ceramics," *J. Am. Ceram. Soc.,* **75**[8] 2037-43 (1992).

29. L. K. L. Falk and G. L. Dunlop, "Crystallization of the glassy phase in an Si_3N_4 material by post-sintering heat-treatments," *J. Mater. Sci.,* **22**[12] 4369-76 (1987).

30. A. H. Heuer and V. L. K. Lou, "Volatility Diagrams for Silica, Silicon Nitride, and Silicon Carbide and Their Application to High-Temperature Decomposition and Oxidation," *J. Am. Ceram. Soc.,* **73**[10] 2789-803 (1990).

31. G. A. Gogotsi, Y. G. Gogotsi, and D. Y. Ostrovoj, "Mechanical behaviour of hot-pressed boron carbide in various atmospheres," *J. Mater. Sci. Lett.,* **7**[8] 814-16 (1988).

32. V. A. Lavrenko and Y. G. Gogotsi, "Influence of oxidation on the composition and structure of the surface layer of hot-pressed boron carbide," *Oxid. Met.,* **29**[3-4] 193-202 (1988).

33. E. W. Neuman, G. E. Hilmas, and W. G. Fahrenholtz, "Mechanical Behavior of Zirconium Diboride-Silicon Carbide Ceramics at Elevated Temperature In Air " *J. Eur. Ceram. Soc.,* **35** 2889-99 (2013).

34. D. He and N. N. Ekere, "Effect of Particle Size Ratio on the Conducting Percolation Threshold of Granular Conductive–Insulating Composites," *J. Phys. D: Appl. Phys.,* **37**[13] 1848 (2004).

35. J. L. Watts, G. E. Hilmas, W. G. Fahrenholtz, D. Brown, and B. Clausen, "Measurement of Thermal Residual Stresses in ZrB_2–SiC Composites," *J. Eur. Ceram. Soc.,* **31**[9] 1811-20 (2011).

36. J. Wachtman, "Mechanical Properties of Ceramics.*"* John Wiley & Sons, Inc.: New York, (1996).

37. E. Eakins, *Nanoscale Characterisation of Effect of SiC on Microstructure and Oxidation Behavior of ZrB_2-Based Ceramics*, Ph.D. thesis., Imperial College London, London, England, (2011).

38. J. Zou, G. J. Zhang, H. Zhanh, Z. R. Huang, J. Vleugels, and O. Van der Biest, "Improving high temperature properties of hot pressed ZrB_2-20 vol% SiC ceramic using high purity powders," *Ceram. Int.,* **39** 871-76 (2013).

39. C. S. Lim, H. Nickel, A. Naoumidis, and E. Gyarmati, "Interface structure and reaction kinetics between SiC and thick cobalt foils," *J. Mater. Sci.,* **31**[16] 4241-47 (1996).

40. R. C. J. Schiepers, F. J. J. van Loo, and G. de With, "Reactions between α-Silicon Carbide Ceramic and Nickel or Iron," *J. Am. Ceram. Soc.,* **71**[6] C-284-C-87 (1988).

Table I. Summary of volume fraction of ZrB_2, SiC, and B_4C in as-processed and heat-treated ZrB_2-30vol% SiC measured by image analysis.

Phase	Heat-treatment Temperature (°C)				
	As Processed	1400°C	1500°C	1600°C	1800°C
ZrB_2	69.7 ± 0.3	69.2 ± 0.4	70.2 ± 0.5	69.9 ± 0.3	68.6 ± 0.4
SiC	28.2 ± 0.3	27.7 ± 0.4	27.7 ± 0.4	27.2 ± 0.3	28.6 ± 0.3
B_4C	2.1 ± 0.1	3.1 ± 0.1	2.1 ± 0.3	2.9 ± 0.2	2.9 ± 0.3

Table II. Summary of average ZrB_2 and SiC grain size, average SiC and B_4C cluster size, and maximum SiC cluster size for ZrB_2-30 vol% SiC ceramics heat-treated at between 1400°C and 1800°C for 10 hours.

Heat-treatment Temperature (°C)	Grain Size (µm)		Cluster Size (µm)			
	ZrB_2	SiC	SiC	SiC_{max}	B_4C	B_4C_{max}
As-processed	1.86 ± 0.91	1.20 ± 0.51	3.77 ± 3.27	32.9	1.16 ± 0.81	11.9
1400	1.85 ± 0.83	1.29 ± 0.57	3.51 ± 3.16	30.0	2.07 ± 1.29	11.3
1500	1.99 ± 1.04	1.16 ± 0.51	3.48 ± 3.04	35.1	1.19 ± 0.80	12.9
1600	2.00 ± 1.04	1.13 ± 0.55	3.71 ± 3.05	27.9	2.00 ± 1.18	10.2
1800	--	--	4.57 ± 3.94	37.8	1.38 ± 1.08	11.7

Table III. Summary of elevated temperature flexure strength for as processed and heat-treated ZrB_2-30 vol% SiC. Number of specimens tested for each condition given in parenthesis.

Test Temperature (°C)	Heat-treatment Temperature (°C)				
	As-processed	1400°C	1500°C	1600°C	1800°C
RT	687 ± 63 (11)	717 ± 58 (8)	706 ± 44 (9)	722 ± 83 (10)	690 ± 47 (10)
800	753 ± 98 (9)	809 ± 130 (6)	845 ± 110 (5)	833 ± 122 (6)	923 ± 30 (3)
1000	725 ± 67 (10)	866 ±14 (6)	739 ± 78 (6)	783 ± 77 (6)	818 ± 38 (3)
1200	564 ± 77 (8)	645 ± 84 (7)	623 ± 30 (8)	635 ± 50 (7)	600 ± 29 (4)
1400	438 ±41 (8)	470 ±35 (7)	455 ± 37 (6)	449 ± 32 (5)	405 ± 24 (5)
1500	358 ± 23 (5)	386 ± 13 (5)	362 ± 20 (5)	371 ± 9 (5)	369 ± 28 (5)
1600	383 ± 42 (5)	427 ± 16 (5)	412 ± 46 (5)	415 ±23 (5)	387 ± 25 (5)

Table IV. Summary of elevated temperature elastic modulus for as-processed and heat-treated ZrB_2-30 vol% SiC.

Test Temperature (°C)	Heat-treatment Temperature (°C)				
	As-processed	1400°C	1500°C	1600°C	1800°C
RT	512 ± 15	515 ± 8	518 ± 6	512 ± 5	520 ± 13
800	439 ± 16	429 ± 10	381 ± 15	426 ± 17	452 ± 8
1000	415 ± 23	435 ± 19	420 ± 11	420 ± 25	441 ± 18
1200	363 ± 17	391 ± 20	364 ± 24	363 ± 13	386 ± 8
1400	255 ± 17	272 ± 34	270 ± 20	271 ± 9	245 ± 8
1500	213 ± 17	219 ± 12	238 ± 2	235 ± 11	198 ± 6
1600	120 ± 5	120 ± 2	142 ± 3	133 ± 18	124 ± 2

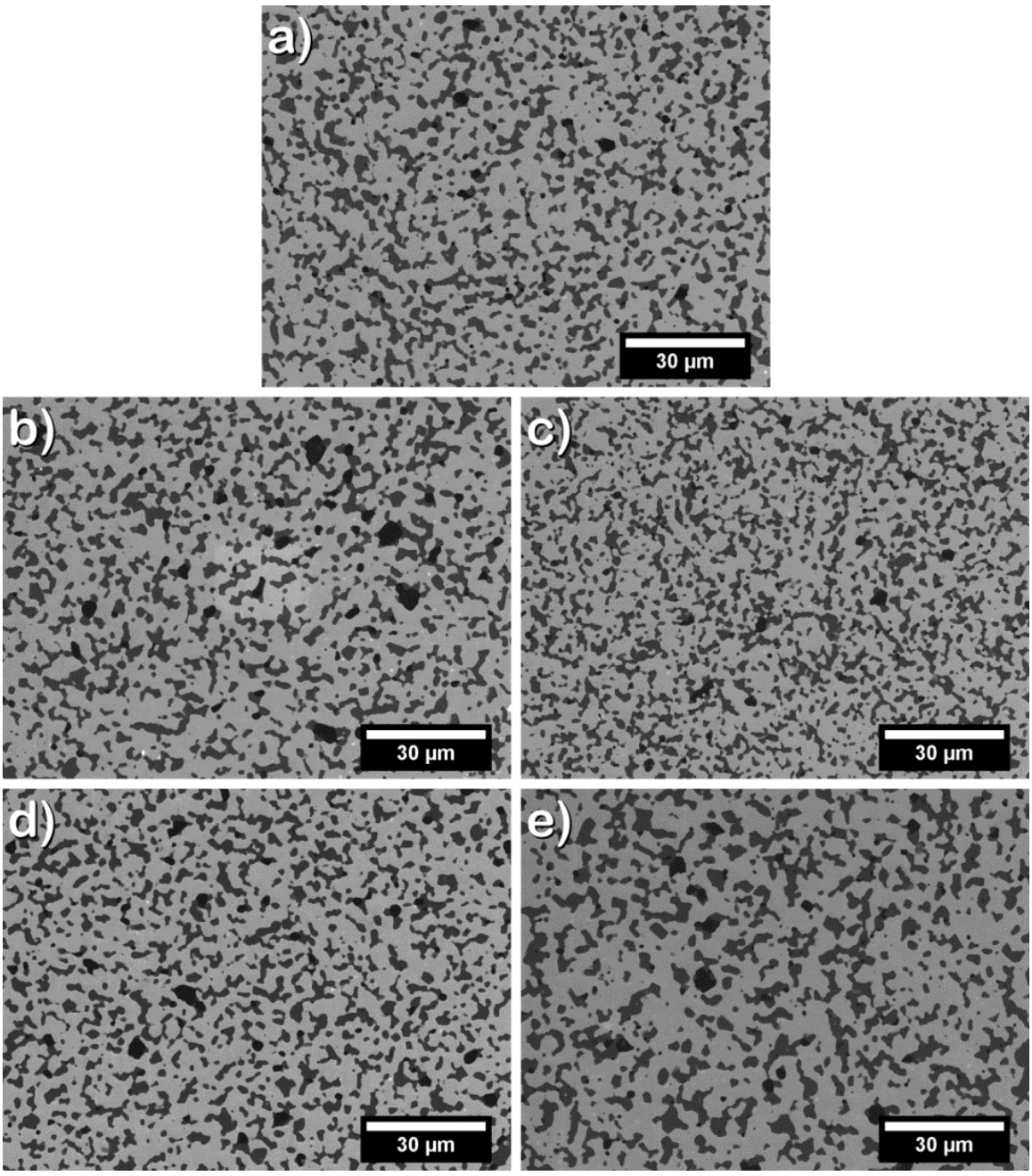

Figure 1. SEM micrographs of polished ZrB_2-30 SiC a) as-processed, and after 10 hour heat-treatments at b) 1400°C, c) 1500°C, d) 1600°C, and e) 1800°C.

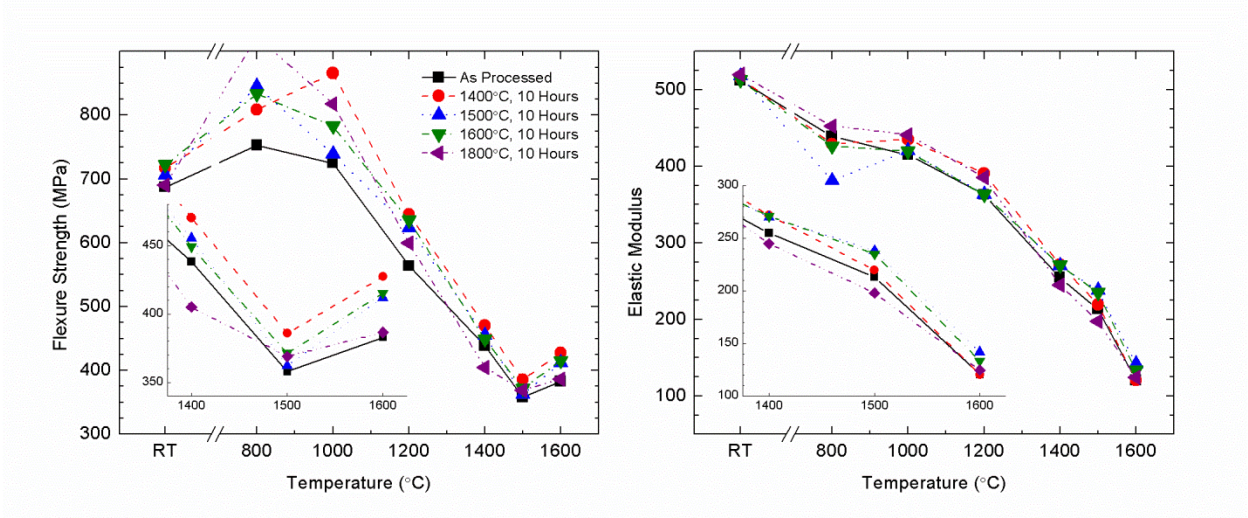

Figure 2. Flexure strength (a) and elastic modulus (b) as a function of test temperature for heat-treated ZrB_2-SiC.

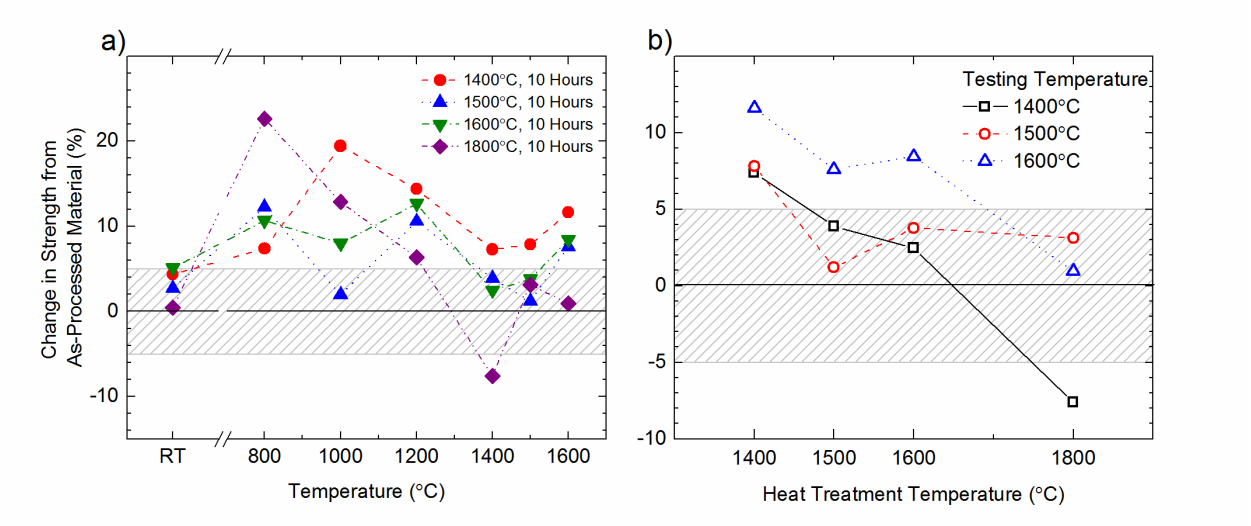

Figure 3. Change in strength from as-processed material as a function of heat-treatment temperature for specimens tested between 1400°C and 1600°C.

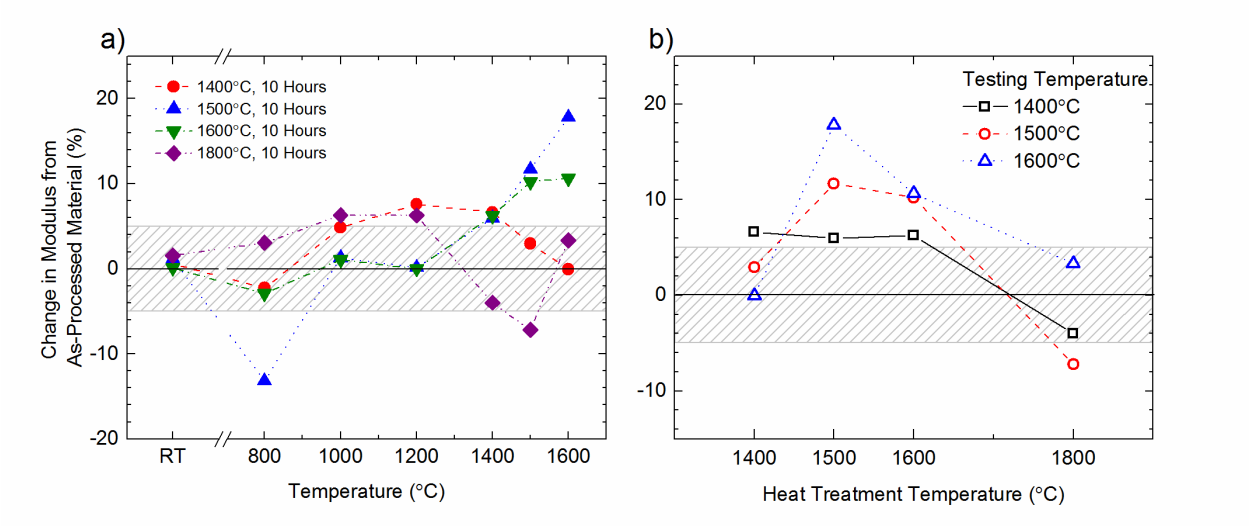

Figure 4. Change in modulus from as-processed material as a function of heat-treatment temperature for specimens tested between 1400°C and 1600°C.

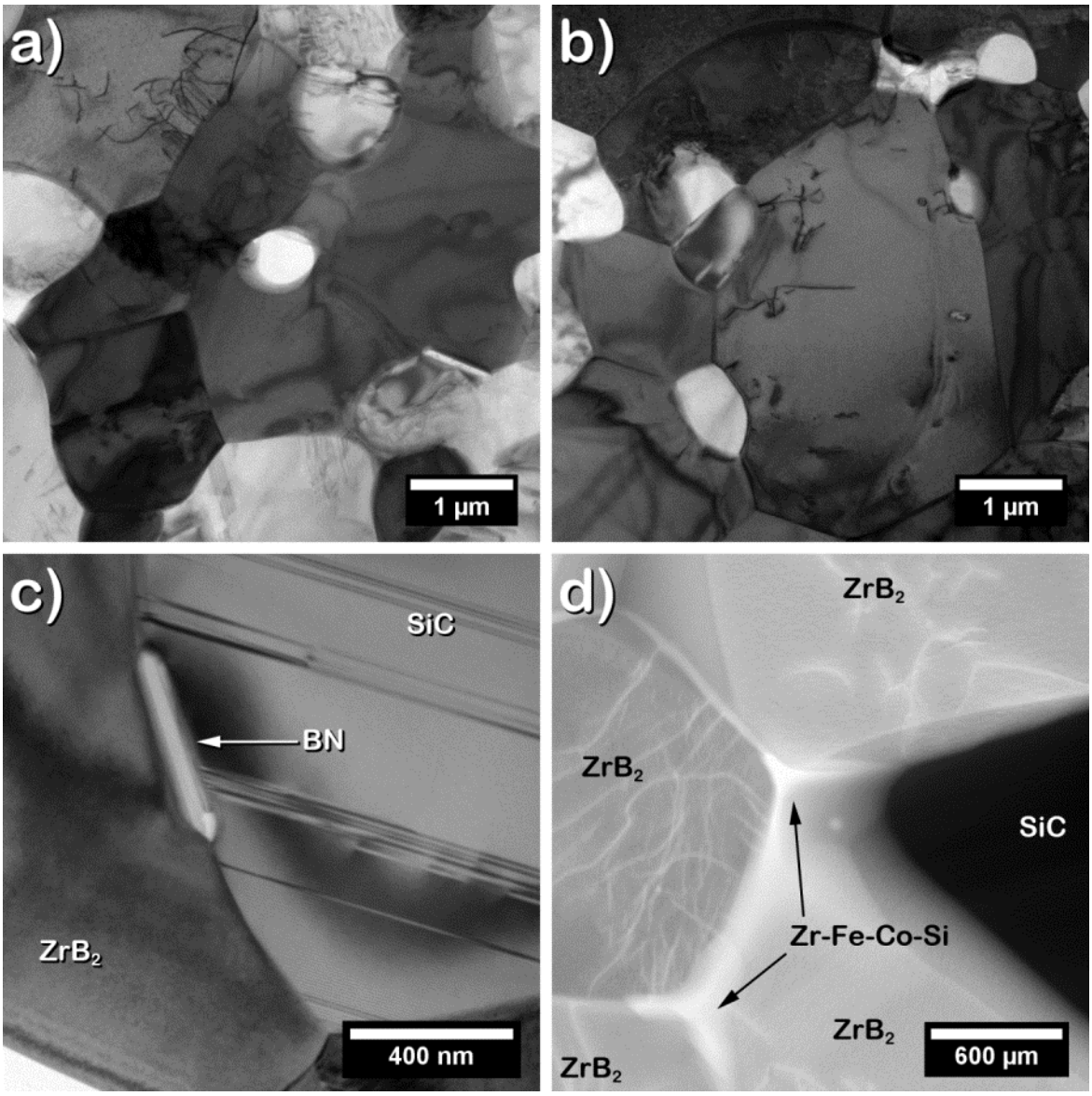

Figure 5. TEM images of AP demonstrating dislocations in ZrB_2 and SiC (a,b), BN inclusion and SiC stacking faults (c), and Zr-Fe-Co-Si rich phase (d).

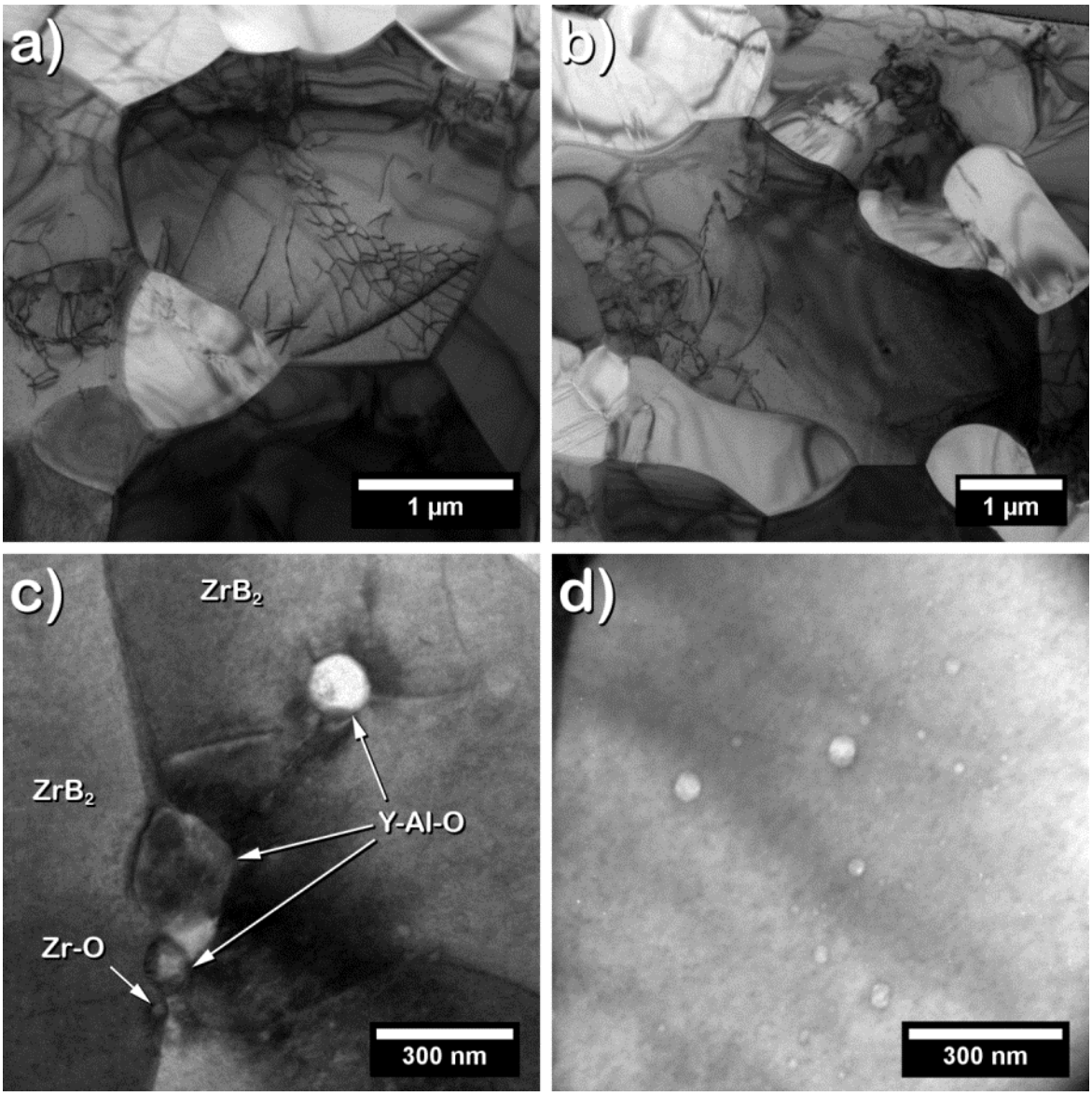

Figure 6. TEM images of HT14 demonstrating increased dislocation in ZrB_2 and SiC (a,b), and Zr-Y-Al-O type inclusions (c), and oxide precipitates intragranular to ZrB_2 (d).

V. ULTRA-HIGH TEMPERATURE STRENGTH, TOUGHNESS AND MODULUS OF A ZIRCONIUM DIBORIDE-ZIRCONIUM CARBIDE CERAMIC

Eric W. Neuman, Gregory E. Hilmas, William G. Fahrenholtz

Department of Materials Science and Engineering, Missouri University of Science and Technology Rolla, MO 65409 USA

Abstract

The mechanical properties of a ZrB_2-10 vol% ZrC ceramic were measured up to 2300°C in an argon atmosphere. Dense billets of ZrB_2-9.5vol% ZrC-0.1vol% C were produced by hot-pressing at 1900°C. The ZrB_2 grain size was 4.9 µm and ZrC cluster size was 1.8 µm. Flexure strength was 695 MPa at ambient, decreasing to 300 MPa at 1600°C, increasing to 345 MPa at 1800 and 2000°C, decreasing to 290 MPa at 2200°C. Fracture toughness was 4.8 $MPa \cdot m^{½}$ at room temperature, decreasing to 3.4 $MPa \cdot m^{½}$ at 1400°C, increasing to 4.5 $MPa \cdot m^{½}$ at 1800°C, decreasing to 3.6 $MPa \cdot m^{½}$ at 2300°C. Elastic modulus was calculated from the crosshead displacement, estimated to be 505 GPa at ambient, relatively unchanging to 1200°C, then decreasing linearly to 385 GPa at 1600°C, more slowly to 345 GPa at 2000°C, then more rapidly to 260 GPa at 2300°C. Surface flaws resulting from machining damage were the critical flaw up to 1400°C. Above 1400°C, plasticity reduces the stress at the crack tip

and the surface flaws experience sub-critical crack growth. Above 2000°C, microvoid coalescence ahead of the crack tip causes failure.

Keywords: zirconium diboride, zirconium carbide, hot pressing, mechanical properties, failure analysis

1. Introduction

Zirconium diboride (ZrB_2) has generated much interest for its potential for uses as a structural material in extreme environments. It belongs to a class of materials known as ultra-high temperature ceramics (UHTCs), characterized by melting points exceeding 3000°C.[1, 2] ZrB_2 has generated particular interest due to its relatively low density (~6.1 g/cm^3) when compared to refractory metals, high strength (400-600 MPa), modulus (515-525 GPa), hardness (~23 GPa), and moderate toughness (3-4 MPa·m^{½}). ZrB_2 also exhibits a high thermal conductivity (60-125 W·(m·K)$^{-1}$) and low electrical resistivity (7.8 – 22 μΩ·cm).[3, 4] These properties make zirconium diboride a candidate for a range of applications including molten metal crucibles, furnace electrodes, cutting tools, and wing leading edges on future hypersonic aerospace vehicles.[2]

The ZrB_2-zirconium carbide (ZrC) system offers several beneficial attributes. ZrB_2-ZrC has a high eutectic temperature of 2660°C for ZrB_2-ZrC and 2830°C for ZrB_2-$ZrC_{0.88}$.[5, 6] This is higher than ZrB_2-SiC which has a eutectic at 2270°C,[7] and ZrB_2-$MoSi_2$ and ZrB_2-$TaSi_2$ where the disilicide phase has melting points of ~2030°C and ~2200°C, respectively.[8] The CTE mismatch between

ZrB_2 (~5.2 ppm/K at 298 K)[2, 9] and ZrC (6.7 to 7.6 ppm/K at 298 to 2973 K)[10, 11] results in residual tensile stress in the ZrC and compressive stresses in the ZrB_2 matrix. This could offer improved mechanical properties at ambient temperatures, similar to TiC or SiC additions to TiB_2. Further, the presence of a second phase should reduce grain growth at elevated temperatures through grain boundary pinning, maintaining a fine grain size and improving strength at temperature. Additions of ZrC may also enhance the densification of ZrB_2, allowing for processing at lower temperatures.

To our knowledge, investigations of the mechanical behavior of the ZrB_2-ZrC system have been limited and there have been no reported investigations of the elevated temperature mechanical properties. Gropyanov et al. showed that additions of ZrC to ZrB_2 improve sintering.[12] They showed that additions of 10 vol% ZrC lowered the activation energy for sintering by ~25% and suppressed grain growth in the ZrB_2 and ZrC phase. Andrievskii et al. hot pressed ZrB_2-5 vol% ZrC with ~5 vol% porosity after hot pressing at 2200°C.[13] They also found that the addition increased the grain size of the ZrB_2 phase from 13 μm to 27 μm for similar hot pressing conditions. Kats et al. showed that 20 vol% additions of ZrC to ZrB_2 reduced the porosity to 2.9% from 10.6%, and reduced the grain size of the ZrB_2 from 6-8 μm to 2-4 μm after hot pressing at 2100°C.[14] More recently, Tsuchida et al. used spark plasma sintering to produce a 97.5% dense compact of ZrB_2-20 vol% ZrC at 1800°C.[15] Though elevated temperature creep behavior has been reported for the ZrB_2-ZrC system, strength has not.[14] Similarly, creep has been studied by numerous authors in the ZrC system,[16-19] but limited

elevated temperature strength data is available for ZrC ceramics.[20, 21] Gridneva et al. reported the strength of $ZrC_{0.95}$ to be ~120 MPa between room temperature and 500°C, increasing to ~350 MPa at ~1000°C, then decreasing to ~120 MPa at ~1800°C.

Recent studies of ZrB_2 based ceramics have begun to systematically investigate the mechanical properties at elevated temperatures.[22-25] These studies have shown that modern powders and processing methods result in ZrB_2 ceramics with improved properties compared to the historical work performed at Manlabs Inc. by Rhodes et al..[26] Neuman et al. reported the strength of monolithic ZrB_2 to be 390 MPa between room temperature and 1200°C, decreasing to ~200 MPa between 1400 and 2300°C.[24, 27] Zou et al. reported the strengths of ZrB_2-20 vol% SiC with[23] and without[22] additions of 5 vol% WC. For ZrB_2-20SiC, the strength was reported to increase to 680 MPa at 1000°C from 550 MPa at ambient, then decrease to 460 MPa at 1600°C. ZrB_2-20SiC-5WC has shown improved strength retention at elevated temperature, increasing to 675 MPa at 1600°C from 605 MPa at room temperature. The improvement in strength was attributed to removal of surface oxides from the starting powders through reaction with WC during sintering. Neuman also reported the strength of a ZrB_2-30 vol% SiC-2vol% B_4C ceramic having a room temperature strength of 700 MPa which decreased to 540 MPa at 1800°C, further decreasing to 260 MPa at 2200°C.[25] The strength of this ceramic was found to be controlled by the SiC cluster size up to 1800°C, and the formation of large B-O-C-N phases at higher temperatures.

The goal of the current study was to investigate the mechanical properties of a ZrB_2-10 vol% ZrC ceramic. The flexure strength, elastic modulus, and fracture toughness were measured for temperatures up to 2300°C in an argon atmosphere. Fractography was performed following testing to investigate the failure mechanisms.

2. Experimental Procedure

2.1. Processing

ZrB_2 powder (Grade B, H. C. Starck, Karlsruhe, Germany), ZrC powder (Grade A, H. C. Starck), and ZrH_2 (Grade S, Chemetall, Jackson, MI) were the starting materials for this study. A soluble phenolic resin (GP 2074, Georgia Pacific, Atlanta, GA) was added as a carbon precursor (~43%, 800°C, Ar/10H_2) to aid in the removal of surface oxides. The addition of phenolic resin in addition to the free carbon present in the ZrC powder results in an excess of carbon present in the microstructure, pushing the composition into the ZrB_2-ZrC_x-C phase field. Thus, ZrH_2 was added to react with residual carbon and form ZrC during hot-pressing, attempting to keep the system in the ZrB_2-ZrC_x binary phase field. Powders were batched to meet a target composition of ZrB_2-10 vol% ZrC (ZZC10) in the following amounts (wt%): ZrB_2, 88.83; ZrC, 5.98; ZrH_2, 4.16; phenolic resin, 1.03. Powders were dispersed in methyl ethyl ketone by ball milling with a dispersant (DISPERBYK®-110, BYK-Gardner USA, Columbia, MD) using ZrB_2 media.* A slurry of ZrB_2, ZrC, and ZrH_2 was ball milled for 8 hr to

* Fabricated in-house using ZrB_2 with additions of 1 wt% B_4C and 1 wt% C (phenolic source), ball milled with WC-6Co (~1wt% added to powder through

disperse the powders. Phenolic resin was added to the mixture and milled for an additional 16 hr. Contamination from media erosion was 1.02 ± 0.02 wt%. Following ball milling, the slurry was dried by rotary evaporation (Model Rotavapor R-124, Buchi, Flawil, Germany) at a temperature of 70°C, low vacuum (~27 kPa), and a rotation speed of 120 rpm. The dried powders were lightly ground to pass through a 50 mesh screen prior to hot-pressing.

Milled powders were hot-pressed (Model HP50-7010G, Thermal Technology, Santa Rosa, CA) in 63.5 mm square graphite dies lined with BN coated (SP-108, Cerac, Milwaukee, WI) graphite foil (2010-A, Mineral Seal Corp., Tucson, AZ). Prior to hot pressing, the powders were cold compacted in a uniaxial press at ~2 MPa. Powder compacts were pyrolyzed by heating at 5°C/min under flowing Ar/10H_2 to a 1 hr isothermal hold at 800°C. Following charring, the furnace was evacuated, then heated under vacuum (~13 Pa) to 1250°C with an average heating rate of 10°C/min. After holding for 2 hr, the temperature was increased to 1450°C at an average heating rate of 10°C/min. Following a 2 hr hold, the temperature was increased to 1600°C at an average heating rate of 10°C/min. After 1 hour, the furnace was back filled with Ar/10H_2 and a uniaxial load of 32 MPa was applied. Following previous studies, the Isothermal holds were used to promote reactions between surface oxides on the starting powders and carbon to remove the oxides as gaseous species.[33, 34] T he furnace was then heated at ~20°C/min to 1900°C. After 45 min, the furnace was

---

erosion). Uniaxially pressed into cylinders (0.5 in D x 0.5 in H), cold isostatically pressed, then pressurelessly sintered at 2050°C for 90 min in flowing Ar/H_2.

cooled at a rate of 20°C/min. The load was removed when the die temperature dropped below 1600°C.

2.2. Characterization

Microstructures of specimens were examined following elevated temperature testing using scanning electron microscopy (SEM; Helios Nanolab 600, FEI, Hillsboro, OR) equipped for energy dispersive spectroscopy (EDS; X-Max, Oxford Instruments, Abingdon, UK). The tensile surfaces of the specimens following testing were examined both as-tested and polished, and the fracture surfaces examined as-tested. The as-tested specimens were ultrasonically cleaned to remove furnace deposits. The polished specimens were plane ground to remove ~100 μm from the tensile surface, polished to a 0.05 μm surface finish using diamond abrasives, then etched using molten KOH at 200°C for ~2 s. ZrB_2 and SiC grain sizes were measured from SEM images using computerized image analysis (ImageJ, National Institutes of Health, Bethesda, MD). The grain size distribution of the ZrB_2 phase, and the cluster size distribution of the ZrC phase, were estimated by fitting ellipses to at least 1000 grains, or clusters, respectively.

2.3. Mechanical testing

Room temperature flexure strengths were measured in four-point bending using a fully-articulated test fixture using type-B bars (45 mm x 4 mm x 3 mm) according to ASTM C1161-02c. Flexure strength was measured at elevated temperatures (1000, 1200, 1400, 1600, 1800, 2000, 2200, and 2300°C) using the same type-B bars and following the testing procedures outlined in ASTM C1211-

08. Ten specimens were tested at room temperature and five specimens were tested at each elevated temperature. Bars were machined from the hot-pressed billets by diamond grinding on a fully automated surface grinder (FSG-3A818, Chevalier, Santa Fe Springs, CA). The flexure surface was polished to a 1 μm surface finish using diamond abrasives. Tests were performed using a screw-driven instrumented load frame (Models: 33R4204 or 5881, Instron, Norwood, MA). Elevated temperature testing was performed in an environmental chamber using an induction heated (SI-30KWLF, Superior Induction Technology, Pasadena, CA) graphite hot zone and load train, under a flowing argon atmosphere.[28] Temperature was controlled by a two-color optical pyrometer (SR-24C05, Ircon Inc., Santa Cruz, CA) and a programmable PID controller (2404, Eurotherm, Ashburn, VA). The heating profile was 100°C/min to 100°C below the test temperature, then 50°C/min to the test temperature, followed by a 5 min isothermal hold. The crosshead rate was varied with temperature (Table I) such that the load-displacement curve was linear to failure (as required by ASTM C1211).

Elastic constants were determined using the static bend test method according to ASTM standard E411-04. The elastic modulus was calculated from the slope of the load displacement curves, with the beam displacement estimated from the crosshead displacement. A minimum of five measurements were averaged to calculate the reported values. Fracture toughness was measured by the chevron notch beam method in four-point bending using a fully articulated test fixture using chevron notch type-A bars (45 mm x 3 mm x 4 mm) according

to ASTM Standard C1421-10. The chevron notch was machined using a dicing saw (Accu-cut 5200, Aremco Products, Ossining, NY) with a 0.006 in thick diamond wafering blade. The crosshead rate was varied with temperature (Table I). For elevated temperature testing, a heating rate of 50°C/min was used, followed by an isothermal hold of 5 min at the desired temperature. The notch dimensions were measured after testing using a digital microscope (KH-3000, Hirox-USA, Hackensack, NJ). Five specimens were tested at room temperature, and three specimens were tested at each of the same elevated temperatures used for flexure testing.

3. Results and discussion

Measured bulk densities for the hot-pressed specimens were 6.15 g/cm^3. The composition following hot-pressing was determined by image analysis to be 90.4 vol% ZrB_2, 9.5 vol% ZrC, and 0.1 vol% C (Figure 1). Approximately 0.05 vol% porosity was observed in the hot-pressed microstructure. Figure 1 shows a typical cross-section of a polished and chemically etched ZZC10. The average ZrB_2 grain size was 4.9 ± 3.0 μm with an aspect ratio of 1.7 ± 0.5, and a maximum observed grain size of 20.0 μm. Average ZrC cluster size was 1.8 ± 1.5 μm with an aspect ratio of 1.7 ± 0.7, and a maximum observed size of 9.8 μm. Residual carbon was observed at the grain boundaries and triple junctions, while porosity was observed at grain boundaries, triple junctions, and entrapped within ZrB_2 grains. Measured values for the flexure strength, fracture toughness, and elastic modulus are summarized in Table I. All specimens showed linear-

elastic behavior to failure, and no macroscopic creep was observed from the bars following testing.

Elastic modulus (Figure 2) was calculated from the crosshead displacement during testing, and should be considered an estimate. The modulus at room temperature was 505 GPa, which is lower than the predicted modulus of 518 GPa from rule of mixtures using 524 GPa for ZrB_2[24] and 465 GPa for ZrC.[29] However, given that the range of values reported for the modulus of ZrB_2 and ZrC range from 490-530 GPa[1, 24, 30, 31] and 350-465 GPa,[29, 32] the measured value is consistent. Modulus was relatively unchanged up to 1200°C, decreasing linearly to 385 GPa at 1600°C. A similar trend is observed in monolithic ZrB_2 by Rhodes,[26] Zhu,[33] and Neuman,[24] however, the values of ZZC10 are ~100 GPa higher than those reported between 1000 and 1600°C. This decrease has previously been attributed to the softening of oxide phases at grain boundaries and triple junctions.[26] Since the ZrC lattice can accommodate a large amount of oxygen, even forming ZrOC phases, this may account for the less severe decrease in modulus compared to monolithic ZrB_2. Further, SEM and EDS analysis revealed that some of the ZrC grains contained significant amounts of oxygen (not shown), suggesting that the ZrC is acting as a sink for oxygen, reducing the amount of oxide phase present in the microstructure. The modulus then steadily decreases to 345 GPa at 2000°C, decreasing more rapidly to 205 GPa at 2200°C and 260 GPa at 2300°C. Wachtman et al. showed that the elastic modulus of polycrystalline ceramics displayed a gradual linear decrease with increasing temperature, followed by a more rapid increase at

higher temperatures.[34] This rapid decrease in modulus at elevated temperature has been primarily attributed to grain boundary sliding and diffusional creep. Further, the transitions in modulus trend correspond to the transitions in deformation mechanism shown by Wang and Vandeperre,[35] showing power law creep for ZrB_2 between 1000 and 2000°C, low temperature power law creep for ZrC from 1000 to 1600°C and high temperature power law creep above 1600°C, with diffusional creep for ZrB_2 above 2000°C. Additionally, some of the decrease in modulus at 2200 and 2300°C may be a result of the proximity of the ZrB_2-ZrC-C eutectic at 2360°C.[5]

Figure 3 shows flexure strength as function of temperature. Strength decreased from 695 MPa at room temperature to 660 MPa at 1000°C. Between 1000°C and 1600°C, strength decreases to 300 MPa. A similar decrease in strength has been observed for monolithic ZrB_2 between 1200°C and 1400-1600°C by Rhodes,[26] Zhu,[33] and Neuman.[24] This decrease in strength has also been observed between 1000°C and 1600°C for monolithic TiC by Kharchenko,[36] and monolithic ZrC by Gridneva.[20] The strength increases above 1600°C to ~345 MPa at 1800 and 2000°C, decreasing to ~290 MPa at 2200 and 2300°C. A similar increase in strength with temperature at 1800-2000°C was observed by Rhodes for monolithic ZrB_2, while Neuman observed a plateau in strength above 1600°C. Leipold and Nielsen reported a decreasing tensile strength with increasing temperature for ZrC between 1600 and 2600°C, but the results were likely influenced by nearly 2% carbon impurities present at grain boundaries.[21] Kharchenko reports similar behavior in monolithic TiC where the flexure strength

increased from ~60 MPa at 1500°C to ~80 MPa at 1900°C, returning to ~60 MPa at 2200°C.

Fracture toughness as a function of temperature is shown in Figure 2. Toughness was ~4.8 MPa·$m^{½}$ at room temperature increasing to 5.1 MPa·$m^{½}$ at 1000°C, decreasing to 3.4 MPa·$m^{½}$ at 1400°C. The increase at 1000°C may be a result of flaw healing of machining damage occurring through oxidation of the specimen surface. Decreases in toughness and modulus are a result of changes in the microstructure and/or stress state of the material. Improvements in the toughness of two-phase particulate ceramics have been shown to be a result of thermal residual stresses generated from the CTE mismatch between the phases upon cooling from processing temperatures.[37-39] Upon heating, these stresses are reduced and the toughness decreases.[39] While not investigate for the ZrB_2-ZrC system, previous research by Watts in the ZrB_2-SiC system has suggested that thermal residual stresses begin to accumulate at approximately 1400°C on cooling.[40] It is reasonable to expect accumulation of thermal residual stresses to accumulate in the ZrB_2-ZrC system at similar temperatures. Unsurprisingly then, a discontinuous change in toughness is observed at around 1400°C in ZZC10, the stress relaxation temperature in ZrB_2-SiC as reported by Watts.[40] Since no microcracking is observed in ZZC10, it is assumed that the reduction in toughness is a result of the reduction of thermal residual stress upon heating. Increasing in temperature from 1400°C observes an increase in toughness between 1600 and 2000°C, with a maximum toughness of 4.5 MPa·$m^{½}$ occurring at 1800°C. Toughness then decreases to ~3.5 MPa·$m^{½}$ at 2200 and 2300°C.

The increase in toughness between 1600°C and 2000°C is attributed to stress relief ahead of the crack tip by plastic flow. Plasticity has been observed in both ZrB_2 and ZrC ceramics at these temperatures by numerous researchers.[19, 26, 41, 42] Fracture in ceramics at elevated temperature typically involves the nucleation, growth, and coalescence of microvoids.[43] The reduction in toughness observed at 2200 and 2300°C is attributed to enhanced dislocation motion, resulting in the coalescence of microvoids ahead of the crack tip. Enhanced creep was observed in ZrB_2 above 2000°C by Rhodes[26] and in ZrC by Leipold[21] and Zubarev.[16, 17] In the case of ZrC, the enhanced creep was characterized by increased cavitation and microvoid coalescence,[17, 21] and that the creep activation energies at temperatures above 2000°C corresponded to the diffusion of carbon through ZrC.[44] Thus, the residual carbon impurities at the grain boundaries and triple junctions contribute to increased microvoid formation and coalescence in ZZC10, resulting in a reduction in toughness above 2000°C.

Following strength testing, the fracture surfaces of the specimens were examined to identify the failure origins. The critical flaw size was estimated using a Griffith type analysis (Figure 3), utilizing the measured flexure strength, fracture toughness, and a geometric stress intensity factor of Y = 1.59 and Y= 1.99 (typical crack geometries observed by fractography). Between room temperature and 1400°C, the observed critical flaws were surface flaws typically between 25 and 30 μm, with semi-circular (Y=1.29) to semi-elliptical (Y=1.59) geometries. Despite the polishing procedure used, these flaws appear to be the result of machining and/or handling damage, with multiple smaller surface flaws visible on

the tensile side of the fracture surface. Figure 4 shows a typical zipper crack following fracture. Figure 5 shows an example of a critical flaw observed at 1400°C, but typical of the failure origins observed between room temperature and 1400°C. The primary crack can be seen emanating from a large region of damage associate with the zipper crack, with secondary cracks emanating from smaller regions of damage along the tensile surface of specimen. The critical flaw between room temperature and 1400°C was typically the largest region of damage in a zipper crack.

Above 1600°C, the critical flaw size increases to between 40 and 60 µm. The flaws appear to be a result of the sub-critical growth and link-up of the surface flaws introduced by machining/handling, having a long semi-elliptical geometry (Y=1.99). The estimated (from Griffith type analysis) and observed flaw sizes decrease from ~60 µm at 1600°C to ~40 µm at 2300°C. Figure 6 shows a failure origin observed after fracture at 1600°C, which is typical of flaws seen between 1600°C and 2000°C. Several cracks of similar depth can be seen emanating from the zipper crack seen at lower temperatures. At these temperatures however, no single crack appears to be the cause of failure. Instead, the cracks continue to grow until several link-up, changing the crack's geometry from a short semi-ellipse to a long semi-ellipse, exceeding K_{IC} and resulting in failure of the specimen. From the discussion above, it is thought that plasticity at these temperatures is relieving stress at the crack tip, allowing these cracks time to grow and link-up. This plasticity increases toughness, resulting in larger flaws prior to failure than is observed below 1600°C. Above 2000°C, the

same type of flaw is observed, but is slightly changed. As discussed above, increased amounts of cavitation and microvoid coalescence are observed in ZrC containing ceramics resulting from carbon impurities at grain boundaries and junctions. Figure 7 shows a failure origin at 2300°C, which is similar to that shown in for 1600°C in Figure 6. However, the detail of the crack front shows numerous microvoids, which were not observed between 1600°C and 2000°C. These microvoids were also not observed in regions of the tensile side of the fracture surface away from the surface cracks. Since the fracture toughness was also observed to decrease at 2200 and 2300°C, it is suggested that microvoid coalescence was occurring in advance of the crack tip, resulting in the formation of the critical flaws at 2200 and 2300°C.

In order to produce a ZrB_2-ZrC ceramic with improved high temperature mechanical properties, several methods are suggested. First, the material is sensitive to flaws introduced during specimen preparation by machining and polishing. In this study, polishing was conducted such that two to three times the depth of the diamond grit size used for each polishing step was removed. Despite this, surface damage was still the source of failure in these materials. Second, since ZrC can form ZrOC compounds of varying stoichiometry, the surface oxides present may not be reduced through previously suggested methods of vacuum isothermal holds and carbothermal reduction. Instead, they may simply diffuse into the ZrC phase forming ZrO_xC_{y-x}, which may be influencing the observed stiffness of the material. Finally, residual phases, such

as carbon, should be eliminated from the microstructure, as they have been shown to promote creep in ZrB_2 and ZrC based ceramics.

4. Summary

Flexure strength, fracture toughness, and elastic modulus of a ZrB_2-10vol% ZrC ceramic were measured up to 2300°C in an argon atmosphere. These are the first results reported for a ZrB_2-ZrC composite at elevated temperatures. Dense billets of ZrB_2-ZrC with a ZrB_2 grain size of 4.9 and ZrC cluster size of 1.8 were produced by hot-pressing at 1900°C. Flexure strength was 695 MPa at ambient, decreasing to 300 MPa at 1600°C, increasing to 345 MPa at 1800 and 2000°C, finally decreasing to 290 MPa at 2200 and 2300°C. Fracture toughness was measured using the chevron notch beam method, finding toughness to be 4.8 $MPa \cdot m^{½}$ at room temperature, decreasing to 3.4 $MPa \cdot m^{½}$ at 1400°C, then increasing to 4.5 $MPa \cdot m^{½}$ at 1800°C, and finally decreasing to 3.6 $MPa \cdot m^{½}$ at 2300°C. Elastic modulus was calculated from the crosshead displacement, estimated to be 505 GPa at ambient, relatively unchanging to 1200°C. Modulus then decreased near linearly to 385 GPa at 1600°C, decreasing more slowly to 345 GPa at 2000°C, then decreasing more rapidly to 260 GPa at 2300°C. Surface flaws resulting from machining and handling damage were determined to be the critical flaw up to 1400°C. Above 1400°C, it is suggested that plasticity reduces the stress at the crack tip, allowing the surface flaws to experience sub-critical crack growth. Above 2000°C, micro void coalescence is the suggested failure mechanism, due to enhanced diffusion resulting from carbon impurities at grain junctions.

Acknowledgements

The authors would like to thank Dr. Jeremy Watts for his assistance in the design and fabrication of the ultra-high temperature mechanical testing furnace. We thank Mr. Lucas Showalter and Mr. Conner Wittmaier for their assistance with the production of the ZrB_2 grinding media used in this study, and for their assistance with powder processing and specimen preparation. We would also like to the Advanced Materials Characterization Laboratory at Missouri S&T for their assistance with specimen characterization. Research at Missouri S&T was supported by the High Temperature Aerospace Materials Program (Dr. Ali Sayir, program manager) in the Air Force Office of Scientific Research through grant FA9550-09-1-0168.

References

1. R. A. Cutler, "Engineering Properties of Borides," pp. 787-803. in Ceramics and Glasses: Engineered Materials Handbook, Vol. 4**.** Edited by S. J. S. Schneider Jr. ASM International, Materials Park, OH, 1991.
2. W. G. Fahrenholtz, G. E. Hilmas, I. G. Talmy, and J. A. Zaykoski, "Refractory Diborides of Zirconium and Hafnium," *J. Am. Ceram. Soc.,* **95**[5] 1347-64 (2007).
3. M. Rahman, C. C. Wang, W. Chen, S. A. Akbar, and C. Mroz, "Electrical Resistivity of Titanium Diboride and Zirconium Diboride," *J. Am. Ceram. Soc.,* **78**[5] 1380-82 (1995).
4. J. W. Zimmerman, G. E. Hilmas, W. G. Fahrenholtz, R. B. Dinwiddie, W. D. Porter, and H. Wang, "Thermophysical Properties of ZrB_2 and ZrB_2-SiC Ceramics," *J. Am. Ceram. Soc.,* **91**[5] 1405-11 (2008).
5. E. Rudy and S. Windisch, "Part II: Ternary Systems: Volume XIII: Phase Diagrams of the Systems Ti-B-C, Zr-B-C, and Hf-B-C" Ternary Phase Equilibria in Transition Metal-Boron-Carbon-Silicon Systems, Report No. AFML-TR-65-2, Air Force Materials Laboratory, Wright-Patterson Air Force Base, OH, (1966).
6. S. S. Ordan'yan and V. I. Unrod, "Reactions in the System ZrC-ZrB_2," *Powder Metall. Met. Ceram.,* **14**[5] 393-95 (1975).
7. S. S. Ordan'yan, A. I. Dmitriev, and E. S. Moroshkina, "Reaction of Silicon Carbide with Zirconium Diboride," *Inorg. Mater.,* **25**[10] 1487-89 (1989).

8. A. K. Vasudévan and J. J. Petrovic, "A comparative overview of molybdenum disilicide composites," *Materials Science and Engineering: A,* **155**[1–2] 1-17 (1992).

9. Y. S. Touloukian, C. Ho, and D. Dewitt. in Thermal Expansion: Nonmetallic Solids*,* Vol. 13**.** Edited by Touloukian. New York: IFI/Plenu, 1977.

10. J. H. Richardson, "Thermal Expansion of Three Group IVA Carbides to 2700°C," *J. Am. Ceram. Soc.,* **48**[10] 497-99 (1965).

11. B. R. Miccioli and P. T. B. Shaffer, "High-Temperature Thermal Expansion Behavior of Refractory Materials: I, Selected Monocarbides and Binary Carbides," *J. Am. Ceram. Soc.,* **47**[7] 351-56 (1964).

12. V. M. Gropyanov and L. M. Bel'tyukova, "Sintering and Recrystallization of ZrC-ZrB_2 Compacts," *Powder Metall. Met. Ceram.,* **7**[7] 527-33 (1968).

13. R. A. Andrievskii, L. A. Korolev, V. V. Klimenko, A. G. Lanin, I. I. Spivak, and I. L. Taubin, "Effect of Zirconium Carbide and Carbon Additions on Some Physicomechanical Properties of Zirconium Diboride," *Powder Metall. Met. Ceram.,* **19**[2] 93-94 (1980).

14. S. M. Kats, S. S. Ordan'yan, and V. I. Unrod, "Compressive Creep of Alloys of the ZrC-ZrB_2 and TiC-TiB_2 Systems," *Powder Metall. Met. Ceram.,* **20**[12] 886-90 (1981).

15. T. Tsuchida and S. Yamamoto, "Spark Plasma Sintering of ZrB_2–ZrC Powder Mixtures Synthesized by MA-SHS in Air," *J. Mater. Sci.,* **42**[3] 772-78 (2007).

16. P. V. Zubarev and A. G. Shmelev, "Creep process kinetics and long-term strength of zirconium carbide. Communication 2," *Strength Mater.,* **12**[3] 264-68 (1980).

17. P. V. Zubarev and A. G. Shmelev, "Creep process kinetics and long-term strength of zirconium carbide. Communication 1," *Strength Mater.,* **12**[2] 142-48 (1980).

18. Y. V. Miloserdin, K. V. Naboichenko, L. I. Laveikin, and A. G. Bortsov, "The high-temperature creep of zirconium carbide," *Strength Mater.,* **4**[3] 302-05 (1972).

19. D. W. Lee and J. S. Haggerty, "Plasticity and Creep in Single Crystals of Zirconium Carbide," *J. Am. Ceram. Soc.,* **52**[12] 641-47 (1969).

20. I. V. Gridneva, Y. V. Mil'man, G. A. Rymashevskii, V. I. Trefilov, and S. I. Chugunova, "Effect of temperature on the strength characteristics of zirconium carbide," *Powder Metall. Met. Ceram.,* **15**[8] 638-45 (1976).

21. M. H. Leipold and T. H. Nielsen, "Mechanical Properties of Hot-Pressed Zirconium Carbide Tested to 2600°C," *J. Am. Ceram. Soc.,* **47**[9] 419-24 (1964).

22. J. Zou, G. J. Zhang, C. F. Hu, T. Nishimura, Y. Sakka, H. Tanaka, J. Vleugels, and O. Van der Biest, "High-Temperature Bending Strength, Internal Friction and Stiffness of ZrB_2–20vol% SiC ceramics," *J. Eur. Ceram. Soc.,* **32**[10] 2519-27 (2012).

23. J. Zou, G. J. Zhang, C. F. Hu, T. Nishimura, Y. Sakka, J. Vleugels, and O. Van der Biest, "Strong ZrB_2–SiC–WC Ceramics at 1600°C," *J. Am. Ceram. Soc.,* **95**[3] 874-78 (2012).

24. E. W. Neuman, G. E. Hilmas, and W. G. Fahrenholtz, "Strength of Zirconium Diboride to 2300°C," *J. Am. Ceram. Soc.,* **96**[1] 47-50 (2013).

25. E. W. Neuman, G. E. Hilmas, and W. G. Fahrenholtz, "Mechanical Behavior of Zirconium Diboride-Silicon Carbide Ceramics up to 2200°C," (Manuscript in Progress).

26. W. H. Rhodes, E. V. Clougherty, and D. Kalish, "Research and Development of Refractory Oxidation-Resistant Diborides Part II, Volume IV: Mechanical Properties", Report No. AFML-TR-68-190, Part II, Volume IV, ManLabs Incorporated and Avco Corporation, Wright Patterson Air Forse Base, OH, (1970).

27. G. E. Hilmas, W. G. Fahrenholtz, and E. W. Neuman, "Ultra High Temperature Mechanical Testing of ZrB_2 Based Ceramics." in 38th International Conference and Expo on Advanced Ceramics and Composites. Daytona Beach, FL, USA, 2014.

28. I. Tanaka, G. Pezzotti, T. Okamoto, Y. Miyamoto, and M. Koizumi, "Hot Isostatic Press Sintering and Properties of Silicon Nitride without Additives," *J. Am. Ceram. Soc.,* **72**[9] 1656-60 (1989).

29. D. Sciti, S. Guicciardi, and M. Nygren, "Spark plasma sintering and mechanical behaviour of ZrC-based composites," *Scripta Mater.,* **59**[6] 638-41 (2008).

30. F. Monteverde, S. Guicciardi, and A. Bellosi, "Advances in Microstructure and Mechanical Properties of Zirconium Diboride Based Ceramics," *Mater. Sci. Eng., A,* **346** 310-19 (2003).

31. A. L. Chamberlain, W. G. Fahrenholtz, and G. E. Hilmas, "High-Strength Zirconium Diboride-Based Ceramics," *J. Am. Ceram. Soc.,* **87**[6] 1170-72 (2004).

32. H. O. Pierson, "Handbook of Refractory Carbides & Nitrides: Properties, Characteristics, Processing and Applications.*"* William Andrew Publishing/Noyes: Westwood, NJ, (1996).

33. S. Zhu, *Densification, Microstructure, and Mechanical Properties of Zirconium Diboride Based Ultra-High Temperature Ceramics*, Ph. D. thesis.*,* Missouri University of Science and Technology, Rolla, MO, (2008).

34. J. B. Wachtman and D. G. Lam, "Young's Modulus of Refractory Materials as a Function of Temperature," *J. Am. Ceram. Soc.,* **42**[5] 254-60 (1959).

35. J. Wang and L. J. Vandeperre, "Variation of Mechanical Properties of UHTCs with Temperature." in Ultra-High Temperature Ceramics: Materials for Extreme Environment Applications**.** Edited by W. G. Fahrenholtz, E. J. Wuchina, W. E. Lee, andY. Zhou. John Wiley & Sons, Inc, 2014.

36. V. K. Kharchenko, "High-temperature strength of refractory materials," *Strength Mater,* **12**[10] 1284-94 (1980).

37. J. Wachtman, "Mechanical Properties of Ceramics.*"* John Wiley & Sons, Inc.: New York, (1996).

38. M. Taya, S. Hayashi, A. S. Kobayashi, and H. S. Yoon, "Toughening of a particulate-reinforced ceramics-matrix composite by thermal residual stress.," *J. Am. Ceram. Soc.,* **73**[5] 1382-91 (1990).

39. R. L. Brett and P. Bowen, "Fracture toughness assessment of silicon carbide-based ceramics and particulate-reinforced composites," *Compo,* **24**[2] 177-83 (1993).

40. J. Watts, G. Hilmas, W. G. Fahrenholtz, D. Brown, and B. Clausen, "Stress measurements in ZrB_2–SiC composites using Raman spectroscopy and neutron diffraction," *J. Eur. Ceram. Soc.,* **30**[11] 2165-71 (2010).

41. J. S. Haggerty and D. W. Lee, "Plastic deformation of ZrB_2 single crystals," *J. Am. Ceram. Soc.,* **54**[11] 572-76 (1971).

42. R. Darolia and T. F. Archbold, "Plastic deformation of polycrystalline zirconium carbide," *J. Mater. Sci.,* **11**[2] 283-90 (1976).

43. A. G. Evans and A. Rana, "High temperature failure mechanicsms in ceramics," *Acta Metall.,* **28** 129-41 (1980).

44. P. V. Zubarev and L. N. Dement'ev, "Relation between the activation energies of high-temperature creep and diffusion in transition metal carbides," *Strength Mater.,* **3**[9] 1058-61 (1971).

Table I. Elevated temperature mechanical properties of ZrB_2-10 vol% ZrC in argon.

Temperature (°C)	Crosshead Rate (Strength, Toughness) (mm/min)	Strength (MPa)	Modulus (GPa)	Toughness ($MPa \cdot m^{½}$)
RT	0.5, 0.03	696 ± 82	505 ± 12	4.8 ± 0.5
1000	0.5, 0.03	660 ± 28	508 ± 40	5.1 ± 0.1
1200	0.5, 0.03	525 ± 45	512 ± 42	4.6 ± 0.3
1400	1.0, 0.04	378 ± 19	456 ± 21	3.4 ± 0.2
1600	2.0, 0.05	301 ± 9	384 ± 35	4.1 ± 0.4
1800	3.0, 0.05	348 ± 15	368 ± 23	4.5 ± 0.2
2000	4.0, 0.06	341 ± 45	347 ± 57	4.3 ± 0.2
2200	5.0, 0.15	287 ± 24	305 ± 30	3.5 ± 0.1
2300	7.0, 0.50	294 ± 40	261 ± 32	3.6 ± 0.2

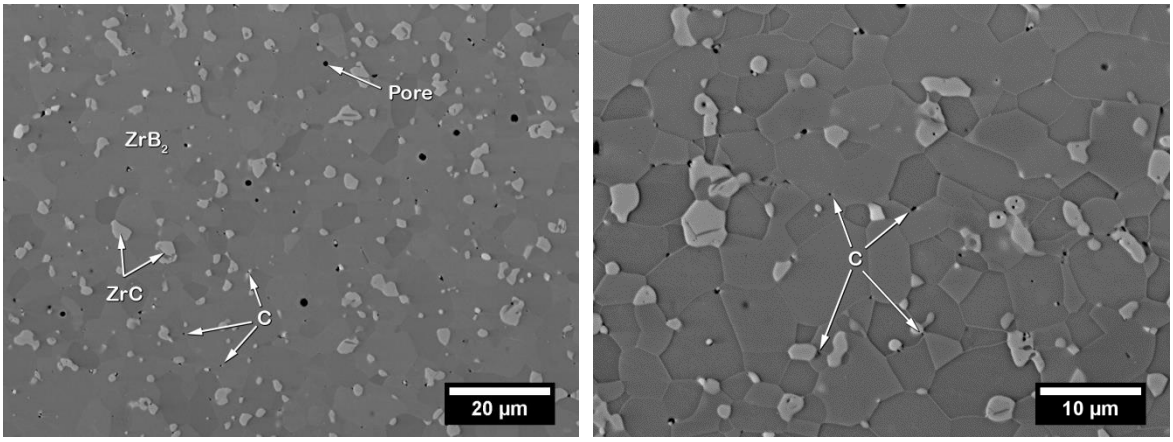

Figure 1. SEM image of polished (left) and chemically etched (right) cross-sections of ZZC10 ceramic.

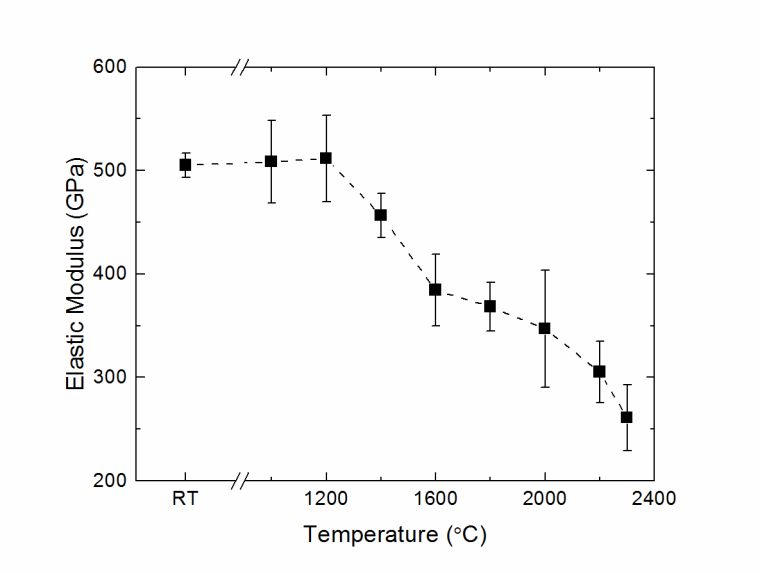

Figure 2. Elastic modulus of ZZC10 tested in argon atmosphere as a function of temperature.

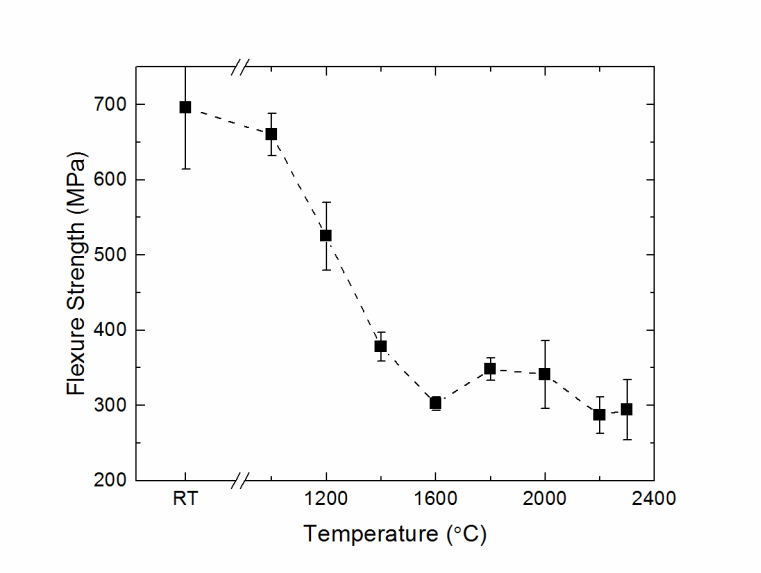

Figure 3. Four-point flexure strength of ZZC10 ceramics tested in argon atmosphere as a function of temperature.

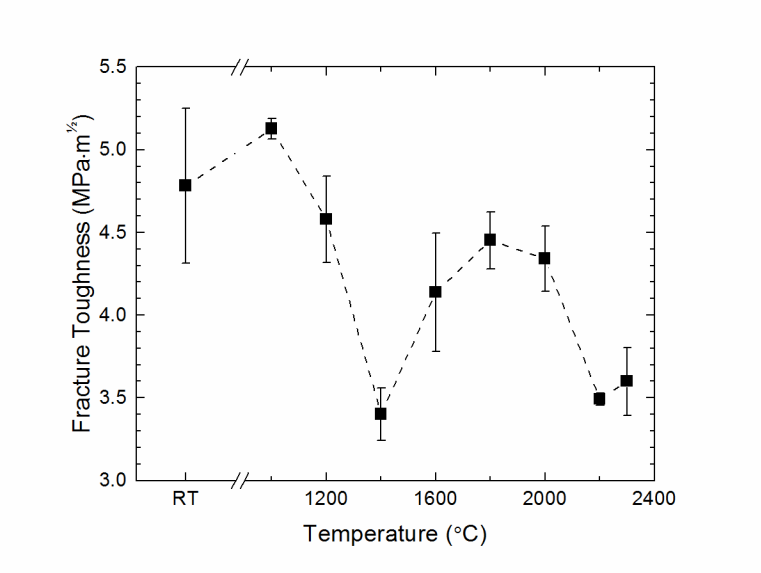

Figure 2. Chevron notch beam, in four-point flexure, fracture toughness of ZZC10 tested in argon atmosphere as a function of temperature.

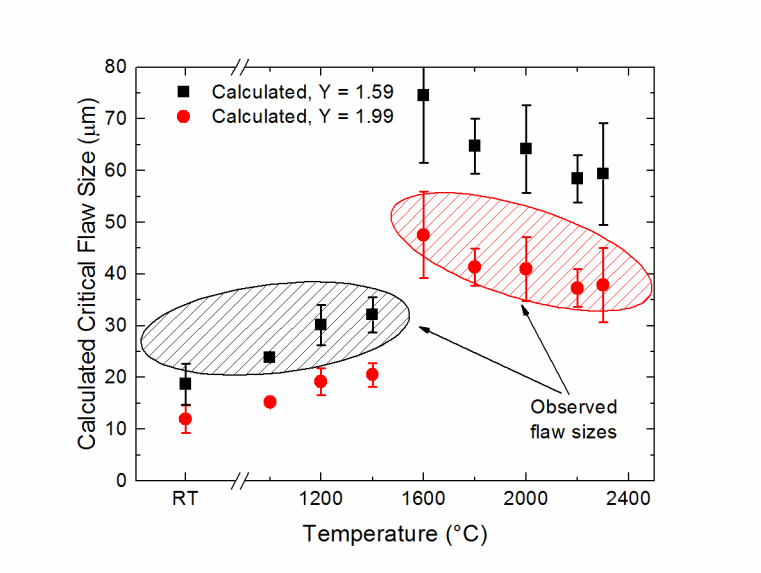

Figure 3. Estimated critical flaw size as a function of temperature for Y = 1.59 (black) and 1.99 (red). Shaded regions represent typical flaw sizes observed by fractography.

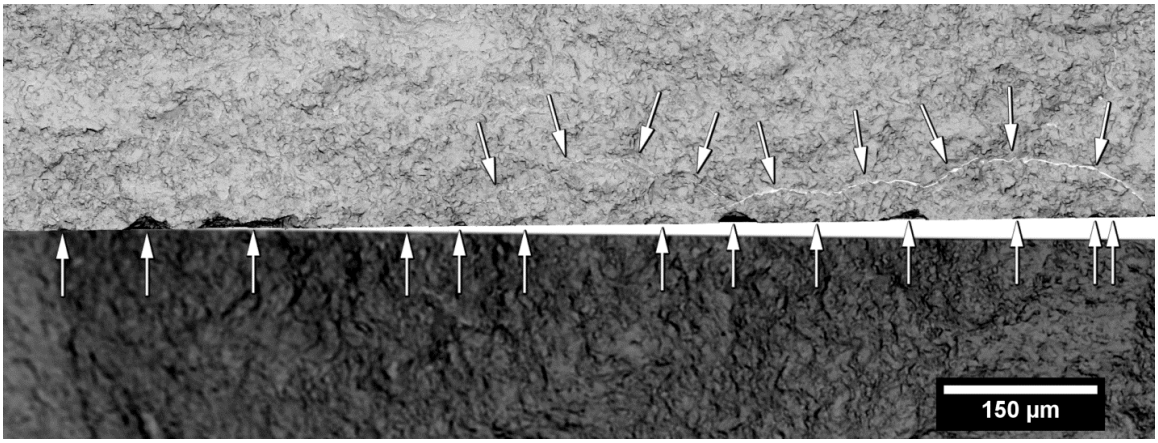

Figure 4. SEM image of tensile side of fracture surface for ZZC10 tested at room temperature demonstrating a “zipper” crack resulting from machining/handling damage, and a sub-surface crack that propagated during fracture (downward arrows).

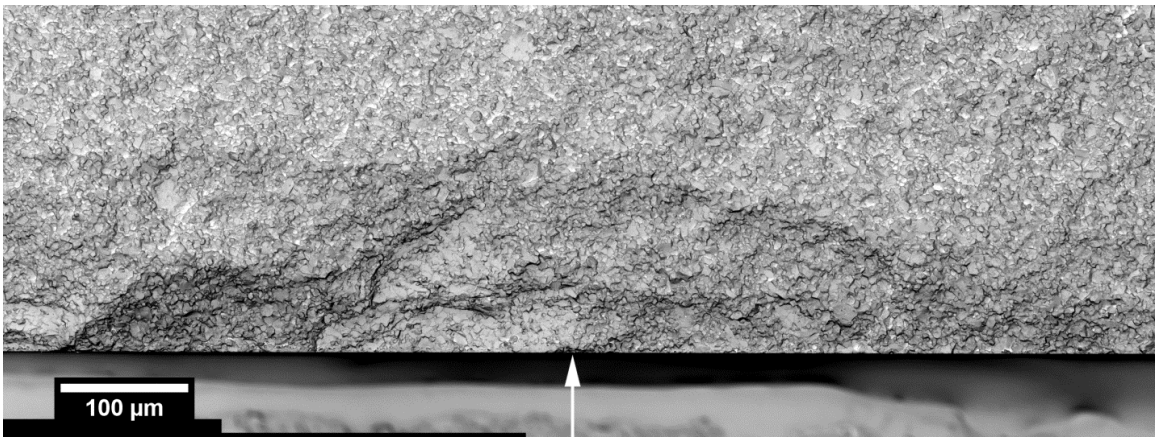

Figure 5. SEM image of tensile side of fracture surface for ZZC10 tested at 1400°C. Arrow indicates failure origin. Several smaller secondary flaws can also be observed near the failure origin.

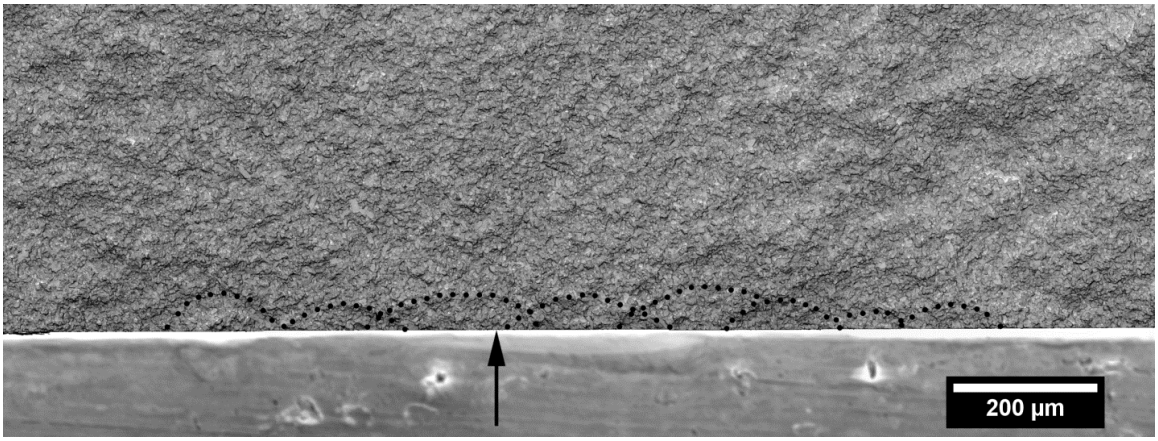

Figure 6. SEM image of tensile side of fracture surface of ZZC10 tested at 1600°C. Arrow indicates failure origin as suggested by the mist-hackle region, while dotted line indicates approximate location of crack front prior to failure.

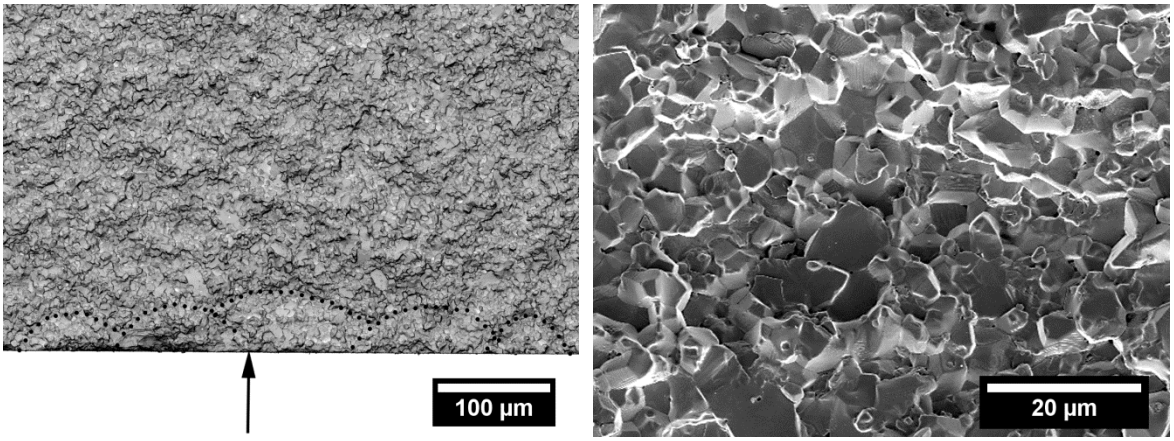

Figure 7. SEM image of tensile side of fracture surface of ZZC10 tested at 2300°C. Arrow indicates failure origin as suggested by the mist-hackle region, while dotted line indicates approximate location of crack front prior to failure. Image on right shows detail of flaw region, highlighting prevalence of cavitation at grain junctions (dark spots).

SECTION

3. SUMMARY AND CONCLUSIONS

The purpose of this dissertation was to investigate the mechanical properties of ZrB_2 based ceramics at elevated temperatures. Since the studies performed by Manlabs Inc. in the 1960's, studies of the elevated temperature mechanical properties of ZrB_2 based ceramics have been limited to temperatures primarily below 1500°C. Further, these studies have typically not been performed in a systematic manner with regard to temperature, and have typically only reported strength. This dissertation reports the strength, modulus, and toughness of several ZrB_2 ceramics at temperatures as high as 2300°C, and has made effort to investigate the source of failure for these materials as a function of temperature and environment where applicable. This section presents a summary of the results designed to answer the questions that formed the basis for the dissertation research, followed by several conclusions that were reached for the overall project.

3.1. SUMMARY

1. *How can the mechanical properties of ultra-high temperature ceramics be measured a temperatures relevant to their intended uses?*

The mechanical properties of ZrB_2 ceramics were measured up to temperatures as high as 1600°C in air, and 2300°C in an argon atmosphere. Tests conducted up to 1600°C were accomplished using a commercially

available testing system. Testing conducted up to 2300°C required construction of a specialty testing apparatus. The system consists of an induction heated graphite hot zone, with a graphite load train, mounted in an environmental chamber with atmospheric control. Mechanical load and data recording was achieved using a commercially available, computer controlled, screw-driven universal test frame. The system was qualified to a temperature of 2600°C; however, testing was limited to below 2300°C due to the ZrB_2-C eutectic at 2390°C. This testing system is currently one of only a handful in the world that is capable of testing at these temperatures. This system will allow researchers at Missouri S&T to advance the understanding of the mechanical properties of UHTCs at ultra-high temperatures.

2. *How have advances in powder purity and processing affected the mechanical behavior of ZrB_2 at elevated temperatures compared to the historical work presented by Manlabs Inc. in the 1960's?*

The mechanical behavior of monolithic ZrB_2 was investigated. The material was produced by hot pressing commercially available ZrB_2 powder with 0.5 wt% carbon added as a sintering aid at 2150°C. The final material was >99.4% dense, with no additional secondary phases observed. The grain size was tailored to ~19 μm, in an effort to match that reported in the historical work. The strength was ~390 MPa between ambient and 1200°C, decreasing to ~200 MPa between 1600°C and 2300°C. Though not reported in the manuscript

included in this dissertation, the toughness and modulus were also measured (Appendix II), and fractography was performed on the tested specimens. For all temperatures tested, the critical flaw size calculated using Griffith type analysis correlated well with the maximum ZrB_2 grain size measured. Compared to the historical work, the modern ZrB_2 material was able to be hot pressed to a higher density at a lower temperature and exhibited higher purity (>98% versus <94%). The material exhibited improved strength at all temperatures tested, and maintained a higher modulus at all elevated temperatures.

3. *What are the mechanical properties (strength, toughness, modulus) of a ZrB_2 – 30 vol% SiC at elevated temperatures, what is controlling the mechanical response, and what is the effect of atmosphere on the mechanical behavior?*

The mechanical behavior of a hot-pressed ZrB_2 – 28.5 vol% – 2.0 vol% B_4C ceramic was evaluated up to 1600°C in air, and up to 2200°C in an argon atmosphere. In air, room temperature strength was 680 MPa increasing to 750 MPa at 800°C. Strength decreased to ~360 MPa at 1500°C and 1600°C. The elastic modulus at room temperature was 510 GPa, decreasing near linearly with temperature to 210 GPa at 1500°C, with a more rapid decrease to 110 GPa at 1600°C. The fracture toughness was 3.6 $MPa \cdot m^{½}$ at room temperature, increased to 4.8 $MPa \cdot m^{½}$ at 800°C, and then decreased linearly to 3.3 $MPa \cdot m^{½}$ at 1600°C. Strength was found to be controlled by the largest SiC clusters up to

1000°C, and by oxidation damage above 1200°C. In argon, room temperature flexural strength decreased from 700 MPa to 540 MPa at 1800°C, further decreasing to 260 MPa at 2200°C. Elastic modulus steadily decreased with temperature from 510 GPa at room temperature to 340 GPa at 1800°C, with a more rapid decrease to 160 GPa at 2200°C. Fracture toughness was 4.9 $MPa \cdot m^{½}$ at room temperature, decreasing to 4.0 and 3.5 $MPa \cdot m^{½}$ at 2000°C and 2200°C. Strength was controlled by the SiC cluster size up to 1800°C. At higher temperatures, strength was controlled by formation of liquid phases, and precipitation of large BN and B-O-C-N inclusions within the microstructure.

4. Can thermal annealing be used to improve the elevated temperature mechanical properties of ZrB_2-SiC?

Post sintering thermal annealing was performed on the ZrB_2-SiC ceramic discussed above. Thermal annealing was conducted following hot-pressing at 1400°C, 1500°C, 1600°C, or 1800°C for 10 hours. For nearly all temperatures tested, heat-treatment resulted in an increase in strength and modulus compared to the as-processed material. Annealing at 1400°C resulted in the largest increases in flexure strengths at the highest test temperatures, with strengths of 470, 385, and 425 MPa at 1400, 1500, and 1600°C, corresponding to increases of 7, 8, and 12%. Thermal treatment at 1500°C resulted in the largest increase in elastic modulus, with values of 270, 240, and 120 GPa at 1400, 1500, and 1600°C, corresponding to increases of 6, 12, and 18%. Changes in ZrB_2 grain

size and SiC cluster size were not observed for these heat-treatment temperatures. TEM analysis suggests that additional phases may be forming during heat-treatment and/or changes in dislocation density may be occurring. These results show that thermal annealing may be a promising method for improving the elevated temperature mechanical properties of ZrB_2 based ceramics.

5. *Does a ZrB_2-ZrC composite offer improved mechanical properties at temperatures above 2000°C compared to the more widely studied monolithic ZrB_2, ZrB_2-SiC, and ZrB_2-$MoSi_2$ ceramics? What are its mechanical properties at temperature, and what leads to failure?*

Dense billets of ZrB_2-9.5vol% ZrC-0.1vol% C were produced by hot-pressing at 1900°C with a ZrB_2 grain size of 4.9 μm and ZrC cluster size of 1.8 μm. Flexure strength was 695 MPa at ambient, decreasing to 300 MPa at 1600°C, increasing to 345 MPa at 1800 and 2000°C, finally decreasing to 290 MPa at 2200°C. Fracture toughness was 4.8 $MPa \cdot m^{½}$ at room temperature, decreasing to 3.4 $MPa \cdot m^{½}$ at 1400°C, increasing to 4.5 $MPa \cdot m^{½}$ at 1800°C, decreasing to 3.6 $MPa \cdot m^{½}$ at 2300°C. Elastic modulus was estimated to be ~505 GPa from ambient to 1200°C, decreasing near linearly to 385 GPa at 1600°C, more slowly to 345 GPa at 2000°C, then more rapidly to 260 GPa at 2300°C. Surface flaws resulting from machining damage were identified as the critical flaw up to 1400°C. Above 1400°C, plasticity reduced the stress at the

crack tip and the surface flaws experienced sub-critical crack growth. Above 2000°C, creep cavitation ahead of the crack tip resulted in micro void coalescence, causing failure.

3.2. CONCLUSIONS

Several conclusions were reached based on the work presented in the papers:

1. At elevated temperatures, the mechanical properties of ZrB_2 based ceramics can be improved through the use of higher purity powders. The use of higher purity powders and modern processing leads to microstructures of higher density and with fewer residual phases than otherwise shown from the historical studies.
2. Control of the microstructure is essential for controlling the mechanical properties of ZrB_2 based ceramics. The formation of SiC percolation clusters in ZrB_2-SiC ceramics results in spontaneous matrix microcracking, resulting in a reduction in strength and toughness from the otherwise expected values. Formation of additional secondary phases at higher temperatures results in changes to the microstructure that result in further reductions of strength, toughness, and modulus.
3. ZrB_2 – 30 vol% SiC exhibits the highest strength for all temperatures between ambient and 2000°C. However, the mechanical properties deteriorate rapidly above this temperature due to the ZrB_2-SiC eutectic at 2270°C.

4. Post-sintering thermal annealing improves the strength and modulus of ZrB_2-SiC at elevated temperatures in air. Annealing at 1400°C for 10 hours resulted in the largest increase in strength to 425 MPa at 1600°C, the highest temperature tested, corresponding to an increase of 12%. Heat-treatment at 1500°C for 10 hours resulted in the largest increase in elastic modulus to 120 GPa 1600°C, the highest temperature tested corresponding to an increase of 18%.
5. The composition ZrB_2 – 10 vol% ZrC, had the highest strength at 2300°C, the highest temperature tested. The composition improves upon both ZrB_2-SiC and ZrB_2-$MoSi_2$ ceramics, both of which underwent partial melting at this temperature. More importantly, the composition improves upon monolithic ZrB_2 at 2300°C, with a strength of 295 MPa compared to 170 MPa.

In examining the dissertation as a whole, several observations can be made. The strength of ZrB_2 composites at all temperatures was correlated with the largest flaws present in the microstructure. Reducing the size of these flaws, through grain size refinement, improved processing, and improved machining practices, will improve the strength of the composites. Although ZrB_2-SiC displayed the highest strength up to 2000°C, more refractory composites are needed for use temperatures above 2200°C, such as the ZrB_2-ZrC composite presented, or other boride-carbide and carbide-carbide type composites. The presence of impurities in the powders used produce detrimental effects at these highest temperatures, and should be eliminated (using higher purity powders and

processing), or mitigated (recrystallization to more refractory phases, diffused into more refractory phases, such as ZrOC). Finally, these materials experience significant loss of mechanical properties during exposure to oxidizing environments. It will be necessary to develop composites with improved oxidation resistance or suitable environmental barrier coatings that will be capable of protecting load bearing regions of these ceramics.

4. SUGGESTIONS FOR FUTURE WORK

Research presented in this dissertation discussed the effects of microstructure on the mechanical properties of several ZrB_2 based ceramics at elevated temperatures. Several suggestions are presented in this section for advancing understanding and improving the mechanical properties of ZrB_2 based ceramics

1. It was discovered during the testing of ZrB_2 that the reported eutectic for the ZrB_2-C system is accurate. To enable testing of ZrB_2 based materials at temperatures above 2300°C, a different material from graphite is needed for the fixturing, load-train, and/or hot zone. ZrB_2, ZrC, HfB_2, and HfC are a few examples of materials that may allow testing of diboride based materials at these higher temperatures.
2. Varying the grain size of monolithic ZrB_2. It is expected that a finer grain size should result in an increase in the strength if grain size is the strength limiting flaw. However, finer grain size typically enhances the creep response at elevated temperatures. It would be useful to explore the trade-off between strength and creep resistance at elevated temperatures resulting from variations in grain size distributions.
3. It is urged that future work not be conducted on systems that have exceeded the percolation threshold. When percolation clusters begin to form, the threshold for spontaneous matrix microcracking can be exceeded, resulting in reduced mechanical properties. Percolation clusters are typically many times larger than the grain size, and thus may

also act as larger critical flaws in materials than otherwise would be the case without percolation clusters.

4. Varying the second phase content and matrix/secondary phase grain sizes. The current work did not explore composition or microstructure optimization. It is recommended that further work be conducted to determine the effect of additive concentration, as well as the effect of matrix/additive grain size on mechanical properties at elevated temperatures. Future studies should also explore new composite systems, as several other higher temperature binary systems exists in addition to ZrB_2-ZrC.

5. TEM characterization of inclusions and grain boundary phases. This work showed that thermal annealing can improve the strength and modulus of ZrB_2-SiC ceramics. This work also showed that additional secondary phases form at elevated temperatures during testing. TEM characterization may improve the understanding of what changes are occurring at the grain boundaries, what inclusions are forming, and dislocation behavior during thermal annealing and/or testing at elevated temperature.

APPENDIX A

CASE STUDY: BUILDING AN ULTRA-HIGH TEMPERATURE MECHANICAL TESTING SYSTEM

Eric W. Neuman, Harlan J. Brown-Shaklee, Jeremy Watts, Greg E. Hilmas, and William G. Fahrenholtz

Ultra-high temperature ceramics (UHTCs), such as refractory metal borides and carbides, are candidate materials for use in the extreme environments associated with hypersonic flight, scramjet engines, rocket propulsion, and atmospheric re-entry.[1] For example, zirconium diboride and hafnium diboride-based ceramics are being evaluated for the sharp wing leading edges of future hypersonic aerospace vehicles where temperatures in excess of 2000°C are predicted. The ability to test these materials near their expected service temperatures is an important step in their continued development. However, the upper test temperature for most commercial testing systems is limited to about 1500°C. As a result, little is known about the mechanical behavior of UHTCs at temperatures relevant to the proposed applications.

The high-temperature testing lab in the Department of Materials Science and Engineering at Missouri University of Science and Technology recently expanded its capabilities to include atmosphere-controlled mechanical testing at temperatures up to 2600°C. Figure 1 shows the ultra-high temperature test system, which consists of a screw driven universal test frame equipped with a custom-built environmental chamber and an inductively heated hot zone with a

graphite susceptor. The environmental chamber is capable of operating in inert or reducing atmospheres, or mild vacuum (to about 35 kPa). The furnace temperature is regulated using a PID (proportional integral derivative) controller with temperatures measured by a type-B thermocouple below 1600°C and a two-color pyrometer above 1500°C. Heating rates as high as 500°C/min have been achieved. To date, four point bend tests as described by ASTM C1211 (Flexural Strength for Advanced Ceramics at Elevated Temperature) have been performed, but the system is capable of conducting tensile and compression tests with the proper test fixtures.

An initial study to validate the system tested ZrB_2 based ceramics in flexure up to 2300°C using a graphite test fixture. The ZrB_2-C eutectic that occurs around 2390°C limited the upper test temperature to 2300°C. Figure 2 shows examples of load-deflection curves with insets showing fractured bars. One curve is for a ZrB_2 specimen tested at 2200°C in argon, and the other is for a ZrB_2-30SiC particulate composite tested at 1800°C, also in argon. The average strength of the ZrB_2 was about 300 MPa at 2200°C while the average strength of ZrB_2-SiC was about 220 MPa at 1800°C.[2] These are the first mechanical property measurements for ZrB_2 ceramics at temperatures over 1600°C that have been reported since work performed by Rhodes, et al. at Manlabs Inc. in 1970.[3]

Design challenges

The system originally was designed for testing at temperatures up to 2500°C. One approach would be to purchase a traditional graphite or refractory

element vacuum furnace and integrate it into an existing test frame. However, these types of furnaces raised several concerns including chemical compatibility with fixturing and specimens at elevated temperatures; limited heating rates; and atmosphere limitations. Selecting an induction furnace overcame some of these limitations. One advantage of induction heating is the ability to change the hot zone material and test fixturing based on the type of material being tested and the atmosphere required. Induction furnaces also enable higher heating and cooling rates than graphite element resistance furnaces, which allows for testing multiple specimens per day. The drawback to this approach was that no commercially available systems appeared to meet our design requirements.

The test system was constructed in several stages over a period of about six years. The environmental chamber (Detroit Tool and Die), induction power supply (Superior Induction), pyrometer (Ircon), temperature controller (Eurotherm), and load cell (Omega Engineering) were purchased, and the load frame (Instron 33R4204) was acquired from another department on campus. Graduate students at Missouri S&T designed and fabricated most of the rest of the load train assembly, induction coil, hot zone, and gas handling system. Graduate students also designed the test fixtures and rigid graphite components, which were fabricated by Graphite Products Inc. in Madison Heights, Mich.

The most significant challenges encountered during construction of the system were related to the induction coil. During initial testing, we discovered that the original induction coil did not have sufficient electrical insulation to operate in an environment with graphite dust, which caused the coil to electrically short to

the insulation pack surrounding the susceptor. The short melted a portion of the coil and burned a hole through the insulation. Adding several additional layers of electrical and thermal tape isolated the coil from the graphite insulation pack. For the current design, the coil was wrapped with mica tape, followed by fiberglass tape, and finally covered with Nextel sleeving. A sheet of alumina paper further isolated the graphite insulation from the induction coil. This furnace design has been tested successfully up to 2600°C.

We have already made several modifications to improve the design. The original design required the ability to operate under vacuum, so the environmental chamber design accommodated the constraints imposed by the size of the load frame, while giving maximum space for the furnace, insulation, and fixturing. However, the original design did not include feed-throughs for water, gas, or instrumentation. Holes were added for additional access points, but this created concerns regarding the mechanical stability of the chamber. To determine whether the holes would compromise the structural integrity of the chamber, a graduate student in the Mechanical Engineering Department at Missouri S&T performed finite element analysis of the chamber under vacuum stresses. Based on the results of this analysis, operation is limited to mild vacuum levels (about 35 kPa). In addition, the chamber body is not actively cooled. While the induction coil is capable of sustained operation at temperatures up to 2600°C, the lack of cooling loops on the chamber limits the time that specimens can be held at test temperature to several minutes.

The original design did not incorporate direct strain measurement capability. Hence, estimating strain requires compliance corrected axial displacement measurements, which, in turn, limits the precision of elastic moduli calculated from load-displacement curves. Finally, the first test fixture was constructed from graphite, which limits the maximum test temperature for ZrB_2 to 2300°C. To address this limitation, a ZrC test fixture is being fabricated, which should increase the upper test temperature for ZrB_2 specimens to about 2600°C.

Working with the system

To perform a test, a specimen is secured to the fixture using a high-strength adhesive like Super Glue and placed in the hot zone. The environmental chamber is closed, evacuated, and backfilled with argon several times to remove air as much air as possible. The chamber is purged with argon for 30 minutes, which is enough to cycle the atmosphere through the chamber twice. After purging, the induction coil is energized. The typical heating rate is 100°C/min until the temperature is about 100°C below the testing temperature and reduced to 50°C /min to reach the testing temperature. A five minute hold prior to applying the load allows for thermal equilibration before testing. The test frame is operated using standard commercial software, which controls the displacement rate and captures the resulting displacement and load. Once the specimen has failed, the induction coil is de-energized and the furnace is allowed to cool. Because of the low thermal mass of the insulation, the furnace cools to below 600°C in about one hour. Below 600°C, the environmental chamber can be opened to allow the hot zone to cool more rapidly. Using this methodology, we

can test up to four specimens at temperatures of 2000°C or more in a typical workday.

This project eliminates the barriers that used to prevent ultra-high temperature mechanical testing and enables us to study the mechanical behavior of UHTCs at the extreme temperatures likely to be encountered during hypersonic flight.

Acknowledgemnts

Research on ultra-high temperature mechanical testing is supported at Missouri S&T by the Aerospace Materials for Extreme Environments program of the Air Force Office of Scientific Research. The authors wish to thank program manager Dr. Ali Sayir for his guidance and support.

About the authors

Eric W. Neuman is a graduate student in the Department of Materials Science and Engineering at Missouri University of Science and Technology, Rolla, Mo. Jeremy Watts, Greg Hilmas, and William G. Fahrenholtz are faculty in the same department at Missouri S&T. Harlan Brown-Shaklee is a former graduate student in the MSE Department at Missouri S&T and is currently a post-doctoral researcher at Sandia National Laboratories. Contact: G. Hilmas, ghilmas@mst.edu.

References

1. W.G. Fahrenholtz, G.E. Hilmas, I.G. Talmy, and J.A. Zaykoski, "Refractory Diborides of Zirconium and Hafnium," *J. Am. Ceram. Soc.,* **90** [5] 1347-64 (2007).

2. E.W. Neuman, G.E. Hilmas, and W.G. Fahrenholtz, “Strength of Zirconium Diboride to 2300°C,” accepted for publication in the Journal of The American Ceramic Society.

3. W.H. Rhodes, E.V. Clougherty, and D. Kalish, "Research and Development of Refractory Oxidation-Resistant Diborides Part II, Volume IV: Mechanical Properties," Technical Report AFML-TR-68-190, Part II, Volume IV, ManLabs Incorporated and Avco Corporation, Wright Patterson Air Force Base, OH, 1970

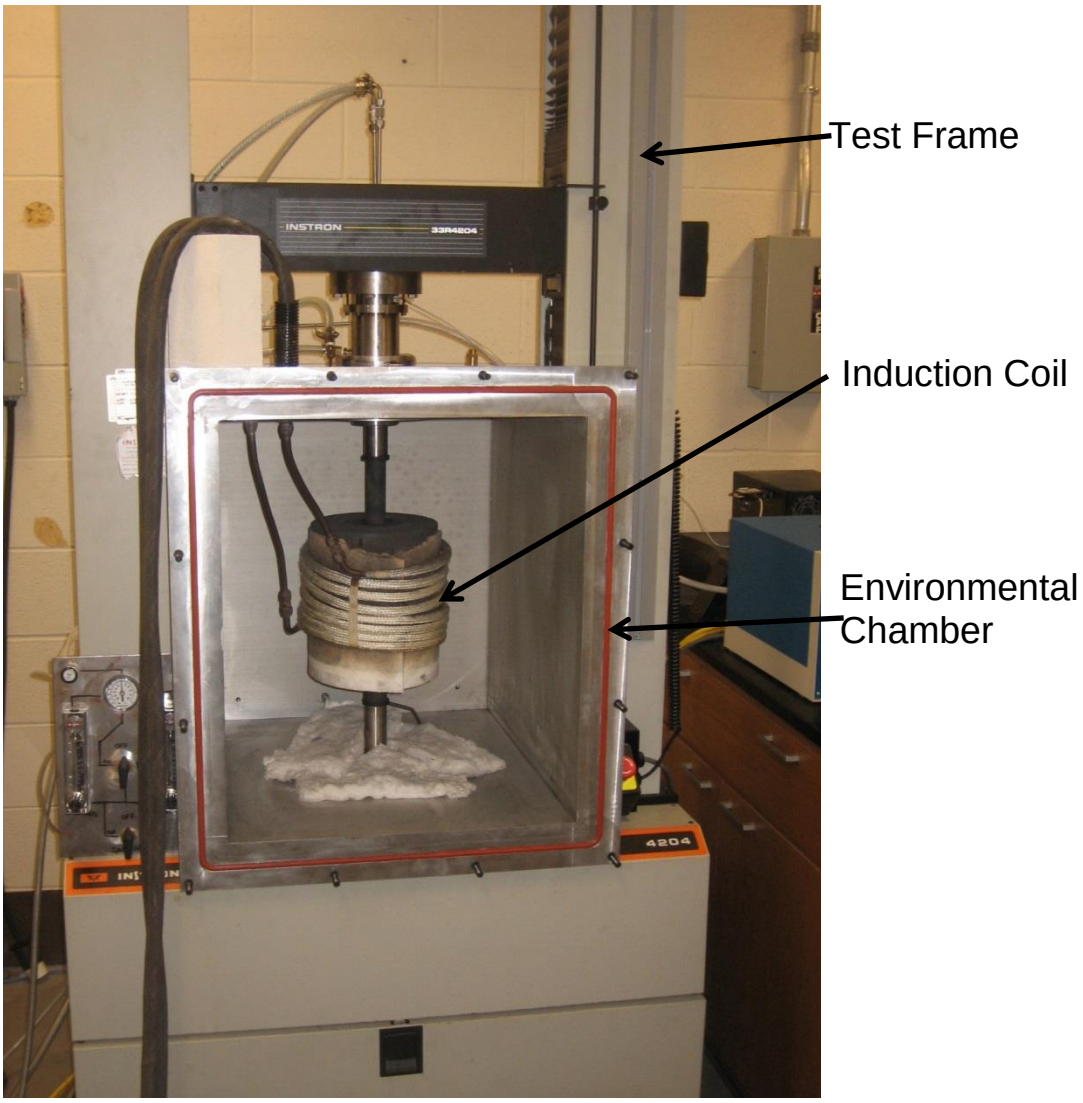

Figure 1. Ultrahigh temperature mechanical testing apparatus showing the environmental chamber, induction coil, and test frame.

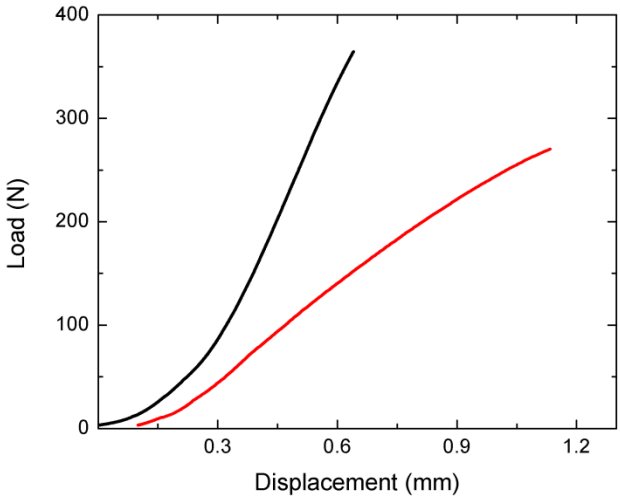

Figure 2. Examples load-displacement curves for ZrB_2 tested at 2200°C and ZrB_2-SiC tested at 1800°C.

APPENDIX B

SUPPLIMENTARY ZIRCONIUM DIBORIDE DATA

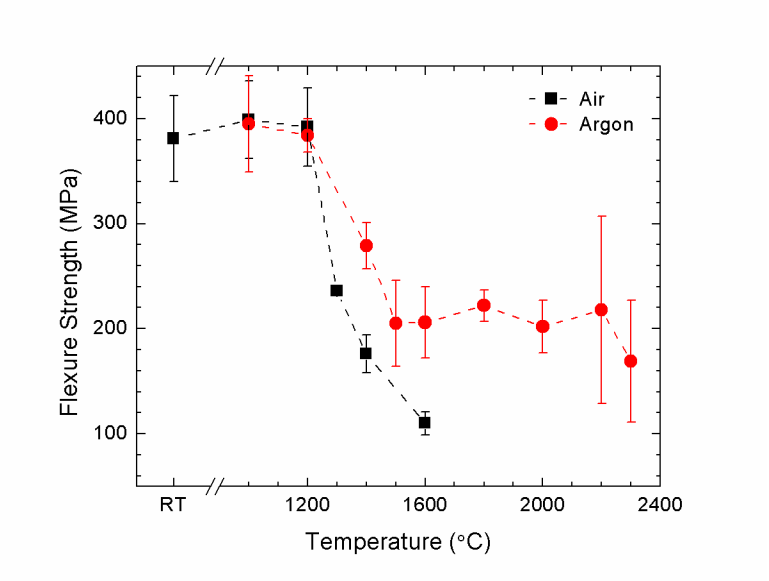

Figure 1. Flexure strength as function a of temperature for hot-pressed ZrB_2 – 0.5 wt% C material described in Paper 1. Figure shows the completed data set for the study.

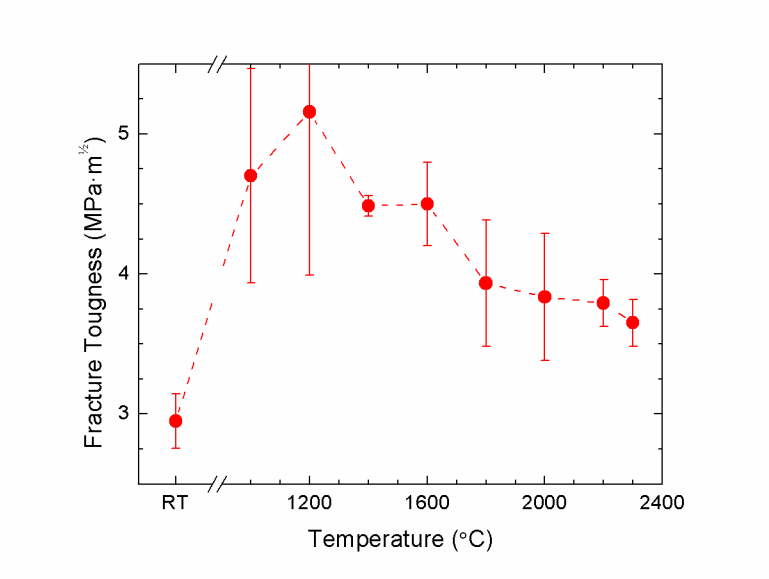

Figure 2. Chevron notch beam, in four-point flexure, fracture toughness as a function of temperature for hot-pressed ZrB_2 – 0.5 wt% C material described in Paper 1. Figure shows the completed data set for the study.

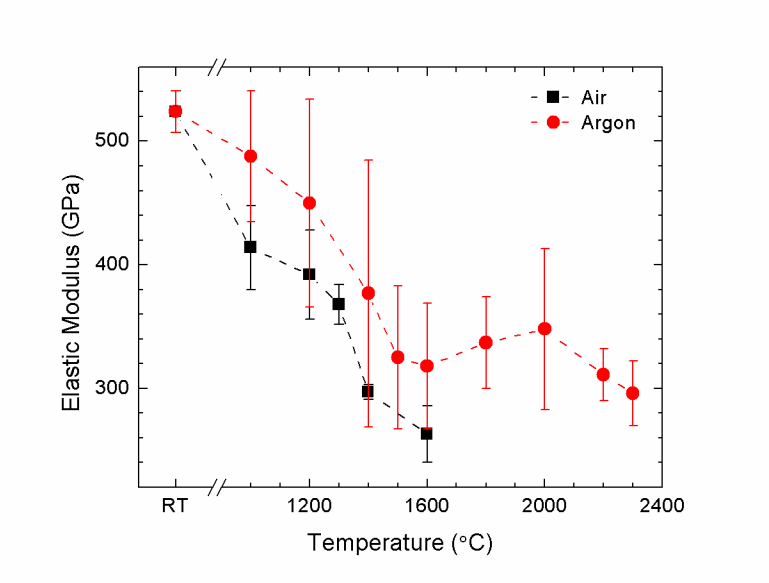

Figure 3. Elastic modulus as a function of temperature for hot-pressed ZrB_2 – 0.5 wt% C material described in Paper 1. Modulus of material in argon atmosphere was calculated from the stress-strain curve, using the crosshead displacement to estimate strain. This figure shows the completed data set for the study.

VITA

Eric Neuman was born in March 1985 in Kansas City Missouri. Until 2003 he resided in Lenexa Kansas. He met his wife Rebecca in 2002. They had their first daughter Kaelyn Elizabeth in November 2005, their son Otto Willhelm in 2009, and their second daughter Beatrix Adelaid in 2014.

Eric worked as a studio production potter at Hillcreek Pottery between 2003 and 2005 while pursuing his undergraduate degree. He changed majors and schools several times while pursuing this degree. He enrolled at the University of Missouri Rolla in 2007. He graduate Summa Cum Laude from Missouri University of Science and Technology in 2009 with a Bachelor's of Science in ceramic engineering in 2009 at Missouri University of Science and Technology.

Eric began his PhD research in 2009 under the advisement of Drs. Gregory E. Hilmas and William G. Fahrenholtz. In 2012, he was a visiting researcher at the Center for Advanced Structural Ceramics at Imperial College London under the advisement of Dr. William E. Lee. His PhD research focused on the mechanical properties of boride based ceramics. He presented work at 15 conferences nationally and internationally, published four manuscripts, with three pending, and one book chapter. In May 2014, he received his Ph.D. in Ceramic Engineering from Missouri University of Science and Technology. He will continue his career at Intel Corporation in Hillsboro Oregon.